INFORMATION TO USERS

This manuscript has been reproduced from the microfilm master. UMI films the text directly from the original or copy submitted. Thus, some thesis and dissertation copies are in typewriter face, while others may be from any type of computer printer.

The quality of this reproduction is dependent upon the quality of the copy submitted. Broken or indistinct print, colored or poor quality illustrations and photographs, print bleedthrough, substandard margins, and improper alignment can adversely affect reproduction.

In the unlikely event that the author did not send UMI a complete manuscript and there are missing pages, these will be noted. Also, if unauthorized copyright material had to be removed, a note will indicate the deletion.

Oversize materials (e.g., maps, drawings, charts) are reproduced by sectioning the original, beginning at the upper left-hand corner and continuing from left to right in equal sections with small overlaps.

Photographs included in the original manuscript have been reproduced xerographically in this copy. Higher quality 6" x 9" black and white photographic prints are available for any photographs or illustrations appearing in this copy for an additional charge. Contact UMI directly to order.

ProQuest Information and Learning
300 North Zeeb Road, Ann Arbor, MI 48106-1346 USA
800-521-0600

University of Alberta

Development and Application of Capillary Electrophoresis-Electrospray Mass Spectrometry

By

Chun-Sheng (Charles) Liu 

A thesis submitted to the Faculty of Graduate Studies and Research in partial fulfillment of the requirements for the degree of Doctor of Philosophy

Department of Chemistry

Edmonton, Alberta

Spring 2001

University of Alberta

Library Release Form

Name of Author: Chun-Sheng (Charles) Liu

Title of Thesis: Development and Applications of Capillary Electrophoresis-Electrospray Mass Spectrometry

Degree: Doctor of Philosophy

Year this Degree Granted: 2001

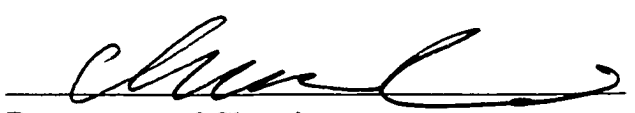

Department of Chemistry
University of Alberta
Edmonton, Alberta
Canada T6G 2G2

December 11, 2000

University of Alberta

Faculty of Graduate Studies and Research

The undersigned certify that they have read, and recommend to the Faculty of Graduate Studies and Research for acceptance, a thesis entitled **Development and Application of Capillary Electrophoresis-Electrospray Mass Spectrometry** submitted by **Chun-Sheng (Charles) Liu** in partial fulfillment of the requirements for the degree of Doctor of Philosophy.

Dr. Norman J. Dovichi

Dr. Liang Li

Dr. John S. Klassen

Dr. Charles A. Lucy

Dr. David S. Wishart

Dr. Frank Turecek

November 02, 2000

Abstract

The coupling of capillary electrophoresis (CE) with mass spectrometry (MS) using electrospray ionization (ESI) interface has reached a significant level of maturity since its inception in 1987. However, the commercialization of a CE-MS system for widespread applications on a routine basis has not occurred yet. This is mainly due to the lack of robustness of both the CE methodology and the interfacing technique. Improvement in CE method development for the on-line CE-MS analysis has proven the robustness of this technique. With the use of a nonaqueous buffering system, the on-line coupled CE-MS analysis for antidepressant drugs can be very sensitive and reproducible. The method has been successfully employed in metabolism studies of amitriptyline by *Cunninghamella elegans*. Aqueous CE separation coupled with ESI-MS detection has also been developed for analysis of nucleosides, nucleotides, carbohydrates, and peptides. With the use of volatile electrolytes such as ammonium acetate or carbonate at an optimized pH, sufficient sensitivity and separation efficiency has been achieved for anti-HIV nucleosides and their phosphorylated forms. Application of this methodology to detection and recognition of naturally occurring nucleotides in a Hep G2 cell extract, and intracellular characterization of 3TC in Hep G2 cell lines, has been demonstrated.

Sheathless microspray or nanospray MS provide superior sensitivity. The commonly used micro- or nano- sprayers have limited lifetime and are hard to fabricate; applications of those sprayers for coupled CE-MS analysis often provide signals with low stability. To take advantage of an increased ESI efficiency of microspray and nanospray and the long-term stability of a conventional stainless-steel sheath-flow interface, a silica sheath-liquid

interface has been constructed and operated at a flow rate in the mid- to high- nanoliter per minute range. The liquid sheath and the gold layer deposited on the outer surface of the CE column at the detection end make the electrical contact for CE and ESI. Overall, the interface showed a gain in sensitivity of at least one order of magnitude over the conventional interface. This low flow interface also shows promise in terms of its endurance and ability in producing highly stable ion signals.

Acknowledgement

I wish to extend a special thanks to my supervisor, Dr. Norman Dovichi for not only offering me the chance to join his group four years ago but for his encouragement, inspiration, and support throughout my graduate program.

I would also like to thank all my co-workers. Jianzhong Zhang provided much interesting input in exploring new technologies. Dev Pinto helped me to set-up the CE-MS for the lab. Special thanks to Woei Tan and Nan Li for contributing to one project and for those much joyful topics, and foods, in those *Da Leng* evening events after experiments. I thank Dr. Palcic, Jyy Huang, Dr. Tyrell, Xingfang Li, Robert Polakowski, Eugene Hansen Jr. (FDA), and Dr. Cerniglia (FDA) for collaborations with various projects. I appreciate my friends who gave help freely and cheerfully. Thank you to Dawn Richards for editing my thesis. I thank Eric Carpenter for his expertise in computing technologies and the help during my data analysis. Special thanks to Zheru Zhang for sitting beside me not only in the office but also in the rain and snow waiting for buying special merchandises. All present and former department members, in particular Edgar Arriaga, Kym Schreiner, Chris Dambrowitz, Amy Dambrowitz, Shen Hu, Le Zhang, Lillian Cook, Minghui Ma, Dieter Starke, and Ilona Baker deserve special mention for the help during my time with the department. I would like to thank Dr. Cantwell for his friendship and excellence in teaching. Thanks also to Dr. Li, Dr. Lucy, Dr. Kebarle, Dr. Klassen, Dr. Wishart, and Dr. Turecek for their advice and input on my thesis studies. Dr. Jianyi Sun (Agilent), Ms. Xiaofang Wang (Agilent), and Dr. Tonghui Zhou (CAMS) encouraged me for my advanced studies. I thank them.

Most importantly, I would like to express my gratitude to my wife Angela who supported me unconditionally and put up with my long working hours throughout my studies. In

addition to their warmth and support, my children, Wendy and Eric gave me endless joy of life. They also, on occasion, pulled me away from my word processor. I thank them for their impatience, as well as for their patience, their love and the pleasure of their company.

Table of Contents

1. Introduction 1

1.1. Introduction 2

1.2. Capillary Electrophoresis 3

1.2.1. Capillary Zone Electrophoresis 7

1.2.2. Separation Efficiency 11

1.2.3. Resolution 14

1.3. Electrospray Ionization 14

1.3.1. Production of Charged Droplets 17

1.3.2. Electrolytic Feature of Electrospray 18

1.3.3. Electrophoretic Feature of Electrospray 19

1.3.4. Theoretical Prediction of Gas Phase Ion Formation 19

1.4. On-line CE-MS Considerations 21

1.4.1. Ion Source 22

1.4.2. ESI Interface 23

1.4.3. CE Modes and Buffer Compatibility 26

1.5. Mass Spectrometer 28

1.6. Thesis Overview 29

1.7. Bibliography 34

2. On-line Nonaqueous CE-ESI-MS of Tricyclic Antidepressants and Metabolic Profiling of Amitriptyline by *Cunninghamella elegans* 44

2.1. Abstract 45

2.2. Introduction 46

2.3. Experimental 49

2.3.1. Materials and Chemicals 49

2.3.2. Culture Incubation and Sample Preparation..... 50

2.3.3. CE..... 51

2.3.4. ESI-MS..... 52

2.4. Results and Discussion..... 53

2.4.1. Modification of Separation Conditions..... 53

2.4.2. Optimization of ESI..... 58

2.4.3. Sample Stacking Effect, Quantification Calibration Curve, and Detection Limits..... 62

2.4.4. ESI-MS Characterization of TCAs..... 70

2.4.5. CE-MS Profiles of Amitriptyline and its Metabolites..... 70

2.5. Conclusion..... 78

2.6. Bibliography..... 79

3. CE-ESI-MS of Nucleosides and Nucleotides: Application to Phosphorylation Studies of Anti-HIV Nucleosides *in Vitro*..... 83

3.1. Abstract..... 84

3.2. Introduction..... 85

3.3. Experimental Section..... 88

3.3.1. Chemicals..... 88

3.3.2. Apparatus..... 88

3.3.3. Cell Preparation..... 90

3.3.4. Intracellular Phosphorylation of 3TC by Isolated Hep G2... 90

3.3.5. Preparation of Blank Hep G2 Cell Extract..... 90

3.3.6. CE Separations..... 91

3.3.7. ESI MS Detection..... 91

3.4. Results and Discussion..... 93

3.4.1. Separation of ddNs..... 93
3.4.2. Positive ESI-MS Detection for ddNs..... 96
3.4.3. Analyte Discrimination in CE Injection..... 99
3.4.4. Calibration Curves and Detection Limits..... 102
3.4.5. Profiling of ddNs in Positive ESI CE-MS..... 102
3.4.6. Negative ESI-MS Detection for ddNs and Nucleotides..... 106
3.4.7. BGE Concentration versus Separation of ddNs and Nucleotides..... 115
3.4.8. Mass Interval versus Ion Intensity and Sensitivity..... 115
3.4.9. Profiling of ddNs and Nucleotides in Negative ESI CE-MS..... 118
3.4.10. Calibration Curves and Detection Limits..... 121
3.4.11. Detection of Nucleotides in a Hep G2 Cell Extract..... 121
3.4.12. Phosphorylation of 3TC in Hep G2 Cell Lines..... 121
3.5. Conclusion..... 126
3.6. Bibliography..... 127
4. Characterization of Oligosaccharides by Micro-ESI-MS and CE-ESI-MS..... 131
4.1. Abstract..... 132
4.2. Introduction..... 133
4.3. Experimental..... 135
4.3.1. Chemicals and Materials..... 135
4.3.2. Procedures..... 135
4.4. Results and Discussion..... 139
4.4.1. Infusion-μESI-MS..... 139
4.4.2. Aqueous CE in an APS-Coated Column..... 144

4.4.3. Nonaqueous CE in an Untreated Column..... 148

4.5. Conclusion..... 151

4.6. Bibliography..... 153

5. A Novel Electrospray Interface for Capillary Electrophoresis-Mass Spectrometry..... 157

5.1. Abstract..... 158

5.2. Introduction..... 159

5.3. Experimental..... 161

5.3.1. Reagents and Materials..... 161

5.3.2. Sheath Low-Flow Interface for Infusion-ESI-MS..... 162

5.3.3. Sheath Low-Flow Interface for CE-ESI-MS..... 164

5.3.4. ESI-MS and CE-ESI-MS..... 164

5.4. Results and Discussion..... 166

5.4.1. Sheath Liquid Low Flow Electrospray for CE-MS..... 166

5.4.2. Sample Flow Effect on Sensitivity..... 167

5.4.3. Sheath Flow Effect on Sensitivity..... 172

5.4.4. Calibration Curves..... 175

5.4.5. Infusion-ESI Mass Spectra..... 175

5.4.6. CE-MS Performance..... 182

5.5. Conclusion..... 186

5.6. Bibliography..... 187

6. Electrospray Artifacts of Peptides: A Unique Behavior of Doubly Charged Ions..... 192

6.1. Abstract..... 193

6.2. Introduction..... 194

6.3. Experimental..... 195

6.3.1. Materials and Chemicals..... 195

6.3.2. CE-ESI-MS..... 195

6.4. Results and Discussion..... 198

6.5. Conclusion..... 213

6.6. Bibliography..... 216

7. An Observation of Clusters in Electrospray Mass Spectra of Dideoxynucleosides..... 219

7.1. Abstract..... 220

7.2. Introduction..... 221

7.3. Experimental..... 222

7.3.1. Chemicals and Materials..... 222

7.3.2. Procedures..... 222

7.4. Results and Discussion..... 223

7.4.1. ESI Mass Spectra of Dideoxynucleosides..... 223

7.4.2. Pseudo-Molecular Ions and Base Fragments..... 223

7.4.3. Dimers and Oligomers of Dideoxynucleosides in the Gas Phase..... 226

7.5. Conclusion..... 234

7.6. Bibliography..... 235

8. Conclusion..... 236

List of Tables

Table 2.1 CE-ESI-MS data of amitriptyline and its metabolites 76, 77

Table 3.1 pKa values of ribosenucleosides and deoxyribosenucleosides 94

List of Figures

Figure 1.1 Database-searched results of publications on CE-MS 4

Figure 1.2 A Schematic diagram illustrating a system for capillary electrophoresis with on-column detection 6

Figure 1.3 A representation of the flow profile resulting from electroosmotic flow in an uncoated capillary and the separation of charged species in CZE mode 9

Figure 1.4 A representation of electrospray process in positive ion mode 16

Figure 1.5 Schematic of interfaces for CE-MS 24

Figure 1.6 Schematic representation of CE-MS set-up used in this thesis 31

Figure 2.1 Structures of the five tricyclic antidepressants 47

Figure 2.2 TIEs (baseline subtracted) showing the effects of organic composition on resolution and migration times 54

Figure 2.3 TIEs (baseline subtracted) showing the influence of ammonium acetate concentration on separation and migration of the five TCAs 56

Figure 2.4 TIEs showing the influence of CE voltage on separation efficiency and migration of analytes 57

Figure 2.5 TIEs showing the influence of sheath flow-rate on detection sensitivity of analytes 60

Figure 2.6 TIEs showing the effect of nebulizing gas flow rate on separation and migration times of five TCAs 61

Figure 2.7 Total ion current (baseline) signals showing the effect of nebulizing gas flow rate on signal stability 63

Figure 2.8 Effects of ammonium acetate concentration in the sample solution on total ion current 64

Figure 2.9 TIEs (baseline-subtracted) showing the effects of ammonium acetate concentration in the sample solution on TIC 65

Figure 2.10 Calibration curves for the TCAs in full scan mode 67

Figure 2.11 TIEs showing the concentration detection limits of five TCAs in full scan mode 68

Figure 2.12 TIEs showing the concentration detection limits of five TCAs in SIM mode 69

Figure 2.13 ESI-MS spectra of five TCAs 71, 72

Figure 2.14 Proposed ESI-MS fragmentation pathways of tricyclic antidepressants and metabolites 73

Figure 2.15 CE-ESI-MS profiles of AMI and its metabolites 74

Figure 3.1 Structures of dideoxynucleosides and nucleotides 89

Figure 3.2 Total ion electropherograms of ddNs showing the effect of BGE pH on separation of ddNs with positive ESI-MS detection 95

Figure 3.3 Mass electropherograms showing the effects of BGE concentration on separation and migration of ddNs 97

Figure 3.4 Positive ESI mass spectra of ddNs separated by CE-MS 98

Figure 3.5 Frontal electropherograms of 3 ddNs in (A) 25 mM (B) 50 mM ammonium acetate BGE obtained by continuous electrokinetic infusion 100

Figure 3.6 Mass electropherograms showing the discrimination of analytes

during their injection process 101

Figure 3.7 Calibration curves of ddNs obtained in positive ESI CE-MS analysis 103

Figure 3.8 Total ion electropherograms of four ddNs showing the concentration limits of detection 104

Figure 3.9 Total ion electropherogram showing the separation of ddNs in a positive ESI-MS detection mode 105

Figure 3.10 Total ion electropherograms showing the effects of ESI operational modes on detection sensitivity of ddNs and nucleotides 107

Figure 3.11 Total ion electropherogram and mass spectra of nucleosides and nucleotides 108, 109

Figure 3.12 Negative ESI spectra of dGMP showing the influence of solvent on ion intensity and fragmentation 111

Figure 3.13 Negative ESI spectra of ddG, dGMP, GDP and GTP showing the influence of solvent on ion intensity 112

Figure 3.14 Negative ESI spectra of ddG, dGMP, GDP and GTP showing the influence of infusion methods on ion intensity 113

Figure 3.15 Total ion electropherograms of ddC, dCMP, CDP and ddCTP showing the effects of solvent ionic strength on peak shapes and intensities 114

Figure 3.16 Total ion electropherograms of ddNs and nucleotides showing the influence of BGE concentration on CE separation 116

Figure 3.17 Total ion electropherograms of ddNs and nucleotides showing the effects of MS scanning mass step size on ion intensity and

sensitivity 117

Figure 3.18 Total ion electropherograms showing the separation of ddNs and nucleotides 119

Figure 3.19 Total ion electropherogram and mass spectra showing the separations of ddG, dG and G by CE-MS 120

Figure 3.20 Total ion electropherograms showing the concentration limits of detection 122

Figure 3.21 Total ion electropherogram of a Hep G2 cell extract. Sample pretreatment was described in the experimental section 123, 124

Figure 3.22 Selected ion electropherograms showing the detection of 3TC and its metabolites in Hep G2 cell lines 125

Figure 4.1 Structures of the TRSE-labeled sugars 136

Figure 4.2 A schematic diagram of the microspray interface set-up 137

Figure 4.3 The μESI mass spectra of the TRSE-labeled sugars 141

Figure 4.4 The μESI mass spectra of sugars without the TRSE label 142

Figure 4.5 The μESI mass spectra of Trig-L at various orifice voltages 143

Figure 4.6 Calibration curves of the TRSE labeled sugars obtained by μESI-MS 145

Figure 4.7 μESI mass spectra of 10 μM TR in a cell incubation media 146

Figure 4.8 Total ion electropherogram showing the separation of the TRSE labeled and non-labeled sugars by CE-MS using an APS coated column and acidic separation buffer 147

Figure 4.9 Extracted ion electropherograms showing the separation of mono-, di-, and tri-saccharide labeled with TRSE 149

Figure 4.10 The ESI mass spectra of the TRSE-labeled sugars separated by CE-MS shown in **Figure 4.8** 150

Figure 4.11 Total ion electropherogram showing the separation of the TRSE labeled sugars by CE-MS using an untreated column and nonaqueous separation buffer 152

Figure 5.1 Schematic diagram of the sheath low-flow electrospray interface. 163

Figure 5.2 A modified version of the sheath low-flow electrospray interface for CE-MS 165

Figure 5.3 Effects of sample-flow rates on the selected ion signal of ddC 168

Figure 5.4 Effects of sample flow rates on the selected ion signal of ddC 169

Figure 5.5 Total ion current (TIC) signal intensity of ddI versus sample flow rate 171

Figure 5.6 Effects of sheath flow rates on the selected ion signal of ddC 173

Figure 5.7 Effects of sheath-flow rates on observed signals (TIC) of ddI..... 174

Figure 5.8 Calibration curves for ddNs by infusion ESI-MS..... 176

Figure 5.9 ESI mass spectra of bradykinin obtained from (a) ion spray and (b) low-flow interfaces..... 177

Figure 5.10 ESI mass spectra of rhodamine obtained from the sheath silica low-flow interface..... 178

Figure 5.11 Negative and positive ESI mass spectra of AttoPhos obtained from the sheath silica low-flow interface..... 179

Figure 5.12 ESI mass spectra of ddI showing the sensitivity comparison of ion spray and low-flow interfaces..... 180

Figure 5.13 Total ion electropherogram of antidepressants by CE-MS using

a low flow rate ESI interface shown in **Figure 5.1**..... 183

Figure 5.14 Total ion electropherograms of tricyclic antidepressants by CE-MS 184

Figure 6.1 A schematic diagram of the interface set-up for electrospray and CE-MS 197

Figure 6.2 ESI mass spectra of bradykinin showing the influence of analyte concentration on relative intensities of doubly charged ions over singly charged ions 199

Figure 6.3 Calibration curves of bradykinin by infusion ESI-MS 200

Figure 6.4 Calibration curves of angiotensin II by infusion ESI-MS 201

Figure 6.5 Extracted ion electropherogram (XIE) for singly charged ions (m/z 1040-1140) and doubly charged ions (m/z 520-570) obtained from a total ion electropherogram (TIE) of bradykinin... 202

Figure 6.6 Intensity of singly-charged and doubly-charged ions versus water content in a sample solution prepared in methanol-water 204

Figure 6.7 Intensity ratio of doubly-charged ions to singly-charged ions (++/+) versus water content in a sample solution prepared in methanol-water 205

Figure 6.8 Effects of solution pH on ESI mass spectra of bradykinin 208

Figure 6.9 Spatial effects of Y-axis on charge distribution of bradykinin in the gas phase 209

Figure 6.10 Spatial effects of Y-axis on charge formation as plotted with a ratio of ++/+ versus the Y-axis 210

Figure 6.11 Effects of infusion flow rates of the sample solution on charge

distribution of bradykinin in the gas phase 211

Figure 6.12 Effects of orifice potential on charge formation 212

Figure 6.13 Effects of ring potential on charge formation 214

Figure 6.14 Total ion electropherogram showing the separation of bradykinin and tyr-bradykinin 215

Figure 7.1 Average of 10 spectra of (A) ddI, (B) d4T, (C) ddC, (D) AZT, and (E) 3TC 224, 225

Figure 7.2 Cluster intensities versus concentration of d4T 227

Figure 7.3 Effects of analyte concentration on dimer formation for ddC 229

Figure 7.4. Orifice voltage versus total ion intensities of base, molecular, and dimer ions of ddC 231

Figure 7.5. Orifice voltage versus signal intensities of protonated and sodiated ions of ddC. (A) dimers, (B) monomers, (C) base fragments 232

Figure 7.6. Orifice voltage versus ion intensities of sodiated monomer and oligomers of ddC (a re-plot of **Figure 7.5**) 233

List of Symbols, Nomenclature, and Abbreviations

$[2M+H]^+$: protonated dimeric ion

$[2M+Na]^+$: sodiated dimeric ion

$[A^-]$: concentration of conjugate base A^-

$[A^+]$: concentration of charged analyte A

$[B^+]$: concentration of charged analyte B

$[BH_2]^+$: protonated base-fragment ion

$[BHNa]^+$: sodiated base-fragment ion

$[HA]_0$: initial concentration of acid HA

$[M+H]^+$: protonated molecular ion

$[M+Na]^+$: sodiated molecular ion

$1/\kappa$: thickness of double layer

3TC: lamivudine

3TCDP: lamivudine 5'-diphosphate

3TCMP: lamivudine 5'-monophosphate

3TCTP: lamivudine 5'-triphosphate

A: adenosine

A^+: charged analyte A

ACN: acetonitrile

ADP: adenosine 5'-diphosphate

AIDS: acquired immune deficiency syndrome

AMI: amitriptyline

AMP: adenosine 5'-monophosphate

amu: atomic mass unit

APCI: atmospheric pressure chemical ionization

API: atmospheric pressure ionization

APS: aminopropyltrimethoxysilane

aq: aqueous

ATP: adenosine 5'-triphosphate

AZT: azidothymidine

B^+: charged analyte B

BGE: background electrolyte

C. elegans: Cunninghamella elegans

C: cytidine

CCD: charge-coupled device

CDP: cytidine 5'-monophosphate

CE: capillary electrophoresis

CEC: capillary electrochromatography

CEM_v: channel electron multiplier voltage

CEM: charge-residue model

CF-FAB: continuous-flow fast-atom bombardment

CGE: capillary gel electrophoresis

CID: collision induced dissociation

CIEF: capillary isoelectric focusing

CITP: capillary isotachophoresis

Cl^-: chloride anion

Cl_2: chlorine gas

CLO: clomipramine

cps: counts per second

CTP: cytidine 5'-triphosphate

CUR: curtain gas flow rate

CZE: capillary zone electrophoresis

D: diffusion coefficient

d: distance between the sprayer tip and the counter plate

d4T: stavudine

dA: 2'-deoxyanosine

Da: Dalton

dAMP: 2'-deoxyadenosine 5'-monophosphate

dC: 2'-deoxycytidine

dCMP: 2'-deoxycytidine 5'-monophosphate

ddA: 2',3'-dideoxyadenosine

ddATP: 2',3'-dideoxyadenosin 5'-triphosphate

ddC: 2',3'-dideoxycytidine

ddCTP: 2',3'-dideoxycytidine 5'-triphosphate

ddG: 2',3'-dideoxyguanosine

ddI: 2',3'-dideoxyinosine

ddNs: dideoxynucleosides

ddU: 2',3'-dideoxyuridine

DES: desipramine

dG: 2'-deoxyguanosine

dGMP: 2'-deoxyguanosine 5'-monophosphate

DNA: deoxyribonucleic acid

DR: disaccharide labeled with TRSE

dT: 2'-deoxythymidine

dU: 2'-deoxyuridine

E: electric field

e^-: electronic charge

E_{CE}: electric field for CE separation

E_{inj}: electric field for injection

EOF: electroosmotic flow

ESI: electrospray ionization

f: fraction of droplet charge converted to gas phase ions

fmol: femtomole

FWHM: peak width at half maximum

g: gas

G: guanosine

GC-MS: gas chromatography-mass spectrometry

GDP: guanosine 5'-monophosphate

GTP: guanosine 5'-triphosphate

h: Plank's constant

H: plate height

HAc: acetic acid

Hep G2: human hepatoma cell line

HIV: immunodeficiency virus

HPLC: high-performance liquid chromatography

I: ionic strength

I_{A+}: ion current of charged analyte A

ICP: inductively coupled plasma

ID: inner diameter

IEM: ion-evaporation model

IMI: imipramine

IS: ion spray voltage

IU: international unit

k: Boltzmann constant

k_I: rate constant of ion evaporation

k_{A+}: rate constant of A^+ ion evaporation

k_{B+}: rate constant of B^+ ion evaporation

kV: kilovolts

L/min: liter per minute

L: total capillary length

l: liquid

Lac: lactose

Lac-L: lactose with a linker-arm

LC-MS: liquid chromatography-mass spectrometry

L_d: capillary length between injection and detection ends

l_{Det}: length of the detector window

LIF: laser-induced fluorescence

L_{Inj}: length of sample plug injected

m/z: mass to charge ratio

M: molar; mole per liter

MALDI: matrix-assisted laser desorption/ionization mass spectrometry

MEKC: micellar electrokinetic capillary chromatography

MEM: minimum essential media

MeOH: methanol

Met: metabolite

mM: millimolar; millimole per liter

MR: monosaccharide with TRSE label

MS: mass spectrometry

M_s: capillary metal

$M_{(aq)}^+$: capillary metal cation

MW: molecular weight

N/m: Newton per meter

n: number of repeated runs

N: number of theoretical plates

Na_2HPO_4: sodium hydrogenphosphate

NaOH: sodium hydroxide

NEB: nebulizing gas flow rate

NH_4Ac: ammonium acetate

nL: nanoliter

nM: nanomolar; nanomole per liter

NMR: nuclear magnetic resonance

NOR: nortriptyline

OD: outer diameter

OR: orifice voltage

X^2_ν: reduced chi squared for ν degrees of freedom

p: probability

p: constant expressing the sampling efficiency of mass spectrometer

PA: proton affinity

PBS: phosphate buffered saline

pg: picogram

pI: isoelectric point

pKa: acidic dissociation constant

PSD: post-source decay

psi: pounds per square inch

Q: charge on particle

Q_0: surface charge density on capillary wall

QqTOF: quadrupole-quadrupole time-of-flight

QTOF: quadrupole time-of-flight

R: gas constant

R_s: resolution

R^2: correlation coefficient

r_c: radius of the electrospray capillary

RNG: focusing ring voltage

RSD: relative standard deviation

S/N: signal to noise ratio

SDS: sodium dodecylsulfate

SIM: selected ion monitoring

SS: stainless steel

T^0: temperature

T: thymidine

TCA: tricyclic antidepressant agent

TIC: total ion current

TIE: total ion electropherogram

t_{inj}: injection time

TLC: thin-layer chromatography

$t_{m,i}$: migration time of analyte i

$t_{m,j}$: migration time of analyte j

t_m: migration time

t_{mig}: migration time

TOF: time of flight

Torr: pressure unit

TR: trisaccharide with TRSE label

Trig-L: trisaccharide with a linker-arm

TRSE: 5-carboxytetramethylrhodamine

U: uridine

UDP: uridine 5'-diphosphate

UV: ultra-violet light

V: voltage; volts

V_{cap}: capillary inner volume

V_{inj}: injection volume

Vis: visible light

V_{on}: onset potential leading to formation of the charged liquid jet

W_i: peak width of analyte i

W_j: peak width of analyte j

$W_{1/2}$: peak width at half maximum

XIE: extracted ion electropherogram

ΔG: free energy of activation

ΔH^0: standard enthalpy

$\Delta\mu_{ep}$: electrophoretic mobility difference between analyte i and j

α: dissociation ratio

ε: dielectric constant of solvent

ε_0: permitivity of the solvent

γ: surface tension

η: viscosity of solution

μA: microampere

μ_{app}: apparent electrophoretic mobility of a charged particle

μ_{eo}: electroosmotic mobility

$\mu_{ep,i}$: electrophoretic mobility of analyte i

$\mu_{ep,j}$: electrophoretic mobility of analyte j

μ_{ep}: electrophoretic mobility

μESI: microelectrospray ionization

μL/min: microliter per minute

μm: micrometer

μM: micromolar; micromole per liter

ν_{app}: apparent velocity of the electrophoretic migration of a charged particle

ν_{eo}: linear velocity of electroosmotic flow

σ: noise variance

σ^2: peak variance

σ^2_A: peak variance due to adsorption

σ^2_{Cond}: peak variance due to conductivity difference

σ^2_{Det}: peak variance due to detection

σ^2_{Inj}: peak variance due to injection

σ^2_{JH}: peak variance due to Joule heating

σ^2_{LD}: peak variance due to longitudinal diffusion

σ^2_{other}: peak variance due to all other factors

σ^2_{pH}: peak variance due to pH difference during electrophoresis

ζ': zeta potential of the charged particle

ζ: zeta potential of the charged surface

CHAPTER 1

Introduction

1.1 INTRODUCTION

In the past two decades, the on-line coupling of separation techniques and spectrometric detection methodologies has become an important topic in analytical and bioanalytical chemistry. The most significant examples of the widely employed hyphenated technologies have been gas chromatography-mass spectrometry (GC-MS), high-performance liquid chromatography-ultraviolet absorbance (HPLC-UV), and high-performance liquid chromatography-mass spectrometry (LC-MS). Capillary electrophoresis (CE) is a relatively young technique and since its introduction in 1981[1,2], CE has played increasingly important roles in the analytical development of the Human Genome Project[3], biopolymer analysis[4], and pharmaceutical analysis[5]. The combination of CE separations and ultraviolet and visible (UV/Vis) absorbance, laser-induced fluorescence (LIF), and electrochemical detection schemes has been commonly utilized in many microscale applications. In recent years, MS detection for CE has been actively pursued as well. MS detection not only provides molecular weight and structural information, but also adds a second dimension in separation. The addition of this second dimension in separation helps achieve differentiation of co-eluted species with different nominal masses.

The coupling of CE with MS has reached a significant level of maturity since the first publication on CE-MS in 1987 utilizing an electrospray ionization (ESI) interface[6]. ESI is the most versatile ionization technique in existence today[7]. The only absolute prerequisite for ESI is that the analytes of interest be soluble in a solvent, and, therefore, ESI affords a near-ideal marriage between CE and MS. It will likely remain the preferred approach for the foreseeable future of CE-MS hyphenation. In addition to ESI, the continuous flow fast atom bombardment MS interface has also been employed for

coupling CE and MS[8-10]. **Figure 1.1** shows the number of the published articles on on-line coupled CE-MS studies in the past thirteen years. The number shown was obtained by searching the Analytical Abstracts Database with "Electrophoresis AND Mass Spectrometry" as key words, subtracting (manually) the number of papers on off-line CE/MS and CE-inductively coupled plasma-MS. The number of publications on LC-MS is also listed in the figure for comparison. The same search performed on the Medline Database produced very similar results. It is clear that the number of applications of LC-MS is much larger than of CE-MS. Although the acceptance of CE-MS has increased tremendously in the past five years, some limitations of this technique hinder its widespread application. Continuous developments in CE separation, further understanding of the ESI mechanism, improvements in interface designs, and availability of novel mass spectrometers will mediate CE-MS's limitations and lead to increased use of CE-MS in research and development of biotechnology and the pharmaceutical industry. The news[11] that the commercial CE-MS product joint-ventured by Beckman Coulter and ThermoQuest won the second-place award for Best New Products on Show during PittCon 2000 should stimulate wider acceptance of this CE-MS technology in analytical chemistry, biochemistry, and health care markets.

1.2 CAPILLARY ELECTROPHORESIS

Electrophoresis is a separation method based upon the differential mobilities of charged species in a condensed medium under the influence of an electric field. The development of electrophoresis in capillary tubes offers several exciting features for fast, highly efficient separations of ionic species and macromolecules. Initial work on electrophoresis in smaller open tubes was first reported in 1974 when Virtanen[12] performed electrophoretic separations in 200-500 μm ID glass tubes. Mikkers[13] repeated

Figure 1.1 Database-searched results of publications on CE-MS (1987-2000).

The data was obtained from the **Analytical Abstracts Database** by searching **Electrophoresis AND Mass Spectrometry**, or **Liquid Chromatography AND Mass Spectrometry**. The number shown in the figure is the total number of papers related to on-line CE-MS or LC-MS, excluding off-line combination and CE-ICP MS or LC-ICP MS.

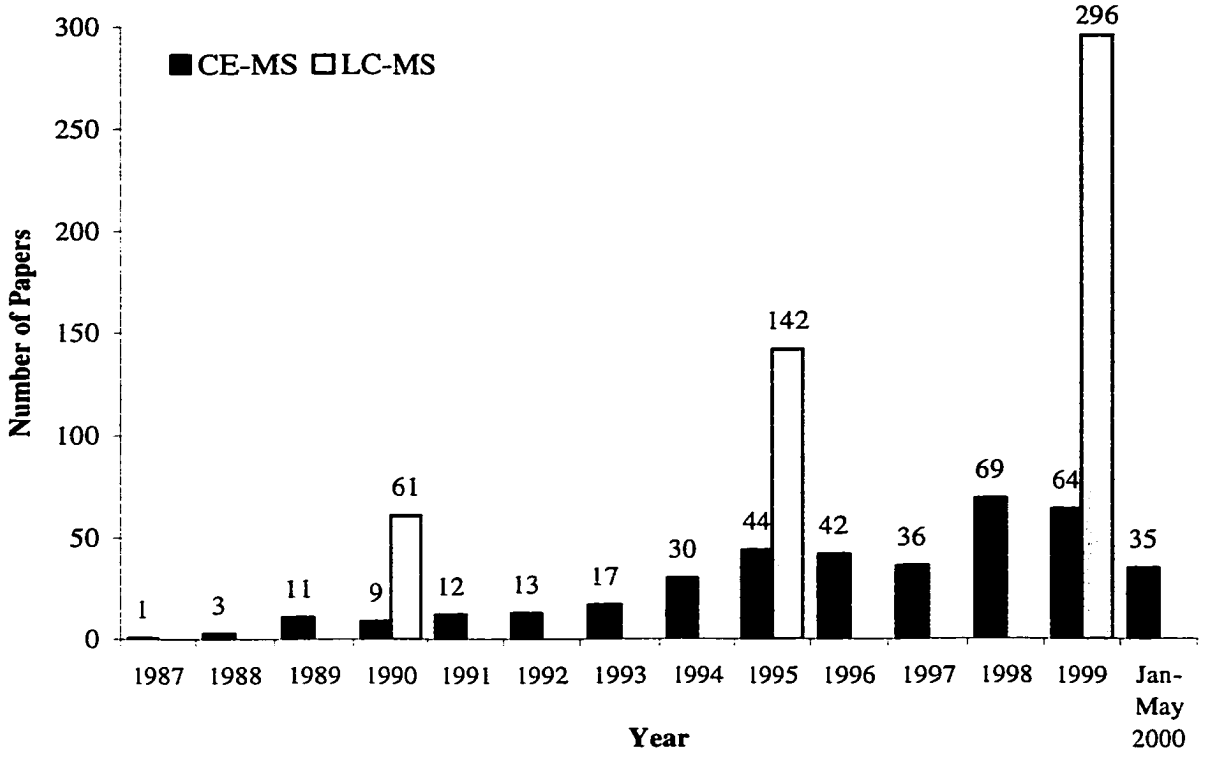

this technique with 200 μm ID Teflon tubes with separation efficiencies of nearly 100,000 theoretical plates. Jorgenson and Lukacs[1,2,14] improved the technique by using 75 μm ID fused-silica capillaries in the early 1980s with separation efficiencies of over a million theoretical plates in less than 20 minutes. A key advantage with the use of capillary tubes for electrophoresis is an enhanced heat dissipation that permits the use of high electric fields for separations. Utilizing high electric field results in extremely high efficiency and dramatically decreased analysis times[14]. The small flow rates obtained in CE permit sampling from picoliter environments, even for the measurements of chemical composition of single cells[15]. Finally, the use of a fused-silica capillary for CE allows easy automation of the separation apparatus.

In the past 20 years, CE has found widespread applications in many areas related to chemical and biomedical research[12]. Frequently used modes of CE have been capillary zone electrophoresis (CZE), capillary gel electrophoresis (CGE), capillary isoelectric focusing (CIEF), capillary isotachophoresis (CITP), micellar electrokinetic chromatography (MEKC), and capillary electrochromatography (CEC). A schematic diagram of a CE instrument with on-column detection is illustrated in **Figure 1.2**. A buffer-filled capillary column is placed between two buffer reservoirs. One end is kept at high voltage in a Plexiglass box (dashed box) and the other end is at ground potential. An electric field is applied across the capillary after a narrow solute (sample) plug has been introduced into the column. Separations of analytes are conducted according to mass-to-charge ratio in CZE or by other mechanisms in other separation modes, such as size in CGE or isoelectric point (pI) in CIEF.

Figure 1.2 A Schematic diagram illustrating a system for capillary zone electrophoresis with on-column detection.

The box with the dashed line indicates the injection end is in a safety-locked Plexi-Glass device.

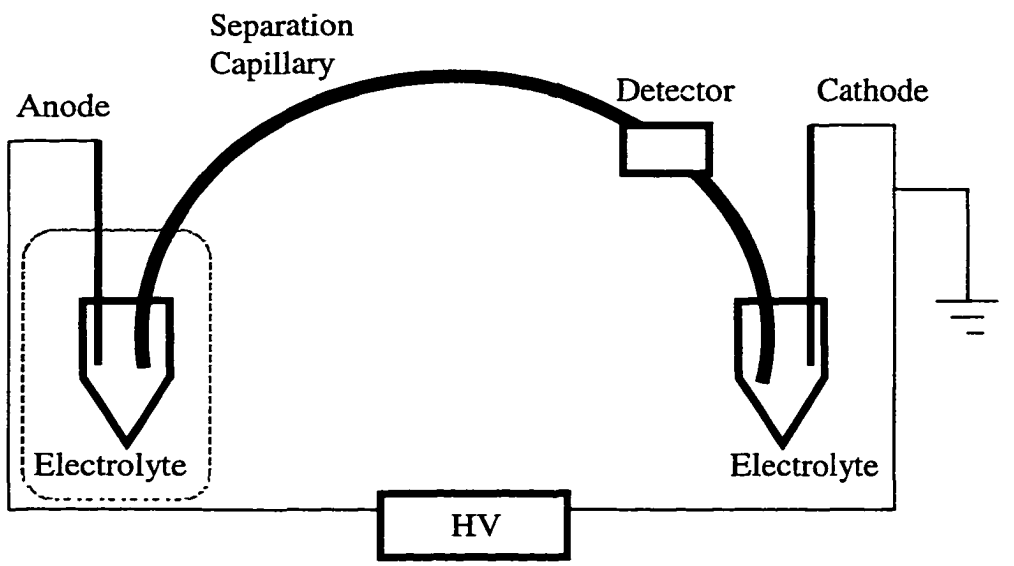

1.2.1 Capillary Zone Electrophoresis

CZE is the basic mode of CE and is usually performed in a bare capillary column. Under the influence of an electric field, ionic solutes migrate differentially in a homogeneous buffer to provide discrete, moving zones in a buffer-filled capillary. This is generally the simplest and perhaps the most universally employed mode of CE. A key property of capillaries for electrophoretic separations is the presence of an electroosmotic flow (EOF) originating from the capillary wall[14,16]. Under normal aqueous conditions with small binary electrolytes, the solid surface has an excess of anionic charge resulting from ionization of surface functional groups, i.e. the silanol groups of silica capillaries. Counterions to these anions move from the medium to this stationary surface and create an ionic layer. A compromise between electrostatic attraction and diffusion creates a thin stagnant double layer adjacent to the capillary walls. This cationic nature extends into the diffuse layer, which is the bulk of solution and is mobile. The charge density of excess cations decreases exponentially away from the capillary wall in the diffuse layer. The potential across the layers is termed the zeta potential, ζ, and is related to the thickness ($1/\kappa$) of the double layer. With an approximation, the ζ on a plane surface can be expressed as[17]:

$$\zeta = (Q_0 / \varepsilon_o)\,(1/\kappa) \qquad (1.1)$$

$$1/\kappa = 3.04 \times 10^{-10} / I^{1/2}\text{ , in meters} \qquad (1.2)$$

where Q_0 is the surface charge density on the capillary wall, ε_o is the permittivity of the solvent, and I is the ionic strength of the bulk solution. The double layer thickness ranges from 3 to 300 nm for a binary electrolyte with concentrations of 10^{-2} to 10^{-6} M. During CE, an electric field is applied tangentially to the double layer, along the axis of the capillary. This electric field forces the excess cations near the double layer to migrate

parallel to the wall toward the cathode. As these cations are solvated, they drag solvent with them resulting in a flow of the bulk solution. The linear velocity of the EOF, v_{eo}, is given by:

$$v_{eo} = \mu_{eo} E \tag{1.3}$$

where μ_{eo} is the electroosmotic mobility, E is the electric field strength (where E is the ratio of voltage applied across the capillary (V) to the capillary length (L)). According to the Helmoltz-Smoluchowski equation, the electroosmotic mobility can be described by:

$$\mu_{eo} = \varepsilon \zeta / (\eta/10) \tag{1.4}$$

where ε is the dielectric constant and η is the viscosity of the solution. The velocity of the solution is zero at the wall and reaches v_{eo} in the bulk solution at some distance away from the wall, **Figure 1.3**. The presence of double layer results in a flat flow profile of solution as long as the capillary radius is at least 7 times larger than the thickness of the double layer[18]. Changing the ζ potential will modify the EOF. For instance, the number of ionized silanol groups on the inner capillary wall increases at elevated pH, therefore the charge density at the wall increases, the ζ potential increases, and the EOF increases. Similarly, modification of the inner surface of the capillary can eliminate EOF or alter its direction. The thickness of the double layer can be affected by the ionic strength of the buffer solution; high ionic strength produces low EOF due to a reduced thickness of the double layer and thus a reduced ζ potential. The electric field applied across the capillary and the solution viscosity also have large effects on EOF as depicted by equation 1.3. Other parameters that have been shown to affect the EOF include the presence of organic solvents in the buffer and aging of the capillary. The EOF process can be easily controlled, and because of the EOF, anions and cations can be separated and detected in the same run.

Figure 1.3 A representation of the flow profile resulting from electroosmotic flow in an uncoated capillary and the separation of charged species in CZE mode.

Neutral species co-elute with EOF. + is the cation from the solution, $^-$ is the negative charge on the capillary wall. Different sized circles represent different sized ions. The arrow represents the direction of the EOF. The lower scheme is the electropherogram resulting from the separation.

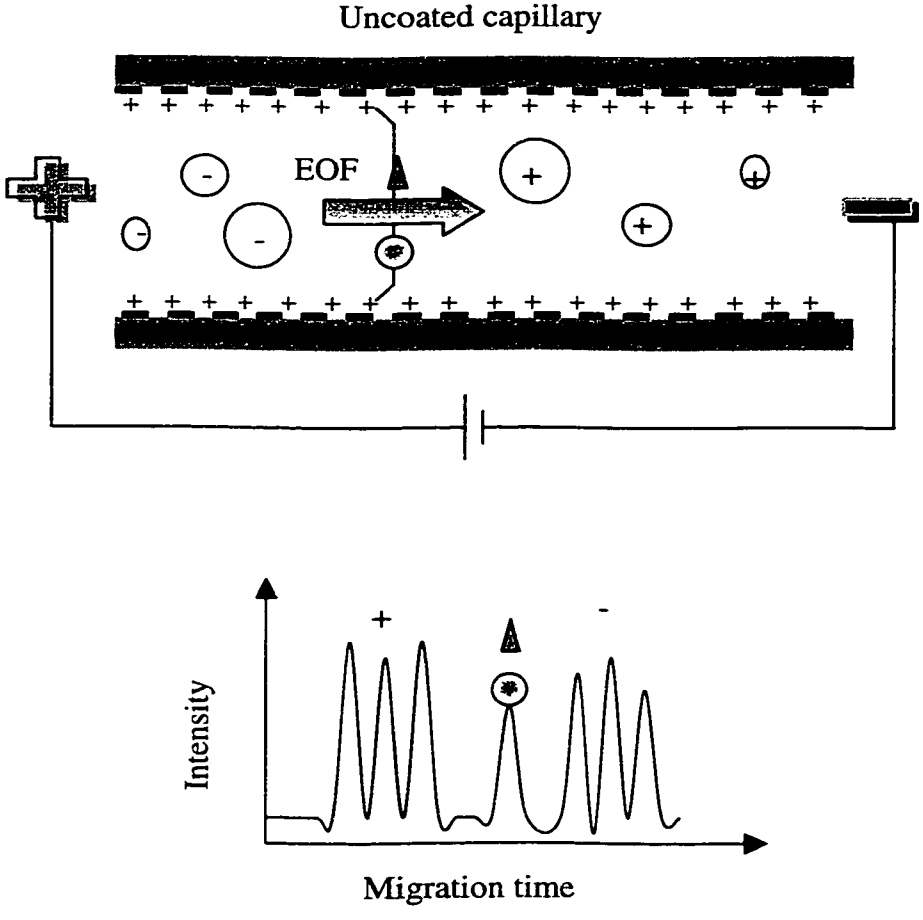

According to the Debye-Huckel limiting law theory, the electrophoretic mobility of a small charged particle (ion), μ_{ep}, can be described as:

$$\mu_{ep} = \varepsilon \zeta / \{1.5 (\eta/10)\} \quad (1.5)$$

and

$$\zeta' = (Q / 4 \pi \varepsilon_o r) \quad (1.6)$$

where ζ' is the zeta potential of the charged particle, Q is the charge on particle, ε_o is the permittivity of the solvent, r is the radius of the charged particle. In the presence of EOF, the apparent velocity of the electrophoretic migration of a charged particle, v_{app}, can be expressed as:

$$v_{app} = \mu_{app} E = (\mu_{ep} + \mu_{eo})E = (\mu_{ep} + \mu_{eo}) V / L \quad (1.7)$$

where μ_{app} is the apparent mobility of the particle. The separations of charged species are due to their differences in electrophoretic mobility. The migration time, t_m, is expressed as the function of the apparent velocity of electrophoretic migration and the length from the injection end to the detector, L_d:

$$t_m = L_d / v_{app} = L_d L / \{(\mu_{ep} + \mu_{eo})V\} \quad (1.8)$$

where L_d is the capillary length between injection and detection ends. In cases of post column detection, $L_d = L$. Therefore the equation can be revised as:

$$t_m = L^2 / \{(\mu_{ep} + \mu_{eo})V\} \quad (1.9).$$

1.2.2 Separation Efficiency

According to the rate theory of column band broadening, the number of theoretical plates (N) can be defined as:

$$N = L / H \tag{1.10}$$

where H is the plate height. H is related to the peak variance, σ^2, as expressed in the following eqation:

$$H = \sigma^2 / L \tag{1.11}$$

where σ^2 is the total variance of the peak and is constituted by variances from injection (σ^2_{Inj}), longitudinal diffusion (σ^2_{LD}), convection caused by Joule heating (σ^2_{JH}), adsorption (σ^2_{A}), gravity flow caused by the height difference of the two ends of capillary (σ^2_{GF}), conductivity difference between the solute zone and the background electrolyte (σ^2_{Cond}), pH difference during electrophoresis (σ^2_{pH}), and detection (σ^2_{Det}). The total variance σ^2 can be expressed as:

$$\sigma^2 = \sigma^2 = \sigma^2_{Inj} + \sigma^2_{LD} + \sigma^2_{JH} + \sigma^2_{A} + \sigma^2_{GF} + \sigma^2_{Cond} + \sigma^2_{pH} + \sigma^2_{Det} + \sigma^2_{other} \tag{1.12}.$$

Gravity flow is minimized by assuring that each end of the capillary is at the same height. Adsorption is caused by the interaction between analyte and the capillary wall. This interaction can be electrostatic and/or hydrophobic, causing significant tailing of peaks or irreversible retention. In cases of protein separations, this adsorption can become serious. Methods have been developed for reducing the interactions of analytes with the capillary wall using a separation buffer at low pH or with high ionic strength[19,20]. Dynamic coating or covalent coating of the inner capillary wall to deactivate the capillary surface has also been employed for this purpose[2,21-23]. The conductivity difference between analyte and

buffer leads to elution of asymmetrical zones and therefore causes peak asymmetry with either a fronting or a tailing peak shape[24]. The conductivity variance can be minimized by using a buffer concentration of 1000 times higher than that of the solute ions[14].

An electric current passing through the conducting buffer solution generates Joule heating. The heat increases the temperature at the center of the capillary relative to that at the walls. The cross-sectional temperature gradient leads to a viscosity difference of solution, and therefore introduces a parabolic flow profile. When large diameter capillaries or high conductivity buffers are employed, the convection variance can be problematic[25]. Providing enough surface area (e.g. use of small ID capillaries to dissipate the heat) minimize Joule heating effects. An alternative is to utilize an external cooling device to lower the thermal effect[26].

Sample injection is usually performed electrokinetically or hydrodynamically. The variance can be expressed as:

$$\sigma^2_{Inj} = l^2_{Inj} / 12 \qquad (1.13)$$

where l_{Inj} is the length of the sample plug injected. Usually a sample plug with a length of less than 1% of total capillary length encounters minimal band broadening effect caused by the injection variance[27]. The variance of on-column and post-column detection is described as:

$$\sigma^2_{Det} = l^2_{Det} / 12 \qquad (1.14)$$

where l_{Det} is the length of the detection window.

Providing the experiment is conducted properly and the aforementioned parameters are controlled carefully, variance caused by diffusion is the major contribution to the total

variance. Diffusion of molecules occurs when the concentration of analyte is different along the capillary. Molecules diffuse from high to low concentration regions. According to the Stokes-Einstein equation, the diffusion variance can be expressed as:

$$\sigma^2_{LD} = 2\ D\ t_m \qquad (1.15)$$

where D is the diffusion coefficient. Molecules possessing smaller diffusion coefficients (such as proteins) show less diffusion variance if the migration time is not prolonged significantly. In an ideal situation where the diffusion variance is the major contributor of the total variance, an arrangement of equations 1.9, 1.10, 1.11, and 1.14 can be obtained as:

$$N = L^2 / (2\ D\ t_m) = (\mu_{ep} + \mu_{eo})\ V / 2\ D \qquad (1.16).$$

This equation indicates that a high number of theoretical plates can be achieved by employing an ultra-high potential for separation[28], but Joule heating in the capillary often limits the efficiency gain from the increased potential. Increasing the apparent mobility ($\mu_{ep} + \mu_{eo}$) is another way to obtain high separation efficiency. As stated in Equations 1.4 and 1.5, an increased electrophoretic mobility and electroosmotic mobility can be achieved by increasing the ζ potential and decreasing the solution viscosity.

The number of theoretical plates, N, can be calculated from experimental results according to the following equation:

$$N = t^2_m / \sigma^2 = 5.54\ (t_m / W_{1/2})^2 \qquad (1.17)$$

where $W_{1/2}$ is the peak full width at half maximum (FWHM) in the time scale.

1.2.3 Resolution

Similar to conventional chromatography, the resolution, R_s, of two analytes (i and j) in CE can be estimated using the following equation:

$$R_s = 2\,(t_{m,j} - t_{m,i}) / (W_i + W_j) \qquad (1.18).$$

Resolution is also related to the number of theoretical plates as follows:

$$R_s = (N^{1/2} / 4)\,\Delta\mu_{ep}\{\mu_{eo} + (\mu_{ep,i} + \mu_{ep,j})/2\}^{-1} \qquad (1.19)$$

Combining Equations 1.16 and 1.18, a relationship between resolution and applied potential across the capillary can be shown as:

$$R = (V / 32\,D)^{1/2}\,\Delta\mu_{ep}\,\{\mu_{eo} + (\mu_{ep,i} + \mu_{ep,j})/2\}^{-1/2} \qquad (1.20).$$

Increasing the potential has less effect on resolution enhancement than on the number of theoretical plates as depicted in Equations 1.20 and 1.16. The resolution gained by elevating the potential is limited by the Joule heating. However, improved resolution of analytes can be achieved by adjusting operational parameters such as the solution pH to enlarge analyte differences in electrophoretic mobility, $\Delta\mu_{ep}$. Neutral species or analytes with similar electrophoretic mobilities cannot be separated by CZE. CE operated in other modes such as CGE, MEKC and CEC need to be employed.

1.3 ELECTROSPRAY IONIZATION

Electrospray ionization (ESI) produces gas phase ions directly from the solution phase at atmospheric pressure. Dole first proposed ESI as an ion source in the late 1960s and early 1970s for mass spectrometric detection of polymeric species such as polystyrenes[29-31]. In the late 1970s Iribarne and co-workers first demonstrated that

macroions could be liberated from charged droplets and detected using mass spectrometry[32]. In 1984, Fenn and Yamashita[33,34] introduced the direct coupling of an ESI source and a mass spectrometer for studies of organic and inorganic solutes. Since 1984 the development of ESI-MS has demonstrated its importance in the world of biochemical applications and has revolutionized mass spectrometry technology. The groups of Smith[6,35-38], Henion[39-43], Fenn[44, 45], and others[46-49] explored the applicability of an ESI source as an interface for coupling CE and liquid chromatography to mass spectrometry, or ESI-MS alone for analyses of polar, thermally labile compounds and macromolecules. Presently ESI-MS, along with matrix-assisted laser desorption/ionization time of flight mass spectrometry (MALDI-TOF MS), has become an outstanding technique for analyses of small to high molecular weight compounds of all types including pharmaceuticals, peptides, proteins, nucleotides, and synthetic polymers. These two techniques are also utilized for studies of solution chemistries and gas phase chemistries, such as the kinetics and dynamics of inter-/intra-molecular reactions and processes of biologically active species. Other analytical techniques cannot provide the same level of detailed information of molecular weight, structure, and kinetics from extremely small quantities of samples as these two MS techniques can.

Efforts have been aimed towards fundamental studies which will elucidate the mechanism of the electrospray process responsible for the production of gaseous ions of ionic molecules from solution phase. Generally, the ESI process can be classified into four main steps[50]. Under atmospheric pressure, the electric field at the electrospray needle tip charges the emerging liquid, dispersing it by Coulomb forces into a fine spray of large charged droplets, **Figure 1.4**. Driven by the electric field, the charged droplets migrate towards the counter plate. At the same time, the droplets' size decreases while the surface charge density increases due to solvent evaporation. Once the size of the charge droplets

Figure 1.4. A representation of electrospray process in positive ion mode.

The different sized circles represent the different sized charged droplets and ions.

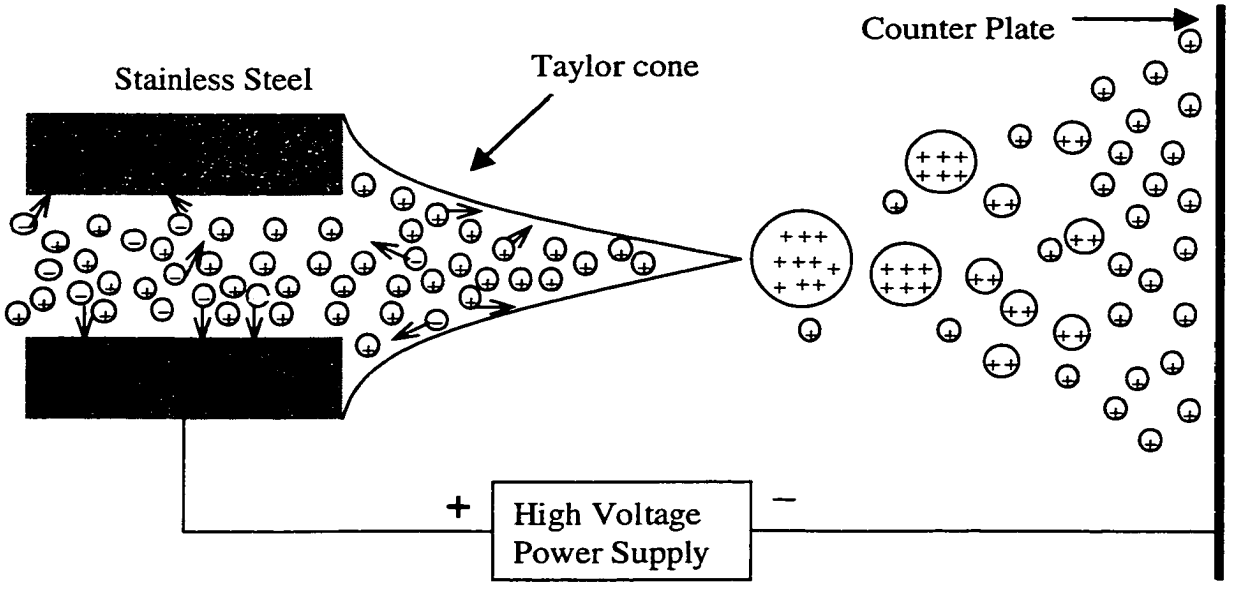

approaches to the Rayleigh limit, "Coulomb explosion" or fission occurs, producing small, highly charged offspring droplets. This process of droplet shrinkage and disintegration repeats, leading ultimately to very small charged-droplets capable of producing gaseous ions. Finally, the gas phase ions are liberated from the droplets. The first two steps are observable[50]. Practicing mass spectrometrists can optimize parameters involved in these steps (e.g., solvent volatility, electric field, temperature, and countercurrent gas flow rate) for the best performance of the electrospray ionization. The mechanism of the gaseous ion production, however, is still not well understood[51]. Investigations of the electrospray plume by different means have been developed in recent years in attempts to model the ion transition from solution-phase to the gas phase[52-55]. Three features of ESI set it apart from other ionization techniques. In addition to the unique characteristic of ESI producing gas phase ions directly from the solution phase, the production of multiply charged ions[45,56,57] and preservation of ion complexes in the gas phase[58,59] are two other distinctive features that enable ESI mass spectrometry to be used in macromolecule analysis and in probing the solution chemistry of biomolecules such as noncovalent interactions[58-61] and conformational structure[62-64].

1.3.1 Production of Charged Droplets

Charging of liquid emerging from the electrospray capillary tip (**Figure 1.4**) under high voltage is a natural phenomenon[50,65]. If the applied potential is sufficiently high, a stable Taylor cone will form, and a fine filament jet from the tip of the cone will appear and break up into small charged droplets[50,66]. The onset potential, V_{on}, applied at the sprayer tip leading to the formation of the charged jet can be expressed as[50]:

$$V_{on} = 2 \times 10^5 (\gamma r_c)^{1/2} \ln(4 d / r_c) \qquad (1.21)$$

where γ is the surface tension of the solvent, r_c is the radius of the electrospray capillary, and d is the distance between the sprayer tip and the planar counter plate. For a given solvent and its surface tension value, the onset potential can be calculated. For instance, the surface tension of methanol and water are 0.023 and 0.073 N/m. Thus the estimated onset potential applied to a 200 μm ID sprayer tip with a distance of 10 mm from the curtain plate are 2.25 kV and 4.05 kV, respectively. The actual potential applied at the sprayer is often adjusted a few hundred volts higher to achieve a stable electrospray operation. However, it has been reported that multi-jet modes will be observed[66] if the potential is too high. Use of water as the solvent can also lead to severe electric discharge from the capillary tip which is more likely to occur in negative ion mode[67,68].

1.3.2 Electrolytic Feature of Electrospray

The generation of charged droplets by the electrospray process involves electrolytic reactions that occur at the metal-solution interface. Redox reactions of some species occur at the counter electrode which complete the electrical circuit. These reactions maintain charge balance in the continuous-current electrospray device[69-72]. According to Kebarle *et al.*[69] the possible oxidation reactions that occur when the sprayer capillary is held at a high positive potential for a methanol solution containing chloride impurities are as follows:

$$2Cl^-_{aq} = Cl_{2,g} + 2e^- \quad (1.22)$$

$$4OH^-_{aq} = O_{2,g} + 2H_2O + 4e^- \quad (1.23)$$

$$2H_2O = O_{2,g} + 4H^+_{aq} + 4e^- \quad (1.24)$$

$$M_s \text{ (capillary metal)} = M_{(aq)}^{n+} + ne \qquad (1.25).$$

In the negative ion mode, possible reactions that might occur include reductions of dissolved oxygen or protons to produce OH^- and H_2. It was shown that the charge balance at the metal-solution interface is dependent on factors including the magnitude of the electric field at the tip and the availability of species at the metal-solution interface (which is related to the capillary dimensions, flow rate, and species concentration)[72,73]. Cook[74] pointed out that some redox reactions of solute species might cause unstable spray and loss of stable current due to the formation of gas products. Van Berkel *et al.*[72,73] have shown that electrospray ionization is actually a controlled-current electrolytic cell. They and others[75-81] have used this feature to provide enhanced detection of otherwise difficult to ionize species.

1.3.3 Electrophoretic Feature of Electrospray

Under the electric field, ions of the same polarity migrate from the bulk of the solution to the Taylor cone tip, while ions of opposite polarity migrate to the capillary wall where the potential is applied. This charge separation process necessitates the continuous formation of charged droplets and the production of gas phase ions drifting to the counter electrode, which is similar to an electrophoretic separation of ions performed in solution. Smith[82] and Hyati *et al.*[83] have reported recognition of the electrophoretic mechanism of electrospray.

1.3.4 Theoretical Prediction of Gas-Phase Ion Formation

Fission and offspring production is observable for droplets with radii over a micrometer[50]. When fission occurs, there are about 20 offspring droplets ejected from the

parent droplet with radii about one-tenth of that of the parent; 2% mass and 15% of the charge of the parent droplet is lost[50,84]. It is assumed that the first generation offspring droplets have about 280 charges and radii of 80 nm; the second generation offspring have 2 charges and radii of 3 nm[51]. Droplets with radii less than a micrometer have not yet been observed and these assumptions have not been verified experimentally[51].

The mechanism of the gas phase ion formation from the last generation offspring droplets has been proposed to occur by two theories: Dole's charged-residue model (CRM)[29,85] and Iribarne-Thomson's ion-evaporation model (IEM)[32,86-88]. In fact, Dole's model was one of the earliest efforts to predict the formation of multiply-charged macromolecular ions upon solvent evaporation. According to Dole, Coulomb fission of charged droplets occurs repeatedly until each offspring droplet contains only one solute molecule. The analyte in the droplet becomes a gas-phase ion by retaining some of droplet charge after all of the solvent has evaporated. As stated by Fenn *et al.*[89,90] and Kebarle[51], Dole's CRM seems to be a natural mechanism for large molecules. The increasing charge/mass ratios of the offspring droplets likely yield multiple charged ions.

The Iribarne-Thomson model predicts that after certain generations of fission, ions can be evaporated from the highly charged droplets. The rate constant, k_I, of ion evaporation could be expressed as:

$$k_I = (k\,T / h)\, e^{-(\Delta G / R\,T')} \qquad (1.26)$$

where k is the Boltzmann constant, T' is the temperature of the droplet, h is Planck's constant, ΔG is the free energy of activation, and R is the gas constant. The rate constant can also be determined from experimental results[50]. Qualitative agreement has been reached with this theoretical description, as ions predicted to have the highest rate

constants for desorption were indeed observed to appear in the highest abundance in the ESI mass spectra[50]. For a binary mixture, the signal intensity of a given singly-charged analyte (A^+) in the presence of a competing singly-charged species (B^+) has been described[50] as:

$$I_{A+} = p\, f\, k_{A+}\, [A^+]\, I_{total} / (k_{A+}\, [A^+] + k_{B+}\, [B^+]) \qquad (1.27)$$

where I_{A+} is the ion current of analyte A^+ detected by the mass spectrometer, p is a constant expressing the sampling efficiency of the mass spectrometer, f is the fraction of droplet charge converted to gas phase ions, $[A^+]$ and $[B^+]$ are the electrolyte concentrations initially present in the electrosprayed solution, I_{total} is the total ion current produced by ESI, and k_{A+} and k_{B+} are the rate constants expressing the rate of transfer of the respective ions from charged droplets to the gas phase. Equation 1.27 describes the factors that influence the ion intensity of a specified analyte in solution. A series of experimental results has shown support for the ion evaporation theory[50,51]. However, as discussed by Kebarle[51], neither CRM nor IEM has achieved unanimous acceptance.

1.4 ON-LINE CE-MS CONSIDERATIONS

As shown in **Figure 1.1**, there have been nearly 400 papers published on CE-MS since its inception. In fact, most of the publications describe the development of the technique itself. Only a small portion deal with method development and applications capable of widespread, routine use. The main reason for this trend might be the presence of several difficulties encountered in employing the CE-MS technology that have not yet been solved. For instance, on-column detection using UV/Vis absorption is straightforward; the detection end of the capillary can simply be placed in a buffer reservoir containing an electrode. For MS detection, however, an electrical connection of

another kind has to be developed. A robust interface is crucial for stable and sensitive CE-MS operation and is still a controversial topic. Other issues are related to the optimization of CE separations for real-sample applications of various kinds, and the choice of a mass analyzer for fast and efficient sampling and data acquisition.

1.4.1 Ion Source

An immediate consideration in CE-MS coupling is the type of ion source to use. The first CE-MS paper in 1987 by Smith's group presented the use of an electrospray interface[6]. In that report, a metal coating on the CE column end made contact with a metal capillary to which the electrospray voltage was applied. The following year, the same group presented another paper using the metal capillary as the sheath liquid transporter. The electrical contact for the CE circuit and the ESI emitter was maintained by the sheath liquid[38]. Also in 1988 Henion's group reported a liquid junction interface that successfully coupled CE to a pneumatically assisted electrospray (also called ion spray) MS[41]. Ion spray was introduced by the same group for high flow rate LC-MS[91]. In 1989, CE-MS employing continuous-flow fast-atom bombardment (CF-FAB) sources were reported employing either a liquid junction[92] or a co-axial sheath[93] interface. Since then, CE-ESI-MS and CE-CF-FAB-MS have gained the same attention. Experimental results had indicate that the ESI source has numerous advantages over CF-FAB[94,95], and after 1995, no searchable publications on CE-MS have mentioned the CF-FAB ion source. In addition to ESI and CF-FAB, the use of an atmospheric-pressure chemical ionization (APCI) source[96,97] for on-line coupling of CE-MS, MALDI sources as off-line complements to ESI-MS[98-100] or pseudo-on-line interfaces for CE-MS studies[101], have also been reported. It is interesting to note that CE coupled to inductively coupled plasma (ICP)-MS has recently been an increasingly important topic for metal speciation[102-104].

Chip-based electrophoretic separations coupled to ESI-MS has been reported in recent years[105,106]. However, these techniques share the same categories of ESI interfaces that have been successfully utilized in CE-MS. A notable direction is the development of multiple ESI sprayer coupled to CE or chip-based separations for high throughput analysis.

1.4.2 ESI Interface

Ideally, the interface should maintain the separation efficiency and resolution of CE, be sensitive, precise and linear in response, maintain electrical continuity with the separation capillary, cope with all eluents present in CE, and provide efficient ionization from low flow rates for mass analysis. Until recently, coupling of CZE with MS has relied on coaxial, liquid-junction and sheathless interfaces that were developed a decade ago. Most sheathless interfaces utilize a metalized emitter made of a CE column and a layer of metal coating such as silver[6] or gold[107-109]. The metal coating maintains the electrical contacts for CE and ESI operation, and the tapered tip increases the electric field for electrospray[110]. However, the coatings are not stable. Methods have been developed for improved coating endurance[111-113]. Other approaches are more complicated and delicate for example, inserting a metal electrode inside the outlet of the CE capillary[114,115], **Figure 1.5**. The sheathless interface is generally the simplest for coupling CE to MS, leading to a high ionization efficiency and low mass limits of detection since analytes are not diluted and no additional chemicals (and thus noise) are introduced. However, there are several issues which should be considered carefully when employing the sheathless interface. The tip usually has a short lifetime due to clogging and because the coatings can be easily damaged by the high electric potential. The tip size is critical to maintain a stable electrospray and a sufficient electroosmotic flow. Since the tip is part of the separation

Figure 1.5 Schematic of interfaces for CE-MS.

(A) Gold-coated sheathless interface. (B) Electrode direct-inserted sheathless interface. (C) Liquid junction interface. (D) Sheath flow interface.

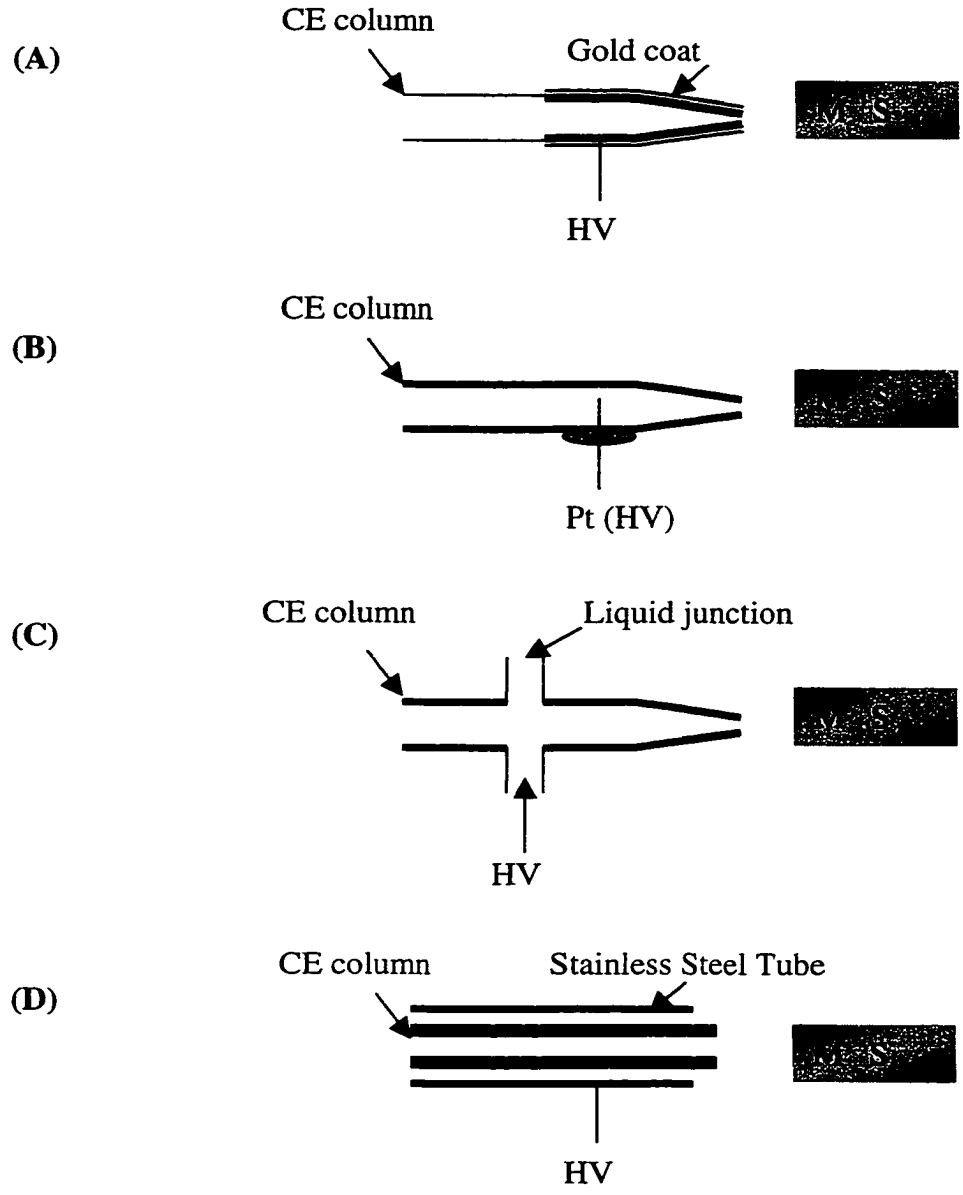

capillary, modification to the tip (e.g. coating and tapering) requires special attention, especially for inner-coated capillaries. The most significant disadvantage of the sheathless design is the limited choice of buffers for CE separations. A crucial point is that CE flow rates are generally much less than those desired for ESI. The ESI response is fully dependent upon the CE buffers which are often substantially conductive and thus generate unstable electrospray. Further, the sensitivity is not comparable among buffers used for different separation systems.

A sheath flow interface normally utilizes a co-axial configuration, **Figure 1.5D**. To date it has been the most commonly employed method for CE-MS coupling. In this arrangement, the CE column is inserted into a narrow metal tube which delivers a sheath liquid to the column exit. As the liquid flows from the tube, it mixes with the column effluent and completes the circuits for CE and electrospray. A sheath liquid, such as methanol, is chosen for its excellent electrospray characteristics and to overcome the volatility and conductivity problems of a CE buffer that usually has poor electrospray capability. The sheath liquid is supplied at a higher flow rate than EOF; the ESI process is mainly dominated by the sheath liquid. The result is that a wide range of CE buffer compositions and solvents can be effectively addressed, though with some constraints owing to background signals from buffer components or sheath liquid. Another advantage is that with the help of the sheath flow, gas bubbles generated by the electrolytic action of electrospray are not detrimental to the separation process. The main problem with this interface is the dilution of analyte caused by the sheath. Also, in some applications, the small magnitude of EOF may affect the electrical contact. When the EOF is minimal, a hydrodynamic flow through the CE capillary introduced by either raising the injection end for a few centimeters or applying a small constant pressure may aid electrical contact while incurring minimal degradation of the CE separation. Effects of

sheath liquid composition on CE resolution and migration variations have also been reported[116].

As shown in **Figure 1.5C**, in a liquid junction interface, electrical contact is established through a liquid reservoir perpendicularly intersecting with the separation capillary and a transfer capillary. The intersection is approximately ten to twenty micrometers, adjusted with the help of a microscope. The make-up flow is maintained by a combination of gravity and the electrospray suction force at the tip. The introduction of the make-up liquid has similar dilution features previously mentioned for sheath flow interfaces. With the use of the liquid junction interface, impaired sensitivity and separation efficiency has been reported, and the operation of the coupling analyses is labor intensive[117].

1.4.3 CE Modes and Buffer Compatibility

Addition of any ionic species to the solution, other than the analyte or small amounts of acids or bases assisting in the ionization of analyte, is usually avoided when possible. The presence of these 'excess' ionic species causes suppression of gas phase ion production of the analyte molecules[118,119]. As demonstrated by Equation 1.27, compounds which have surface active properties, detergents for instance, give the highest response with ESI. Surface active compounds can also be the most effective at suppressing the ionization of other less surface active molecules, presumably by shielding the droplet exterior. Bearing this consideration in mind, one can understand that the direct coupling of MEKC to ESI-MS is unlikely to be successful[120]. MEKC is a mode of CE in which micelles are used as a pseudo-stationary phase for neutral and ionic analyte separation. The presence of micelle forming agents such as sodium dodecylsulfate (SDS) causes suppression of any other analyte ion signals when coupled to ESI-MS. Novel approaches

have been reported on MEKC-ESI-MS utilizing a partial filling technique[121], employing an anionic surfactant that does not migrate to the ion source[122], or by inserting a CZE capillary between the MEKC and the ion source for surfactant removal in combination with voltage switching[123].

CIEF is a highly efficient separation technique for complex protein mixtures. Proteins with different pIs are separated in a pH gradient which is formed by ampholytes in an electric field. On-line coupling of CIEF with ESI-MS has been demonstrated by several groups[124-129]. The focusing effect of CIEF permits analysis of very dilute protein samples. A typical concentration factor of 50-100 times has been observed for analytes with concentrations on the order of 10^{-7} M[124]. The presence of ampholytes, however, not only causes a marked reduction in the protein peak intensity but also results in a decrease of the net charge of protein ions in the mass spectra compared to the average charge state measured in the absence of ampholytes[124,127]. An interesting solution to solve the interference of the ampholytes has been reported recently, employing an on-line coupled microdialysis device[125,126] or an integrated microfabricated device[128] for dual microdialysis for rapid fractionation and cleanup of complex biological mixtures.

Capillary gel electrophoresis has been successfully coupled to ESI-MS[130,131]. Up to now, the application of this coupling has been limited by difficulties surrounding the use of buffers containing high concentrations of surfactants and involatile salts. CITP and transient CITP-ESI-MS have also been demonstrated for analysis of peptides[38] and nucleotides[132]. These techniques are far more popular in sample preconcentration for enhanced sample volume injection and concentration limits of detection[133-134]. Several groups have reported coupling of CEC with ESI-MS[135-137]. CEC is a hybrid technique of CE and capillary HPLC, and is of significant importance in analyzing neutral and

nonpolar species. Due to technical and operational difficulties, such as the application of a constant or gradient pressure to the packed column, and gas bubbles' production during CEC which will affect the electrospray process, this coupling technique is still in its infancy. The most successful coupling technique has been CZE-ESI-MS for small and large molecule analyses[138].

1.5 MASS SPECTROMETER

The small solute quantities and the high separation efficiency in CE, with peak widths of only a few seconds or less, presents challenges for most mass spectrometers in terms of sensitive and fast detection. Although virtually all types of mass spectrometers have been coupled to CE with an electrospray interface, most ESI-MS instruments to date are based on quadrupole mass spectrometers. Optimization of quadrupole mass analyzers, however, requires a good understanding of the trade-offs between scan speed, resolution, mass range, and sensitivity. With quadrupole mass spectrometers, the greatest limitation occurs with the practical scan speeds. The use of full-scan detection often results in either limited ion intensities owing to extremely short dwell times at each mass, or too few scans obtained during the CE peak elution. Another limitation of the present ESI-MS instrumentation based on quadrupole analyzers is associated with the small openings of the sampling orifice, which results in only a small fraction of the total ESI ion current being introduced into the spectrometer. An overall sampling efficiency of approximately 0.01% of the ESI current has been reported utilizing the popular ESI-MS ion source and ion optics designs[139]. Thus, ESI quadrupole MS detection requires careful consideration of the experiment and the necessary compromises, such as using a lower resolution and narrowed mass range for a higher ion intensity signal. The situation is much more severe

for tandem MS/MS using triple quadrupole instrumentation, owing to the much lower ion current which exists after collisional dissociation.

These limitations are a major driving force for the implementation of improved MS instrumentation using array detectors[140,141] or ion-trap analyzers[142-145], and more recently, time of flight (TOF) analyzers[109,146-148] or quadrupole time of flight analyzers (Q-TOF)[149,150]. Since TOF MS has unlimited mass range, moderate resolution ($M/\Delta M_{FWHM}$ up to 10,000), fast response, and the ability to record all ions simultaneously without scanning, the coupling of CE with TOF-MS via an ESI interface offers superior advantages to coupling techniques employing other mass analyzers. A comparison of the on-line detection utilizing a quadrupole and a TOF mass analyzer for CE separations has exhibited tremendous differences between the two techniques in maintaining the high separation efficiency of CE[151]. The novel QTOF and quadrupole-quadrupole time of flight (QqTOF) MS offer good MS resolution, mass accuracy and MS/MS capabilities, and these mass analyzers will certainly play important roles in on-line coupled analyses with CE.

The combination of CE-ESI with Fourier-transform ion-cyclotron resonance (FTICR) MS provides high accuracy mass measurements and extremely high resolving powers[127,152-155], over 10^5. The major disadvantage for on-line separations is the relatively slow spectral acquisition speed and, of course, the high instrument prices.

1.6 THESIS OVERVIEW

The material presented in the thesis covers three categories which in many ways parallel the areas of continuing growth of the coupling technique of capillary electrophoresis-electrospray mass spectrometry: methodology, instrumentation, and

associated chemistries in the solution phase and the gas phase. The thesis (**Chapter 2**) begins with a detailed investigation of a nonaqueous capillary electrophoresis for separation of structurally similar tricyclic antidepressants and on-line detection by a quadrupole mass spectrometer via an ion spray interface as shown in **Figure 1.6**. Factors affecting the CE separation efficiency, resolution, injections, and the ESI-MS detection stability and sensitivity are investigated. Applications of the established methods are demonstrated in metabolism studies of amitriptyline by *Cunninghamella elegans*. **Chapter 3** presents a complete methodology developed for analysis of antiretroviral nucleosides and nucleotides. Although there are hundreds of publications on CE-MS in existence, few have explored and compared the capabilities of ESI-MS detection with positive and negative ion modes for the same analytes. The work presented in Chapter 3 summarizes the efforts of separating and detecting both nucleosides and nucleotides, which have distinctive solution-phase and gas-phase properties, in the same run. Applications of the analytical protocol for detection of endogenous nucleotides in a cell extract, and for characterization of intracelluar metabolism of a commonly used anti-HIV drug, 3TC, are described. **Chapter 4** demonstrates studies of a microspray MS and the on-line CE-MS analyses of oligosaccharides. Successful application of CE-MS for carbohydrate analysis requires careful control of sample and CE separation parameters. How these factors affect the quality of resolution is discussed in this chapter.

Femtomole detection limits can be attained although this often requires concentrated samples, usually in the micromolar range. An effective way to increase the concentration sensitivity, sample stacking, is described and results are discussed in **Chapter 2**. Another approach to obtaining high sensitivity in CE-MS analysis is to employ an improved electrospray interface. **Chapter 5** presents a novel sheath flow electrospray interface for

Figure 1.6 Schematic representation of CE-MS set-up used in this thesis.

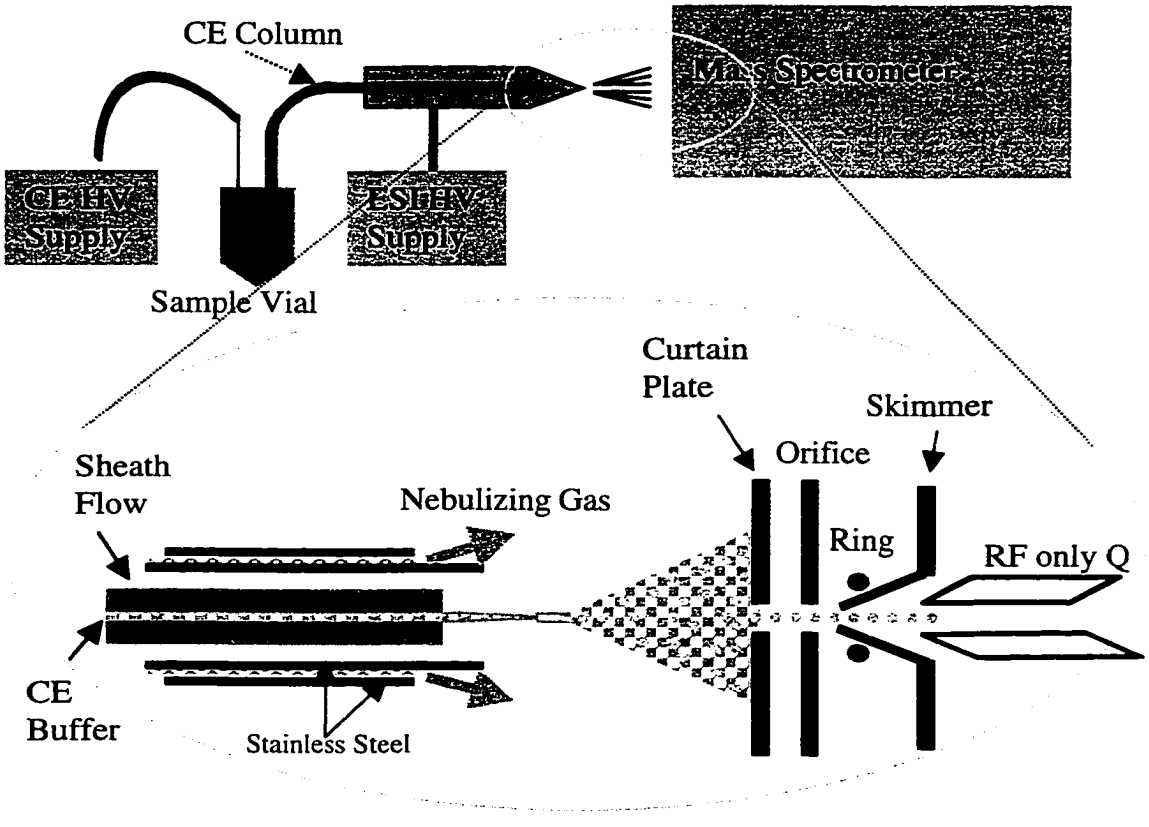

low flow rate operation. A regular sheath flow electrospray device is normally constructed from approximately 0.4 mm OD, 0.2 mm ID stainless steel tubing to which a fused silica CE column is inserted concentrically. Stability at low electroosmotic flow generated by CE and sensitivity in ESI-MS detection require a miniaturized version of the sprayer having both narrower inside and outside diameters. Metalized sheath tubing for this purpose is difficult to fabricate. Instead a fused silica capillary tapered on the outside forming a small opening is employed. Electrical contact with the liquid stream made by the application of a sheath liquid and by the deposition of gold on the outer surface of the CE capillary at the detection end. The improved performance of this interface design is evaluated and a sensitivity comparison with a conventional interfacing design is presented. A discussion of the advantages and disadvantages of sheath liquid and sheathless interfaces for CE-MS coupling is also presented in this chapter.

Before and during mass analysis, gaseous ions produced by ESI experience secondary processes in the sub-atmospheric pressure sampling regions of the mass spectrometer. These secondary processes include the complexation, protonation, deprotonation, and fragmentation of the gas phase ions. The details of these modifications are not well understood and their implications are still of interest to many researchers. The remainder of the thesis, **Chapter 6 and 7**, focuses on the presentation and implementation of some inherent processes in the ion source. **Chapter 6** is devoted to developing an understanding of the factors which determine the appearance of the distribution of charge states (specifically doubly-charged and singly-charged ions) of small peptides observed in the electrospray mass spectra. The effects of specific operating conditions on doubly charged peptide ion formation and variation in the gas-phase are examined. **Chapter 7** presents results related to the underlying processes of the formation of cluster ions of nucleosides that appeared in the electrospray mass spectra. In any design

of an electrospray mass spectrometer, the formation of solvated-(cluster) ions is addressed. Procedures have been taken into consideration with respect to hardware designs of a mass spectrometer to prevent the clustering (for instance with the use of a counter-current nebulizing gas). Self-complexation of analytes in mass spectra, however, is still a noteworthy phenomenon by which some intrinsic properties of gas phase chemistry such as proton affinity and origin of noncovalent interaction of biomolecules in the solution phase and the gas phase may be determined. A discussion concerning the cluster ion formation as a function of analyte concentration and collisional activation is provided.

1.7 BIBLIOGRAPHY

(1) Jorgenson, J.W.; Lukacs, K.D. *J. Chromatogr.* **1981**, *218*, 209-216.

(2) Jorgenson, J.W.; Lukacs, K.D. *Anal. Chem.* **1981**, *53*, 1298-1302.

(3) Zhang, J.Z.; Voss, K.O.; Shaw, D.F.; Roos, K.P.; Lewis, D.F.; Yan, J.; Jiang, R.; Ren, H.; Hou, J.Y.; Fang, Y.; Puyang, X.; Ahmadzadeh, H.; Dovichi, N.J. *Nucleic Acids Research* **1999**, *27*, E36.

(4) Krylov, S.N.; Dovichi, N.J. *Anal. Chem.* **2000**, *72*, 111-128.

(5) Nishi, H. *Electrophoresis* **1999**, *20*, 3237-3258.

(6) Olivares, J.A.; Nguyen, N.T.; Yonker, C.R.; Smith, R.D. *Anal. Chem.* **1987**, *59*, 1230-1232.

(7) Cole, R.B., Editor, *Electrospray Ionization Mass Spectrometry* **1997**, John Wiley & Sons, Inc., New York.

(8) Moseley, M. A.; Deterding, L. J.; Tomer, K. B.; Jorgenson, J. W. *Rapid Commun. Mass Spectrom.* **1989**, *3*, 87-93.

(9) Caprioli, R. M.; Moore, W. T.; Martin, M.; DaGue, B. B.; Wilson, K.; Moring, S. *J. Chromatogr.* **1989**, *480*, 247-257.

(10) Moseley, M. A.; Deterding, L. J.; Tomer, K. B.; Jorgenson, J. W. *J. Chromatogr.* **1989**, *480*, 197-209.

(11) Sparkman, O.D. *J. Am. Soc. Mass Spectrom.* **2000**, *11*, 472-480.

(12) Landers, J.P. *Handbook of Capillary Electrohphoresis,* 2nd Ed., CRC Press Inc., Boca Raton, **1997**.

(13) Mikkers, F.E.P.; Everaerts, F.M.; Verheggen, T. *J. Chromatogr.* **1979**, *169*, 11-20.

(14) Jorgenson, J.W.; Lukacs, K.D. *Science* **1983**, *222*, 266-272.

(15) Krylov, S.N.; Zhang, Z.; Chan, N.W.C.; Arriaga, E.; Palcic, M.M.; Dovichi, N.J. *Cytometry* **1999**, *37*, 14-20.

(16) Pretorius, V.; Hopkins, B.J.; Schieke, J.D. *J. Chromatogr.* **1974**, *99*, 23-30.

(17) Cantwell, F.F. *Separation Sciences-Chemistry 421 Textbook,* **1996**, *Chapter 15,* pp3.

(18) Stevens, T.S.; Cortes, H.J. *Anal. Chem.* **1983**, *55*, 1365-1370.

(19) McCormik, R.M. *Anal. Chem.* **1988**, *60*, 2322-2328.

(20) Lauer, H.; McManigill, D. *Trends in Anal. Chem.* **1986**, *5*, 11-15.

(21) Zhao, Z.; Malik, A.; Lee, M.L. *Anal. Chem.* **1993**, *65*, 2747-2752.

(22) Hjerten, S.; Kubo, K. *Electrophoresis* **1993**, *14*, 390-395.

(23) Schomburg, G.; Belder, D.; Gilges, M.; Motsch, S. *J. Cap. Electrophor.* **1994**, *1*, 219-230.

(24) Albin, M.; Weinberger, R.; Sapp, E.; Moring, S. *Anal. Chem.* **1991**, *63*, 417-422.

(25) Davis, K.L.; Liu, K.L.; Lanan, M.; Morris, M.D. *Anal. Chem.* **1993**, *65*, 293-298.

(26) Heiger, D.N. *Higher Performance Capillary Electrophoresis-An Introduction,* 2nd Ed., **1992**, Hewlett-Packard, pp 28-33.

(27) Huang, X.; Gordon, M. J.; Zare, R.N. *J. Chromatogr.* **1989**, *480*, 285-288.

(28) Hutterer, K. M.; Jorgenson, J. W. Anal. Chem. **1999**, 71, 1293-1297.

(29) Dole, M.; Mack, L.L.; Hines, R.L.; Mobley, R.C.; Ferguson, L.D.; Alice, M.B. *J. Chem. Phys.* **1968**, *49*, 2240-2249.

(30) Mack, L.L.; Kralik, P.; Rheude, A.; Dole, M. *J. Chem. Phys.* **1970**, *52*, 4977-4986.

(31) Teer, D.; Dole, M. *J. Polymer Sci.* **1975**, *13*, 985-995.

(32) Thomson, B.A.; Iribarne, J.V. *J. Chem. Phys.* **1979**, *71*, 4451-4463.

(33) Yamashita, M. Fenn, J.B. *J. Phys. Chem.* **1984**, *88*, 4451-4459.

(34) Yamashita, M. Fenn. J.B. *J. Phys. Chem.* **1984**, *88*, 4671-4675.

(35) Smith, R.D.; Olivares, J.A.; Nguyen, N.T.; Udseth, H.R. *Anal. Chem.* **1988**, *60*, 436-441.

(36) Smith, R.D.; Barinaga, C.J.; Udseth, H.R. *Anal. Chem.* **1988**, *60*, 1948-1952.

(37) Loo, J.A.; Udseth, H.R.; Smith, R.D. *Anal. Biochem.* **1989**, *179*, 404-412.

(38) Smith, R.D.; Loo, J.A.; Barinaga, C.J.; Edmonds, C.G.; Udseth, H.R. *J. Chromatogr.* **1989**, *480*, 211-232.

(39) Bruins, A. P.; Covey, T. R.; Henion, J. D. *Anal. Chem.* **1987**, *59*, 2642-2646.

(40) Bruins, A. P.; Weidolf, L. O. G.; Henion, J. D.; Budde, W. L. *Anal. Chem.* **1987**, *59*, 2647-2652.

(41) Lee, E.D.; Mueck, W.; Henion, J.D.; Covey, T.R. *J. Chromatogr.* **1988**, *458*, 313-321.

(42) Covey, T. R.; Bruins, A. P.; Henion, J. D. *Org. Mass Spectrom.* **1988**, *23*, 178-186.

(43) Lee, E. D.; Henion, J. D.; Covey, T. R. *J. Microcolumn Sep.* **1989**, *1*, 14-18.

(44) Whitehouse, C. M.; Dreyer, R. N.; Yamashita, M.; Fenn, J. B. *Anal. Chem.* **1985**, *57*, 675-679.

(45) Fenn, J.B.; Mann, M.; Meng, C.K.; Whitehouse, C.M. *Science* **1989**, *246*, 64-71.

(46) Siu, K.; Gardner, G.J.; Berman, S.S. *Rapid Commun. Mass Spectrom.* **1988**, *2*, 69-71.

(47) Shumate, C.B.; Hill, H.H., Jr. *Anal. Chem.* **1989**, *61*, 601-606.

(48) Henry, K.D.; Williams, E.R.; Wang, B.H.; McLafferty, F.W.; Shabanowitz, J.; Hunt, D,F. *Proc. Nat. Acad. Sci. USA.* **1989**, *86*, 9075-9078.

(49) Hallen, R.W.; Shumate, C.B.; Siems, W.F.; Tsuda, T.; Hill, H.H., Jr. *J. Chromatogr.* **1989**, *480*, 233-245.

(50) Kebarle, P.; Tang, L. *Anal. Chem.* **1993**, *65*, 972A-986A.

(51) Kebarle, P.; Ho, Y. Editor: Cole, R.B. *Electrospray Ionization Mass Spectrometry* **1997**, John Wiley & Sons, New York, pp 3-63.

(52) Kiselev, P.; Rosell, J.; Fenn, J.B. *Ind. Eng. Chem. Res.* **1997**, *36*, 3081-3084.

(53) Chillier, X.F.D.; Monnier, A.; Bill, H.; Gulacar, F.O.; Buchs, A.; McLuckey, S.A.; Van Berkel, G.J. *Rapid Commun. Mass Spectrom.* **1996**, *10*, 299-304.

(54) Zhou, S.L.; Edwards, A.G.; Cook, K.D.; Van Berkel, G.J. *Anal. Chem.* **1999**, *71*, 769-776.

(55) Zhou, S.L.; Cook, K.D. *Anal. Chem.* **2000**, *72*, 963-969.

(56) Siu, K.; Gardner, G.J.; Berman, S.S. *Org. Mass Spectrom.* **1989**, *24*, 931-942.

(57) Le Blanc, J.Y.C.; Wang, J.; Guevremont, R.; Siu, K. *Org. Mass Spectrom.* **1992**, *29*, 587-593.

(58) Aplin, R.T.; Robinson, C.V.; Schofield, C.J.; Westwood, N.J. *J. Chem. Soc., Chem. Commun.* **1994**, *20*, 2415-2417.

(59) Smith, R.D.; Wahl, K.J.; Winger, B.E.; Loo, J.A. *Org. Mass Spectrom.* **1992**, *27*, 811-821.

(60) Bruce, J.E.; Smith, V.F.; Liu, C.; Randall, L.L.; Smith, R.D. *Protein Sci.* **1998**, *7*, 1180-1185.

(61) Veenstra, T.D. *Biochem. & Biophys. Res. Commun.* **1999**, *257*, 1-5.

(62) Winger, B.E.; Wahl, K.J.; Rockwood, A.J.; Smith, R.D. *J. Am. Chem. Soc.* **1992**, *114*, 5897-5898.

(63) Lee, V.W.; Chen Y.L.; Konermann, L. *Anal. Chem.* **1999**, *71*, 4154-4159.

(64) Bouchard, M.; Benjamin. D.R.; Tito, P.; Robinson, C.V.; Dobson, C.M. *Biophys. J.* **2000**, *78*, 1010-1017.

(65) Hager, D.B.; Dovichi, N.J.; Klassen, J.; Kebarle, P. *Anal. Chem.* **1994**, *66*, 3944-3949.

(66) Cloupeau, M.; Prunet-Foch, B. *J. Aerosol Sci.* **1994**, *25*, 1021-1036.

(67) Ikonomou, M.G.; Blades, A.T.; Kebarle, P. *J. Am. Soc. Mass Spectrom.* **1991**, *2*, 497-503.

(68) Wampler, F.W.; Blades, A.T.; Kebarle, P. *J. Am. Soc. Mass Spectrom.* **1993**, *4*, 289-295.

(69) Blades, A.T.; Ikonomou, M.G.; Kebarle, P. *Anal. Chem.* **1991**, *63*, 2109-2114.

(70) Van Berkel, G.J.; McLuckey, S.A.; Glish, G.L. *Anal. Chem.* **1992**, *64*, 1586-1593.

(71) Xu, X.; Nolan, S.P.; Cole, R.B. *Anal. Chem.* **1994**, *66*, 119-125.

(72) van Berkel, G.J.; Zhou, F. *Anal. Chem.* **1995**, *67*, 2916-2923.

(73) van Berkel, G.J.; Zhou, F. *Anal. Chem.* **1995**, *67*, 3958-3964.

(74) Cook, K.D. *Mass Spectrom. Rev.* **1986**, *5*, 467-519.

(75) Hop, C.; Saulys, D.A.; Gaines, D.F. *J. Am. Soc. Mass Spectrom.* **1995**, *6*, 860-866.

(76) Bond, A.M.; Colton, R.; D'Agostino, A.; Downard, A.J.; Traeger, J.C. *Anal. Chem.* **1995**, *67*, 1691-1695.

(77) Zhou, J.; Hefta, S.; Lee, T.D. *J. Am. Mass Spectrom.* **1997**, *8*, 1165-1174.

(78) van Berkel, G. J.; Quirke, J. M. E.; Tigani, R. A.; Dilley, A. S.; Covey, T. R. *Anal. Chem.* **1998**, *70*, 1544-1554.

(79) Bateman, K.P. *J. Am. Soc. Mass Spectrom.* **1999**, *10*, 309-317.

(80) Wang, H. J.; Agnes, G. R. *Anal. Chem.* **1999**, *71*, 4166-4172.

(81) Deng, H. T.; van Berkel, G. J. *Anal. Chem.* **1999**, *71*, 4284-4293.

(82) Smith, D.P.H. *IEEE Trans. Ind. Appl.* **1986**, *IA-22*, 527-535.

(83) Hayati, I.; Bailey, A.I.; Tadros, T.F. *J. Colloid Interface Sci.* **1987**, *117*, 205-221.

(84) Gomez, A.; Tang, K. *Phys. Fluids* **1994**, *6*, 404-409.

(85) Dole, M.; Hines, R.L.; Mack, L.L.; Mobley, R.C.; Ferguson, L.D.; Alice, M.B. *Macromolec.* **1968**, *1*, 96-97.

(86) Iribarne, J.V.; Thomson, B.A. *J. Chem. Phys.* **1976**, *64*, 2287-2294.

(87) Thomson, B.A.; Iribarne, J.V.; Dziedzic, P.J. *Anal. Chem.* **1982**, *54*, 2219-2224.

(88) Iribarne, J.V.; Dziedzic, P.J.; Thomson, B.A. *Int. J. Mass Spectrom. Ion Phys.* **1983**, *50*, 331-334.

(89) Fenn, J.B.; Mann, M.; Meng, C.K.; Wong, S.K.; Whitehouse, C.M. *Mass Spectrom. Rev.* **1990**, 9, 37-70.

(90) Fenn, J.B. *J. Am. Soc. Mass Spectrom.* **1993**, *4*, 524-535.

(91) Bruins, A.P.; Covey, T.R.; Henion, J.D. *Anal. Chem.* **1987**, *59*, 2642-2646.

(92) Caprioli, R.M.; Moore, W.T.; Martin, M.; DaGue, B.B.; Wilson, K.; Moring, S. *J. Chromatogr.* **1989**, *480*, 247-257.

(93) Moseley, M.A.; Deterding, L.J.; Tomer, K.B.; Jorgenson, J.W. *J. Chromatogr.* **1989**, *480*, 197-209.

(94) Deterding, L.J. Parker, C.E.; Perkins, J.R.; Moseley, M.A.; Jorgenson, J.W.; Tomer, K.B. *J. Chromatogr.* **1991**, *554*, 329-338.

(95) Nichols, W.; Zweigenbaum, J.; Garcia, F.; Johansson, M.; Henion, J.D. *LC-GC* **1992**, *10*, 676-686.

(96) Andrien, B.A.; Boyle, J.G. *Spectroscopy* **1995**, *10*, 42-44.

(97) Takada, Y.; Sakairi, M.; Koizumi, H. *Anal. Chem.* **1995**, *67*, 1474-1476.

(98) Castoro, J.A.; Chiu, R.W.; Monnig, C.A.; Wilkins, C.L. *J. Am. Chem. Soc.* **1992**, *114*, 7571-7576.

(99) Apffel, A.; Chakel, J.; Udiavar, S.; Hancock, W. S.; Souders, C.; Pungor, E., Jr. *J. Chromatogr. A,* **1995**, *717*, 41-60.

(100) Cruz, L.; Garden, R. W.; Kaiser, H. J.; Sweedler, J. V. *J. Chromatogr. A,* **1996** , *735*, 375-385.

(101) Preisler, J.; Foret, F.; Karger, B. L. *Anal. Chem.* **1998**, *70*, 5278-5277.

(102) Olesik, J.W.; Kinzer, J.A.; Olesik, S.V. *Anal. Chem.* **1995**, *67*, 1-12.

(103) Liu, Y.; Lopez-Avila, V.; Zhu, J.J.; Wiederin, D.R.; Beckert, W.F. *Anal. Chem.* **1995**, *67*, 2020-2025.

(104) Silva da Rocha, M.; Soldado, A.B.; Blanco-Gonalez, E.; Sanz-Medel, A. *J. Anal. Atomic Spectrom.* **2000**, *15*, 513-518.

(105) Li, J.; Thibault, P.; Bings, N.H.; Skinner, C.D.; Wang, C.; Colyer, C.; Harrison, J.D. *Anal. Chem.* **1999**, *71*, 3036-3045.

(106) Zhang, B.; Liu, H.; Karger, B.L.; Foret, F. *Anal. Chem.* **1999**, *71*, 3258-3264.

(107) Kriger, M.S.; Cook, K.D.; Ramsey, R.S. *Anal. Chem.* **1995**, *67*, 385-389.

(108) Hofstadler, S.A.; Severs, J.C.; Smith, R.D.; Swanek, F.D.; Ewing, A.G. *Rapid Commun. Mass Spectrom.* **1996**, *10*, 919-921.

(109) McComb, M.E.; Krutchinsky, A.N.; Ens, W.; Standing, K.G.; Perreault, H. *J. Chromatogr. A,* **1998**, *800*, 1-11.

(110) Chowdhury, S.K.; Chait, B.T. *Anal. Chem.* **1991**, *63*, 1660-1664.

(111) Wahl, J.H.; Smith, R.D. *J. Cap. Electrophor.* **1994**, *136*, 167-171.

(112) Kelly, J.F.; Ramaley, L.; Thibault, P.; *Anal. Chem.* **1997**, *69*, 51-60.

(113) Barnidge, D.R.; Nilsson, S.; Markides, K.E. *Anal. Chem.* **1999**, *71*, 4115-4118.

(114) Fang, L.; Zhang, R.; Williams, E.R.; Zare, R.N. *Anal. Chem.* **1994**, *66*, 3696-3701.

(115) Cao, P.; Moini, M. *J. Am. Soc. Mass Spectrom.* **1997**, *8*, 561-564.

(116) Foret, F.; Thompson, T.J.; Vouros, P.; Karger, B.L.; Gebauer, P.; Bocek, P. *Anal. Chem.* **1994**, *66*, 4450-4458.

(117) Pleasance, S.; Thibault, P.; Kelly, J. *J. Chromatogr.* **1992**, *591*, 325-339.

(118) Tang, L. and Kebarle, P. *Anal. Chem.* **1991**, *63*, 2709-2715.

(119) Tang, L. and Kebarle, P. *Anal. Chem.* **1993**, ***65***, 3654-3668.

(120) Ozaki, H.; Ito, N.; Terabe, S.; Takada, Y.; Sakairi, M.; Koizumi, H. *J. Chromatogr. A.* **1995**, *716*, 69-79.

(121) Wiedmer, S.K.; Jussila, M.; Riekkola, M.L. *Electrophoresis* **1998**, *19*, 1711-1718.

(122) Lu, W.; Shamsi, S.A.; McCarley, T.D.; Warner, I.M. *Electrophoresis* **1998**, *19*, 2193-2199.

(123) Lamoree, M.H.; Tjaden, U.R.; van der Greef, J. *J. Chromatogr. A.* **1995**, *712*, 219-225.

(124) Tang, Q.; Harrata, K.; Lee, C.S. *Anal. Chem.* **1995**, *67*, 3515-3519.

(125) Lamoree, M.H.; Tjaden, U.R.; van der Greef, J. *J. Chromatogr. A.* **1997**, *777*, 31-39.

(126) Lamoree, M.H.; van der Hoeven, R.A.M.; Tjaden, U.R.; van der Greef, J. *J. Mass Spectrom.* **1998**, *33*, 450-460.

(127) Yang, L.; Lee, C.S.; Hofstadler, S.A.; Pasa-Tolic, L.; Smith, R.D. *Anal. Chem.* **1998**, *70*, 3235-3241.

(128) Xiang, F.; Lin, Y.; Wen, J.; Matson, D.W.; Smith, R.D. *Anal. Chem.* **1999**, *71*, 1485-1490.

(129) Shen, Y.; Xiang, F.; Veenstra, T.D.; Fung, E.N.; Smith, R.D. *Anal. Chem.* **1999**, *71*, 5348-5353.

(130) Garcia, F.; Henion, J. D. *Anal. Chem.* **1992**, *64* , 985-990.

(131) Banks, J. F. *Electrophoresis* **1997**, *18*, 2255-2266.

(132) Zhao, Z.; Wahl, J.H.; Udseth, H.R.; Hofstadler, S.A.; Fuciarelli, A.F.; Smith, R.D. *Electrophoresis*, **1995**, *16*, 389-395.

(133) Guzman, N.A.; Park, S.S.; Schaufelberger, D.; Hernandez, L.; Paez, X. Rada, P.; Tomlinson, A.J.; Naylor, S. *J. Chromatogr. B,* **1997**, *697*, 37-66.

(134) Yang, Q.; Tomlinson, A.J.; Naylor, S. *Anal. Chem.* **1999**, *71*, 183A-189A.

(135) Wu, J.; Qian, M.K.; Li, M.X.; Zheng, K.; Huang, P.; Lubman, D.M. *J. Chromatogr. A,* **1998**, *697*, 37-66.

(136) Schmeer, K.; Behnke, B.; Bayer, E. *Anal. Chem.* **1995**, 67, 3656-3658.

(137) Lane, S. J.; Boughtflower, R.; Paterson, C.; Underwood, T. *Rapid Commun. Mass Spectrom.* **1995**, *9*, 1283-1287.

(138) Ding, J.; Vouros, P. *Anal. Chem.* **1999**, *71*, 378A-385A.

(139) Smith, R.D.; Loo, J.A.; Edmonds, C.G.; Barinaga, C.J.; Udseth, H.R. *Anal. Chem.* **1990**, *62*, 882-888.

(140) Reinhoud, N.J.; Schroder, E.; Tjaden, R.R.; Niessen, W.M.A.; Ten Noever de Brauw, M.C.; van der Greef, J. *J. Chromatogr.* **1990**, *516*, 147-156.

(141) Tomlinson, A.J.; Benson, L.M.; Johnson, K.L.; Naylor, S. *Electrophoresis* **1994**, *15*, 62-71.

(142) Mordehai, A. V.; Hopfgartner, G.; Huggins, T. G.; Henion, J. D. *Rapid Commun. Mass Spectrom.* **1992**, *6*, 508-516.

(143) Ramsey, R.S.; Goeringer, D.E.; McLuckey, S.A. *Anal. Chem.* **1993**, *65*, 3521-3524.

(144) Wahl, J. H.; Hofstadler, S. A.; Smith, R. D. *Anal. Chem.* **1995**, *67*, 462-465.

(145) Jin, X. Y.; Kim, J. K.; Parus, S.; Lubman, D. M.; Zand, R. *Anal. Chem.* **1999**, *71*, 3591-3597.

(146) Fang, L.; Zhang, R.; Williams, E. R.; Zare, R. N. *Anal. Chem.* **1994**, *66*, 3696-3701.

(147) Chang, S. Y.; Yeung, E. S. *Anal. Chem.* **1997**, *69*, 2251-2257.

(148) Lazar, I. M.; Rockwood, A. L.; Lee, E. D.; Sin, J. C. H.; Lee, M. L. *Anal. Chem.* **1999**, *71*, 2578-2581.

(149) Deforce, D. L. D.; Raymackers, J.; Meheus, L.; Van Wijnendaele, F.; De Leenheer, A.; Van den Eeckhout, E. G. *Anal. Chem.* **1998**, *70*, 3060-3068.

(150) Li, J. J.; Wang, C.; Kelly, J. F.; Harrison, D. J.; Thibault, P. *Electrophoresis* **2000**, *21*, 198-210.

(151) Andrien, B.A.; Banks, J.F.; Boyle, J.G.; Dresch, T.; Haren, P.J.; Whitehouse, C.M. *Proceedings of the 43rd ASMS Conference on Mass Spectrometry and Allied Topics;* **1995**, Atlanta, GA, pp 999.

(152) Hofstadler, S.A.; Swanek, F.D.; Gale, D.C.; Ewing, A.G.; Smith, R.D. *Anal. Chem.* **1995**, *67*, 1477-1480.

(153) Hofstadler, S.A.; Severs, J.C.; Smith, R.D.; Swanek, F.D.; Ewing, A.G. *Rapid Commun. Mass Spectrom.* **1996**, *10*, 919-922.

(154) Severs, J.C.; Hofstadler, S.A.; Zhao, Z.; Senh, R.T.; Smith, R.D. *Electrophoresis* **1996**, *17*,1808-1817.

(155) Valaskovic, G.A.; Kelleher, N.L.; McLafferty, F.W. *Science* **1996**, *273*, 1199-1202.

CHAPTER 2 [1]

On-line Nonaqueous Capillary Electrophoresis and Electrospray Mass Spectrometry of Tricyclic Antidepressants and Metabolic Profiling of Amitriptyline by *Cunninghamella elegans*

[1] Parts of this chapter have been published as:
Liu, C.S.; Li, X.F.; Pinto, D.; Hansen, E.B., Jr.; Cerniglia, C.E.; Dovichi, N.J. *Electrophoresis* **1998**, *19*, 3183-3189.
Li, X.F.; Liu, C.S.; Roos, P.; Hansen, E.B., Jr.; Cerniglia, C.E.; Dovichi, N.J. *Electrophoresis* **1998**, *19*, 3178-3182.

2.1 ABSTRACT

An on-line nonaqueous capillary electrophoresis-electrospray mass spectrometry (CE-ESI-MS) technique was developed using a commercial ion spray interface. The nonaqueous CE-ESI-MS system was employed to profile tricyclic antidepressants of similar structures and mass-to-charge ratios. A mixture of methanol and acetonitrile with ammonium acetate as the separation buffer was essential to achieve baseline resolution of these compounds. We found that pure methanol can be utilized as a sheath liquid to obtain stable ion spray from nonaqueous capillary electrophoresis. The flow rate of the coaxial nebulizing gas affected baseline signals, CE separation efficiency, and migration time. Other nonaqueous capillary electrophoresis operating conditions and electrospray parameters were optimized to enhance baseline separation and for high sensitivity detection. The effect of sample stacking on separation and detection was evaluated. The calculated detection limits were approximately 1.0 fmol of analyte injected onto the capillary. ESI-MS spectra of tricyclic antidepressants from a single quadrupole MS were obtained and elucidated. The resulting information was used to propose fragmentation pathways of the tricyclic antidepressants. This method was also employed to analyze the metabolites of amitriptyline produced by the fungus *Cunninghamella elegans* (*C. elegans*). Sixteen metabolites of amitriptyline were detected and most of them were tentatively identified as demethylated and/or hydroxylated, and/or N-oxidized products.

2.2 INTRODUCTION

Tricyclic antidepressant agents (TCAs), amitriptyline, imipramine, desipramine, and nortriptyline are widely used medications to treat depression and mania[1,2]. These compounds are secondary or tertiary amines with very similar structures and masses (**Figure 2.1**). The clinical effects of these drugs are characterized by changes in mood, which may be related to their capabilities to inhibit the neuronal uptake of biogenic norepinephrine[3]. Toxic effects involve antimuscarinic effects and cerebral and cardiac toxicity[4]. In addition lethal overdose toxicity has been proverbially reported[5]. The pharmacological effects and toxicity of these compounds are caused, in part, by the formation of active metabolites[3,6]. The major metabolite, 11-OH-amitriptyline is about as potent as amitriptyline in inhibition of noradrenaline uptake by rat brain slices[7], whereas the N-demethylated metabolite of amitriptyline, nortriptyline, is 5 times more potent than the parent drug[3,8]. Thus, it is of high interest to develop a methodology of separation and determination of these compounds and their principle metabolites.

The structural similarity of these drugs poses difficulties in achieving a highly efficient separation and determination. Traditional approaches to the analysis of these compounds and their metabolites include thin layer chromatography (TLC) with fluorescence detection[9], gas chromatography[10,11], high performance liquid chromatography (HPLC)[12-17], and gas chromatography-mass spectrometry (GC-MS) with pre-derivatization of the analytes before analysis[18-21]. Spectroscopic analysis is often employed for structural characterization of metabolites after tedious HPLC fractionation[22-25]. Fast atom-bombardment mass spectrometry has been employed to directly characterize quaternary ammonium-linked glucuronides of three TCAs[26]. In

Figure 2.1. Structures of the five tricyclic antidepressants.

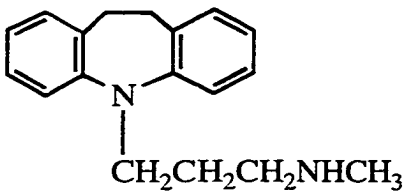

1. Desipramine(DES)

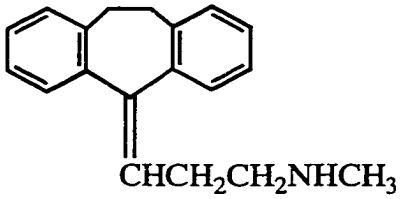

2. Nortriptyline(NOR)

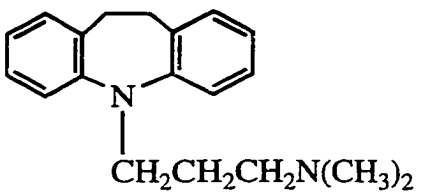

3. Imipramine(IMI)

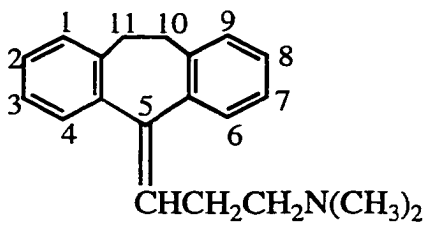

4. Amitriptyline(AMI)

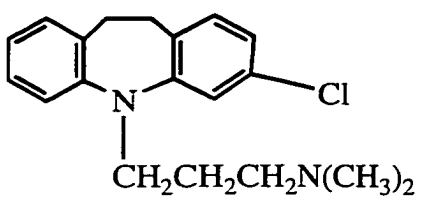

5. Clomipramine(CLO)

addition, thermospray liquid chromatography-mass spectrometry has been employed to determine TCAs and neuroactive indoleamines with 10 picograms detection limits[27].

Capillary electrophoresis (CE) has been widely employed for separations of polar compounds and macromolecules[28,29]. Most CE separations, however, are carried out in an aqueous buffer system. Due to this fact, application of CE for the analysis of pharmaceuticals is limited because most drugs are hydrophobic. Conventional aqueous CE methods do not generate useful separations of drugs. Nonaqueous buffer systems utilizing organic solvents such as methanol and acetonitrile and a soluble buffer salt provide an alternative to conventional aqueous CE systems. Since 1993, the use of a non-aqueous CE buffer solution for the separation of pharmaceuticals has been reported[30-36]. Very high separation selectivity was obtained in a nonaqueous CE system without adding surfactants or complexing agents to the electrophoresis media. Although absorbance measurement has been the most common detection method, electrospray ionization-mass spectrometry (ESI-MS) provides an information-rich spectrum that may be useful for drug and metabolite identification.

Since the birth of CE-ESI-MS in 1987, its application has been widespread[37-42]. The technique, however, is still in its infancy and has some limitation, including poor sensitivity for neutral molecules such as cholesterol and aromatic hydrocarbons. Poor compatibility of CE running buffers with ESI-MS is another important limitation. Commonly used aqueous separation systems which may contain nonvolatile salts, beta-cyclodextrin, or surfactant additives are not suitable for coupling CE directly to ESI-MS[43-45]. These additives inhibit ionization, leading to very low sensitivity or they can affect both tertiary and quaternary structures of proteins under conditions used for ESI-MS, thereby complicating analysis[46-48]. The completely organic system with a volatile

electrolyte is ideal for coupling CE to an electrospray mass spectrometer. Few reports have documented the application of on-line CE-MS analysis using nonaqueous solvents[31,44]. Tomlinson *et al.* [31,32] discussed the use of nonaqueous separation conditions for the investigation of drug metabolites by on-line CE-MS. Lu *et al.* [46] reported a nonaqueous, surfactant-containing media CE system with on-line coupling to ESI MS for the analysis of tamoxifen and its metabolites. It was reported that SDS lowered the ESI MS signal response by a factor of 3. We present the first report of on-line CE-MS analysis of tricyclic antidepressants.

The filamentous fungi Cunninghamella species has been employed to study the metabolism of a number of pharmaceutical drugs such as (+/-)-N-(n-propyl)amphetamine [49], antihistamines[50], antidepressants[51,52], and other xenobiotics[53,54]. These fungi metabolize drugs in a manner similar to that in mammals. For example, cytochrome P450 monooxygenases are involved in the oxidative drug metabolism reactions in both fungi and mammals[53-55]. Thus, fungal metabolism could model mammalian drug metabolism. Since fungal cultures are inexpensive and easy to maintain the combination of this model system with a simple analytical technique should provide useful metabolic information and reduce the cost of drug development.

2.3 EXPERIMENTAL

2.3.1 Materials and Chemicals

Desipramine (DES), nortriptyline (NOR), imipramine (IMI), amitriptyline (AMI) and clomipramine (CLO) were purchased from Sigma (St. Louis, MO, USA). HPLC-grade methanol and acetonitrile were purchased from BDH (Toronto, ON, Canada). Ammonium acetate (NH_4Ac), acetic acid (HAc) was obtained from Anachemia

(Montreal, PQ, Canada). Other reagents were from Sigma. All stock solutions (10.0 mM) were prepared by dissolving the antidepressants directly into methanol-acetonitrile (1:1, v/v). Before analysis, the stock solutions were diluted to 0.1-100 μM concentrations with the CE running buffers or diluted running buffers before use. Typically, a 100 mM stock solution of nonaqueous electrolyte medium was prepared by dissolving ammonium acetate in methanol, then a portion of this solution was diluted to a proper concentration with methanol and acetonitrile before use. For example, 50 mM NH_4Ac in methanol-acetonitrile (75:25) was used as a running buffer, and 5 mM NH_4Ac in methanol-acetonitrile (75:25) was the sample matrix.

2.3.2 Culture Incubation and Sample Preparation

Six cultures of *Cunninghamella elegans* were prepared and incubated for a total of ten days following the same procedures and under the same conditions described elsewhere[51]. Three of these cultures were dosed with 5 mg amitriptyline and three were dosed with 10 mg of the same drug. Two controls, one containing the growth medium and cell culture without amitriptyline, and another containing only growth media, were also prepared and incubated under the same conditions. Two 5 mg-dosed and two 10 mg-dosed cultures were extracted utilizing the following procedures. A ten-day old culture of *C. elegans* (30 mL) was centrifuged to pellet the cells and the aqueous phase was transferred to a 250 mL separatory funnel. The cell pellet was lysed and extracted with 50 mL of methanol. The methanol cell lysate was centrifuged and the methanol supernatant was added to the separatory funnel. Five grams of sodium hydrogen phosphate (Na_2HPO_4) and 100 mL of water were added to the separatory funnel. The mixture in the separatory funnel was extracted three times using 150 mL of methylene chloride. Each methylene chloride extract was filtered through a plug of sodium sulfate into a 250 mL

round bottom flask, and the organic solvent was evaporated to dryness using a roto-evaporator and a 40°C water bath. The dry residue after the third extraction was redissolved into 5 mL of methylene chloride and transferred to a glass tube. Finally, the methylene chloride was completely evaporated under gentle N_2 flow, and the dry residue was kept at 4 °C prior to analysis.

The dried extracts were concentrated by redissolving the sample in 1mL of methanol. A 25 μL aliquot of the 10 mg-dosed sample and a 50 mL aliquot of the 5 mg-dosed sample was mixed and diluted to 1 mL in a methanol-acetonitrile (75:25) containing 5 mM ammonium acetate. These concentrated solutions contained approximately 0.9 mM of total analytes. Controlled samples, without AMI, and blank samples, without AMI or cells but containing only media were prepared in the same way. Aqueous cell extract solutions were also injected directly without concentration or redissolution in organic solvent.

2.3.3 CE

CE was performed using a SpectraPhoresis 100 system from Thermo Separation Products (San Jose, CA). Untreated fused silica capillaries (Polymicro Technologies, Phoenix, AZ) with 80 cm x 50 μm ID x 184 μm OD were utilized for separations. Fresh running buffers were used to flush the capillaries before and between runs. Samples were introduced into the capillaries by electrokinetic injections at 10 kV for 10 s unless otherwise indicated. The electrical current was 6 μA during injection. The inlet and outlet of the capillary were adjusted to the same height to prevent siphoning. The separations were performed at 25 kV with a current of 17 μA. The operating electrolyte was changed every 5 to 10 runs to avoid contamination and solvent evaporation.

2.3.4 ESI-MS

ESI-MS of CE eluents was conducted on-line with a PE/Sciex API 100 (Thornhill, Canada) single quadrupole mass spectrometer equipped with an ion spray source. The CE column was inserted inside the 15 cm long stainless steel (SS) electrode tube with 0.5-1.0 mm pulling back with reference to the tube outlet, while the electrode tube was inserted inside another SS nebulizer tube with 0.5~1.0 mm protruding out with reference to the electrode outlet. This positioning was optimized for maximum sensitivity of analyte by infusing a standard solution of analyte in running buffer. The coaxial sheath liquid of 100% methanol was pumped by a Harvard Apparatus low pressure syringe infusion pump (Southnatick, MA) at a flow rate of 2.0 μL/min through a capillary of 50 μm ID and 184 μm OD. The transferring sheath capillary was connected to the hold-down tee of the ion sprayer, and the sheath liquid was transferred to the electrode tube surrounding the CE separation column and used as the conducting media for both CE and ESI processes.

Before CE-MS analysis, the position of the ion sprayer was adjusted three-dimensionally for maximum sensitivity while analytes in running buffer were infused through the CE column at a rate of 2 μL/min. Positive ion mode was performed for all measurements. Other operating parameters such as ion spray voltage (IS), orifice voltage (OR), ring voltage (RNG) and curtain gas flow were optimized for maximum total ion electrophoretic signals over a m/z range of 50-325 using the same flow injection method. Lower OR voltage was chosen, which leads to less in-source collision-induced dissociation, to monitor the protonated molecular ions. A working pressure of 1.7×10^{-5} Torr was maintained in the analyzer chamber. The ion detector (CEM) voltage of 2.3 kV was kept constant during routine operation of the instrument.

When CE separation was performed, the IS was set to 4.6 kV, OR was 45 V, RNG was 320 V, curtain gas flow was 0.95 L/min. Nebulizing assistance was provided by passing prepurified nitrogen through the nebulizer tube at a rate of 0.41 L/min (NEB 3) or 0.67 L/min (NEB 4), unless otherwise indicated according to the stability of the baseline signals. During sample injection, the IS was set to 0 and the nebulizer gas flow was set to 0 (NEB 0). Full scan analysis of sample ions was accomplished by scanning the quadrupole in 1.0 amu increments from 50-325 amu in 0.56 s. For the metabolites study, the scan range was m/z 50-650. While screening for glucuronide conjugates, the extended range was used, the step size was set to 1.0 amu, dwell time was 1.5 ms, and the speed was 0.9 s/scan. For selective ion monitoring (SIM), ions m/z 72, 86, 191, 208, 233, 264, 267, 278, 281, 315 and 317 were selected, the step size was 0.2 amu, the dwell time was 5.0 ms, and the scan speed was 0.52 s. CE-MS electropherograms were acquired by LC2Tune software, and then processed by Multiview1.2 and MacQuant software from Sciex.

2.4 RESULTS AND DISCUSSION

2.4.1 Modification of Separation Conditions

We developed a simple and robust nonaqueous electrophoretic separation method for five TCAs that have similar mass-to-charge ratios and similar chemical structures. We used a nonaqueous buffer system containing ammonium acetate as the electrolyte and a mixture of methanol and acetonitrile as solvent. Despite the structural similarities of the five compounds (**Figure 2.1**), baseline separation was achieved using a nonaqueous running buffer containing ammonium acetate in methanol-acetonitrile solvents with a ratio of 75:25 to 100:0, **Figure 2.2**. The total ion electropherograms (TIE) show improved resolution of analytes is obtained when the amount of methanol in buffer is

Figure 2.2. TIEs (baseline subtracted) showing the effects of organic composition on resolution and migration times.

Running buffer was 50 mM ammonium acetate in different methanol-acetonitrile solvents. The CE electrical current was between 16 μA (methanol-acetonitrile, 50:50) and 20 μA (methanol-acetonitrile, 85:15). The sample was a 10 μM drug mixture in methanol-acetonitrile (50:50) with 5 mM NH_4Ac. Nebulizing gas flow was 0.82 L/min (NEB5). Peak orders: (1) DES; (2) NOR; (3) IMI; (4) AMI; (5) CLO.

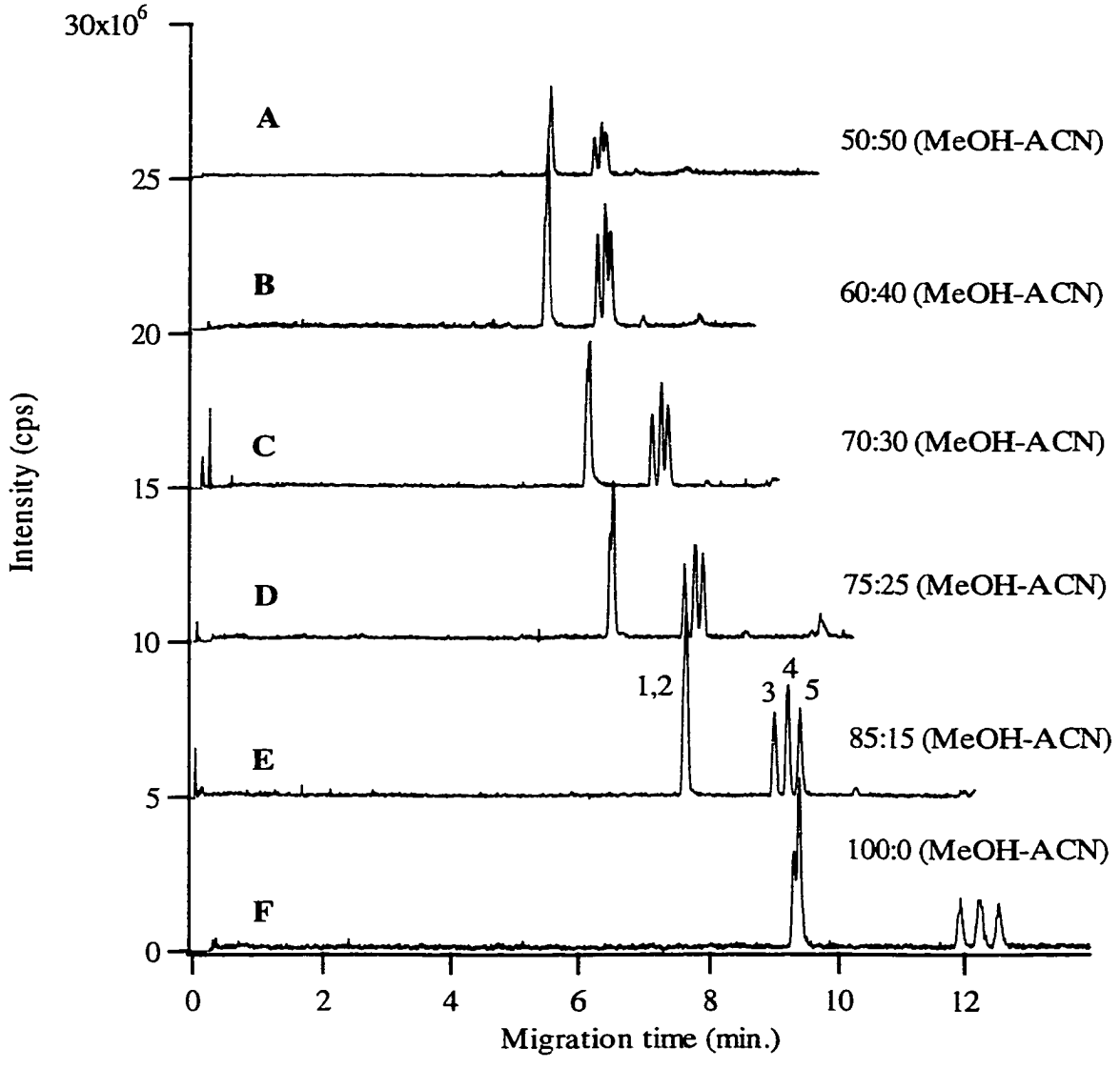

increased, but migration times also increase. This result indicates decreased EOF (**Figure 2.2A-2.2F**). Enhanced CE separation could be attributed to slight differences in electrophoretic mobility of analytes caused by the addition of increased amount of methanol to buffer. To obtain an appropriate resolution of analytes in a short analysis time, 75:25 to 85:15 of methanol-acetonitrile were chosen.

The buffer ionic strength or the concentration of NH_4Ac in the running buffer also has a large influence on the separation efficiency and electro-osmotic flow as shown in **Figure 2.3**. These results were consistent with the observed results in aqueous CE systems[29,56]. Average resolution is not changed much when the concentration of NH_4Ac was increased from 25 mM to 50 mM, i.e. peaks 1 and 2 got closer and peaks 3, 4, and 5 became slightly more separated. In addition, we observed increased sample stacking effects (higher injection amount) when the running buffer concentration increased. For example, the peak height in a 50 mM ammonium acetate buffer is about 1/3 higher than that in a 25 mM buffer while the same sample of 10 μM mixture of analytes in 5 mM ammonium acetate is electrokinetically injected. Sample stacking will be discussed in more detail in the next section.

Changing the voltage is an easy way to modify the electro-osmotic flow because it varies the electric field. The effects of the applied voltage at the injection end on separation efficiency and the electro-osmotic flow are illustrated in **Figure 2.4**. Higher applied voltage provided higher theoretical plate numbers and faster separations. Since nearly 5 kV was applied at the ion sprayer end, the anode of CE, a net voltage of 25 kV across the capillary was used for the remaining experiments due to the upper limit of our 30 kV power supply.

Figure 2.3. TIEs (baseline subtracted) showing the influence of ammonium acetate concentration on separation and migration of the five TCAs.

Running buffer was methanol-acetonitrile (70:30) with various concentrations of NH_4Ac. The CE currents were 18 μA, 15 μA and 10 μA for (a), (b) and (c), respectively. Nebulizing gas flow is 0.82 L/min (NEB 5). Other conditions were as described in the experimental section. Peak orders are as in Figure 2.

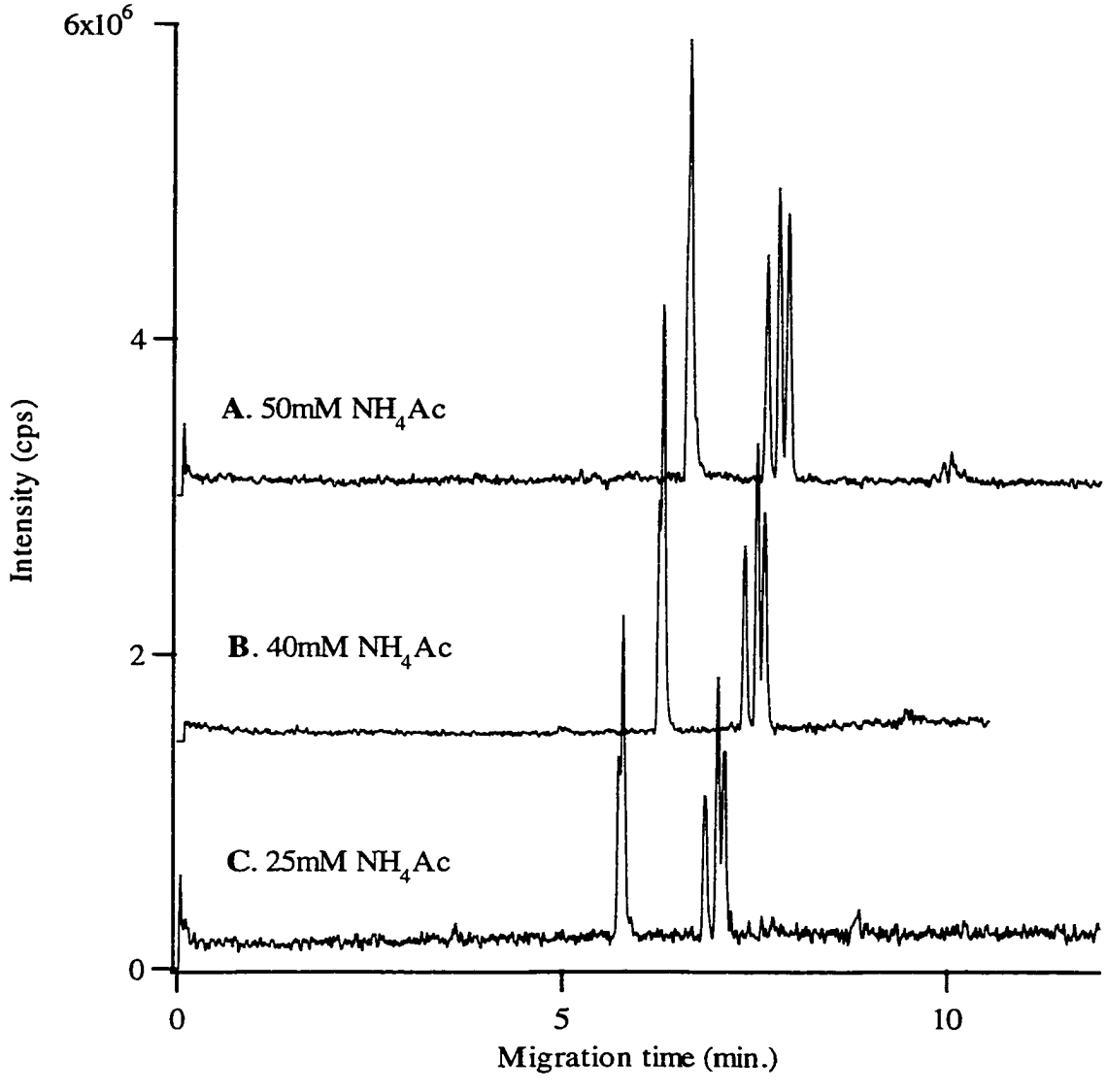

Figure 2.4. TIEs showing the influence of CE voltage on separation efficiency and migration of analytes.

Running buffer was 100 mM ammonium acetate in methanol-acetonitrile (70:30). A mixture of five TCAs with 10 μM of each in 50% (v/v) buffer was injected at 20 kV for 10 s. Nebulizing gas was 0.26 L/min (NEB 2). Other conditions were as described in the experimental section.

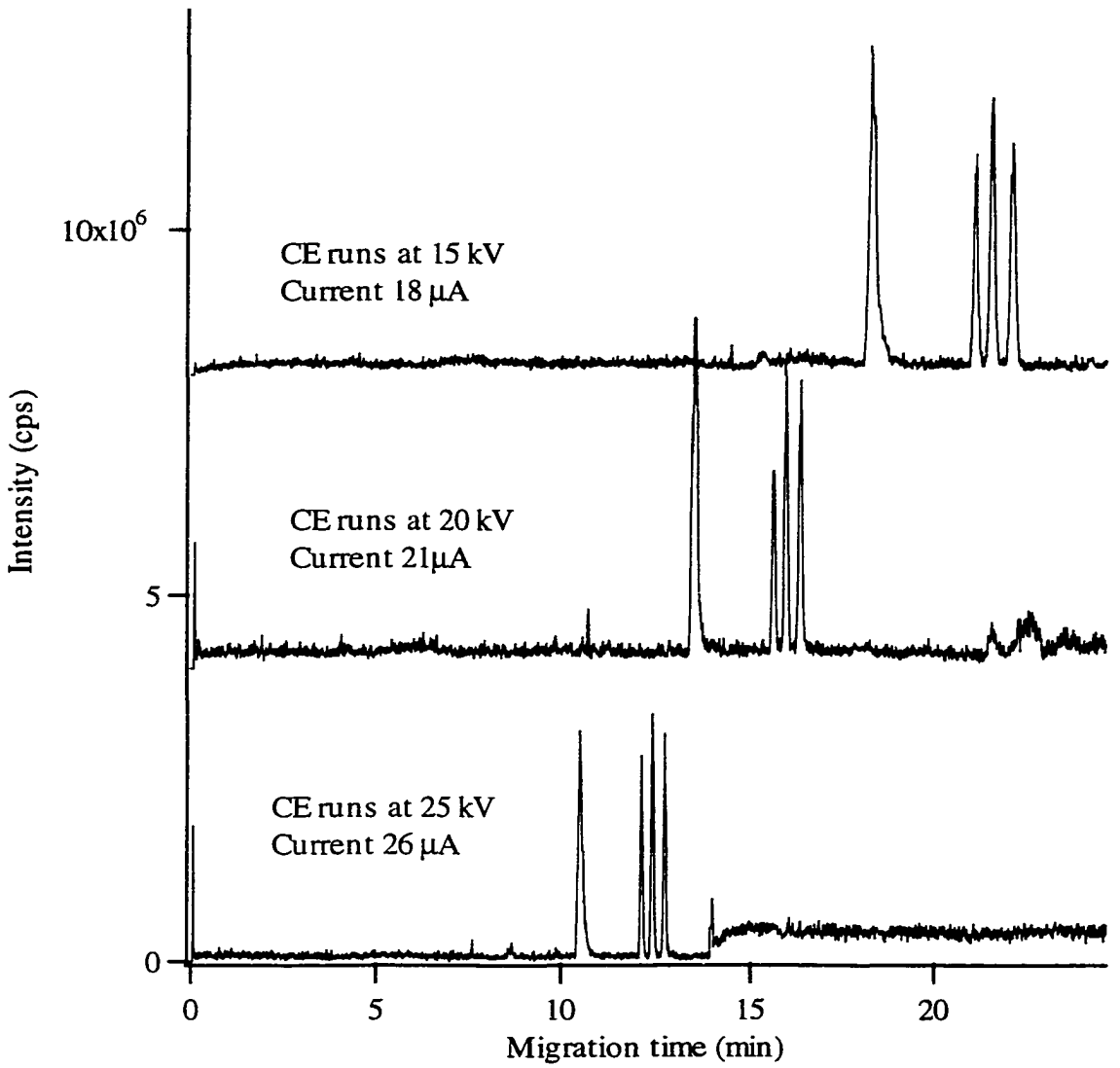

2.4.2 Optimization of ESI

The positioning of the electrode tube and the CE column inside the electrode tube were critical for stable and reproducible signals. It was always advisable to re-align the ion sprayer whenever the column was changed or the interface was cleaned. For tuning purposes, the test sample was a 10 μM mixture of the five TCAs in methanol-acetonitrile (50:50) with 5 mM NH_4Ac in the sample. Other ESI conditions, such as the IS, OR, RNG and nebulizing gas, were optimized during a daily tuning process to the ion spray instrument.

Usually in ESI-MS a sheath liquid containing a dilute solution of electrolyte (in most cases it is ~1% acetic acid for positively charged ions) in aqueous methanol or aqueous isopropanol is coaxially provided. The sheath liquid allows the electrical contact of the electrospray electrode with the outlet of the separation capillary for electrophoresis and simultaneously aids in the ESI process. The choice of a sheath liquid for stable and efficient ion production is crucial for successful CE-MS on-line analysis. For comparison, a mixture of 10 mM each of TCAs dissolved in an acetic acid solution methanol-water-acetic acid (50:50:0.2, v/v/v), in pure methanol, in pure acetonitrile or in a mixed methanol-acetonitrile solvent were infused using the syringe pump. Except for the acetic acid mixture, all solvents gave good electrospray signals for these analytes. When CE-MS mode was performed, and when a mixture of analytes in running buffer was continuously infused electrokinetically via the CE capillary, the effect of different sheath solutions on ESI sensitivity of analytes was evaluated. The acetic acid solution, methanol, acetonitrile, and mixed methanol-acetonitrile solvents as sheath liquids were investigated. The highest signals and most stable baselines were obtained by using methanol as the sheath liquid. The lower surface tension of methanol aids the desolvation

of droplets in the aerosol formed under a high voltage and thus enhances the stability and sensitivity of the electrospray ionization process.

An effect of sheath flow rate on the TIE response of the TCAs migrating from the CE column was also investigated. By changing the sheath flow from 5 μL/min to 2 μL/min, the peak area and height for nortriptyline and amitriptyline both increased by a factor of 1.4 without affecting the CE resolution or efficiency, **Figure 2.5**. The baseline became unacceptable noisy once this rate was lowered to less than 2 μL/min.

For optimal ion production, a stable spray of uniform-sized small charge droplets must be produced; nebulization is a critical step for this purpose. In addition to the sheath liquid, a coaxial nitrogen gas flow was employed to pneumatically assist the electrospray process. The employment of the nebulizing gas substantially enhances nebulization efficiency. For example, large droplets were quite visible when IS voltage was off and nebulizing gas flow was less than 0.67 L/min (NEB 4). Above 0.67 L/min, the spray became focused and a finely divided aerosol was formed. Furthermore, a significant change in CE resolution was observed by varying the gas flow rate as illustrated in **Figure 2.6**. Increasing the rate from 0.17 L/min (NEB 1) to 0.41 L/min (NEB 3) had little influence on CE resolution. However, when this rate was increased to 0.67 L/min (NEB 4) and above, the separation became worse and the migration times of analytes were reduced. This change in migration time could be explained by the pressure difference between inlet and outlet of the CE column. A high gas flow increases the pressure difference across the capillary, which generates more pressure-driven flow in the capillary in addition to electro-osmotic flow. This result suggested the use of nebulizing flow rate of 0.17 L/min to 0.41 L/min (NEB 1 to NEB 3) for a better separation. Moreover, this flow rate should be reduced to 0 during the sample injection procedure to

Figure 2.5. TIEs showing the influence of sheath flow-rate on detection sensitivity of analytes.

Running buffer was methanol-acetonitrile (85:15) with 50 mM ammonium acetate. Nebulizing gas was 0.67 L/min (NEB 4). The sample was a 10 μM mixture of TCAs in 10% (v/v) buffer. Other conditions were as described in the experimental section.

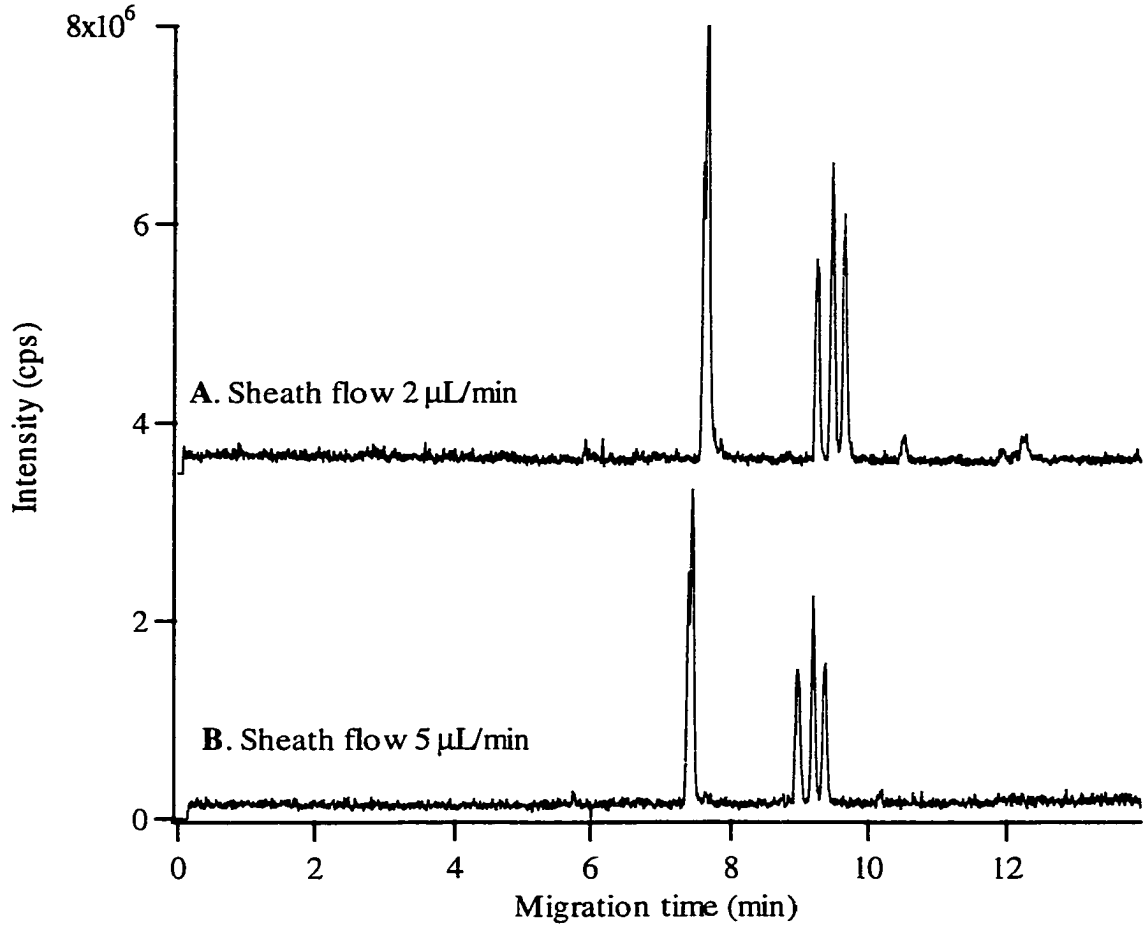

Figure 2.6. TIEs (baseline-subtracted) showing the effect of nebulizing gas flow rate on separation and migration times of five TCAs.

Running buffer was methanol-acetonitrile (60:40) with 50 mM ammonium acetate. Nebulizing gas was 0.67 L/min (NEB 4). The sample was a 10 µM mixture of TCAs in 10% (v/v) buffer. Other conditions were as described in the experimental section.

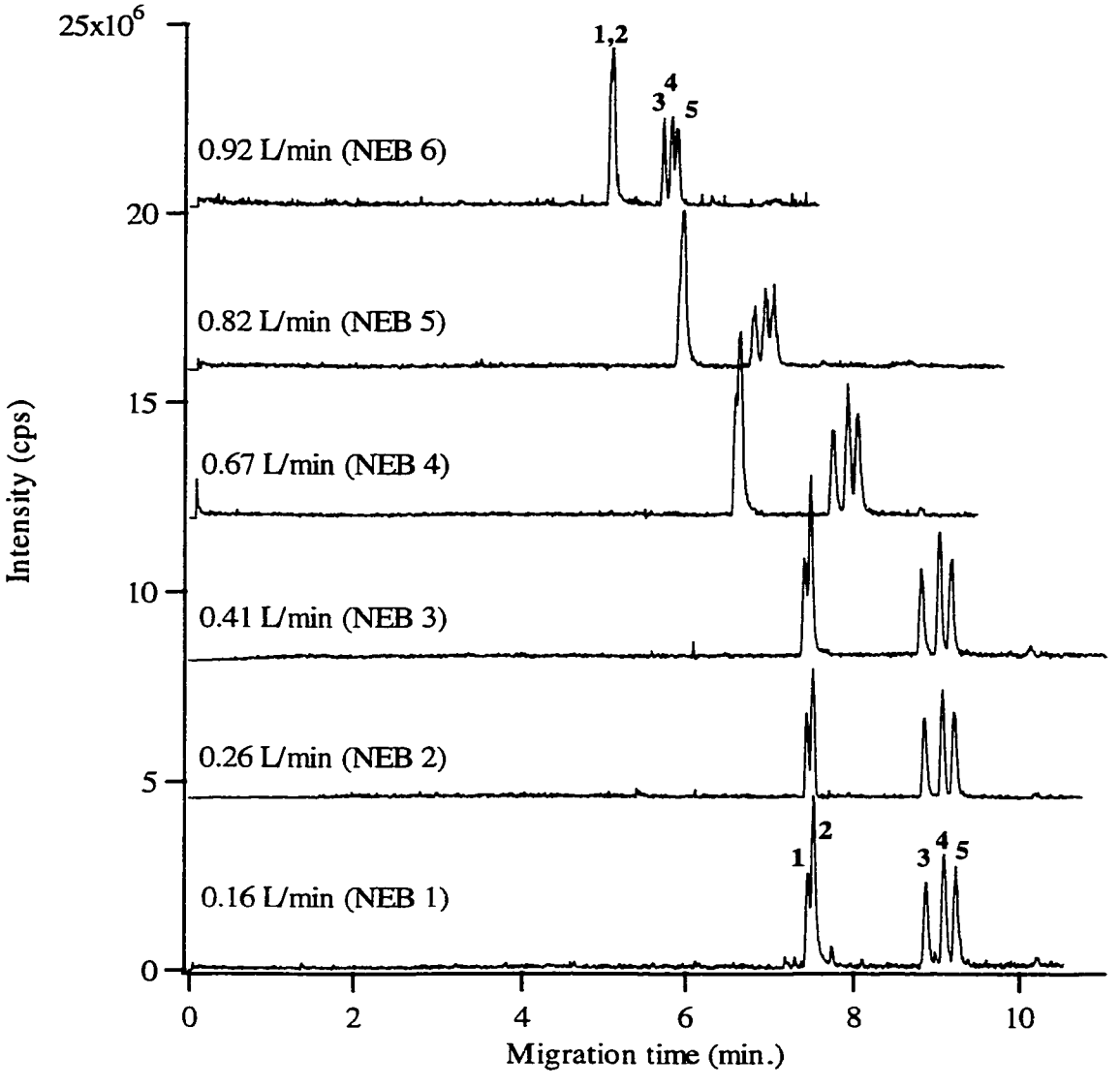

avoid siphoning. However, the TIE baseline was also affected by the flow rate of nebulizing gas as illustrated in **Figure 2.7**; at a lower rate (*e.g.* 0.26 L/min, NEB 2), large spikes in TIE were occasionally observed, probably due to large charged droplets passing into the mass analyzer. In principle, migration times will decrease at very high nebulizing flow rate; however, we did not observe this phenomenon at the flow rates employed for the rest of the study.

Migration times were very reproducible at a given flow rate of nebulizing gas. For example, the average migration time of AMI was 9.87 min with a relative standard of 0.7% (n=12) at a nebulizing gas flow rate of 0.41 L/min (NEB 3). Peak area was also reproducible, with an 8% relative standard deviation for CE-ESI-MS detection of AMI (n=5).

2.4.3 Sample Stacking Effect, Quantification Calibration Curve, and Detection Limits

Stacking has been used to increase sensitivity in CE[57]. In order to evaluate the loading capabilities of the CE-ESI-MS, sample stacking was studied by injecting several sample solutions that varied in the electrolyte concentration (**Figure 2.8**). An increase in the ionic strength of the sample buffer had little effect for concentrations of ammonium acetate below 10^{-4} M. Other ions in the solvent presumably dominated the ionic strength of the solution. Higher ammonium acetate concentration resulted in lower signal. Neither migration time nor resolution were effected by stacking for analyte with concentrations below 10 μM, **Figure 2.9**. Injection in electrophoresis is a coulometric process, wherein passage of charge during injection leads to introduction of a proportional amount of ions. If the analyte ions constitute a large fraction of the total ionic strength of the solution, then they will make up a corresponding fraction of the ions that are injected onto the

Figure 2.7. Total ion current (baseline) signals showing the effect of nebulizing gas flow rate on signal stability.

Running buffer was methanol-acetonitrile (85:15) with 50 mM ammonium acetate. Other conditions were as described in the experimental section.

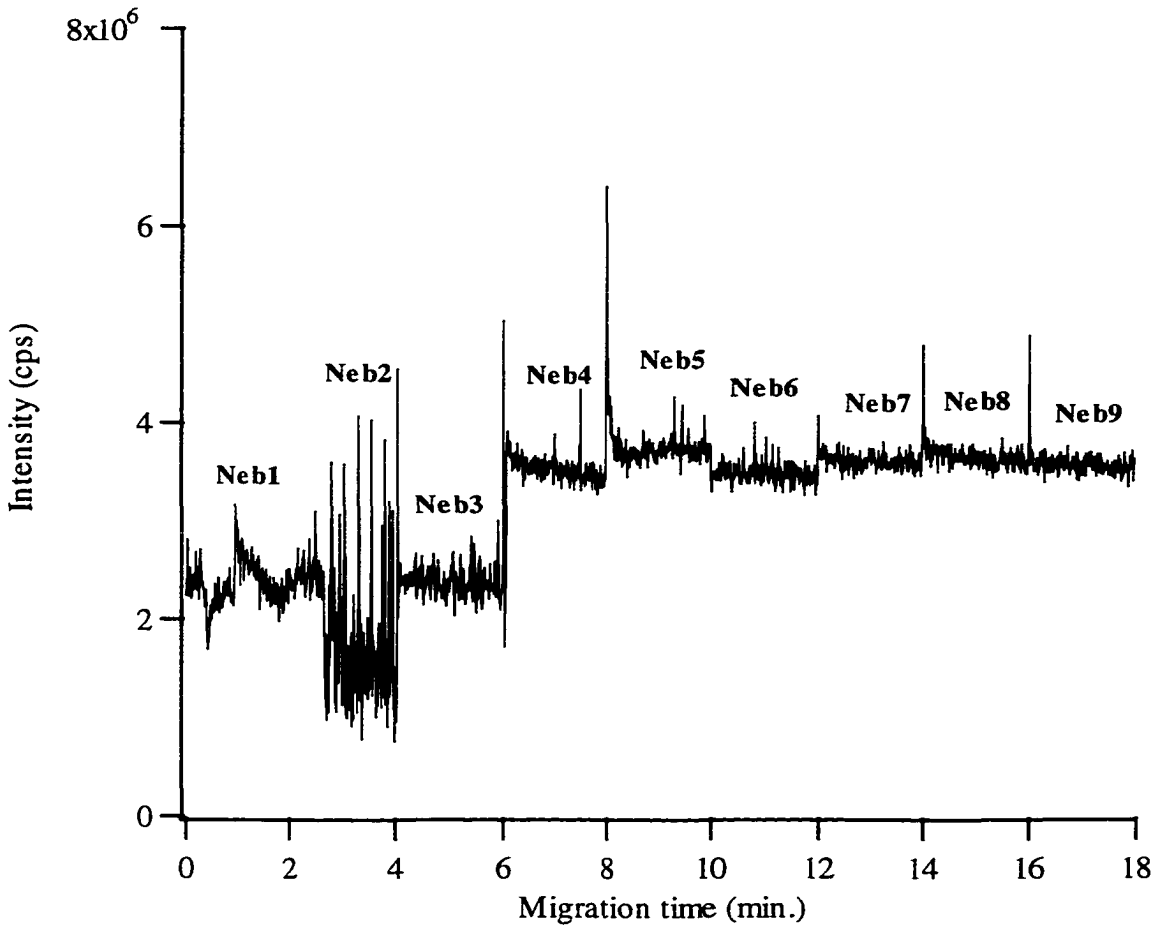

Figure 2.8. Effects of ammonium acetate concentration in the sample solution on total ion current.

The sample mixture, 10 μM, was dissolved in ammonium acetate buffers prepared in methanol-acetonitrile (80:20). The running buffer was 50 mM ammonium acetate in methanol-acetonitrile (80:20). The data are plotted on a log-log graph. Propagation of errors was used to plot the data at +/- one standard deviation. The lines were used to connect the data points as a guide to the eye.

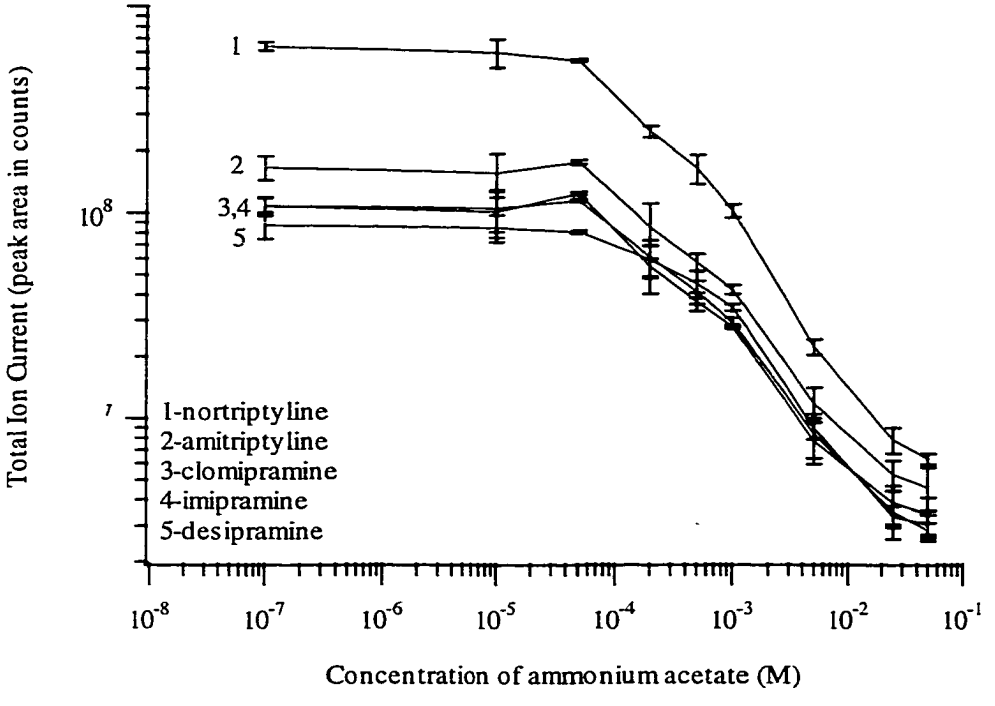

Figure 2.9. TIEs (baseline-subtracted) showing the effects of ammonium acetate concentration in the sample solution on total ion current.

The 10 μM sample mixture was dissolved in ammonium acetate buffers prepared in methanol-acetonitrile (80:20) and (A) 0 (B) 0.2 (C) 1.0 (D) 5.0 and (E) 25 mM ammonium acetate. The running buffer was 50 mM ammonium acetate in methanol-acetonitrile (80:20).

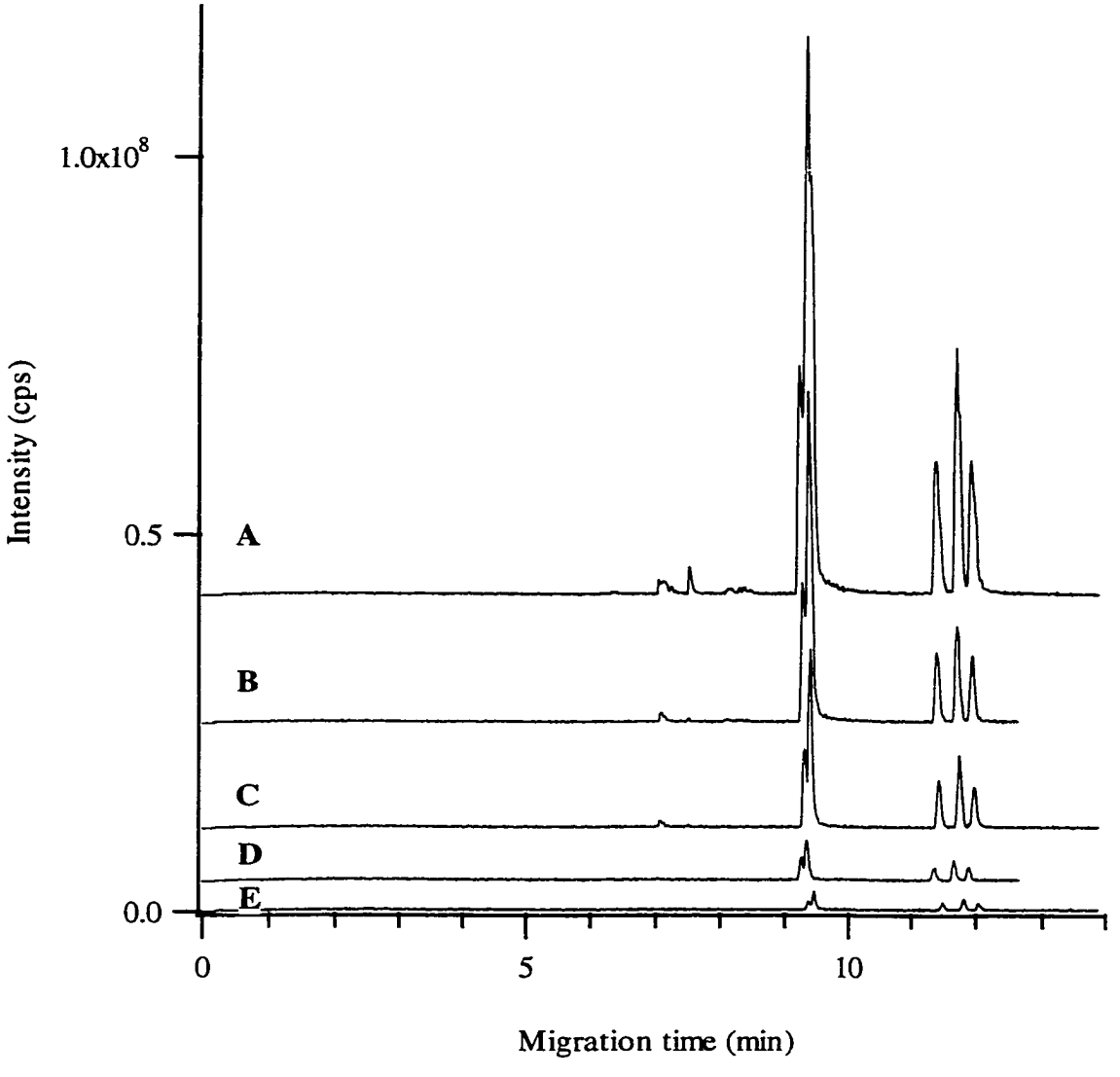

capillary. The slope of the log signal *versus* log ammonium acetate concentration plot was -0.5 for ammonium acetate concentrations above 10^{-4} M and for all analyte. This slope reflects the low dissociation constant of ammonium acetate in the organic solvent; a square-root dependence is expected for the ionic strength as a function of total salt concentration.

CE-ESI-MS calibration curves (**Figure 2.10**) were prepared for samples in 5 mM NH_4Ac , a separation buffer of 50 mM ammonium acetate, 10 kV injection for 10s, and full scan mode detection. The calibration curves were linear over an analyte concentration range of 1 μM-50 μM; the average X^2_v value was 0.74 for four degrees of freedom, $p = 0.55$. The curve became convex due to peak tailing at a concentration of 100 μM and above.

In full scan mode, the concentration detection limits (3σ) were 0.3 μM for desipramine and nortriptyline and 0.5 μM for imipramine, amitriptyline and clomipramine, respectively (**Figure 2.11**). While in SIM mode, detection limits were 0.03 μM and 0.05 μM, respectively (**Figure 2.12**). The injection volume, V_{inj}, was around 11 nL as calculated using the equation:

$$V_{inj} = V_{cap} (t_{inj} / t_{mig}) (E_{inj} / E_{CE}) \qquad (2.1)$$

Where the V_{cap} is the total internal volume of the CE column, t_{inj} is the injection time, t_{mig} is the migration time of an analyte, E_{inj} is the electrical field applied for injection and E_{CE} is the electrical field applied for CE separation. The calculated detection limits of mass for amitriptyline were 5 fmol in full scan mode and 0.5 fmol in SIM mode, respectively.

Figure 2.10. Calibration curves for the TCAs in full scan mode.

The sample mixture was dissolved in ammonium acetate buffers prepared in methanol-acetonitrile (80:20). The running buffer was 50 mM ammonium acetate in methanol-acetonitrile (80:20). Propagation of errors was used to plot the data at +/- one standard deviation. The lines were used to connect the data points as a guide to the eye.

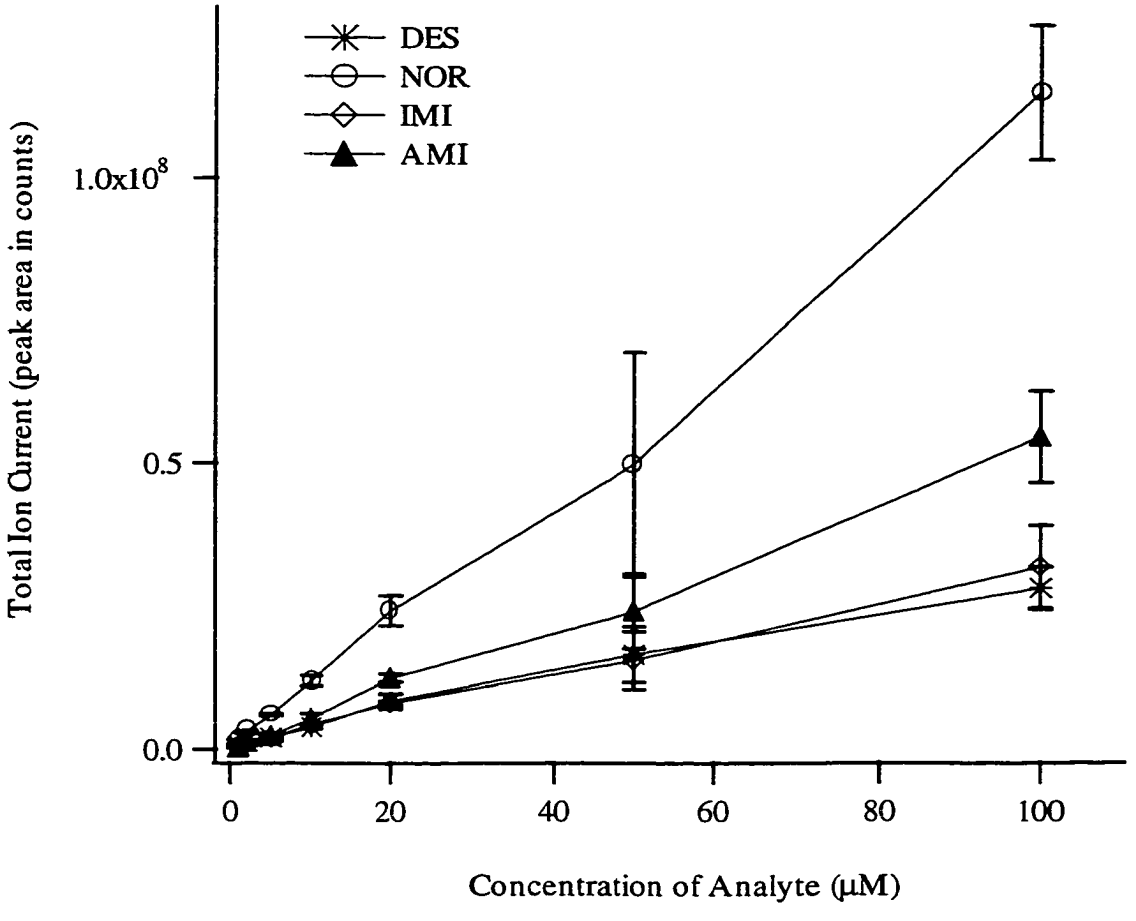

Figure 2.11. TIEs showing the concentration detection limits of five TCAs in full scan mode.

The running buffer was 50 mM ammonium acetate in methanol-acetonitrile (85:15). The sample mixture was dissolved in 10% (v/v) buffer. Other conditions were as described in the experimental section.

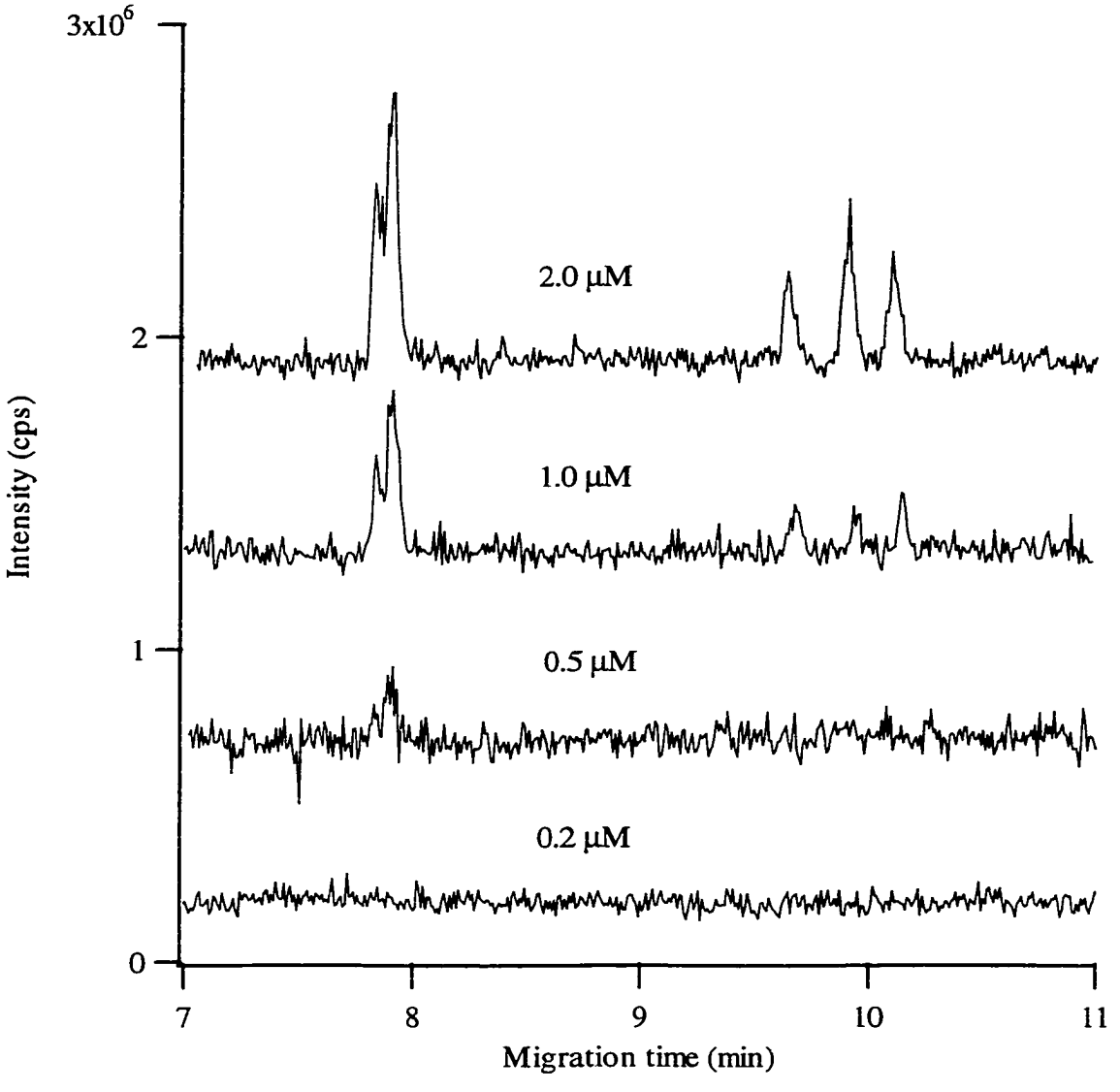

Figure 2.12. TIEs showing the concentration detection limits of five TCAs in SIM mode.

The running buffer was 50 mM ammonium acetate in methanol-acetonitrile (85:15). The sample mixture was dissolved in 10% (v/v) buffer. Other conditions were as described in the experimental section.

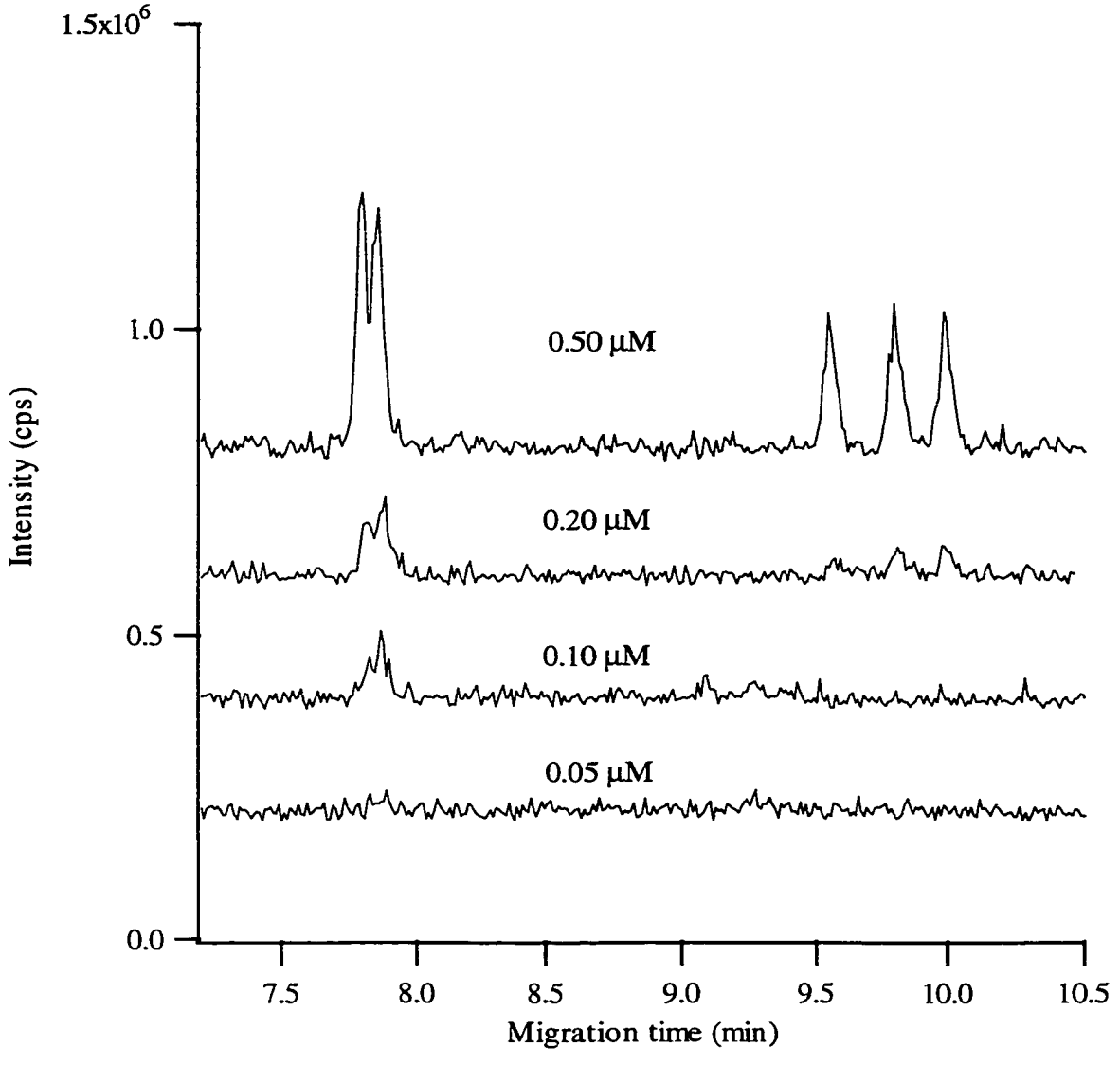

2.4.4 ESI-MS Characterization of TCAs

The N-linked structures of tricyclic antidepressants were detected with the best sensitivity in the positive-ion detection mode. Protonated antidepressants were generated in appreciable abundance even when the in-source collision induced dissociation (CID) potential was increased up to 150 V. It was found that higher CID voltage generates more fragmentation at the expense of lower TIE signals. Moreover, the fragmentation of protonated parent ions still occurred even when the CID voltage was set to a minimum value. In this study, CID voltage was adjusted to 45 V, under which the highest TIE response, abundant protonated molecular ions and some fragment ions were generated (**Figure 2.13**). **Figure 2.14** shows possible fragmentation pathways of those TCAs. The ESI-MS spectra of desipramine, imipramine and clomipramine were relatively simple. Bond cleavages rarely occurred on the tricyclic moiety and fragment ions were mainly due to the side chain breakage. Nortriptyline and amitriptyline showed similar spectra, except for a mass difference of 14 between their protonated molecular ions. In addition to the ions from side chain cleavages, there were also dominant cation peaks at m/z 91, 105, 117 and 155, reflecting the existence of bond cleavage on the tricyclic moiety.

2.4.5 CE-MS Profiles of Amitriptyline and its Metabolites

Figure 2.15 shows the TIEs of a standard mixture of five antidepressants, an extract from 5 mg-dosed *C. elegans* culture solution, and an extract from 10 mg-dosed culture solution. Aqueous culture solutions were either injected directly without further clean-up or with the sample preparation steps. All sample solutions (extracts, vacuum-dried aqueous cultures, and original aqueous cultures) gave similar profiles of metabolites except for different TIE intensities due to different dilution factors. There were few differences in the profiles of the two extracts. In addition to the parent drug,

Figure 2.13. ESI-MS spectra of five TCAs.

The running buffer was 50 mM ammonium acetate in methanol-acetonitrile (85:15). The sample mixture was dissolved in 10% (v/v) buffer. Other conditions were as described in the experimental section.

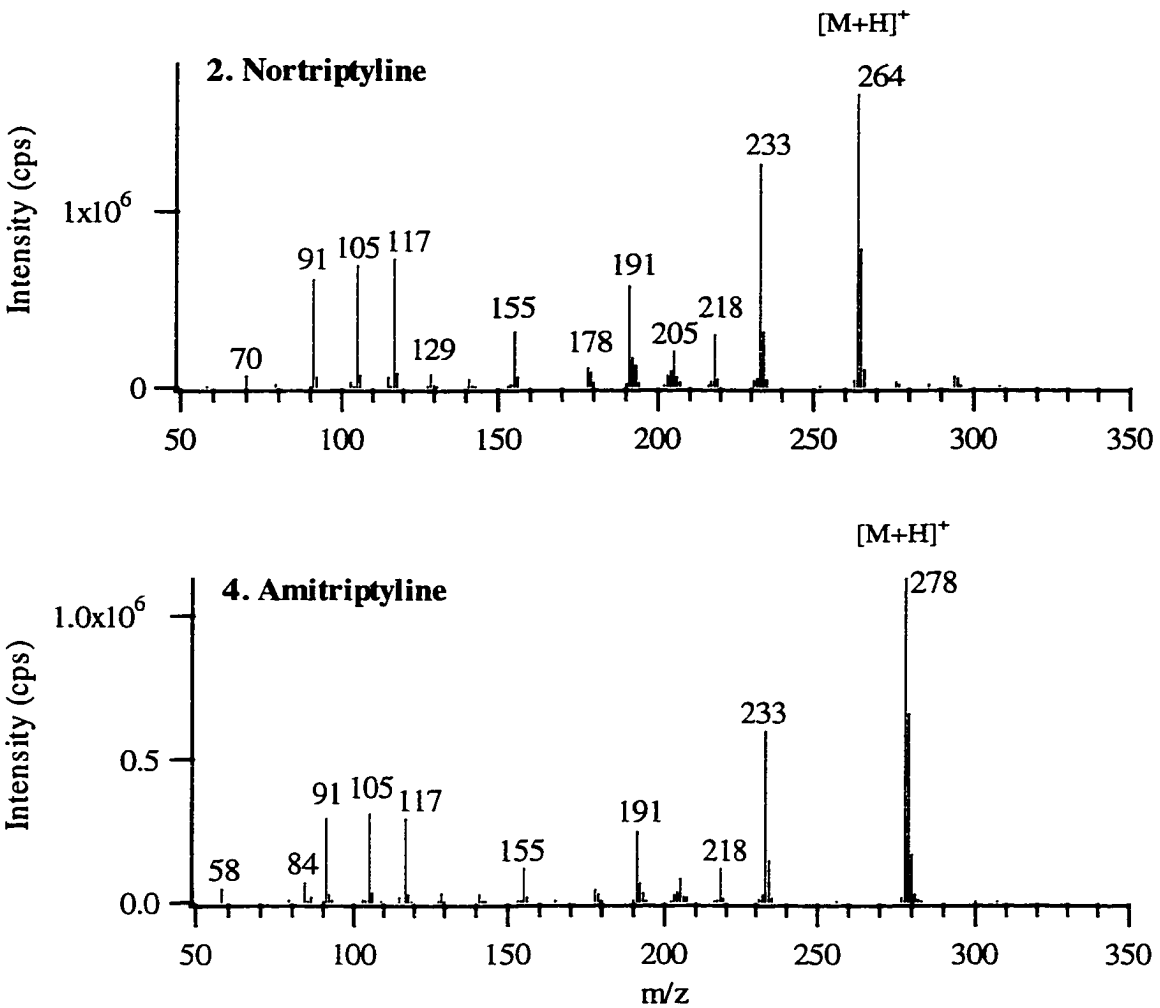

Figure 2.13. (cont'd)

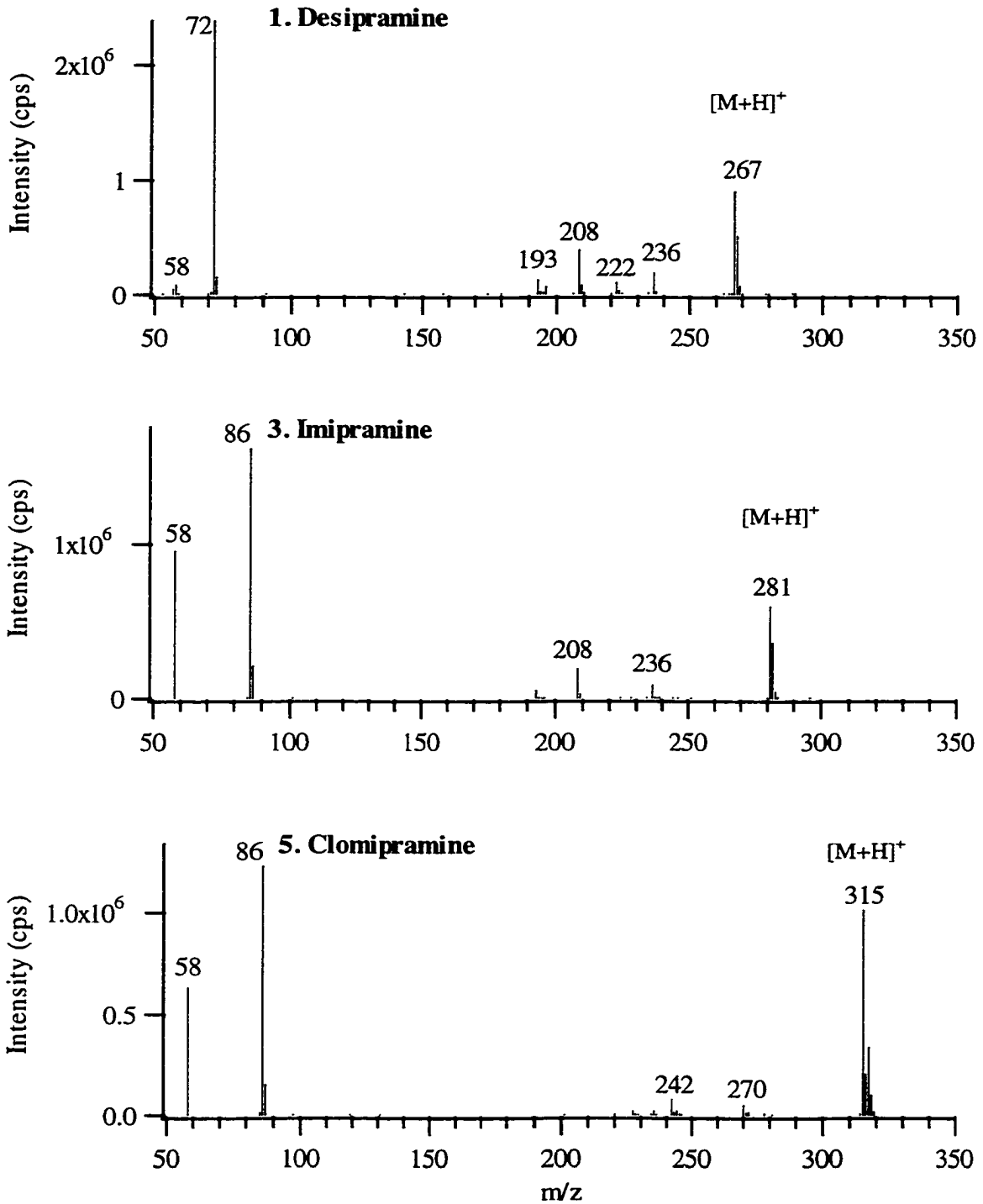

Figure 2.14. Proposed ESI-MS fragmentation pathways of tricyclic antidepressants and metabolites.

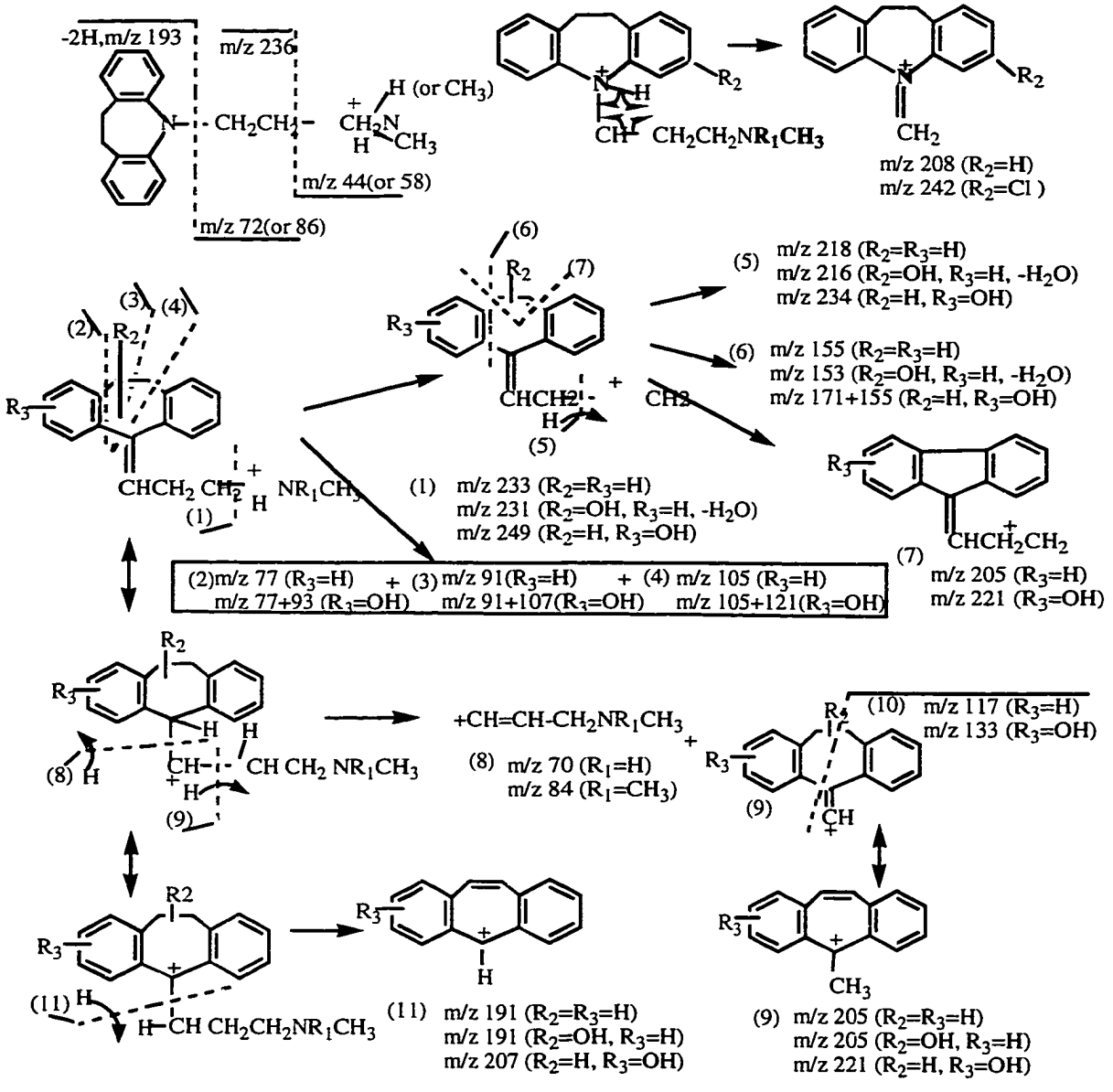

Figure 2.15. CE-ESI-MS profiles of AMI and its metabolites.

The separation was performed at 25 kV in a 50 mM ammonium acetate buffer prepared in methanol-acetonitrile (85:15). The current was 17 μA. Sample dissolved in 10% (v/v) buffer. Injection was performed at 20 kV for 10 s and a current of 13 μA. The nebulizing gas was set at 0.26 L/min (NEB 2). Other conditions were as described in the experimental section. The peak identification is as in **Table 1.** The insert is the selected ion electropherogram at the indicated masses. (A) 10 mg dosed extracts; (B) 5 mg dosed extracts; (C) 10 μM mixture of five antidepressants.

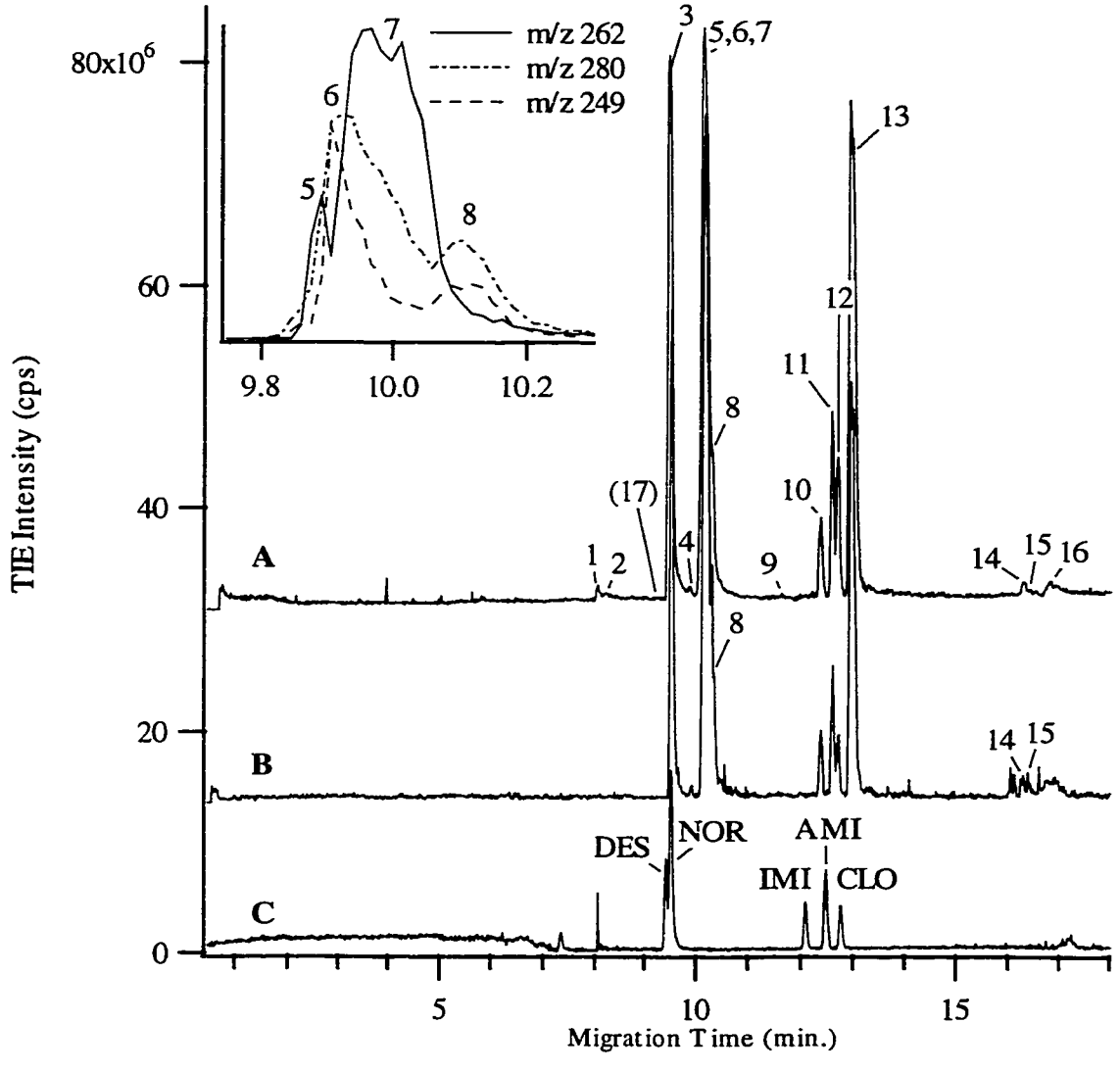

amitriptyline, and 16 new compounds were detected in both extracts that were not observed in the controlled and blank samples. The CE-ESI-MS data are summarized in **Table 2.1**. Based on the comparison of migration times with standards and the interpretation of their spectra, the metabolites could be tentatively identified as demethylated and/or hydroxylated products of amitriptyline. Peak 3, for example, was confirmed as a demethylated metabolite, nortriptyline, by comparing its migration time and spectrum with NOR standard, and by a mass loss of 14 in protonated molecular ion compared to amitriptyline.

Peak 11 was identified as a hydroxylated product of AMI by investigating its abundant protonated molecular ion at m/z 294. The mass spectrum did not permit us to specify the exact position of the hydroxyl group; however, it could be localized in the tricyclic moiety by the appearance of peaks at m/z 58 and 84 of the tertiary amines. Furthermore, the existence of a base peak at m/z 276 indicated that a loss of H_2O from the protonated molecular ion was facile, reflecting the fact that the hydroxyl group was on either carbon 10 or carbon 11. The appearance of peaks at m/z 231, 216, 205, 191 and 153, which were well elucidated from fragmentation patterns, also support this assumption. Peak 9 gave a similar spectrum to peak 11 but more ions existed. Its structure could not be confirmed because of its low concentration.

Peak 12, on the other hand, represented another kind of hydroxylated metabolite. Its spectrum indicated that it was not a 10- or 11-OH-amitriptyline due to the absence of m/z 276; a mass loss of 18 would not be facile. However, the presence of m/z 249 suggested that the OH group was on the aromatic ring, and could be either on carbon 2 or carbon 3. Ions at m/z 234, 221, 207, 155 plus 171, and 133 supported this conclusion.

Table 2.1. CE-ESI-MS data of amitriptyline and its metabolites.

* Data from another run with higher stacking effect. See Figure 1 for ring numbering scheme of amitriptyline. MT: migration time. %: relative abundance.

Peak No.	Compound	MT (min)	$[M+H]^+$ (%)	Characteristic ions (%)
1	Met-1	7.88	?	342(34), 308(6), 294(5), 276(13), 249(6), 231(100), 216(65), 153(3), 58(30)
2	Met-2	8.04	?	342(76), 308(20), 294(69), 276(18), 249(6), 231(100), 221(35), 216(77), 207(28), 153(3), 107(28), 58(41)
3	Nortriptyline (NOR)	9.27	264(100)	233(96), 218(36), 205(26), 191(57), 178(15), 155(33), 117(68), 105(66), 91(60), 70(10)
4	N-Oxide-NOR	9.72	280(45)	264(89), 233(27), 219(100), 191(23), 155(9), 117(24), 105(31), 91(10), 44(54)
5	10(or 11)-OH-NOR	9.87	280(29)	262(93), 231(100), 216(86), 205(16), 191(38), 153(11), 133(5), 115(6), 70(11), 44(8)
6	2(or 3)-OH-NOR	9.92	280(83)	249(86), 234(31), 221(26), 207(46), 171(13), 155(41), 133(33), 121(57), 117(24), 107(57), 105(40), 91(23), 70(4), 44(4)
7	10(or 11)-OH-NOR	10.02	280(26)	262(93), 231(100), 216(93), 205(23), 191(44), 153(15), 115(10), 70(15), 44(17)
8	3(or 2)-OH-NOR	10.13	280(100)	249(71), 234(18), 221(18), 207(52), 171(7), 155(18), 133(25), 121(29), 117(14), 107(34), 105(21), 91(8), 70(17), 44(3)

Table 2.1. (cont'd)

Peak No.	Compound	MT (min)	$[M+H]^+$ (%)	Characteristic ions (%)
9	Met-9	11.44	294(34)	276(100), 231(14), 217(8), 215(16), 185(34), 153(22), 105(5), 84(33), 58(61)
10	Amitriptyline (AMI)	12.19	278(100)	233(67), 218(18), 205(13), 191(30), 178(7), 155(16), 117(45), 105(42), 91(33), 84(10), 58(5)
11	10(or 11)-OH-AMI	12.37	294(48)	276(100), 231(86), 216(64), 205(23), 191(27), 153(8), 117(8), 115(7), 107(4), 91(4), 84(15), 58(48)
12	2(or 3)-OH-AMI	12.51	294(100)	249(64), 234(15), 221(13), 207(21), 171(5), 155(18), 133(17), 121(26), 117(11), 107(24), 105(18), 91(10), 84(6), 58(8)
13	11(or 10)-OH-AMI	12.78	294(57)	276(100), 231(94), 216(78), 205(31), 191(35), 153(12), 133(3), 117(8), 115(8), 107(3), 91(3), 84(20), 58(65)
14	N-Oxide-AMI	16.11	294(52)	278(5), 233(100), 218(12), 205(13), 191(22), 155(13), 117(35), 105(32), 91(29), 55(7), 45(8), 588(13), 316(10)
15	Dihydroxyl-AMI	16.24	310(69)	292(26), 231(100), 216(60), 185(27), 171(24), 115(20), 93(53), 58(35)
16	Met-16	16.66	?	344(64), 304(74), 262(34), 231(100), 216(33), 191(32), 172(11), 153(8), 105(9), 86(16), 45(29)
*17	Met-17	~9.0	250(73)	233(100), 218(30), 191(43), 155(8), 117(40), 105(41), 91(36)

Peaks 5,6,7 and 8 comigrated on the basis of their SIM profiles (insert in **Figure 2.15**). They were characterized by examining either m/z 262 ($[M+H]^+$ - 18) or m/z 249 ($[M+H]^+$ - HNR_1CH_3 + 16), and by examining either m/z 231, 216, 153 or m/z 234, 221, 155.

Peak 4 and peak 14 may be *N*-oxidized products because of the presence of ($[M+H]^+$ - 16) and ($[M+H]^+$ - 61) and the absence of m/z 84 plus 58, or m/z 70 plus 44, and the similarity of other fragments to nortriptyline (peak 4 *vs.* peak 3) or to amitriptyline (peak 14 *vs.* peak 10).

As for the di-OH-amitriptyline, peak 15, the precise positions of two OH- groups have not been determined. Mass spectra of peaks 1, 2 and 16 were related to that of the above-mentioned metabolites, but their identification needs further investigation.

Peak 17 appeared only in the profiles of much higher injection amounts (more stacking effects). Its spectrum indicated that it could be a demethylated nortriptyline.

2.5 CONCLUSION

Nonaqueous CE was coupled with ESI-MS using a commercial ion spray interface to profile tricyclic antidepressants of similar structures and mass-to-charge ratios. Pure methanol generates stable ion spray for the nonaqueous CE separation. Once optimized, the system generated detection limits of sub-femtomole of metabolites injected onto the capillary. More importantly, the ESI spectra of the tricyclic antidepressants provide valuable structural information for the identification of the compounds and their metabolites produced by the fungus *Cunninghamella elegans.* Sixteen metabolites were detected and most of them were tentatively identified as demethylated and/or hydroxylated and/or *N*-oxidized products. In this work, the exact position of OH group on

the aromatic ring of the TCAs has not been confirmed using the single quadrupole mass spectrometer. CE-MS-MS with more detailed structural information should be employed for further confirmation.

2.6 BIBLIOGRAPHY

(1) Feighner, J.P. *J. Clin. Psychiatry* **1999**, *60 Suppl. 22,* 18-22.

(2) Williams J.W., Jr.; Mulrow, C.D.; Chiquette, E.; Noel, P.H.; Aguilar, C.; Cornell, J. *Ann. Internal Med.* **2000**, *132*, 743-756.

(3) Sanchez, C.; Hyttel, J. *Cell. Mol. Neurobiol.* **1999**, *19*, 467-489.

(4) Moller, H.J. *J. Clin. Psychiatry.* **2000**, *61 Suppl. 6,* 24-28.

(5) Henry, J.A. *Drug Saf.* **1997**, *16*, 374-390.

(6) Edelbroek, P.M.; Zitman, F.G.; Schreuder, J.N.; Rooymans, H.G.; de Wolff, F.A. *Clin. Pharmacol. Ther.* **1984**, *31*, 467-473.

(7) Hyttel, J.; Christensen, H.J.; Fjalland, B.A.V. *Acta Pharmacol. Toxicol.* **1980**, *47*, 53-57.

(8) Bertilsson, L.; Mellstrom, B.; Sjoquist, F. *Life Sci.* **1979**, *25*, 1285-1292.

(9) Meola, J.M.; Rosano, T.G.; Swift, T. *Clin. Chem.* **1981**, *27*, 1254-1255.

(10) Roberts, G.M.; Hann, C.S. *Biomed. Chromatogr.* **1986**, *1*, 49-52.

(11) Orsulak, P.J.; Haven, M.C.; Burton, M.E.; Akers, L.C. *Clin. Chem.* **1989**, *35*, 1318-1325.

(12) Swartz, M.E.; Brown, P.R. *Chirality* **1996**, *8*, 67-76.

(13) Sutfin, T.A.; D'Ambrosio, R.; Jusko, W.J. *Clin. Chem.* **1984**, *30*, 471-474.

(14) Labrosse, K.R.; McLoy, H.G. *Clin. Chem.* **1988**, *34*, 859-862.

(15) Minder, E.I.; Schaubhut, R.; Minder, C.E.; Vonderschmitt, D.J. *J. Chromatogr.* **1987**, *419*, 135-154.

(16) Hartter, S.; Hiemke, C. *J. Chromatogr.* **1992**, *578*, 273-282.

(17) Moors, M.; Massart, D.L. *J. Pharm. & Biomed. Anal.* **1991**, *9*, 129-139.

(18) Sasaki, Y.; Baba, S. *J. Chromatogr.* **1988**, *426*, 93-101.

(19) Maurer, H.H. *J. Chromatogr.* **1992**, *580*, 3-41.

(20) Maurer, H.H.; Pfleger, K. *J. Chromatogr.* **1984**, *305*, 309-323.

(21) Baker, G.B.; Coutts, R.T.; Holt, A. *J. Pharm. & Toxic. Methods*, **1994**, *31*, 141-148.

(22) Zhang, D.L.; Evans, F.E.; Freeman, J.P.; Duhart Jr., B.; Cerniglia, C.E. *Drug Met. & Disp.* **1995**, *23*, 1417-1425.

(23) Breger-Pfatt, U.; Prox, A.; Wachsmuth, H.; Yao, P.P. *Drug Met. & Disp.* **1987**, *15*, 882-889.

(24) Baier-Weber, B.; Prox, A.; Breger-Pfatt, U. *Drug Met. & Disp.* **1988**, *16*, 490-496.

(25) Breger-Pfatt, U.; Becher, B.; Nusser, E.; Nill, K.; Baier-Weber, B.; Zaunbrecher, D.; Prox, A. *Xenobiotica* **1990**, *20*, 727-738.

(26) Lehman, J.P.; Fenselau, C.; Depanlo, J.R. *Drug Met. & Disp.* **1983**, *11*, 221-225.

(27) Artigas, F.; Gelpi, E. *J. Chromatogr.* **1987**, *394*, 123-134.

(28) Mikkers, F.; Everaerts, F.M.; Verheggen, T. *J. Chromatogr.* **1979**, *169*, 11-20.

(29) Jorgenson, J.W.; Lukacs, K.D. *Science* **1984**, *222*, 266-272.

(30) Tomlinson, A.J.; Benson, L.M.; Naylor, S. *J. High Resolut. Chromatogr.* **1994**, *17*, 175-186.

(31) Tomlinson, A.J.; Benson, L.M.; Gorrod, J.W.; Naylor, S. *J. Chromatogr. B*, **1994**, 657, 373-381.

(32) Benson, L.M.; Tomlinson, A.J.; Reid, J.M.; Walker, D.L.; Ames, M.M.; Naylor, S.J. *J. High Resolut. Chromatogr.* **1993**, *16*, 324-326.

(33) Sahota, R.S.; Khaledi, M.G. *Anal. Chem.* **1994**, *66*, 1141-1146.

(34) Ng, C.L.; Lee, H.K.; Li, S.F.Y. *J. Liquid Chromatogr.* **1994**, *17*, 3847-3857.

(35) Bjornsdottir, I.; Hansen, S.H. *J. Chromatogr. A*, **1995**, *711*, 313-322.

(36) Tomlinson, A.J.; Benson, L.M.; Naylor, S. *Am. Lab.* **1994**, *26*, 29-33.

(37) Olivares, J.A.; Nguyen, N.T.; Yonker, C.R.; Smith, R.D. *Anal. Chem.* **1987**, *59*, 1230-1232.

(38) Sheppard, R.L.; Tong, X.; Cai, J.; Henion, J.D. *Anal Chem.* **1995**, *67*, 2054-2060.

(39) Lord, G.A.; Gordon, D.B.; Tetler, L.W.; Carr, C.M. *J. Chromatogr. A*, **1995**, *700*, 27-32.

(40) Kelly, J.F.; Locke, S.J.; Ramaley, L.; Thibault, P. *J. Chromatogr. A*, **1996**, *720*, 409-427.

(41) Banks, J.F. *Electrophoresis* **1997**, *18*, 2255-2266.

(42) Foret, F.; Thompson, T.J.; Vouros, P.; Karger, B.L.; Gebauer, P.; Bocek, P. *Anal. Chem.* **1994**, *66*, 4450-4458.

(43) Salomon, K.; Burgi, D.; Helmer, J.C. *J. Chromatogr.* **1991**, *549*, 375-385.

(44) Clark, B.J.; Barker, P.; Large, T. *J. Pharm. & Biomed. Anal.* **1992**, *10*, 723-726.

(45) Spencer, B.J.; Zhang, W.B.; Purdy, W.C. *Electrophoresis* **1997**, *18*, 736-744.

(46) Lu, W.; Poon, G.K.; Carmichael, P.L.; Cole, R.B. *Anal. Chem.* **1996**, *68*, 668-674.

(47) Varghese, J.; Cole, R.B. *J. Chromatogr. A*, **1993**, *652*, 369-376.

(48) Loo, R.R.; Dales, N.; Andrews, P.C. *Protein Sci.* **1994**, *3*, 1975-1983.

(49) Coutts, R.T.; Foster, B.C.; Jones, G.R.: Meyers, G.E. *Appl. Environ. Microbiol.* **1997**, *37*, 429-432.

(50) Cerniglia, C.E.; Hansen, Jr., E.B.; Lambert, K.J.; Korfmacher, W.A.; Miller, D.W. *Xenobiotica* **1988**, *18*, 301-312.

(51) Zhang, D.; Evans, F.E.; Freeman, J.P.; Duhart, Jr., B.; Cerniglia, C.E. *Drug Metab. Dispos.* **1995**, *23*, 1417-1425.

(52) Hufford, C.D.; Capiton, G.A.; Clark, A.M.; Baker, J.K. *J. Pharm. Sci.* **1981**, *70*, 151-155.

(53) Yang, W.; Jiang, T.; Davis, P.J. *Xenobiotica* **1993**, *23*, 973-982.

(54) Smith, R.V.; Rosazza, J.P. in: Rozazza, J.P. (Ed.), *Microbial Transformation of Bioactive Compounds* Vol. II, CRC Press, Boca Raton, **1982**, pp 1-42.

(55) Hezari, M.; Davis, P.J. *Drug Metab. Dispos.* **1992**, *20*, 882-888.

(56) Bruin, G.J.M.; Chang, J.P.; Kuhlman, R.H.; Zegers, K.; Kraak, J.C.; Poppe, H. *J. Chromatogr.* **1989**, *471*, 429-436.

(57) Buzy, A.; Thibault, P.; Laycock, M.V. *J. Chromatogr. A*, **1994**, *688*, 301-306.

CHAPTER 3 [1,2]

Capillary Electrophoresis-Electrospray Mass Spectrometry of Nucleosides and Nucleotides: Application to Phosphorylation Studies of Anti-HIV Nucleosides *in Vitro*

[1] Part of this chapter has been presented at the 48th ASMS Conference on Mass Spectrometry and Allied Topics, Long Beach, CA, June 2000.
Liu, C.S.; Tan, W.; Huang, J.S.; Li, N.; Tyrrell, D.L.J.; Dovichi, N.J.

[2] A version of this chapter has been submitted for publication.
Liu, C.S.; Tan, W.; Huang, J.S.; Li, N.; Tyrrell, D.L.J.; Dovichi, N.J. 2000. Analytical Chemistry.

3.1 ABSTRACT

We report a capillary electrophoresis-electrospray ionization mass spectrometric (CE-ESI-MS) technique for the characterization and determination of antiretroviral dideoxynucleosides and their phosphorylated forms. A CE system for complete separation of most commonly used ddNs has been developed using basic pH conditions with a volatile electrolyte suitable for ESI-MS detection in an untreated capillary column. The separation of nucleotides has also been achieved using the same system. Positive and negative ionization modes were investigated and compared for sensitive and stable electrospray performance. A 14-compound mixture of dideoxynucleosides and nucleotides are well profiled in a single capillary zone electropherogram in less than 18 minutes with a distinct elution order: electro-osmotic flow, dideoxynucleosides, mononucleotides, dinucleotides, and trinucleotides. The fragmentation pathways of the nucleosides and nucleotides in ESI-MS have been interpreted. A 100-200 nM concentration limit of detection with an injection volume of 14 nanoliter is readily achieved. This technique has been used to detect naturally occurring nucleotides in a human hepatocyte (Hep G2) cell extract and applied to the studies of intracellular metabolism of lamivudine (3TC) in Hep G2. The parent compound, 3TC, and its phosphorylated forms, 3TC-monophosphate, 3TC-diphosphate and 3TC-triphosphate were detected after 10 hrs of incubation of 3TC with cells.

3.2 INTRODUCTION

Dideoxynucleosides (ddNs) have been shown to inhibit the replication of the human immunodeficiency virus (HIV), the aetiologic agent of the acquired immunodeficiency syndrome (AIDS). Several ddNs are currently being used as a treatment for HIV infection either by single or combination therapy of homo- and hetero-dimeric derivatives of ddNs for increased antiviral effects.[1-4] The development of analytical methodology for the intracellular characterization and determination of ddNs and their active phosphorylated forms in patients with AIDS, cancer, and related disorders has received increasing attention in the fields of cell biology, medicine, and biochemistry. High performance liquid chromatography (HPLC) of ddNs with UV detection[5-7] or radioactivity detection[3,8-11] has been commonly used. HPLC with radioactivity detection is very sensitive, but obviously entails the undesirable use of radioactive materials. HPLC coupled to electrospray ionization mass spectrometry (ESI-MS) has been developed for analyses of purine and pyrimidine nucleoside antiviral agents[12], DNA adducts[13], and naturally occurring nucleosides[14].

Several reports have detailed the use of capillary electrophoresis (CE) with UV detection for separation of a variety of naturally occurring nucleosides[15, 16]. Micellar electrokinetic capillary chromatography (MEKC) has also been used for the determination of azidothymidine triphosphate[17] or nucleosides[7]. On-column thermo-optical absorbance detection in capillary electrophoretic separations of various nucleosides and nucleotides mixtures in MEKC modes has also been demonstrated.[18] A dynamic pH junction in CE for improved focusing of nucleotides has been introduced to improve concentration sensitivity[19].

The use of CE has dramatically reduced sample requirements and shortened analysis times with high separation efficiency, the detection of labile polar biomolecules with mass spectrometry provides abundant structural information indispensable for unambiguous identification. In attempts to capitalize on the obvious advantages associated with the coupling of the two techniques, since 1989, several groups have investigated interfacing strategies and the application of the CE-MS technique to the analysis of biomolecules such as proteins,[20-25] peptides,[20,21,26-31] small drugs,[32-36] and DNA adducts.[37-43] A general consideration in CE-MS is the choice of the CE running buffer and the compatibility of the buffer with the electrospray process. While sodium borate and sodium carbonate buffers have been commonly used for CE separations of nucleosides and nucleotides, a more volatile buffer, such as ammonium carbonate[41] or ammonium acetate[43], is desirable for CE separation that can be readily employed with mass spectrometry detection.

The profiling of the antiretroviral ddNs and their corresponding nucleotides by CE-MS faces two immediate challenges. As the ddNs are uncharged in the pH region where they are stable, their separation by capillary zone electrophoresis (CZE) in a commonly used buffering system at a moderate pH is not possible. The addition of surfactants to the background electrolyte, such as the frequently used SDS in MEKC separation modes, or the use of complexation of ions with borate employed for the separation of naturally occurring nucleosides, is also difficult for on-line CE-MS analysis because of a severe ion suppression caused by the surfactant and the borate. Nucleotides, however, contain both acidic and basic functional groups which permit the CZE separation of these components under either acidic or basic pH conditions. Because of the ionization of the phosphate, mononucleotides bear negative charges over most of the pH range. Di- and tri-phosphate nucleotides have higher overall negative charges than monophosphates.

Geldart and Brown[15] accomplished the separation of nucleobases by CZE with sodium carbonate buffers. Deforce *et al.*[41] displayed partial separation of some DNA adducts by CE-MS with ammonium carbonate buffers. Zhao *et al.*[42] used an ammonium acetate buffer in the analysis of nucleotides by CE-ESI-MS. Finally Wolf and Vouros[43] used a similar buffer to analyze for DNA adducts by CE coupled to continuous flow fast atom bombardment (CF-FAB) MS. However, the characterization of both antiretroviral dideoxynucleosides and nucleotides within the same run by on-line coupled CE-MS has not been explored.

Another challenging aspect arises from the MS detection. ESI-MS analysis is commonly performed in positive ion mode for nucleosides and nucleobases for maximum sensitivity at neutral and basic pH,[12] In contrast, the presence of negatively charged phosphate groups in nucleotides and oligo-nucleotides would make these analytes well suited for MS detection in negative ionization mode. To cope with these considerations, a thorough understanding of the important influence of experimental conditions on ionization and dissociation of ddNs and nucleotides would be beneficial.

We report the separation of the most common antiretroviral ddNs using CZE with a volatile electrolyte at basic pH conditions suitable for ESI-MS detection in an untreated capillary column. The ddNs and the nucleotides with mono-, di- and tri-phosphate groups on the 5'- position of the ribose sugar are well resolved. Positive and negative ESI-MS ionization modes are investigated and compared for sensitive and stable electrospray performance. The method developed for standards is applied to studies of nucleotides in a cell extract and intracellular metabolism of lamivudine (3TC) in a human hepatoma cell line (Hep G2) is demonstrated.

3.3 EXPERIMENTAL SECTION

3.3.1 Chemicals

The ddNs studied were lamivudine (3TC), 2',3'-dideoxycytidine (ddC), 2',3'-dideoxyadenosine (ddA), stavudine (d4T), azidothymidine (AZT), 2',3'-dideoxyuridine (ddU), 2',3'-dideoxyinosine (ddI), and 2',3'-dideoxyguanosine (ddG) , which were purchased from Sigma (St. Louis, MO). Caffeine and all nucleotide standards were also obtained from Sigma. Their structures are shown in **Figure 3.1**. HPLC-grade methanol and ammonium hydroxide were purchased from BDH (Toronto, ON, Canada). Ammonium carbonate was purchased from ACP (Montreal, PQ, Canada). Ammonium acetate and sodium hydroxide were obtained from Anachemia (Montreal, PQ, Canada). All chemicals and reagents were used without further purification. Water was prepurified by a Nanopure II system (Barnstead, Dubuque, IA). Cell grown media and related compounds were from Life Technologies (Burlington, Canada). Stock solutions of ddNs and nucleotides were prepared initially in water at concentrations of 10^{-2} M of each analyte and stored at -20 °C. They were then mixed and further diluted with water or the CE running buffer prior to CE injection.

3.3.2 Apparatus

All experiments were performed using a PE/Sciex API 100 single quadrupole mass spectrometer equipped with an ion spray source (Thornhill, ON, Canada). CE was performed in an in-house built instrument using a Spellman high-voltage power supply (Plainview, NY).

Figure 3.1. Structures of dideoxynucleosides and nucleotides.

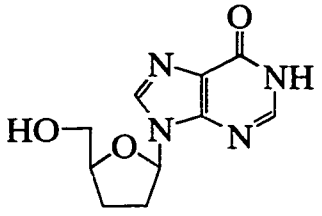

ddI
MW = 236.2

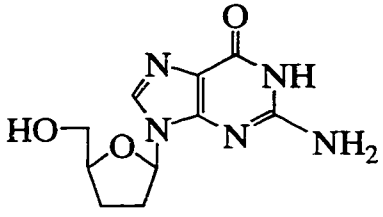

ddG
MW = 251.3

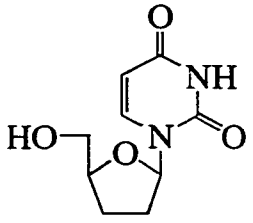

ddU
MW = 212.2

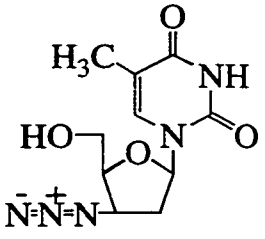

AZT
MW = 267.3

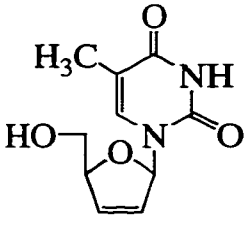

d4T
MW = 224.2

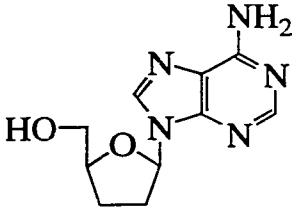

ddA
MW = 235.2

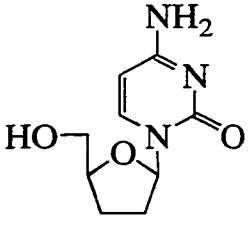

ddC
MW = 211.2

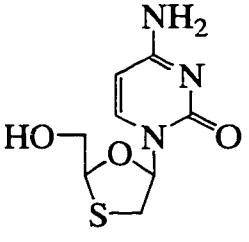

3TC
MW = 229.3

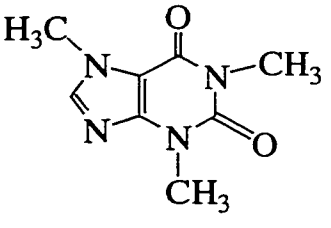

Caffeine
MW = 194.2

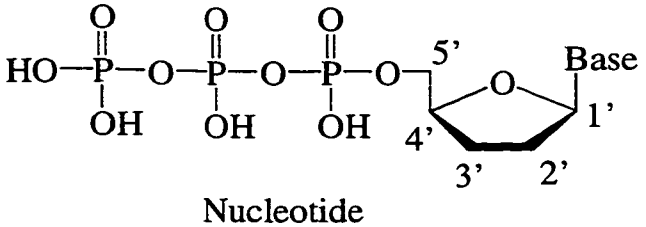

Nucleotide

3.3.3 Cell Preparation

The hepatoblastoma cell line (Hep G2) was purchased from the American Type Culture Collection (Rockville, MD). The monolayer cultures were grown in MEM supplemented with 750 mg/L sodium bicarbonate, 300 mg/L L-glutamine, 50 IU/ml penicillin G, 10 μg/mL streptomycin sulfate and 10% fetal calf serum in a 75-cm^2 flask containing 25 mL of medium until it reached approximately 80% confluency. The cells were trypsinized, counted and seeded at a density of 3 x 10^{-6} cells in per 60-mm tissue culture dish.

3.3.4 Intracellular Phosphorylation of 3TC by Isolated Hep G2

After the cell cultures reached confluency, cells were treated with medium containing 100 μM 3TC and incubated at 37 °C for various time periods. At the appropriate times, the incubation medium was removed and the cells were washed three times with excess phosphate buffered saline (PBS), pH 7.4. Washed cells were lysed and extracted by the addition of 2 mL of 60% methanol, followed by an overnight vortexing and a 1-min sonication at 4 °C. The extracts were then ultra-filtered through a Centricon YM-3 filter (Amicon, Oakville, ON, Canada) at 6000 *g* for 24 hrs at 10 °C. The filtrates were evaporated with a vacuum concentrator (SpeedVac, Savant, Farmingdale, NY) for 4 hrs. The residues were then injected directly for CE-MS analysis.

3.3.5 Preparation of Blank Hep G2Cell Extract

Cell pellets of about 4.1 x 10^6 cells per plate were lysed and extracted with 2 mL of 60% methanol, the extracts were ultra-filtered and stored at -20 °C until analysis.

3.3.6 CE Separations

Untreated fused-silica capillaries (Polymicro Technologies, Phoenix, AZ, USA) of 60-cm x 50 μm ID x 150 μm OD were used for separations of ddNs and nucleotides. Both ends of the column were cut flat and ~ 1 mm of polyimide protective coating was removed with a fiber optic splicer (Orionics, Bozeman, MT). The separation background electrolytes (BGE) were prepared by dissolving the ammonium carbonate or the ammonium acetate in water to an appropriate concentration (15-50 mM) and adjusted to a pH of 10.0 by the same concentrated ammonium hydroxide. A new capillary column was flushed with 0.1 M sodium hydroxide (NaOH) for 5 minutes followed by the BGE for another 5 minutes. Fresh BGE was used to flush the capillary before and between runs. The ESI sprayer tip was moved away from the center of the interface during these flushing procedures to prevent any liquid from entering the sampling orifice. The sample was hydrostatically introduced by raising the injection end of the column with a height of 18-cm above the detection end for 30 s, or was electrokinetically injected at 10 kV for 10 s for comparison studies. The separations were performed at 200-230 V/cm electrical field across the column at room temperature.

3.3.7 ESI MS Detection

The CE column was coupled with the ESI interface using a coaxial sheath configuration. Briefly, the fused silica capillary column was inserted inside the 13-cm long stainless steel electrode (0.2 mm ID and 0.4 mm OD) until the column exit was seen. The column was then pulled back 1-mm with reference to the electrode. The electrode was used as a sheath tube and the ESI sprayer. The electrode was then inserted into the nebulizing gas tube with 1-mm protruding out. The injection end and the sprayer tip were positioned at the same height to avoid siphoning. A sheath liquid of pure

methanol was delivered at 2.0 μL/min using a syringe pump from Harvard Apparatus (South Natick, MA) through a sheath capillary (60 cm x 50 μm ID x 150 μm OD) connected to the electrode with a stainless tee (Valco Instruments, Houston, TX). The optimized sprayer position was adjusted three dimensionally for a maximum sensitivities of each analyte when a mixture of 10^{-4} M of ddG, dGMP, GDP and GTP in the BGE was infused using a syringe pump through the CE column at a flow rate of 160 nL/min. This flow rate was the same as the electro-osmotic flow (EOF) calculated from the migration of caffeine in a typical CE separation. An alternate way to optimize the sprayer position was to tune for a maximum sensitivity while continuously injecting the same mixture under a normal CE-MS separation condition, e.g. a 230 V/cm electrical field applied across the capillary. In both cases, the sheath flow was fixed at 2.0 μL/min methanol. Generally, the sprayer tip was positioned 12 mm from the curtain plate (X-axis), 6 mm from the center of the ion transmission axis (Y-axis) and 0 mm from the center of the Z (vertical)-axis. The sprayer axis was shaped to an angle at 45° on the XY plane. The potentials applied onto the ion sprayer (IS), the orifice (OR), the focusing ring (RNG) and other devices for ion transmission were optimized by adjusting these parameters for maximum sensitivities of the pseudo-molecular ions and major fragments of ddG, dGMP, GDP and GTP. When positive mode ESI was performed, the selected voltages applied to IS, OR, and RNG were 3800 V, 35 V and 250 V, respectively. While in negative mode, they were -3600 V, -35 V and -220 V, respectively. The nebulizing gas flow rate and the curtain gas flow rate were set to 0.41 L/min (NEB 3) and 1.0 L/min (CUR 9), respectively. During sample injection, the ion spray voltage and the nebulizing gas flow were turned off. In a full scan mode the quadrupole analyzer was scanned across a mass range of 105-600 m/z at a scanning speed of 0.99 s/cycle. In selected ion monitoring (SIM) conditions, a single mass or a selected narrow range of multiple ions were scanned

with a mass interval of 0.1 amu. The CE-MS data were acquired by LCTune software (Sciex) and processed by MultiView (Sciex) and IgorPro (WaveMetrics, Inc., Lake Oswego, OR) softwares.

3.4 RESULTS AND DISCUSSION

3.4.1 Separation of ddNs

The pKa values for the standards of ddNs are not known. Therefore the pKa values of the naturally occurring nucleosides[44] were employed as the starting point of separation study. It is believed that very little of the overall pKa value is due to the ribose portion of the nucleoside molecule, and that there are very small differences in the pKa values between the nucleosides and ddNs. For example, the pKa values of dU and U are 9.3 and 9.2, respectively (**Table 3.1**) and similarly, dT and T have a pKa of 9.8 and 9.7, respectively, with only 0.1 unit difference between ribonucleosides and deoxyribonucleosides. One could rationalize that the pKa value for ddU is approximately 9.4 and that for d4T is estimated to be 9.9. The pKa differences among ddNs provide the basis for separation of ddNs by CZE in a buffer with a basic pH. The buffer pH plays a significant role in CZE selectivity and resolution as it determines the ionic charge and thus the electrophoretic mobility of each ddN. As shown in **Figure 3.2** the efficient separation of ddNs was obtained at a pH optimum of 10.0. The 3TC, ddC and ddA have an estimated pKa value of larger than 12.5. according to the well-known Henderson-Hasselbalch equation for acid HA:

$$pH = pKa - \log(1/\alpha - 1) \quad (3.1)$$

$$\alpha = [A^-]/[HA]_0 \quad (3.2)$$

Table 3.1. pKa values of ribosenucleosides and deoxyribosenucleosides.[45]

Compound	pKa
Adenosine (A)	12.5
Cytidine (C)	12.5
Deoxycytidine (dC)	>13
Guanosine (G)	9.2, 12.4
Inosine (I)	8.8, 12.3
Uridine (U)	9.2, 12.5
Deoxyuridine (dU)	9.3, >13
5-Methyluridine (T)	9.7
Thymidine (dT)	9.8, >13

Figure 3.2. Total ion electropherograms of ddNs showing the effect of BGE pH on separation of ddNs with positive ESI-MS detection.

The BGE was (A) 50 mM ammonium carbonate or (B) 50 mM ammonium acetate adjusted to a desired pH by ammonia. Analytes were 1.0 mM each in water and hydrostatically injected at 18-cm for 10 s. CZE separations were performed at 180 V/cm. The ionspray was operated at +4.1 kV, the orifice and the ring focusing potentials were +30 V and +250 V, respectively. The quadrupole mass analyzer was scanned at a speed of 0.59 s/cycle over a mass range of m/z 105-300. Peak orders: (1) 3TC, (2) ddC, (3) ddA, (4) d4T, (5) AZT, (6) ddU, (7) ddI. Other conditions were as described in the experimental section.

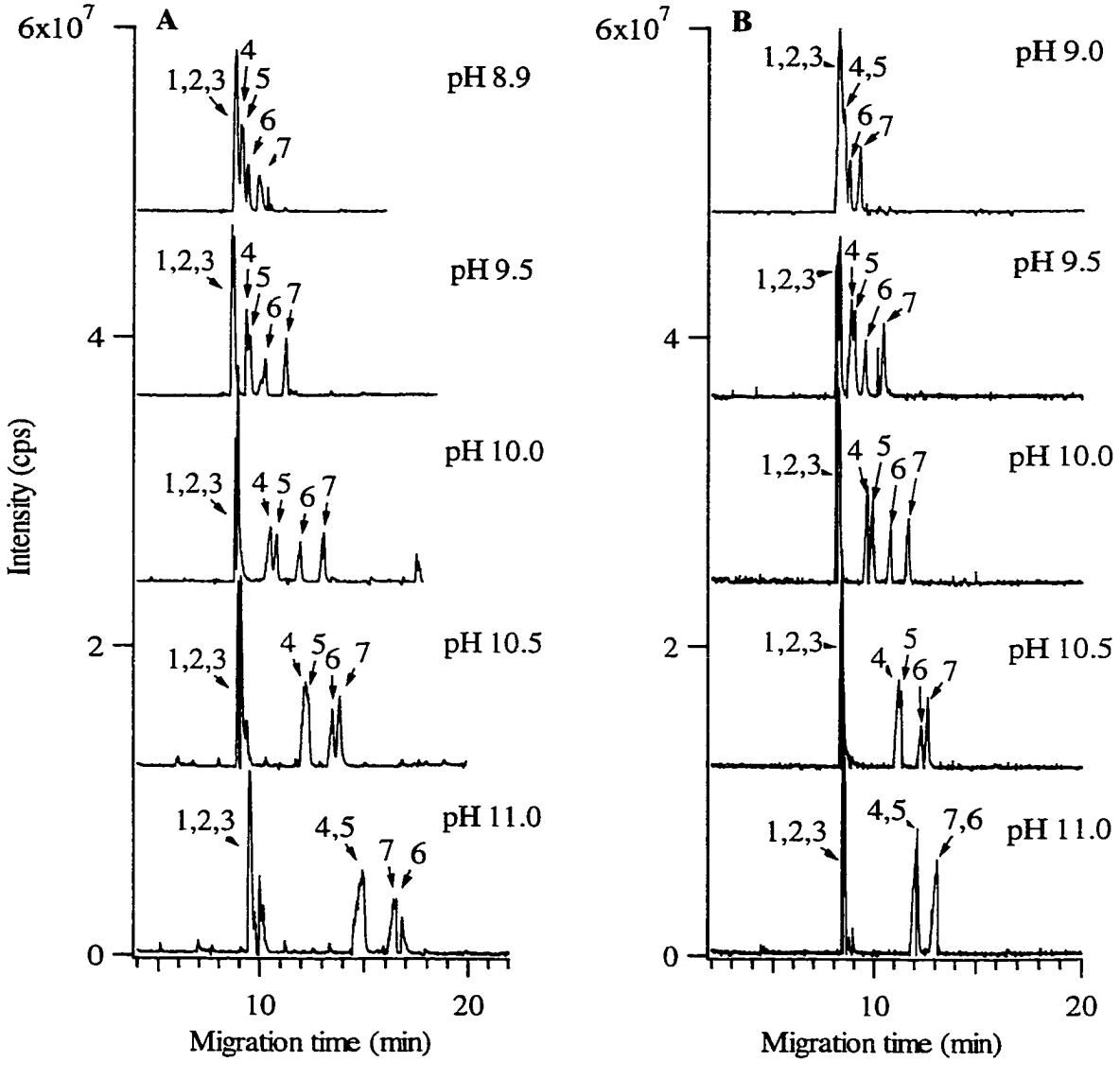

where α is the dissociation ratio of HA, $[A^-]$ is the final concentration of the conjugate base, and $[HA]_0$ is the initial concentration of the acid. The overall dissociation of the three compounds in a solution at a pH of less than 11 would be very minimal and they would co-migrate with the electro-osmotic flow (EOF). Caffeine was used as the EOF marker in these separations. It has been previously employed as the EOF marker for the separation of nucleobases.[15] Compared with that in the ammonium acetate buffer, the prolonged migration time of ddNs in the ammonium carbonate buffer was due to the slower EOF caused by the higher ionic strength of the carbonate electrolyte. Ammonium acetate was chosen as the BGE for the following studies.

The influence of the BGE concentration on separation and migration of ddNs is depicted in **Figure 3.3**. As the BGE concentration increases, the EOF and the migration of ddNs become slower, the separations, especially of d4T/AZT, ddG/ddU, become better. To have an appropriate resolution and analysis time, a 25 mM BGE should be chosen.

3.4.2 Positive ESI-MS Detection for ddNs

In an on-line CE-MS analysis with positive ESI-MS detection, the ddNs gave rise to H^+, Na^+ and K^+ adducts of the molecular ions. The base peak in the spectra is the base fragments (BH_2^+) formed by the cleavage of the glycosidic bond. Cluster ions formed by aggregation of ddNs, such as dimers, trimers, tetramers and so on are also observed, **Figure 3.4**. More cluster ions formed at higher concentrations of analyte. The mechanism governing the formation of aggregated species in the gas phase is complex and not well understood.[14,45,46]

Figure 3.3. Mass electropherograms showing the effects of BGE concentration on separation and migration of ddNs.

BGE was (A) 15 mM (B) 25 mM and (C) 50 mM ammonium acetate at pH 10.0. Samples were 100 μM in corresponding BGE and hydrodynamically injected at 18 cm for 30 s. Positive ESI-MS was operated. Other conditions were as described in the experimental section.

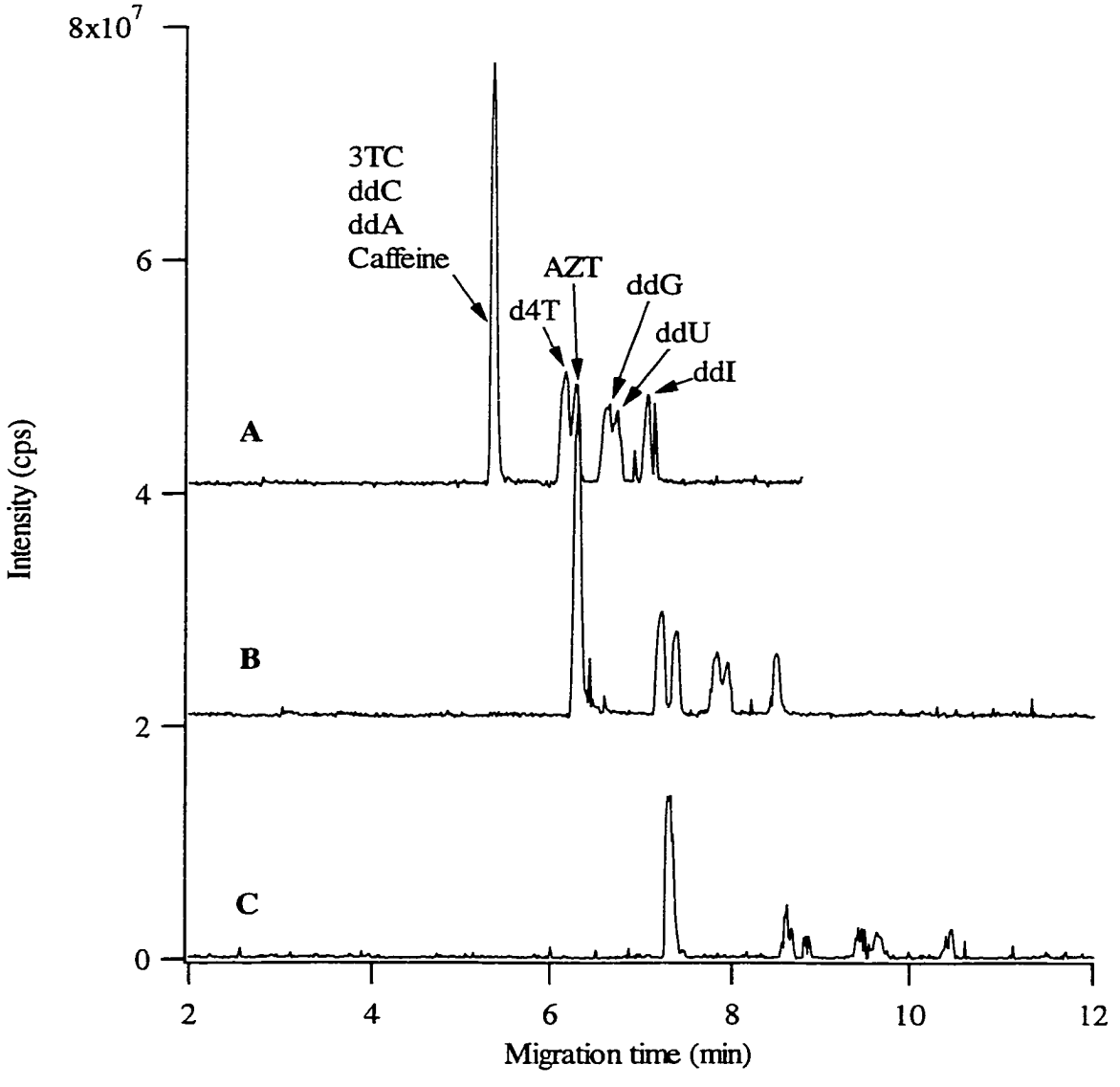

Figure 3.4. Positive ESI mass spectra of ddNs separated by CE-MS.

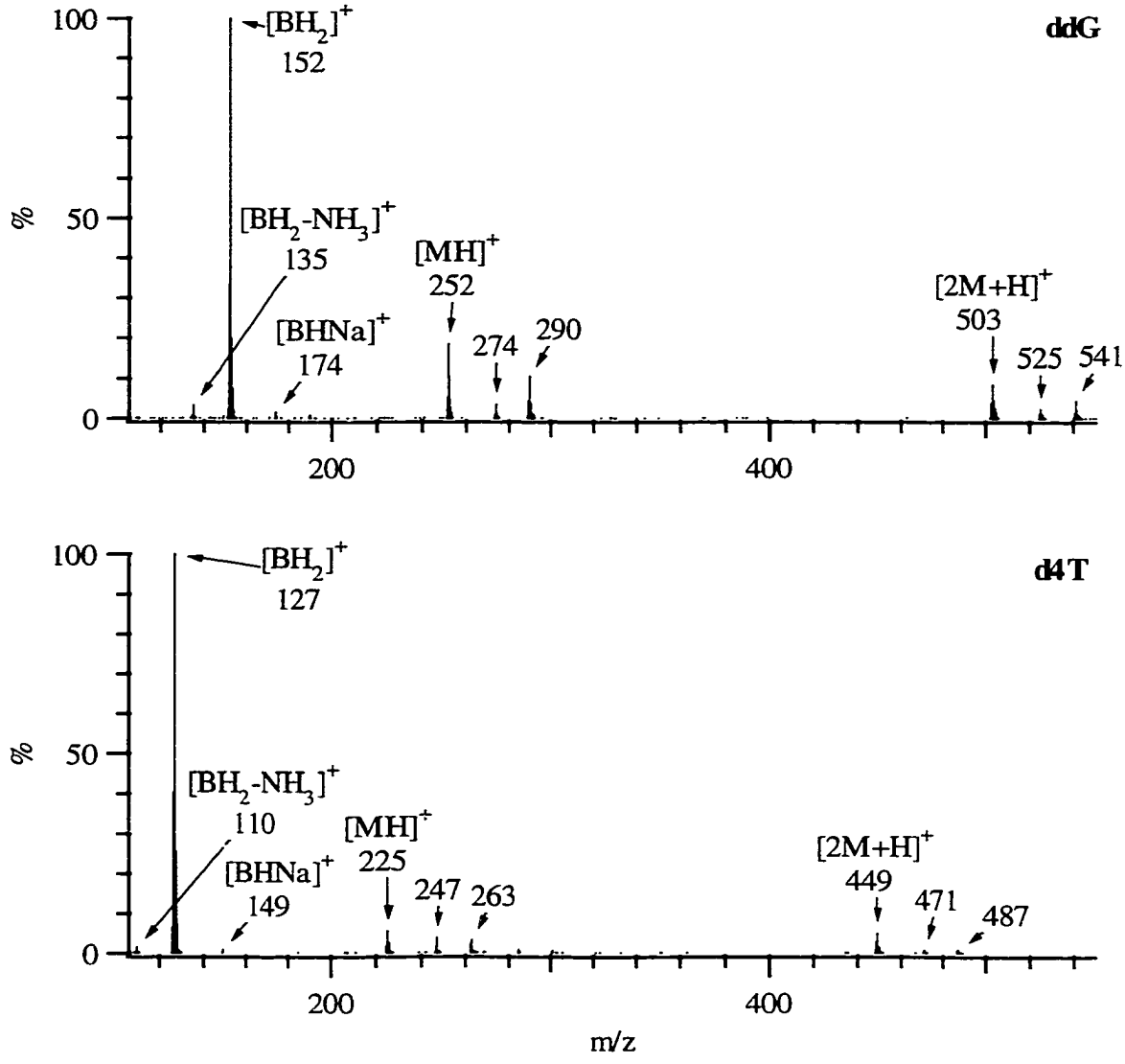

In addition to its effect on CE separation of the analytes, the CE BGE concentration has also a substantial influence on detection sensitivity of ddNs, **Figure 3.3**. The maximum ESI-MS sensitivity and the best baseline stability were obtained at a CE BGE of 25 mM or less of ammonium acetate. When BGE concentration was increased up to 50 mM, large spikes appeared in the baseline and in the peaks of the electropherogram. Frontal electrophoresis obtained from ddNs dissolved in BGE at different concentrations verified that the sensitive and stable signals were achieved when a BGE with 25 mM or less was used (**Figure 3.5**). Since the resolution of ddNs was poorer when the BGE concentration was less than 25 mM, the 25 mM BGE was used for the following studies.

3.4.3 Analyte Discrimination in CE Injection

The choice of injection method, electrokinetic or hydrostatic, has a great influence on discrimination of analyte introduced onto the capillary column during the injection process. Specifically, for an equimolar mixture of ddNs prepared in a BGE, the injected amount of ddNs with a low pKa by the electrokinetic method is less than that with a high pKa. The overall negative charge on an analyte with a lower pKa is larger, its electrophoretic mobility toward the anode (injection end) is higher, and therefore fewer molecules will migrate into the capillary under high positive electrical field. This uneven loading is especially serious when analytes are dissolved in a low conductivity buffer or even water (**Figure 3.6**). With this consideration in mind, the following experiments were performed using the hydrostatic injection method. However, as revealed in the **Figure 3.6**, a much sharper peak shape was obtained in the mass electropherogram with electrokinetic injection. Hydrodynamic flow introduces laminar flow that causes extra-column band broadening.

Figure 3.5. Frontal electropherograms of 3 ddNs in (A) 25 mM (B) 50 mM ammonium acetate BGE obtained by continuous electrokinetic infusion.

The electrical field applied across the CE column was 226 V/cm. Positive ESI-MS was operated. Other conditions were as described in the experimental section.

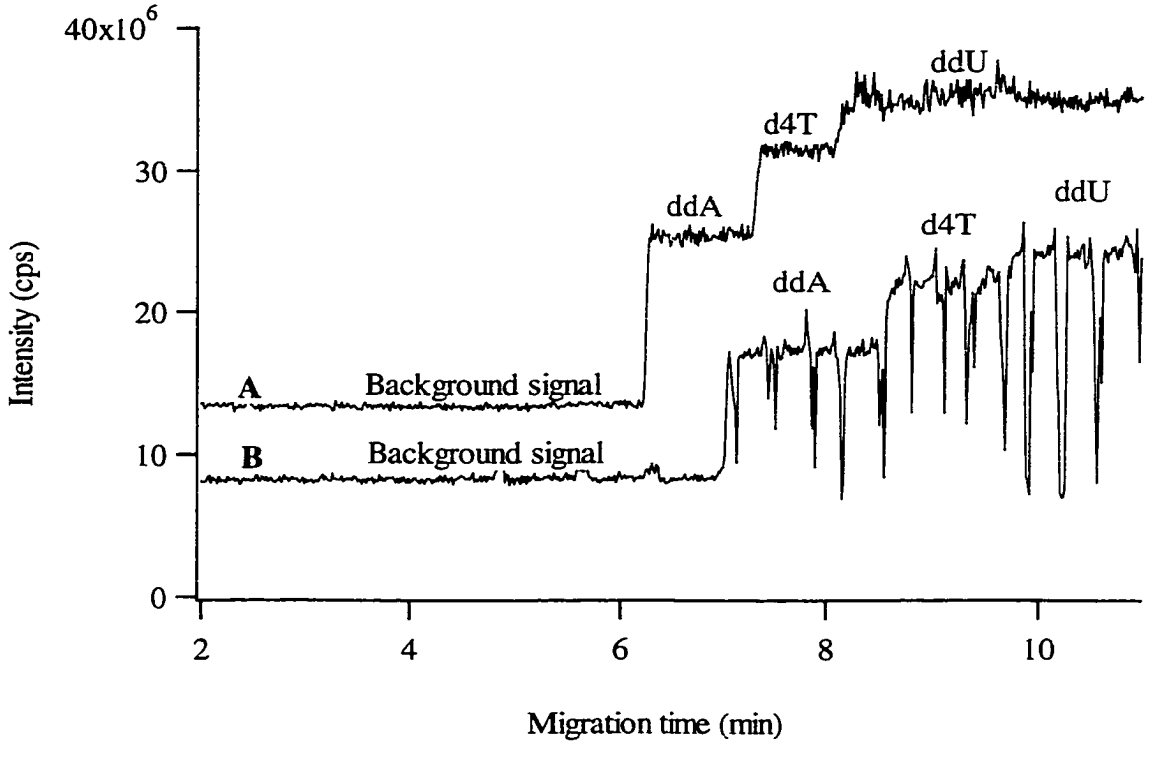

Figure 3.6. Mass electropherograms showing the discrimination of analytes during their injection process.

Samples were ddN mixture of 100 μM dissolved in (A) BGE or (B) water. Separations were made at 226 V/cm. Electrokinetic injection was made at 10 kV for 5 s; hydrodynamic injection was made at 18 cm for 30 s. Positive ESI-MS was operated. Other conditions were as described in the experimental section.

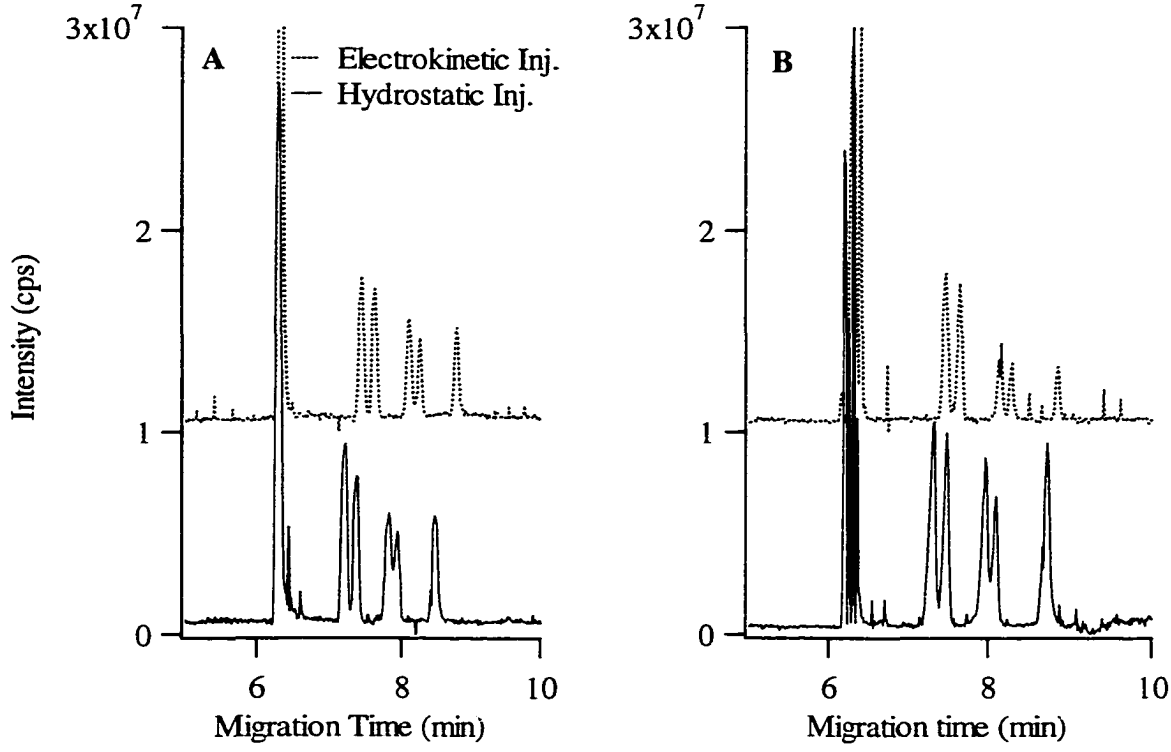

3.4.4 Calibration Curves and Detection Limits

Linear regression plots (**Figure 3.7**) of log(peak area, cps) versus log(concentration, M) of the analytes showed a linear relationship across a concentration range of 10^{-6} to 10^{-3} M. The concentration limits of detection were 1 x 10^{-7} M to 2 x 10^{-7} M determined using a stock solution of 4-ddN (ddA, d4T, AZT, ddI) mixture dissolved and diluted in water, **Figure 3.8**. This detection limit is comparable to the detection limit obtained by Geldart and Brown[15] using CE with UV detection for nucleosides and nucleobases. The injection volume, V_{inj}, of the sample was 14 nL calculated using the equation[47] of:

$$V_{inj} = (\pi r^4 \rho g \Delta h t_{inj}) / (8 \eta L) \quad (3.3)$$

where the r is the radius of the capillary, ρ is the density of the BGE inside the capillary, g is the gravity constant (9.8 m/s^2), Δh is the height difference between the two ends of the capillary, t_{inj} is the injection time, η is the viscosity of the sample solution and L is the total length of the capillary. Therefore, the mass limit of detection was 1.4 fmol. Sensitivity could easily be enhanced by a factor of 10 under single ion monitoring conditions.

3.4.5 Profiling of ddNs in Positive ESI CE-MS

Figure 3.9 shows the separation of ddNs by CZE at 175 V/cm and a positive ESI-MS detection in a full-scan mode. The sample was a 10^{-4} M mixture dissolved in a 50% BGE solution and hydrostatically injected onto an untreated capillary column. It is clear that all ddNs are well separated with nearly equal sensitivity.

Figure 3.7. Calibration curves of ddNs obtained in positive ESI CE-MS analysis.

Hydrodynamic injections were made at 18 cm for 30 s. Other conditions were as described in the experimental section.

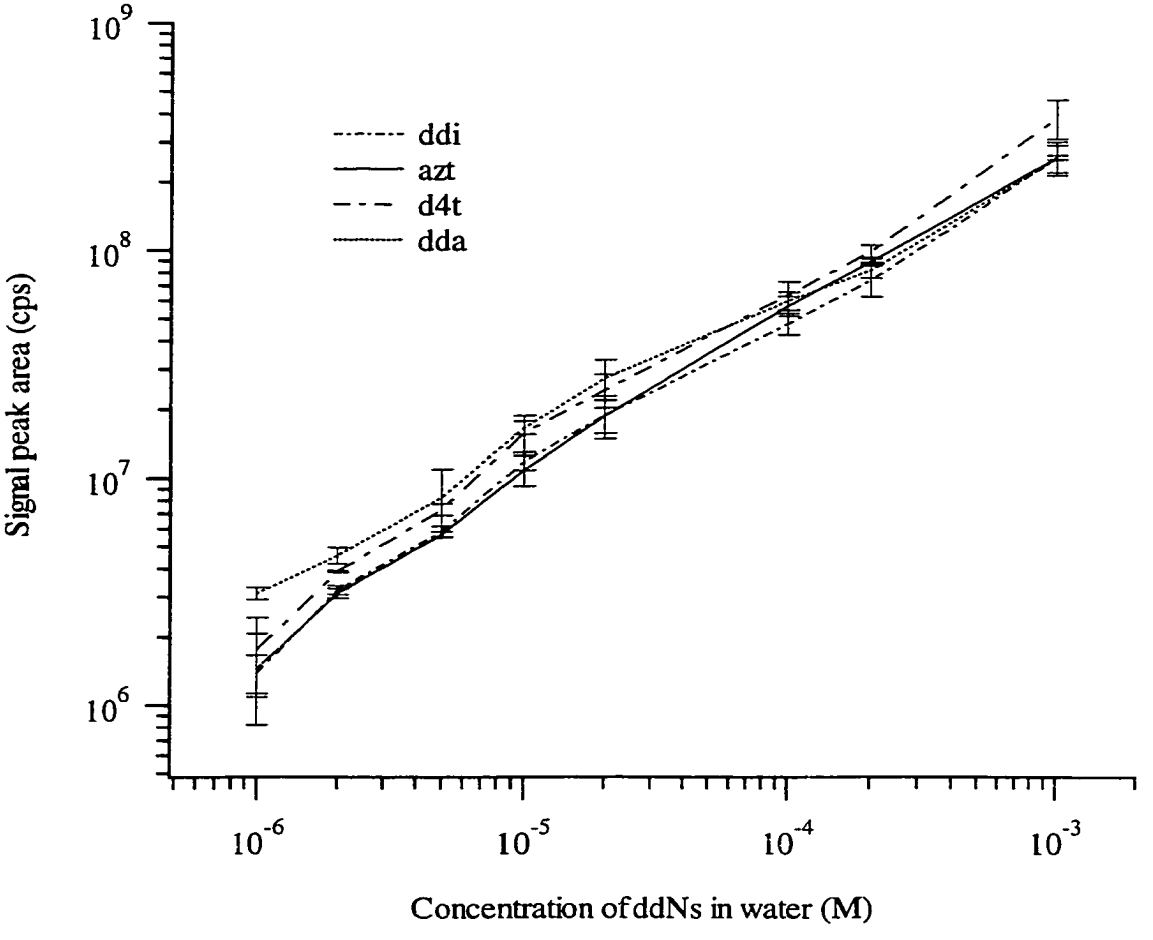

Figure 3.8. Total ion electropherograms of four ddNs showing the concentration limits of detection.

Samples were injected hydrodynamically at 18 cm for 30 s. Separations were made at 235 V/cm in 50 mM ammonium acetate at pH 10.0. The ionspray was operated at +4.1 kV, the orifice and the ring focusing potentials were +30 V and +250 V, respectively. The quadrupole mass analyzer was scanned at a speed of 0.59 s/cycle over a mass range of m/z 105-300. Other conditions were as described in the experimental section.

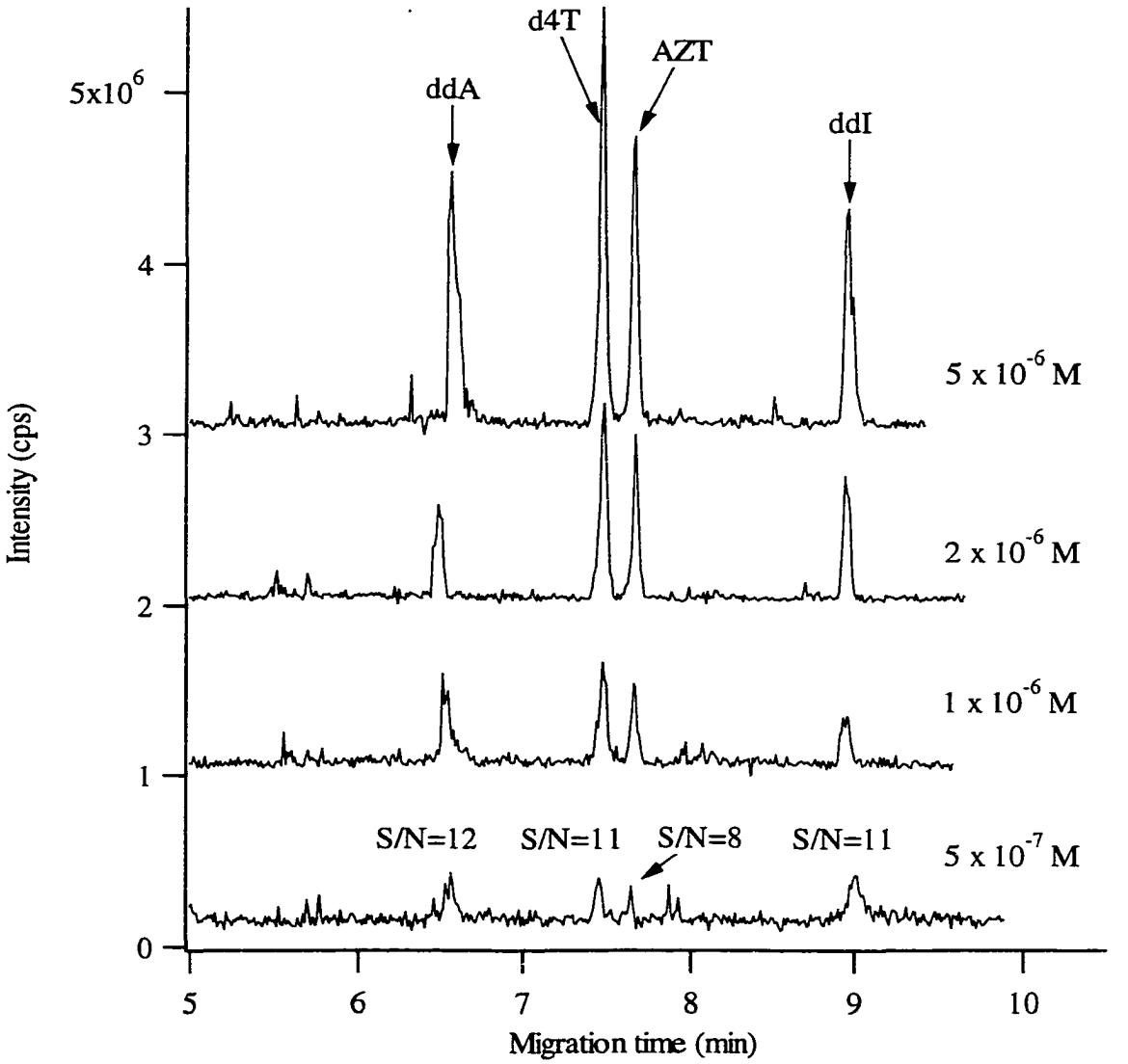

Figure 3.9. Total ion electropherogram showing the separation of ddNs in a positive ESI-MS detection mode.

A 9-ddN mixture with a concentration of 10^{-4} M each in 50% BGE was hydrostatically injected at 18 cm for 30 s. Separation was made in a 25 mM ammonium acetate BGE (pH 10.0) under +10.4 kV (175 V/cm). The mass analyzer was scanned at 0.88 s/cycle from m/z 105 to m/z 550 with a step of 0.5 Da and a dwell time of 1 ms. Potentials applied to the sprayer, the orifice and the focusing ring were 4600 V, 25 V and 250 V, respectively. Other conditions were as described in the experimental section.

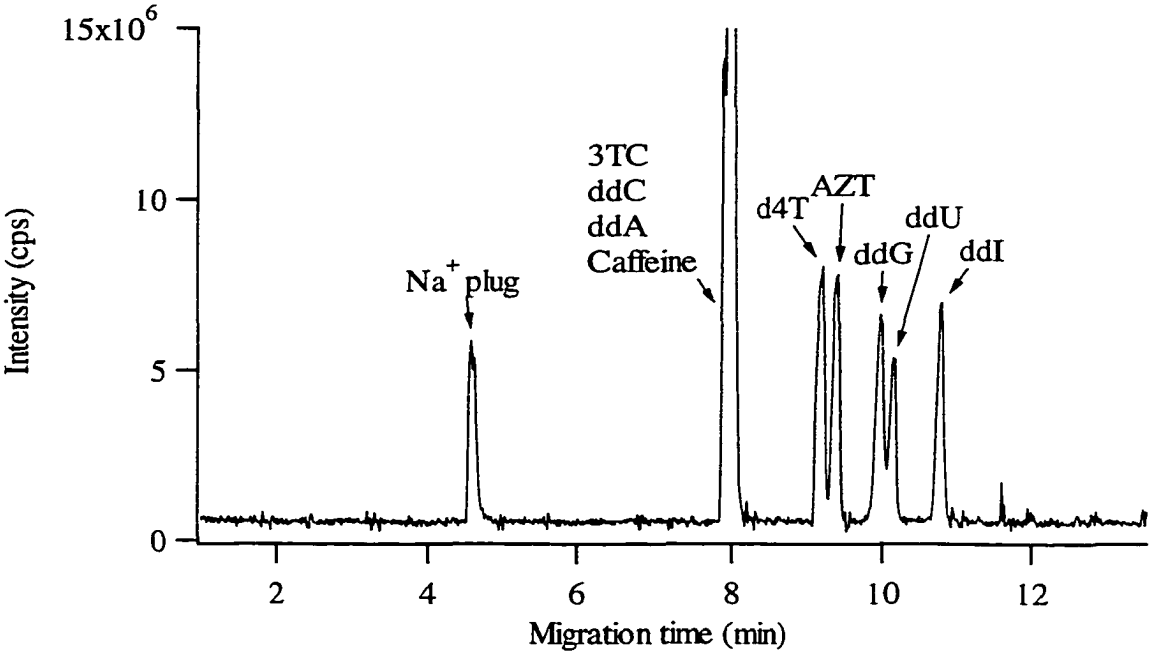

3.4.6 Negative ESI-MS Detection for ddNs and Nucleotides

Nucleotides contain both nucleobases and phosphate groups. In addition to the ionization of the nucleobases that makes the positive ESI-MS detection possible, the ionization of the phosphate groups over most of the pH range accommodates the sensitive detection of nucleotides with negative ESI-MS. **Figure 3.10** shows the profiles of ddNs and nucleotides with both detection modes. It is obvious that the ion intensity and the sensitivity of ddNs in negative mode are the nearly same as that in positive mode. Nucleotides, however, have different sensitivities in the two different detection modes. The sensitivity of nucleotides in negative mode detection is much higher than that in positive detection. That is, negative ion mode produced nearly equal sensitivity for ddNs and nucleotides, whereas in positive ion mode, the response of nucleotides was much lower than that of ddNs. For instance, for a 100 μM mixture of ddNs and nucleotides, negative ion ESI-MS generates a signal of AZT with S/N 128 and of ADP 105; positive ion ESI-MS, however, produces a signal of AZT with S/N 158 and of ADP 57. The sensitivity difference between a ddN and a nucleotide in positive ion mode might be explained by taking account of their differences in gas-phase proton affinity or gas-phase basicity. Green-Church and Limbach[48] have also pointed out that the proton affinity value for a nucleotide is smaller than that for a nucleoside or a nucleobase. The proton affinity of a molecule M is defined as the negative value of enthalpy for the formation of MH^+.

The negative ESI of ddNs in the BGE at pH 10.0 produces simple mass spectra that are similar to the ones in the positive ESI. Generally, the $[M-H]^-$ molecular ion dominates the signal together with the B^- ion produced from the cleavage of the glycosidic bond, the $[B-17\ (NH_3)]^-$ ion and the $[2M-H]^-$ ion, each with a relative abundance of 5-20%. The sodium and potassium adducts are also observed in low abundance, **Figure 3.11d**.

Figure 3.10. Total ion electropherograms showing the effects of ESI operational modes on detection sensitivity of ddNs and nucleotides.

(A) Negative ESI mode with potentials applied to the ion sprayer (IS), the orifice (OR) and the focusing ring (RNG) were -3600 V, -35 V and -220 V, respectively. An electrical field of 226 V/cm was applied across the column for separation. The ESI tip was 6 mm away from the center of the ion transmission axis (Y-axis). (B) Positive ESI mode with IS 3800 V, OR 35 V and RNG 250 V. An electrical field of 236 V/cm was applied for separation. The ESI tip was located at the center of the Y-axis. The BGE was 25 mM ammonium acetate at pH 10.0. The sample was a 10^{-4} M mixture in 50% BGE. Other conditions were as described in the experimental section.

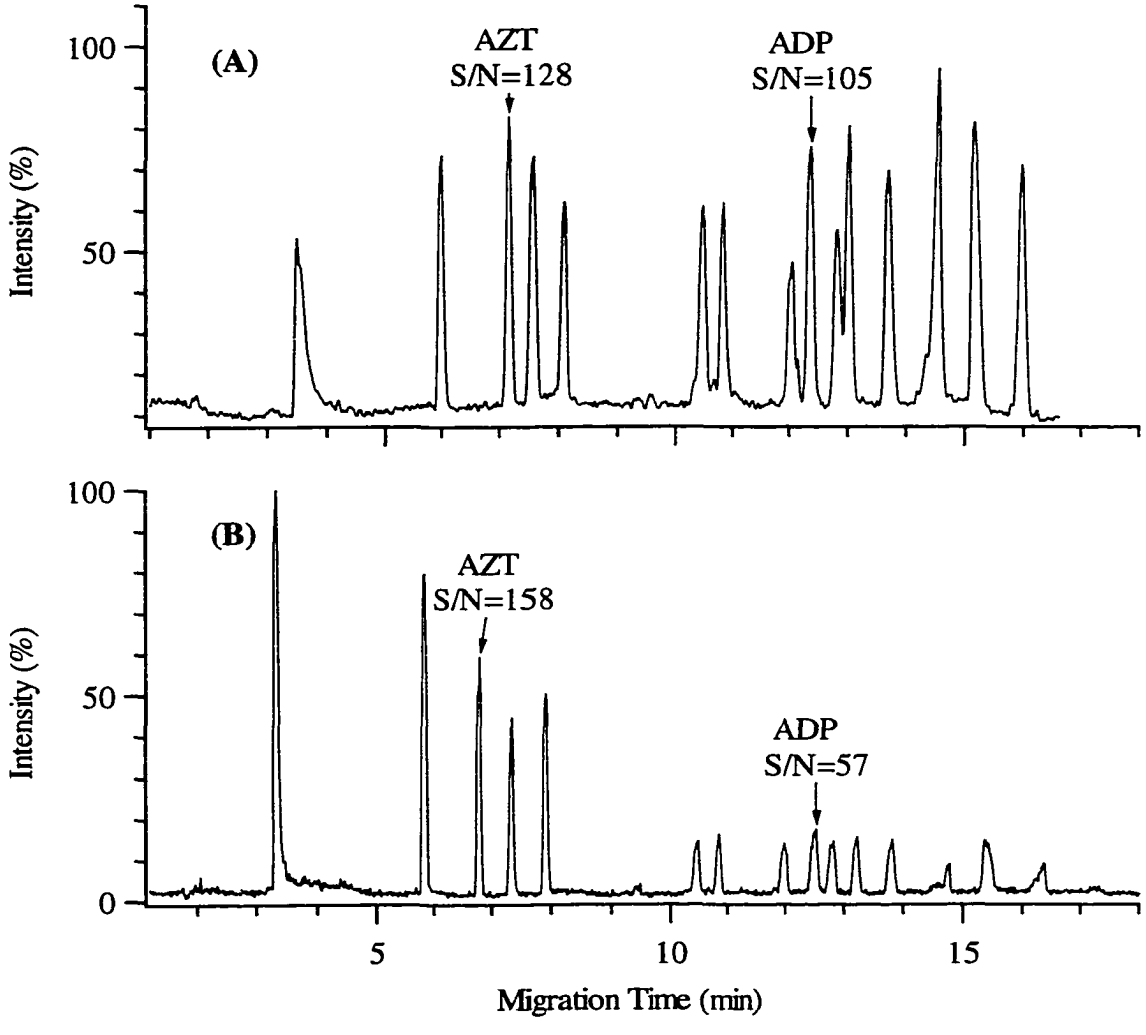

Figure 3.11. Total ion electropherogram and mass spectra of nucleosides and nucleotides.

CE was performed at 234 V/cm in a 25 mM ammonium acetate at pH 10.0. The sample was 100 μM in 50% BGE was hydrodynamically injected. Negative ESI-MS was performed. Other conditions were as described in the experimental section.

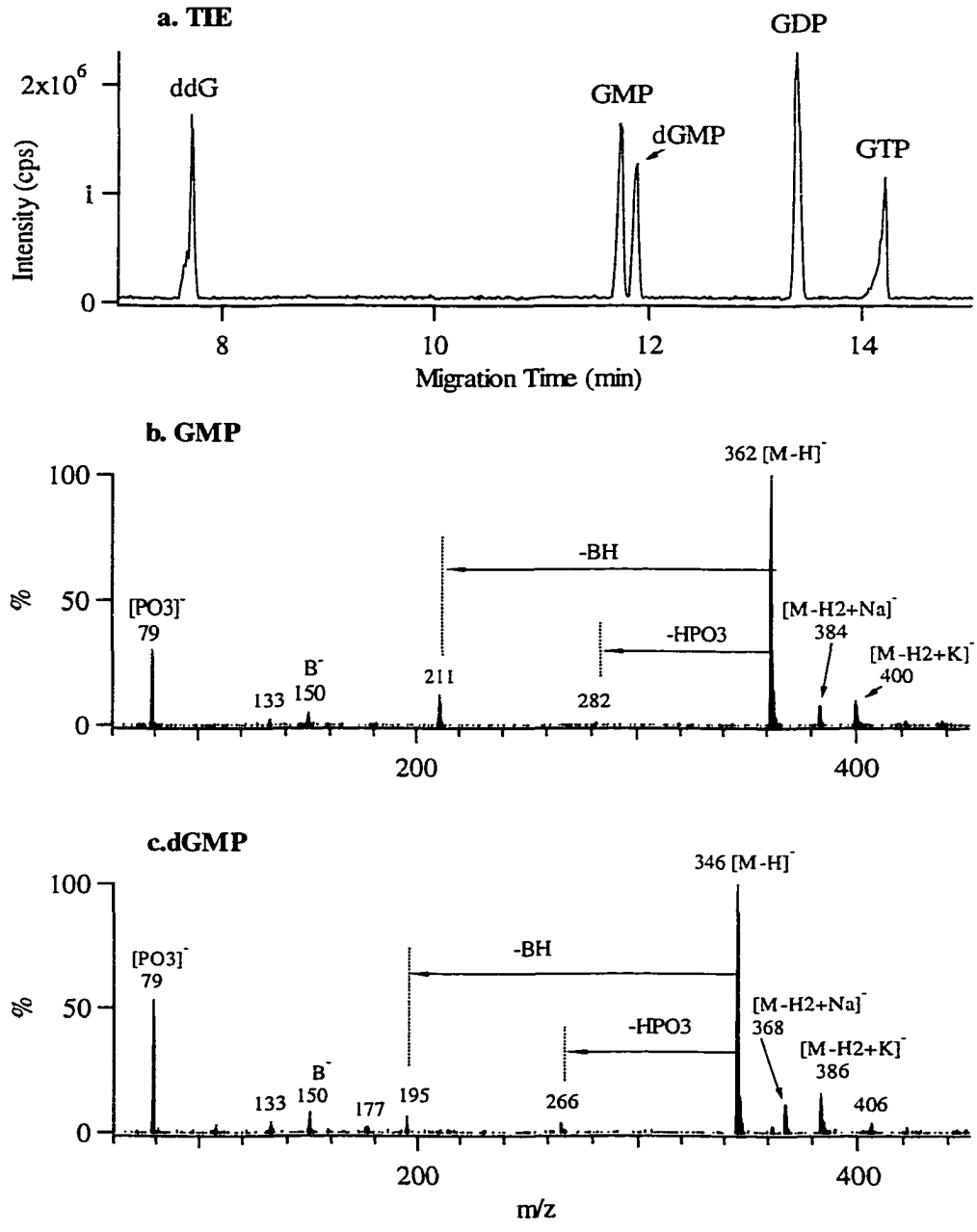

Figure 3.11. (Cont'd)

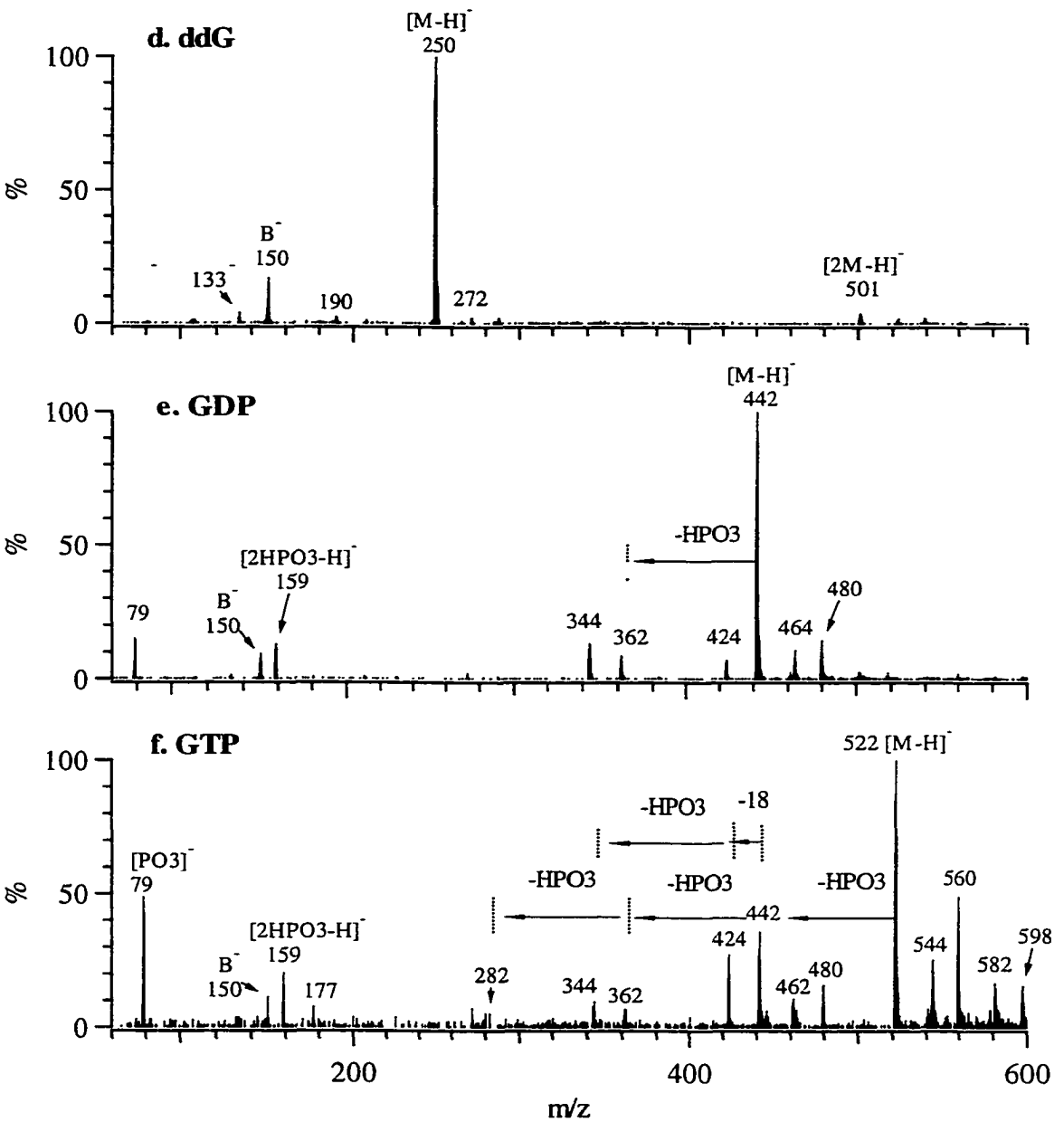

In the case of nucleotides in the BGE at pH 10.0, the base peak in the negative mass spectra (**Figure 3.11 b-f**) is the $[M-H]^-$ molecular ion. Metal ion adducts are also observed. Major fragments are the B^- ions, $[B-17\ (NH_3)]^-$ and $[M-H-BH]^-$; and ions generated from the loss of phosphate groups, such as $[M-H-PO_3]^-$ for diphosphates, $[M-H-PO_3]^-$ and $[M-H-2PO_3]^-$ for triphosphates. $[PO_3]^-$ ions, $[PO_4]^-$ ions are also in high abundance.

It is noteworthy to mention that the solvent has an influence on mass spectra of nucleotides. Compared with that in BGE, the mass spectrum of a nucleotide in water contains more fragmental ions (**Figure 3.12**); ion intensity is also higher (**Figure 3.13**). Except for the ions mentioned above, $[M-H-BH]^-$ phosphorylated sugar ions and the doubly charged molecular ions were also observed. While in the spectrum of dGMP in BGE, those ions were in low abundance, **Figure 3.12**. It is then concluded that it is not appropriate to tune the instrument with standards dissolved in a solvent other than the BGE. In this study, the instrument was tuned on a daily basis with two steps before CE-MS studies. It was tuned to a maximum sensitivity while infusing a mixture of ddG, dGMP, GDP and GTP dissolved in BGE using a syringe pump, then it was adjusted while the same sample mixture was continuously infused at a 230 V/cm electrical filed across the capillary. An example of the final mass spectra after the tuning procedure is shown in **Figure 3.14**.

For an on-line CE-MS analysis, the solvent ionic strength of a sample solution has also a substantial influence on peak shape and intensity. As shown in **Figure 3.15**, a sharper and higher peak produced when sample was prepared in water, while the peak was clearly broadened when the sample was dissolved in 50% BGE. A stacking effect

Figure 3.12. Negative ESI spectra of dGMP showing the influence of solvent on ion intensity and fragmentation.

Samples were 50 μM in (a) water (b) BGE and infused at 0.16 μL/min. The sheath was at 3 μL/min. Other conditions were as described in the experimental section.

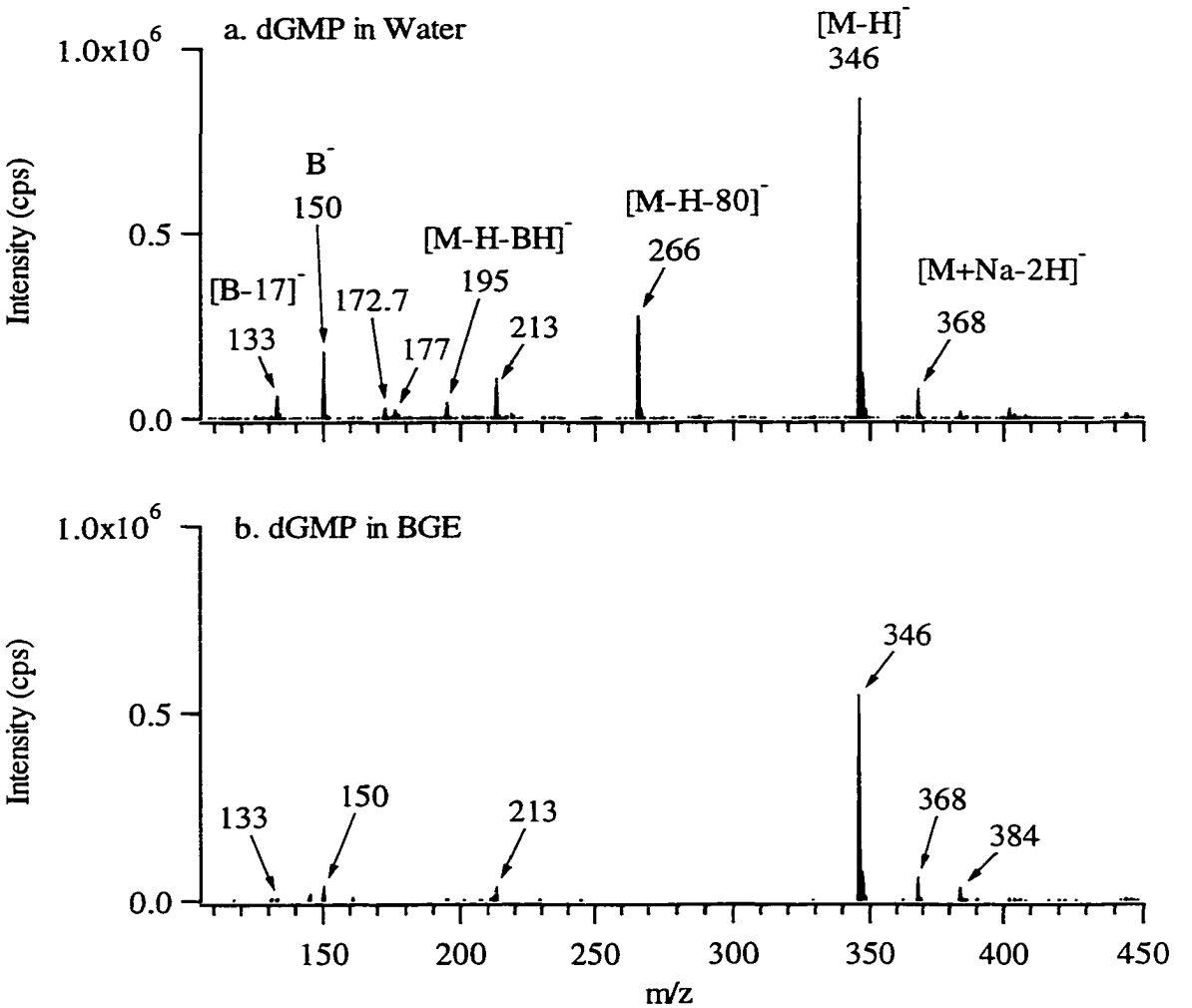

Figure 3.13. Negative ESI spectra of ddG, dGMP, GDP and GTP showing the influence of solvent on ion intensity.

Samples were 100 μM in (a) water (b) BGE and infused at 0.16 μL/min. The sheath was at 3 μL/min. Other conditions were as described in the experimental section.

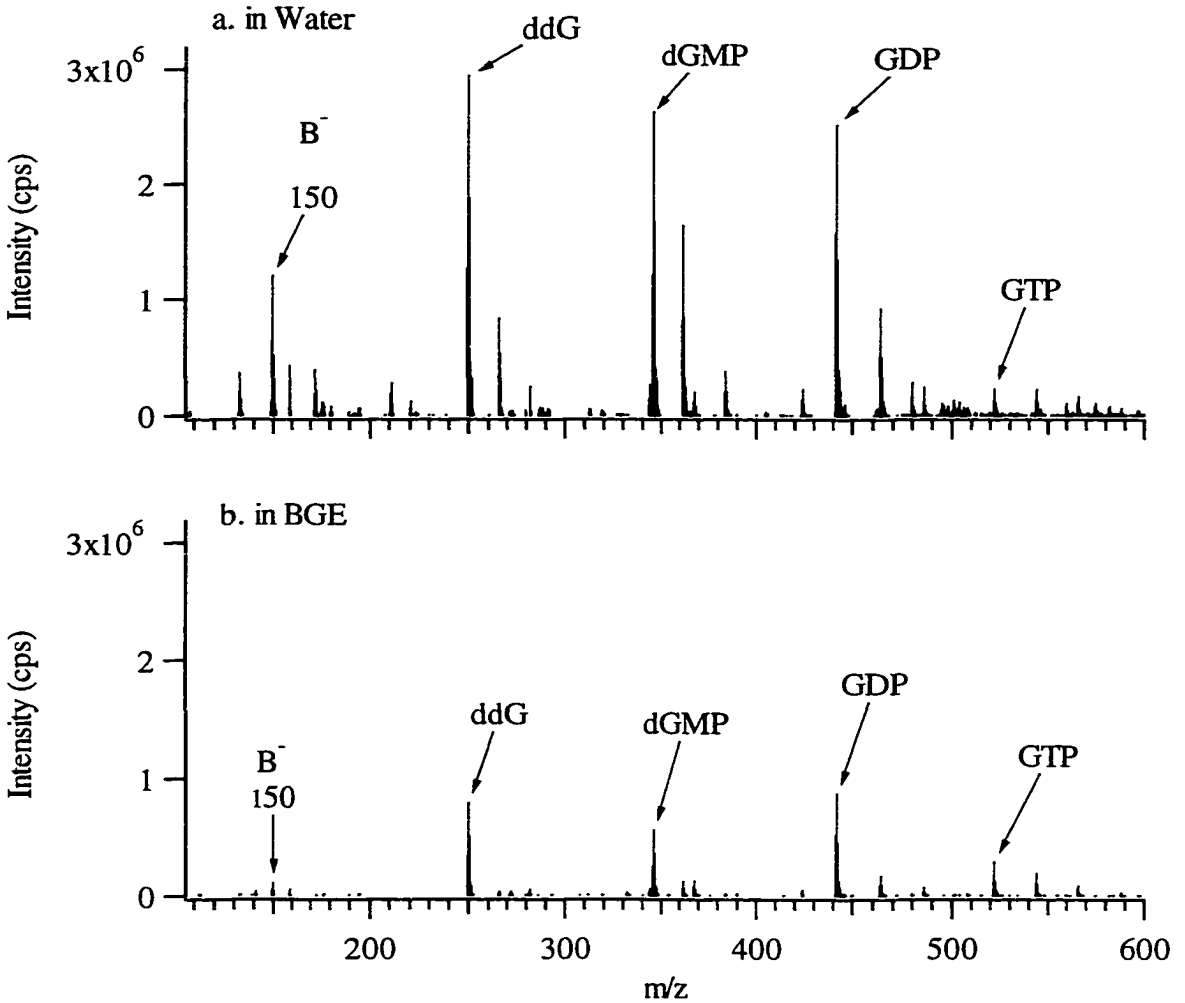

Figure 3.14. Negative ESI spectra of ddG, dGMP, GDP and GTP showing the influence of infusion methods on ion intensity.

(a) Pump infusion at 0.16 μL/min. (b) Electrokinetic infusion at 0.16 μL/min. Samples were 100 μM in BGE. The sheath was at 3 μL/min. Other conditions were as described in the experimental section.

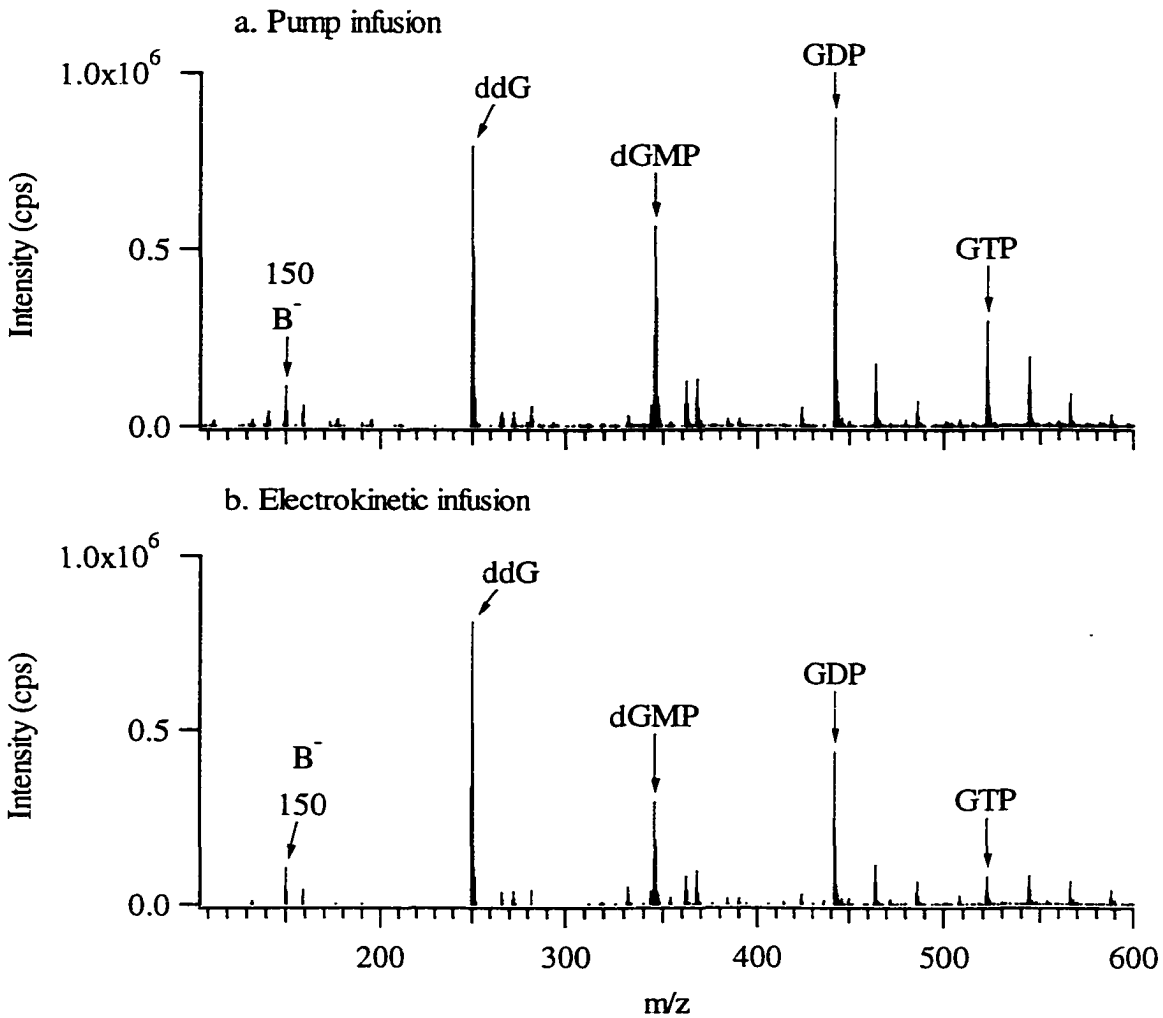

Figure 3.15. Total ion electropherograms of ddC, dCMP, CDP and ddCTP showing the effects of solvent ionic strength on peak shapes and intensities.

CE was performed at 200 V/cm in 15 mM ammonium acetate electrolyte at pH 10.0. Samples of 100 μM were hydrostatically injected. Negative ESI-MS was operated. Other conditions were as described in the experimental section.

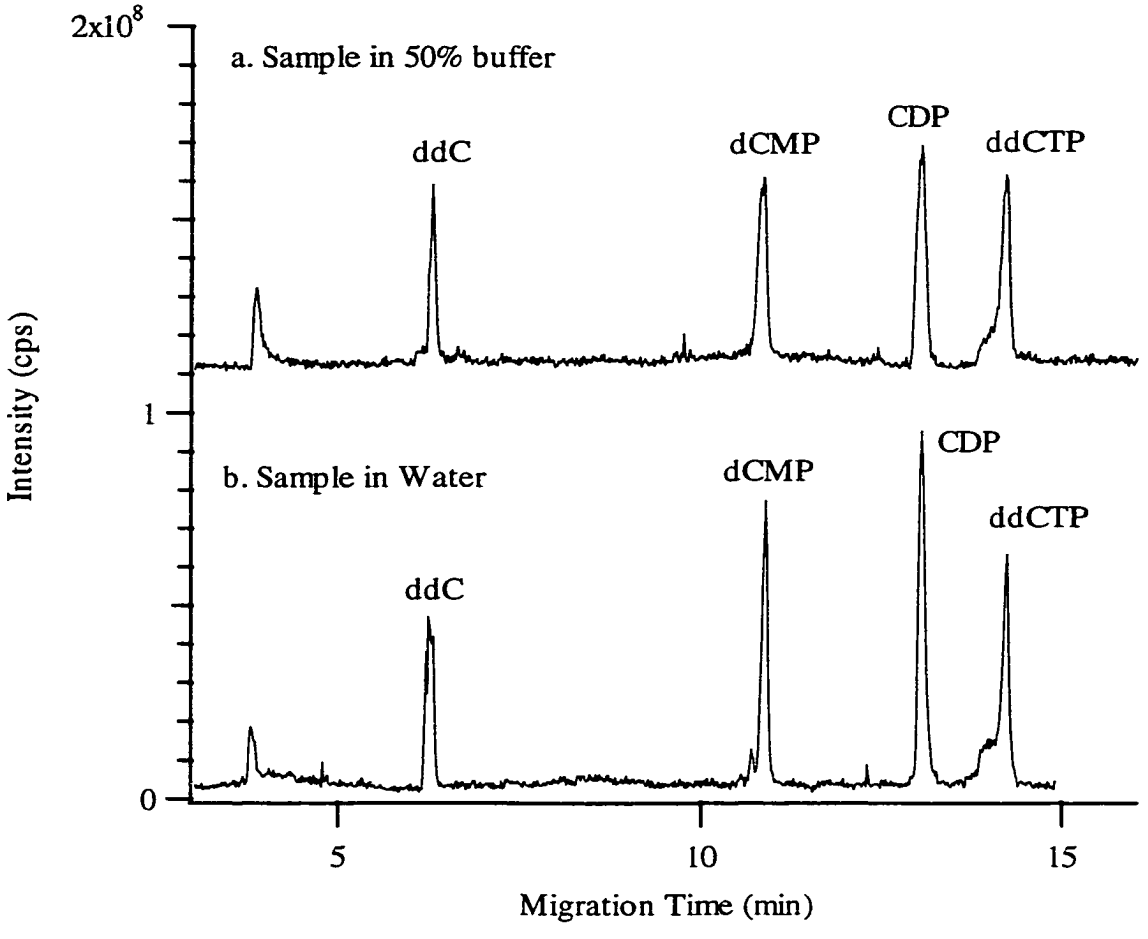

was present for the low conductivity sample plug in the CE capillary when a high electrical field was applied across the column to the BGE.[35]

3.4.7 BGE Concentration versus Separation of ddNs and Nucleotides

Similar to the effects of BGE concentration on ddNs separation shown in **Figure 3.3,** the effects of the BGE concentration on migration and separation of ddNs and nucleotides in a negative ESI detection are shown in **Figure 3.16**. The best sensitivity of analyte and the resolution of peak a, b and c were obtained in a BGE of 25 mM ammonium acetate at pH 10.0.

3.4.8 Mass Interval vs Ion Intensity and Sensitivity

We have observed a change in the ion intensity of analyte versus the change of the mass scanning step size as shown in **Figure 3.17**. When the scanning speed of the mass analyzer is fixed, the total ion current of an analyte is about 10 times higher when the scanning step size of mass is 10 times smaller. However, the S/N of the analyte peak remains the same. These results indicate that one should report a peak height or area with a specified scanning step, while the sensitivity is not affected if the sensitivity is defined as the slope of a calibration curve of log(S/N)-log(concentration of analyte). A possible way to gain higher sensitivity and to have more data points to define a CE peak is to increase the scanning speed of the mass analyzer[49]. However this solution is unlikely in the present study with a quadrupole analyzer since a dwell time needs to be shortened when the scanning speed is increased, *i.e.* the total ion current is not changed. A time-of-flight analyzer should be a better choice for this purpose in a coupled CE-MS analysis.

Figure 3.16. Total ion electropherograms of ddNs and nucleotides showing the influence of BGE concentration on CE separation.

CE was performed at 200 V/cm. Samples of 100 μM were hydrodynamically injected. Negative ESI-MS was operated. Other conditions were as described in the experimental section.

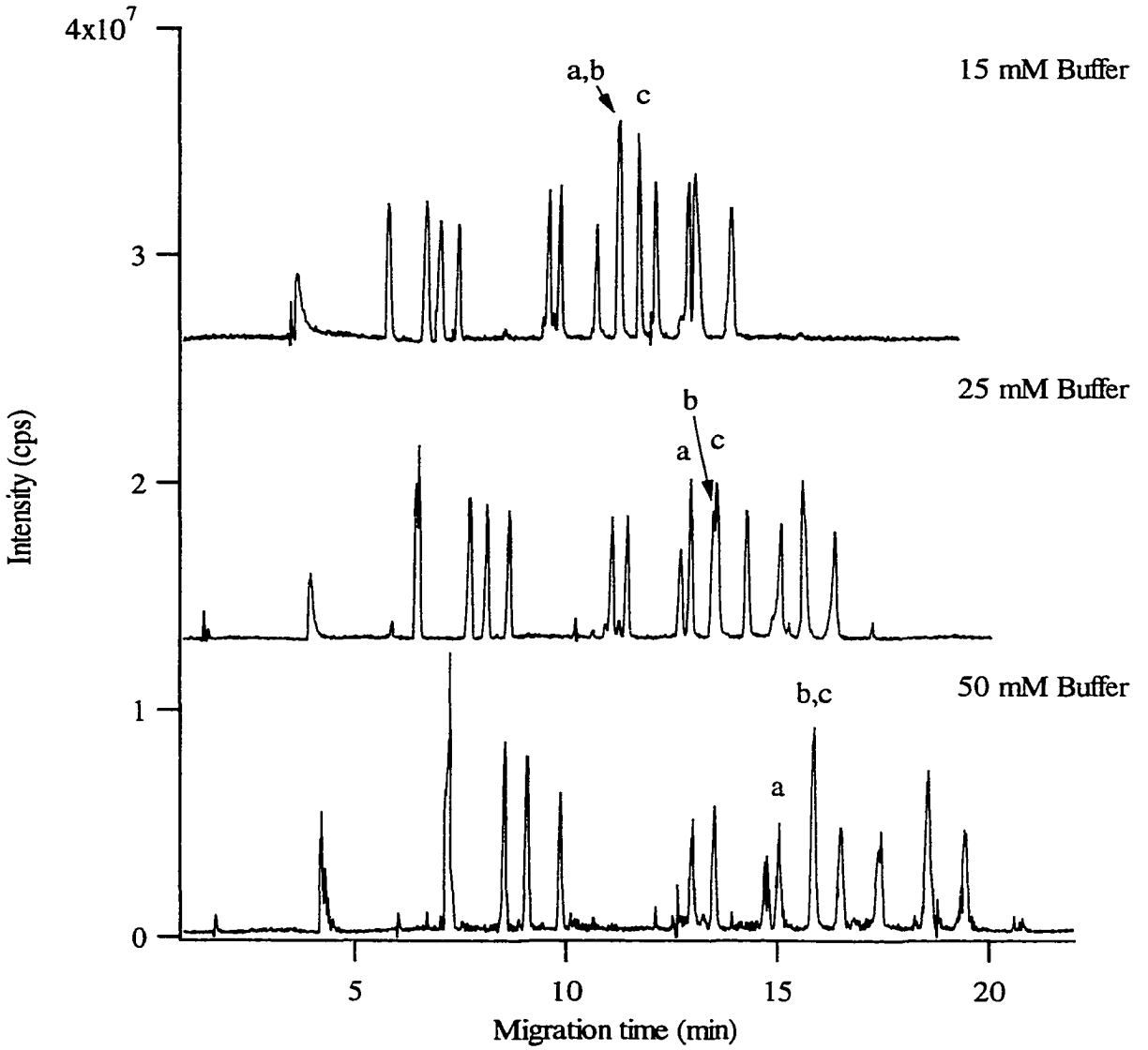

Figure 3.17. Total ion electropherograms of ddNs and nucleotides showing the effects of MS scanning mass step size on ion intensity and sensitivity.

A scanning speed of 0.99 s/scan was fixed by adjusting the step size and a dwell time. CE was performed at 200 V/cm. Samples of 100 μM were hydrodynamically injected. Negative ESI-MS was operated. Other conditions were as described in the experimental section.

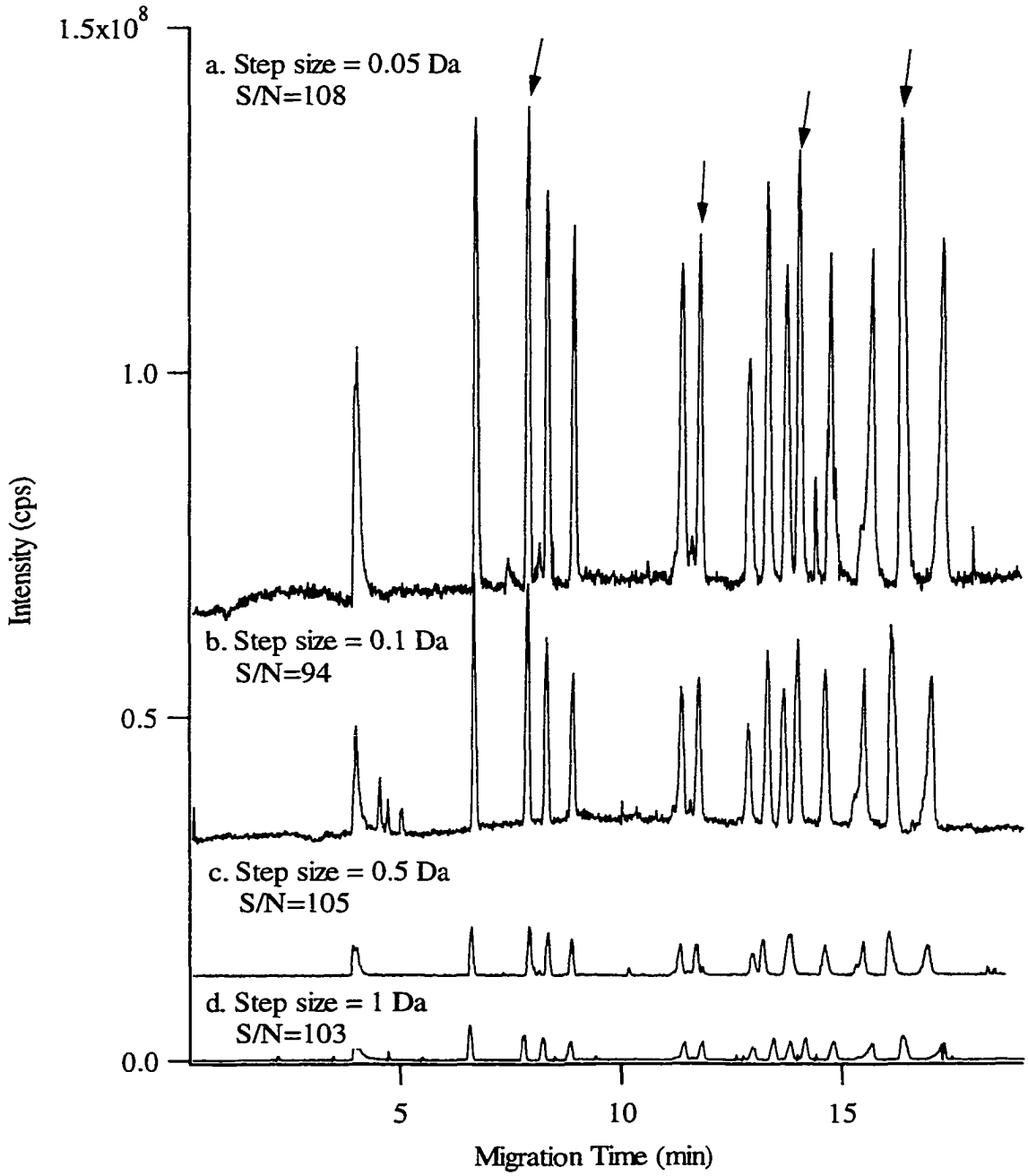

3.4.9 Profiling of ddNs and Nucleotides with Negative ESI CE-MS

As an example of the CE-MS analysis of ddNs and nucleotides, **Figure 3.18A** shows the mass electropherogram of a 14-compound mixture containing ddN and nucleotide standards, with an elution order of EOF and 3TC/ddC/ddA, other ddNs, mononucleotides, dinucleotides and trinucleotides. Panels **B, C, D and E** demonstrate typical profiles of a ddN and its correlated nucleotides. Because of the difficulties in obtaining all dideoxyribonucleotides corresponding to the antiviral dideoxynucleosides, we used other ribonucleotides or deoxyribonucleotides for the method development. Definitive identification of all analytes was accomplished by comparing migration times and typical mass spectra data. The resolving power of CE-MS allowed unambiguous identification of compounds with the same base but with slightly different sugar moieties. For example, one can easily distinguish between the spectra of GMP and the dGMP as shown in **Figure 3.11**. The full scan mass electropherogram showed baseline separations of the GMP and the dGMP, and their definitive assignment was possible from the mass spectra. Another example is the identification of a nucleoside containing a ribose-, a deoxyribose- or a dideoxyribose-sugar. **Figure 3.19** shows the mass electropherogram of ddG, dG and G where these compounds are partially separated. The background-subtracted and interference-subtracted mass spectra were obtained with the help of the MultiView data-processing software. Differences in their elution times were mainly due to their slight differences in their pKa values contributed by the slight differences of their ribose-sugar moieties. Their mass differences might not play any important role in their varying migration orders, based on the experience with the separation of ddG (MW 251), ddU (MW 212) and ddI (MW 236) in **Figure 3.9**, and with the separation of GMP (MW 363) and dGMP (MW 347) in **Figure 3.11**. CE-MS data of all ddNs and nearly 20 nucleotides have been acquired, and interpretation of the data was straightforward. More

Figure 3.18. Total ion electropherograms showing the separation of ddNs and nucleotides.

CE was performed at 200 V/cm in a 25 mM ammonium acetate buffer at pH 10.0. Samples in 50% BGE with concentrations of 10^{-4} M were injected hydrostatically at 18 cm for 30 s. Negative ESI-MS detection was conducted. Other conditions were as described in the experimental section. (A) a 14-compound mixture. (B) a mixture of ddA and related nucleotides. (C) ddC and related nucleotides. (D) ddG and related nucleotides. (E) ddU and related nucleotides.

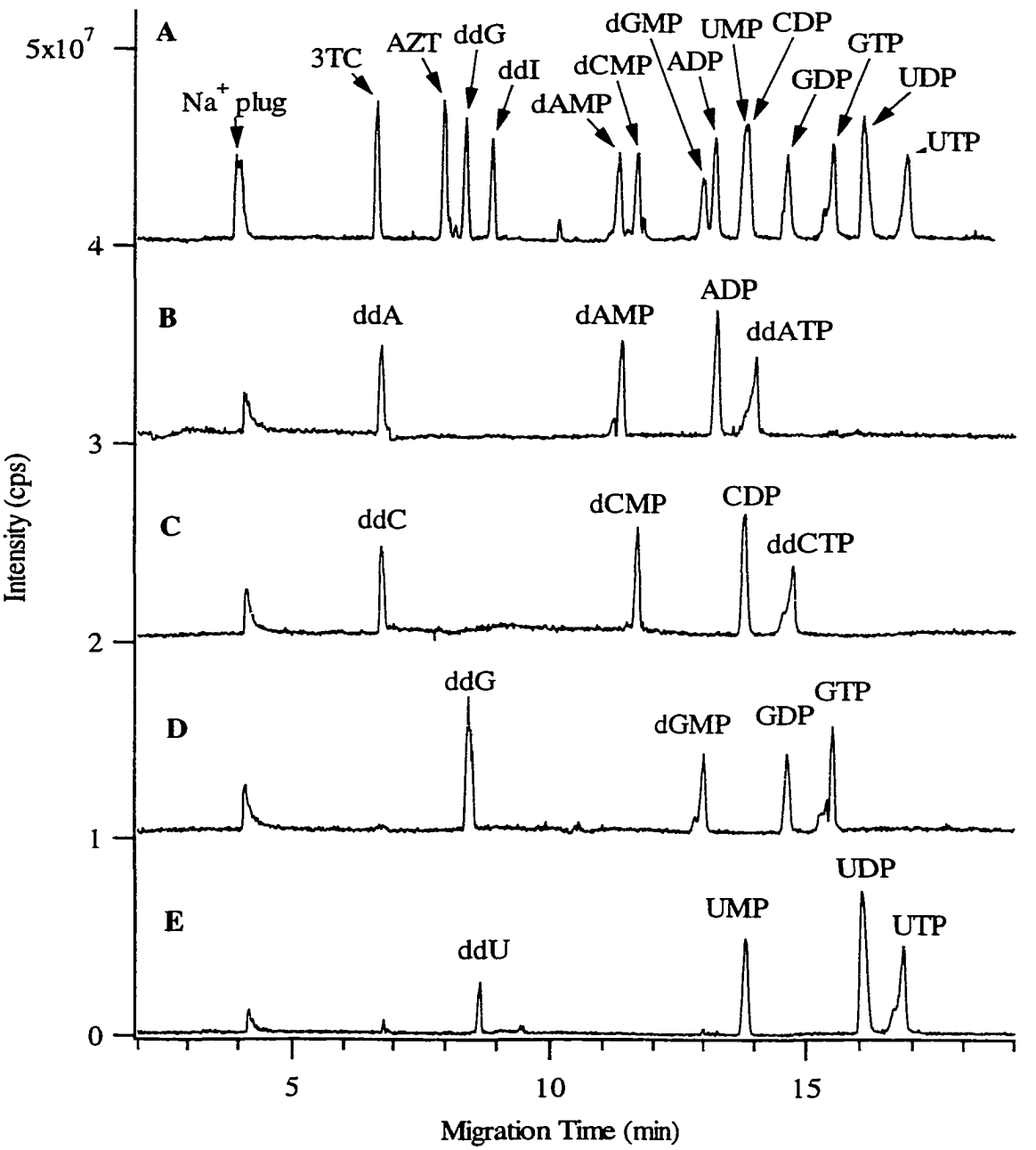

Figure 3.19. Total ion electropherogram and mass spectra showing the separations of ddG, dG and G by CE-MS.

CE was performed at 234 V/cm in a 25 mM ammonium acetate at pH 10.0. The sample was 100 μM in 50% BGE was hydrodynamically injected. Negative ESI-MS was performed. Other conditions were as described in the experimental section.

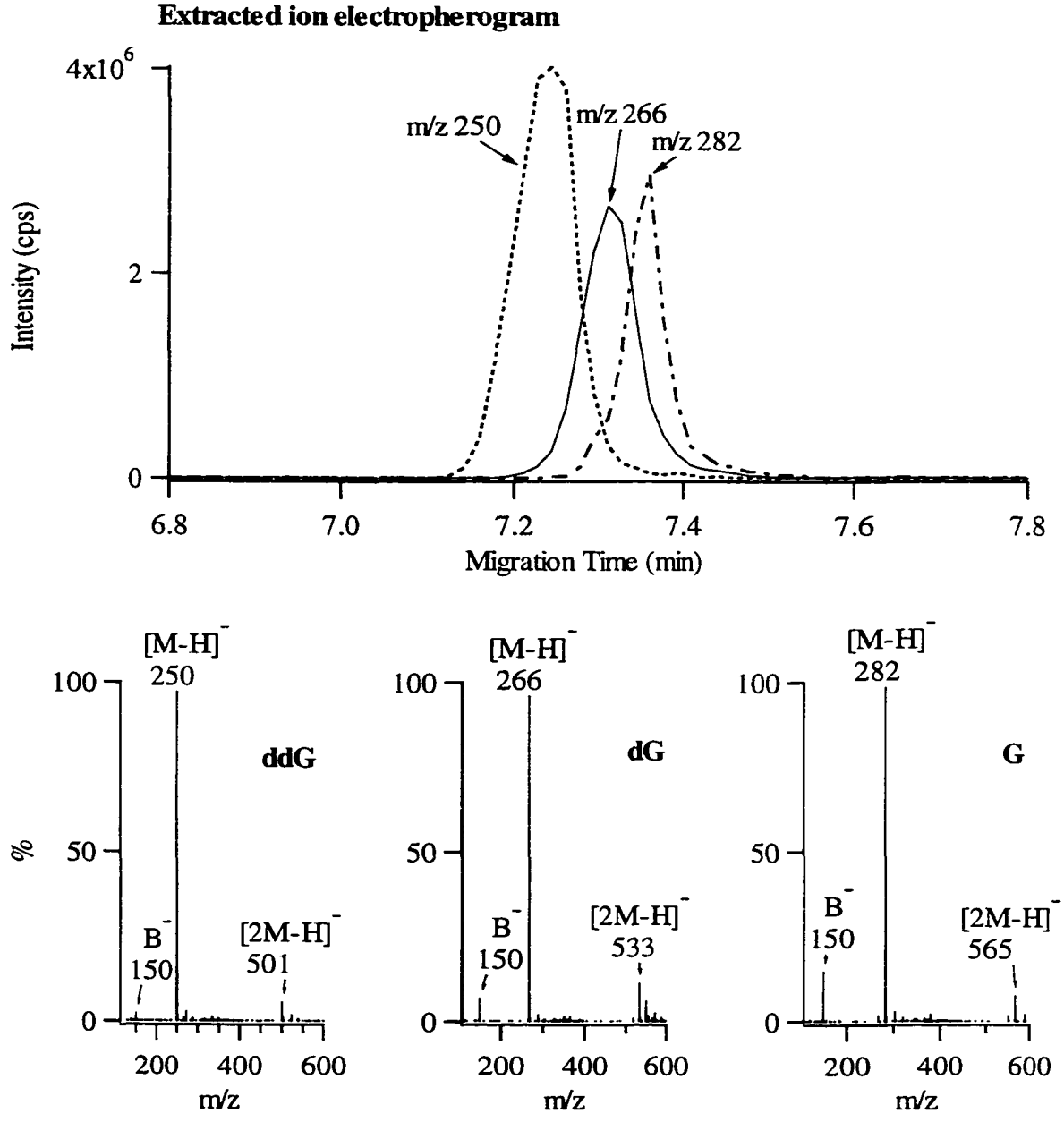

importantly, even in the absence of reference data, identification of the analytes would pose no additional difficulties due to the quality of the acquired on-line CE-MS full scan mass spectra.

3.4.10 Calibration Curves and Detection Limits

With the negative ion detection mode, the CE-MS method gave 3 orders of magnitude of linearity across a range of 5×10^{-7} to 1×10^{-3} M, and concentration limits of detection for ddNs and nucleotides were 100-200 nM, **Figure 3.20**.

3.4.11 Detection of Nucleotides in a Hep G2 Cell Extract

The blank cell extracts were analyzed by CE-MS without further concentration. **Figure 3.21** shows a representative total ion electropherogram and several extracted single ion electropherograms of an extract. Eight nucleotides, namely AMP, ADP, ATP, GDP, CTP, GTP, UDP and UTP have been identified based on their specific migration times and the elucidation of their full-scan mass spectra. The masses showing on the mass electropherogram traces are the molecular ion of those nucleotides. The amount of nucleotides in the final extracts was around 5 μM for ADP, 3 μM for ATP, 2 μM for AMP, and less than 1 μM for other species.

3.4.12 Phosphorylation of 3TC in Hep G2 Cell Lines

Having established the utility of the CE-ESI-MS technique for analysis of representative standards and blank cell extracts, the application of this methodology to the phosphorylation study of 3TC in Hep G2 cell lines was then investigated. **Figure 3.22** shows a representative extracted mass electropherogram for detection of 3TC (m/z 228), 3TCMP (m/z 308), 3TCDP (m/z 388) and 3TCTP (m/z 468) after 10 hr incubations of

Figure 3.20. Total ion electropherograms showing the concentration limits of detection.

CE was performed at 200 V/cm in a 25 mM BGE at pH 10.0. Samples were dissolved in water and injected hydrodynamically. Mass 209-212, 305-308, 401-404, 449-452, 471-474, 487-490 with a step size of 0.05 Da and a dwell time of 2.0 ms was scanned at a speed of 0.74 s/scan. Negative ESI-MS was operated. Other conditions were as described in the experimental section.

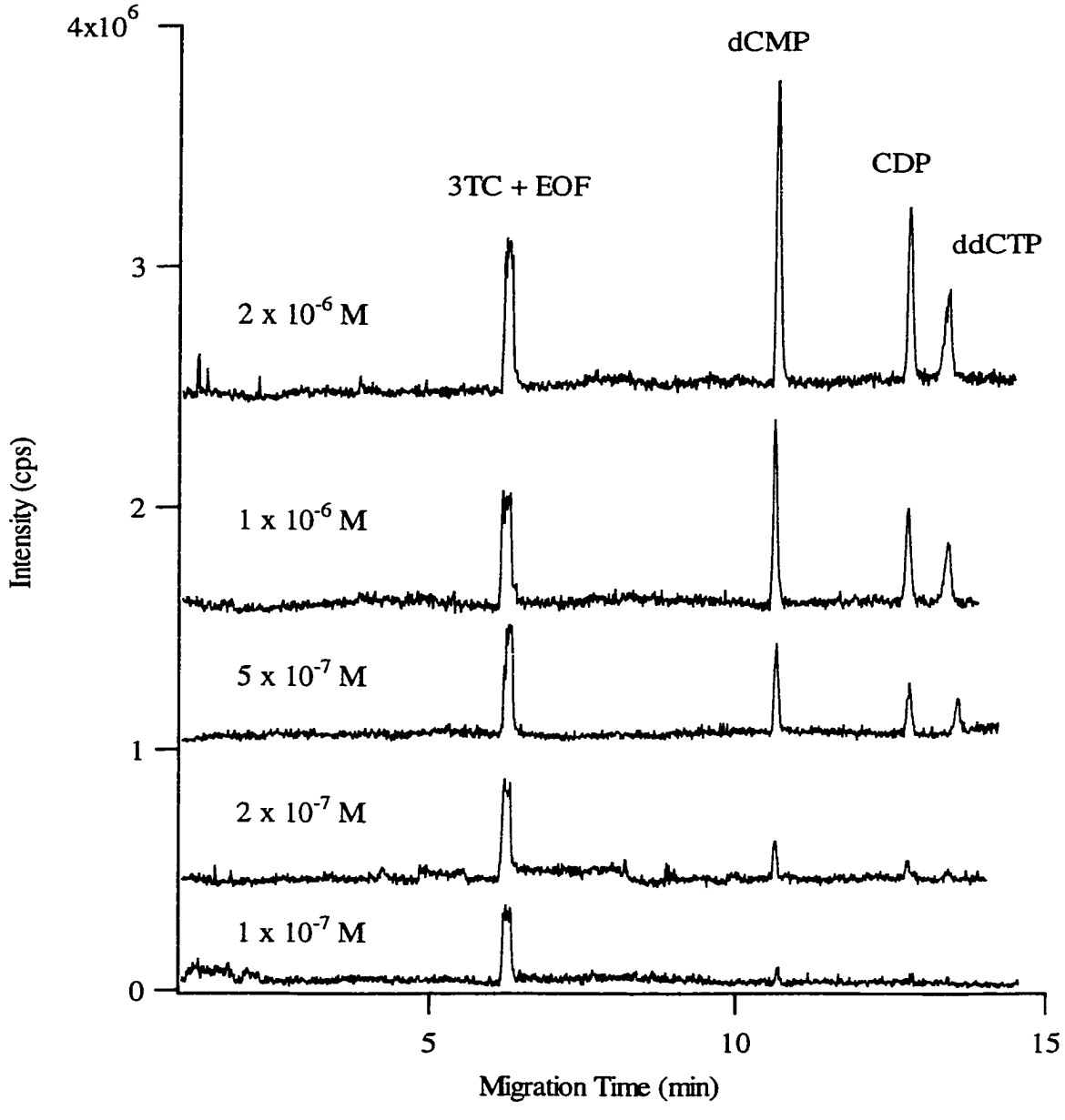

Figure 3.21. Total ion electropherogram of a Hep G2 cell extract. Sample pretreatment was described in the experimental section.

Separation was performed at 230 V/cm in a 25 mM BGE at pH 10.0. Negative ESI-MS was conducted. Other conditions were as described in the experimental section.

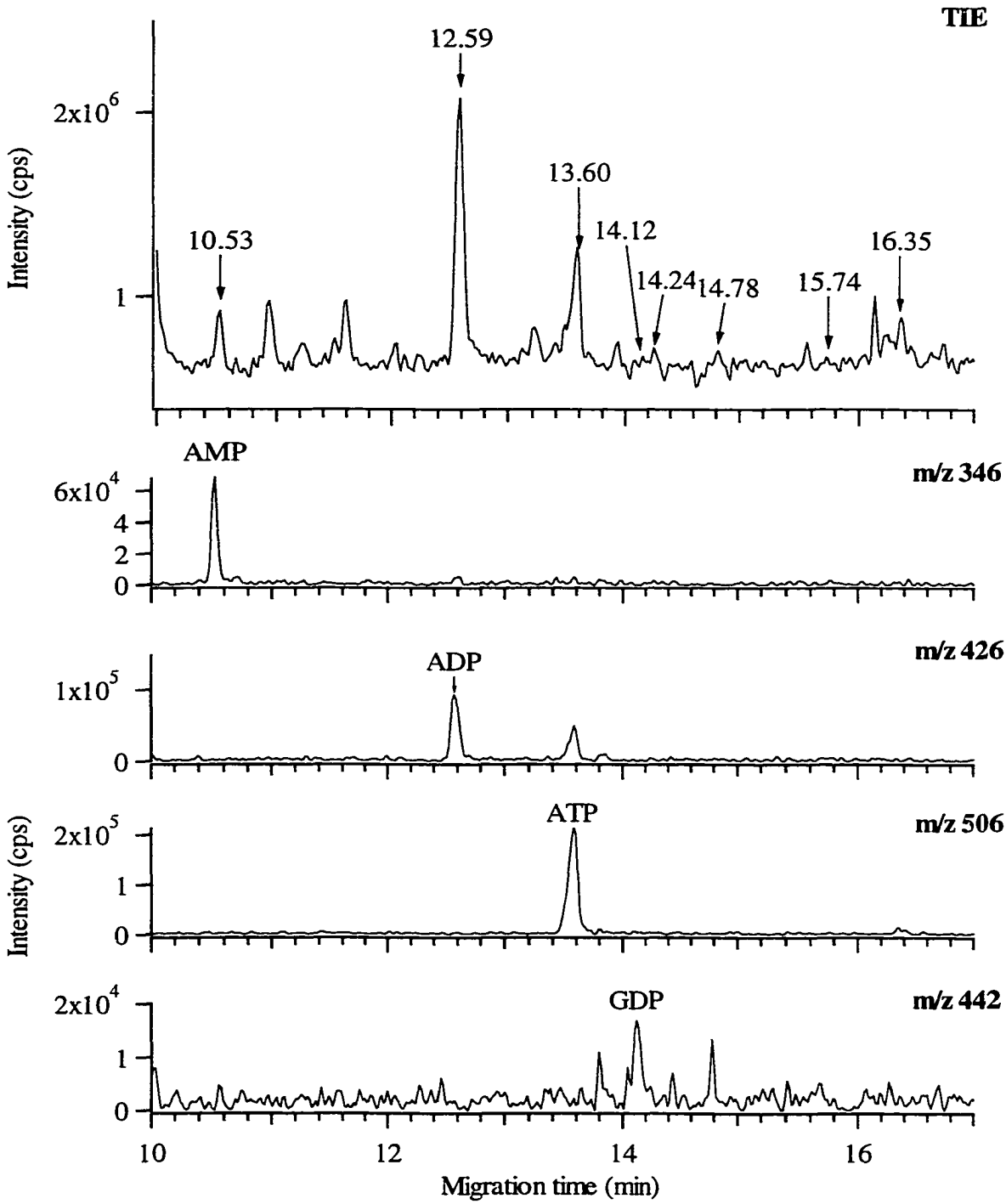

Figure 3.21. (cont'd)

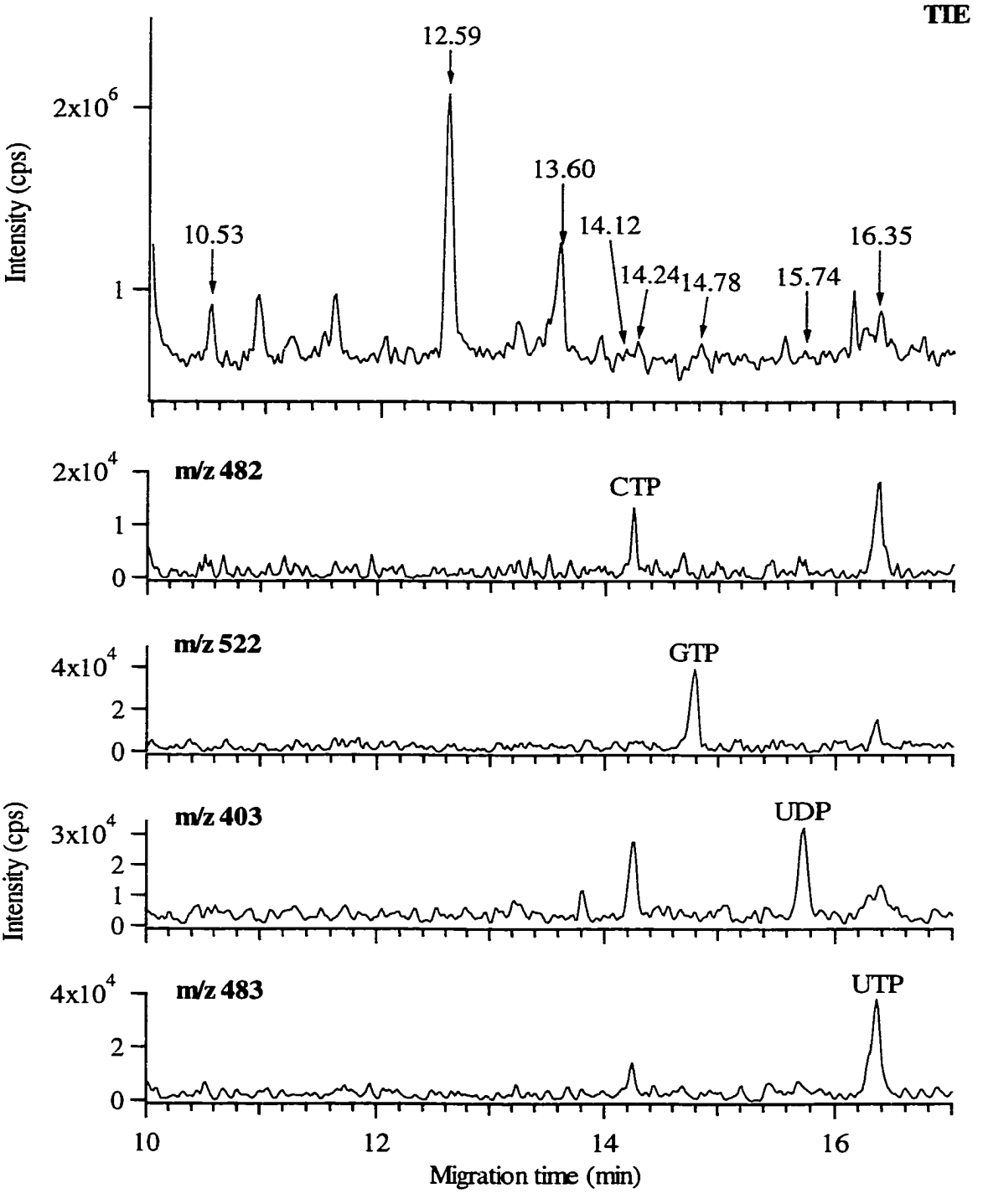

Figure 3.22. Selected ion electropherograms showing the detection of 3TC and its metabolites in Hep G2 cell lines.

Negative ESI-MS was performed. (a) Masses m/z 158.5-159.5, 227.5-228.5, 234.5-236.5, 306.5-310.5, 386.0-390.0, 466.0-470.0, 488.5-492.5, 504.5-508.5 were scanned at a speed of 0.89 s/cycle. (b) Traces for 3TC (m/z 227.9), 3TCMP (m/z 308.1), 3TCDP (m/z 387.9), and 3TCTP (m/z 468.1) were extracted from the trace (a).*Na^+ plug signal, # phosphate anion plug signal.

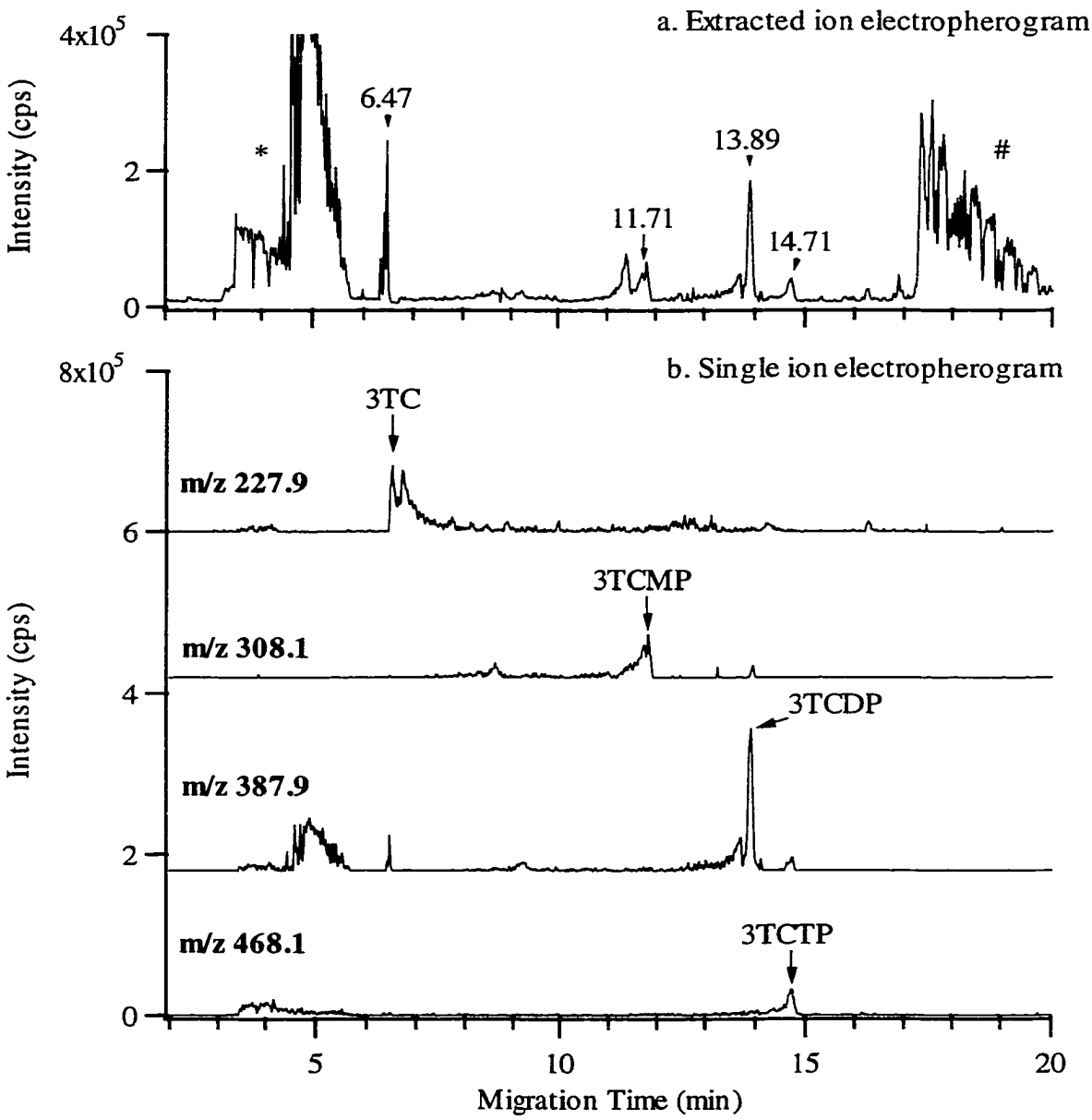

3TC with Hep G2 cells. The signal was obtained from a 100 times concentrated extract, *i.e.*, a combined cell extract with 3 x 2 mL of 60% methanol was evaporated under vacuum to a volume of ~60 μL. These peaks were not shown in a blank cell extract. It is necessary to point out that a simplified extraction procedure has been employed for the demonstration of the phosphorylation studies using the CE-MS method. Large amounts of endogenous species especially the high salt content of the human cell extracts was present in the final preparation of sample prior to CE injection. In fact, we planned to dry the extract and to re-suspend the residue in a small volume of water. However, the final ~60 μL of the oily residue remaining after evaporation was hard to dry again with a common vacuum evaporator. To maintain the content integrity, the residue was injected directly for the following CE-MS analysis. It is therefore predictable that the hydrostatic injection has been affected due to the high viscosity of the sample, and the electrophoretic peak dispersion is present. Nevertheless, using the selected ion monitoring, the profile of 3TC and its phosphorylated forms, 3TCMP, 3TCDP, and 3TCTP has been clearly displayed. The amount of 3TCTP in the cell was estimated at around 10^{-8} M. The sodium ion plug and the phosphate anions plug signals were verified with standards.

3.5 CONCLUSIONS

CE-ESI-MS has been successfully demonstrated for rapid analysis of antiretroviral dideoxynucleosides and their phosphorylated forms. It has been used to study a blank human hepatocyte (Hep G2) cell extract and the intracellular metabolism of 3TC in Hep G2. An optimized ammonium acetate buffer of 25 mM and at pH 10 facilitates efficient separation of the nucleosides and the nucleotides using an untreated fused-silica capillary column under positive electrical field. The best sensitivity is obtained in this buffer with

negative ESI-MS detection. This technique provides 3-4 orders of magnitude of linearity and a 10^{-7} M concentration limit of detection. Future work is being directed to the improvement of sample extraction procedure, and to the application of this analytical approach to permeation and metabolism studies of 3TC and ddG in primary cultures derived from duck hepatocytes and in Hep G2 cell lines.

3.6 BIBLIOGRAPHY

(1) Larder, B.A.; Kemp, S.D.; Harrigan, P.R. *Science* **1995**, *269*, 696-699.

(2) Gazzard, B. *AIDS*. **1996**, *10 Suppl 1*, S3-7.

(3) Barry, M.; Mulcahy, F.; Merry, C.; Gibbons, S.; Back, D. *Clin. Pharmaco.* **1999**, *36*, 289-304.

(4) Zhou, X.J.; Squires, K.; Pan-Zhou, X.R.; Bernhard, S.; Agrofoglio, L.; Kirk, M.; Duchin, K.L.; Sommadossi, J.P. *J. Clin. Pharmacol.* **1997**, *37*, 201-213.

(5) Walters, D.L.; Jacobs, D.L.; Tomaszewski, J.E.; Graves, S. *J. Pharma. Biomed. Anal.* **1999**, *19*, 955-65.

(6) Dobolyi, A.; Reichart, A.; Szikra, T.; Szilagyi, N.; Kekesi, A.K.; Karancsi, T.; Slegel, P.; Palkovits, M.; Juhasz, G. *Neurochem. Int.* **1998**, *32*, 247-256.

(7) Singhal, R.P.; Hughbanks, D.; Xian J. *J. Chromatogr.* **1992**, *609*, 147-161.

(8) Strether, B. N.; PepsiCo, A. J.; Frame, P. T.; Greenberg, K. A.; Stein, D. S. *AIDS* **1994**, *8*, 763.

(9) Kewn, S.; Veal, G.J.; Hoggard, P.G.; Barry, M.G.; Back, D.J. *Biochem. Pharmacol.* **1997**, *54*, 589-595.

(10) Kitos, T.E.; Tyrrell, D.L.J. *Biochem. Pharmacol.* **1995**, *49*, 1291-1302.

(11) Hoggard, P.G.; Manion, V.; Barry, M.G.; Back, D.J. *Br. J. Clin. Pharmacol.* **1998**, *45*, 164-167.

(12) Kamel, A.M.; Brown, P.R.; Munson, B. *Anal. Chem.* **1999**, *71*, 5481-5492.

(13) Andrews, C.L.; Vouros, P.; Harsch, A. *J. Chromatogr. A* **1999**, *856*, 515-526.

(14) Banks, J.F.; Shen, S.; Whitehouse, C.M.; Fenn, J.B. *Anal. Chem.* **1994**, ***66***, 406-414.

(15) Geldart, S.E.; Brown, P.R. *J. Chromatogr. A* **1999**, *831*, 123-129.

(16) Geldart, S.E.; Brown, P.R. *J. Chromatogr. A* **1998**, *828*, 317-336.

(17) Bloom, J; Ortiz, J.; Rodriguez, J.F. *Cellular & Molecular Bio.* **1997**, *43*, 1051-1055.

(18) Krattiger, B.; Bruno, A.E.; Widmer, H.M.; Dandliker, R. *Anal. Chem.* **1995**, *67*, 124-130.

(19) Britz-McKibbin, P; Bebault, G.M.; Chen, D.D.Y. *Anal. Chem.* **2000**, *72*, 1729-1735.

(20) Loo, J.A.; Udseth, H.R.; Smith, R.D. *Anal. Biochem.* **1989**, *179*, 404-12.

(21) Smith, R.D.; Loo, J.A.; Barinaga, C.J.; Edmonds, C.G.; Udseth, H.R. *J. Chromatogr.* **1989**, *480*, 211-32.

(22) Tsuji, K.; Baczynskyj, L.; Bronson, G.E. *Anal. Chem.* **1992**, *64*, 1864-1870.

(23) Issaq, H.J.; Chan, K.C.; Janini, G.M.; Muschik, G.M. *Electrophoresis* **1999**, *20*, 1533-7.

(24) Veenstra, T.D.; Martinovic, S.; Anderson, G.A.; Pasa-Tolic, L.; Smith, R.D. *J. Am. Soc. Mass Spectrom.* **2000**, *11*, 78-82.

(25) Minarik, M.; Foret F.; Karger, B.L. *Electrophoresis* **2000**, *21*, 247-54.

(26) Moseley, M.A.; Deterding, L.J.; Tomer, K.B.; Jorgenson, J.W. *Anal. Chem.* **1991**, *63*, 109-114.

(27) Johansson, I.M.; Huang, E.C.; Henion, J.D.; Zweigenbaum, J. *J. Chromatogr.* **1991**, *554*, 311-27.

(28) Thibault, P.; Paris, C.; Pleasance, S. *Rapid Commun. Mass Spec.* **1991**, *5*, 484-90.

(29) Varghese, J.; Cole, R.B. *J. Chromatogr. A* **1993**, *652,* 369-76.

(30) Zhang, B.; Liu, H.; Karger, B.L.; Foret, F. *Anal. Chem.* **1999**, *71,* 3258-64.

(31) Li, J.; Kelly, J.F.; Chernushevich, I.; Harrison, J.D.; Thibault, P. *Anal. Chem.* **2000**, *72,* 599-609.

(32) Johansson, I.M.; Pavelka, R.; Henion, J.D. *J. Chromatogr.* **1991**, *559,* 515-28.

(33) Perkins, J.R.; Parker, C.E.; Tomer, K.B. *J. Am. Soc. Mass Spectrom.* **1992**, *3,* 139-149.

(34) Tomlinson, A.J.; Benson, L.M.; Johnson, K.L.; Naylor, S. *Electrophoresis* **1994**, *15,* 62-71.

(35) Liu, C.S.; Li, X.F.; Pinto, D.; Hansen, E.B. Jr.; Cerniglia, C.E.; Dovichi, N.J. *Electrophoresis* **1998**, *19,* 3183-3189.

(36) Ruda, S.; Cherkaoui, S.; Dayer, P.; Fanali, S.; Veuthey, J.L. *J. Chromatogr. A* **2000**, *868,* 295-303.

(37) Harsch, A.; Vouros, P. *Anal. Chem.* **1998**, *70,* 3021-3027.

(38) Deforce, D.L.; Lemiere, F.; Esmans, E.L.; De Leenheer, A.; Van den Eeckhout, E.G. *Anal. Biochem.* **1998**, *258,* 331-338.

(39) Ding, J.; Vouros, P. *Anal. Chem.* **1997**, *69,* 379-384.

(40) Schrader, W.; Linscheid, M. *Archiv. Toxicol.* **1997**, *71,* 588-595.

(41) Deforce, D.L.D.; Ryniers, F.P.K.; Van den Eeckhout, E.G.; Lemiere, F.; Esmans, E.L. *Anal. Chem.* **1996**, *68,* 3575-3584.

(42) Zhao, Z.; Wahl, J.H.; Udseth, H.R.; Hofstadler, S.A.; Fuciarelli, A.F.; Smith, R.D. *Electrophoresis* **1995**, *16,* 389-395.

(43) Wolf, S.M.; Vouros, P. *Anal. Chem.* **1995**, *67,* 891-900.

(44) Ts'o, P. O. P. *Basic Principles in Nucleic Acid Chemistry, Vol. 1,* **1974**, Academic Press, New York, pp 461-465.

(45) Rodriguez, A.; Yost, R. *47th Am. Soc. Mass. Spec. Con. Mass Spec. & Applied Topics, Proceedings,* **1999**, 1022.

(46) Ogorzalek, R. R.; Smith, R. D. *J. Mass. Spectrom.* **1995**, *30*, 339-344.

(47) Chen, D.Y. *Ph.D Thesis in Chemistry, University of Alberta*, **1993.**

(48) Green-Church, K.B.; Limbach, P.A. *J. Am. Soc. Mass Spectrom.* **2000**, *11*, 24-32.

(49) Andrien, B.A.; Banks, J.F.; Boyle, J.G.; Dresch, T.; Haren, P.J.; Whitehouse, C.M. *Proceedings of the 43rd ASMS Conference on Mass Spectrometry and Allied Topics;* **1995**, Atlanta, GA, pp 999.

CHAPTER 4 [1]

Characterization of Oligosaccharides by Microelectrospray Mass Spectrometry and Capillary Electrophoresis-Mass Spectrometry

[1] Part of this work has been presented at the 83rd Canadian Society for Chemistry National Meeting & Exhibition, Calgary, AB, Canada, May 2000.

4.1 ABSTRACT

This chapter presents micro-electrospray (μESI) and on-line capillary electrophoresis-electrospray mass spectrometry (CE-ESI-MS) for the characterization of fluorescently labeled and underivatized oligosaccharides at the femtomole level. In the positive-ion mode μESI-MS, numerous intense ions suitable for identification of chromophore-labeled oligosaccharides were generated in high abundance. Underivatized oligosaccharides complexed to alkali metal ions were also detected with high sensitivity. Concentration limits of detection were in the range of 10-100 nM. The very low flow rates inherent to μESI of about 200 nL/min, together with the high signal intensity make it possible to employ μESI-MS for structural analysis. Investigation of a complex mixture of the saccharides however, revealed that the μESI-MS sacrifices sensitivity due to ion suppression arising from other analytes and matrices, and the compound identity is difficult to assign. In a coupled CE-MS analysis, with the help of the first dimensional separations, an individual component in a mixture containing the tetramethylrhodamine-labeled and underivatized oligosaccharides can be identified with high sensitivity.

4.2 INTRODUCTION

The field of glycobiology has been growing rapidly primarily due to the increased awareness among scientists of the critical metabolic functions of carbohydrates in the body, as well as the importance of post-translational glycosylation in the function of recombinant glycoproteins[1, 2]. Research into the physiological roles of carbohydrates has led to a number of carbohydrate-based therapeutics[3], including anti-coagulants such as heparin[4], anti-inflammatories[5], anti-microbials[6], and anti-cancer drugs[7]. The growing interest in biological functions of carbohydrates has stimulated the development of analytical methodology for their determination and structural characterization[2, 8-12].

The main difficulties in carbohydrate analysis arise from their enormous number of possible isomeric forms because of the various possible configurations of the monosaccharides[13], and the presence of nonglycosyl substituents, such as acetyl, methyl, amine, and phosphate groups. The very polar and nonvolatile nature of these compounds as well as the absence of chromophoric or fluorophoric groups further complicate their chemical analysis.

In recent years, mass spectrometry alone or along with chemical/enzymatic degradation has become a key tool for the characterization of oligosaccharides[14-21]. The invention of the electrospray ionization (ESI) and matrix-assisted laser desorption / ionization (MALDI) stimulated the applications of MS on studies of thermally labile oligosaccharides. The sequence and linkage assignments in carbohydrates have been achieved using collisional induced dissociation (CID) or in the case of MALDI-time-of-flight, post-source decay (PSD) capabilities. These techniques, however, have limited sensitivities, at picomole levels, mainly due to ion suppression associated with the ESI or MALDI process of impurities and byproducts[21,22]. A chromatographic separation prior to

MS analysis should provide additional purification and pre-concentration of carbohydrates for sensitive analyses. The most notable analytical methods in the past for carbohydrates have been gas chromatography-mass spectrometry[23] and high-performance liquid chromatography-electrospray mass spectrometry[24-26]. Capillary electrophoresis (CE) has emerged as an alternative technique to conventional chromatographic techniques due to its unprecedented separation efficiencies and its minimal sample requirement[27]. Carbohydrates, however, are difficult to analyze by CE because they lack suitable chromophores for conventional spectrometric detection and are not charged under normal capillary zone electrophoresis (CZE) conditions, with the exception of complex oligosaccharides charged through sialyation and/or sulfation[28, 29]. Derivatization with a suitable tag providing either a chromophore or a flurophore for high sensitivity detection has been the most widely employed strategy[30-33]. *In situ* complexation with borate[34, 35] or metal ions[36] in CE has been utilized in the separation of carbohydrates. Alternatively, the use of micellar electrokinetic chromatography (MEKC) has also been successfully employed for separation of neutral saccharides[37]. Detection methods generally employed for carbohydrate separations employing CE have been UV[34,38,39], laser-induced fluoresence (LIF)[32,35,40,41], electrochemical[42] and thermo-optical absorbance[43]. These methods do not allow a structural characterization of carbohydrates. In this context, the combination of CE and electrospray mass spectrometry (ESI-MS) should be valuable for the analysis of carbohydrates.

CE-ESI-MS has been used for the analyses of negatively charged oligosaccharides[45-48] or glycoform populations of intact glycoproteins[9,49,50]. A major limitation in the development of CE-ESI-MS methodology is the use of volatile buffers, thus limiting the optimization of the CE resolving power. This has been particularly the case for analysis of natural carbohydrates and carbohydrates labeled with a neutral

chromophore, e.g. 5-carboxytetramethylrhodamine succinimidyl ester (TRSE). The present study has investigated the use of μESI and CE-ESI-MS for the characterization of natural and TRSE labeled mono- and oligo-saccharides. The TRSE labeled oligosaccharides have been used to characterize a substrate-enzyme reaction by CE-LIF in this lab[11,32,35,51], in which some product peaks have not been assigned.

4.3 EXPERIMENTAL

4.3.1 Chemicals and Materials

The fluorescently labeled sugar and the natural sugars studied in this chapter were a generous gift from Dr. Monica Palcic, Department of Chemistry, University of Alberta. Their syntheses were described in an earlier paper[52]. Structures of these sugars are shown in **Figure 4.1**. Stock solutions of 100 μM were prepared in water and stored under -20°C until analysis. HPLC-grade methanol, acetonitrile and were purchased from BDH (Toronto, ON, Canada) and were purified by distillation. Sodium hydroxide (NaOH) and acetone were also from BDH. Ammonium acetate (NH_4Ac), acetic acid (HAc) and hydrochloric acid (HCl) were obtained from Anachemia (Montreal, PQ, Canada). Toluene was from Sigma (St. Louis, MO). 3-aminopropyltrimethoxysilane (APS-Silane) was from Sigma. Fused silica capillaries were from Polymicro Technologies (Phoenix, AZ).

4.3.2 Procedures

A PE/Sciex API 100 single quadrupole mass spectrometer equipped with an ion spray interface and a microspray interface was used in this study. The microspray interface is illustrated in **Figure 4.2.** Standards were diluted in 90%MeOH and infused at

Figure 4.1. Structures of the TRSE-labeled sugars.

MR: monosaccharide-TRSE; DR: disaccharide-TRSE; TR: trisaccharide-TRSE. Trig-L: trisaccharide with a linker arm. Lac-L: lactose with a linker arm.

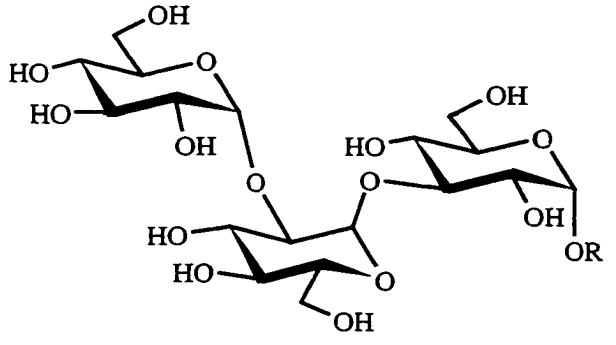

Lac-L, Trig-L:

R =

$-(CH_2)_8-CO-NH-CH_2CH_2-NH_2$

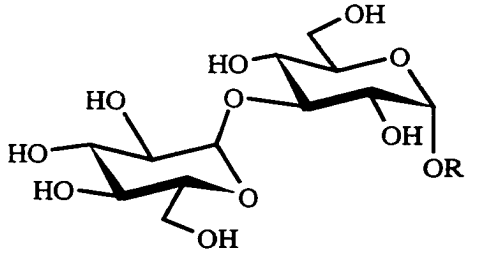

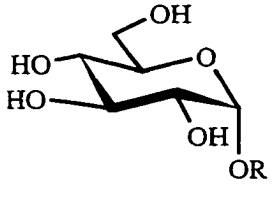

MR, DR, TR:

R =

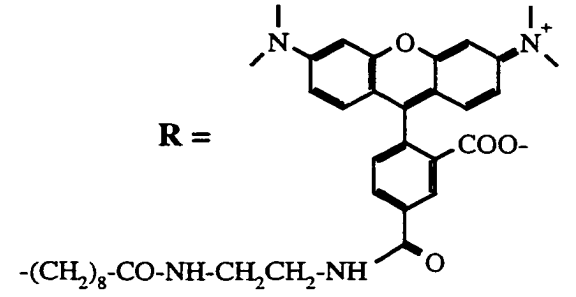

Figure 4.2. A schematic diagram of the microspray interface set-up.

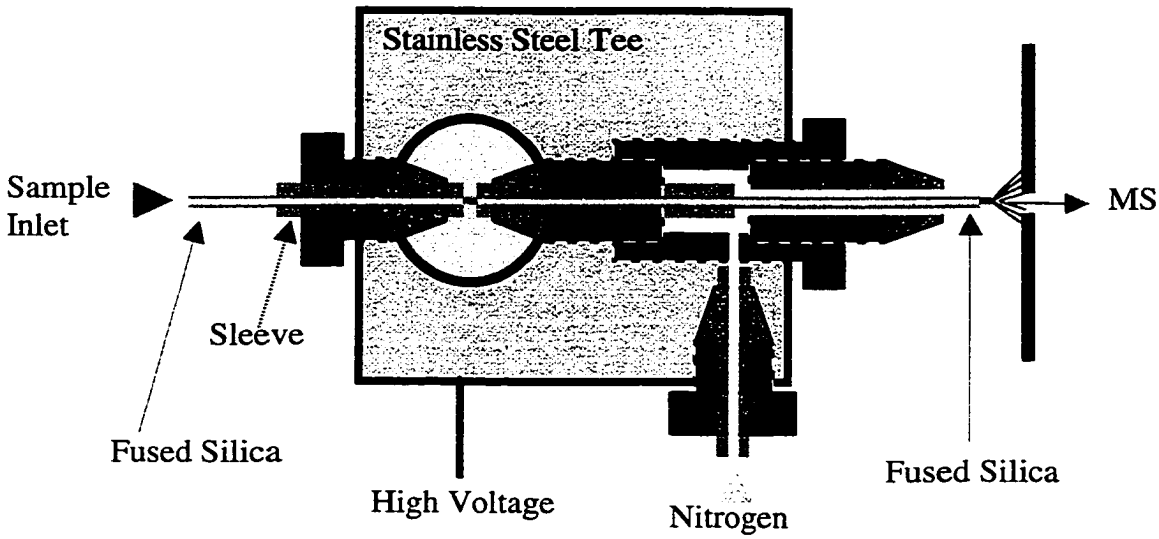

0.2 μL/min in μESI studies with a syringe infusion pump from Harvard Apparatus (Southnatick, MA). Typically a standard solution with 2 μM concentration in distilled methanol was infused to obtain an ESI mass spectrum, with the exception of calibration studies where sample solutions with a concentration range of 5 nM-100 μM were infused to the μESI-MS. Positive ion detection mode was conducted with potentials applied at the ion sprayer, the orifice and the focusing ring of 4.5 kV, 60 V and 400 V, respectively. Typically, a mass range of 30-1200 Da was scanned at a speed of 5.86 s/scan with a mass step size of 1.0 Da and a dwell time of 5 ms, or with a step size of 0.5 Da and a dwell time of 2.5 ms.

The on-line CE-MS studies utilized an in-house designed CE injector coupled to the ion spray MS. The set-up of the CE-MS interface has been described in Chapter 1. Separations were made in a fused-silica capillary column with inner wall derivatized with APS-silane. The APS silane-coating neutralizes the charges of the capillary wall and eliminates the electro-osmotic flow. Therefore a reversed polarity for CE separation was employed. The APS silane-coated capillaries were prepared according to procedures similar to those reported by Tomer and co-workers[53]. Briefly, the fused-silica capillaries (50 μm ID X 150 μm OD X 2 m long) were pre-treated, in order, with 0.1 M NaOH, H_2O, 0.1 M HCl and H_2O infused under a pressure of 60 psi for 3 hrs, 1 hr, 3 hrs and 0.5 hr, respectively. The inner wall was then dried under a stream of nitrogen at 40 psi and at 150 °C for about 3 hrs. The APS, 5% in toluene, was flushed through the capillary at 40 psi and 50 °C for 10 hrs. The coated column was then washed, in order, with toluene at 50 °C for 2 hrs, acetone at room temperature for 1 hr, and methanol at room temperature for 30 min, all under 40 psi. The column was then dried under a nitrogen stream (40 psi) for 2 hrs before use. An 60 cm long piece of the coated capillary was used for CE separation at -200 V/cm with a current of 3 μA. The background electrolyte (BGE) was

10 mM acetic acid. A sample mixture with 10 μM each dissolved in 50% (v/v) BGE was injected at 18 cm for 30 s, *i.e.*, the injected volume was 14 nL. Positive ESI-MS detection was conducted. Typically, the voltages applied at the ion sprayer (IS), the orifice (OR) and the focusing ring (RNG) were 5.0 kV, 80 V, and 400 V, respectively. The quadrupole mass analyzer was scanned at 1.0 s/scan over a mass range of 300-1200 Da with a mass step of 0.5 Da and a dwell time of 0.6 ms. The sheath liquid was methanol at 3.0 μL/min. The nebulizing gas, nitrogen, was supplied at 0.17 L/min (NEB 1), and the curtain gas was at 1.08 L/min (CUR 9).

Separations were also carried out in an untreated capillary column (60 cm x 50 μm ID x 150 μm OD) under positive electrical field at +260 V/cm. The BGE was a nonaqueous buffer of methanol-acetonitrile (70:30) with 40 mM ammonium acetate. Samples with 10 μM concentration dissolved in methanol were injected at 10 kV for 10 s, i.e. 11 nL sample was injected. Positive ESI-MS detection was conducted. The voltages applied at the ion sprayer (IS), the orifice (OR) and the focusing ring (RNG) were 4.2 kV, 35 V, and 230 V, respectively. The quadrupole mass analyzer was scanned at 0.86 s/scan over a mass range of 340-1200 Da with a mass step of 0.5 Da and a dwell time of 0.5 ms. The sheath liquid was methanol at 3.0 μL/min. The nebulizing gas was supplied at 0.41 L/min (NEB 3), and the curtain gas was at 1.08 L/min (CUR 9).

4.4 RESULTS AND DISCUSSION

4.4.1 Infusion-μESI-MS

Six oligosaccharides were characterized by μESI-MS. These standards include the TRSE-labeled monosaccharide (MR), disaccharide (DR), trisaccharide (TR), and the linker-arm derivatized disaccharide (lactose-linker, Lac-L) and trisaccharide (Trig-L), as

well as the nonderivatized lactose. The positive μESI mass spectra of the TRSE-labeled sugars prepared in methanol showed mainly intense peaks of pseudo-molecular ions $[M+H]^+$ and $[M+Na]^+$, as well as doubly charged ions $[M+H+Na]^{2+}$ and $[M+2Na]^{2+}$, **Figure 4.3**. Interestingly, from MR to TR, the presence of doubly charged ions increases. Non-labeled saccharides (lactose, Lac-L and Trig-L), however, exhibited mainly $[M+Na]^+$ ions, **Figure 4.4**. Protonated molecular ions and doubly charged ions were not generated in appreciable abundance. Some typical fragment ions, e.g. $[M-162]^+$, $[M-162-162]^+$, $[M-162-162-162]^+$ and ions from side chain cleavages were observed from the labeled sugars allowing their sequence characterization. Similar ions were only observed in ESI spectra of non-labeled saccharides at elevated orifice voltages (OR) for an increased in-source collision-induced dissociation (CID). For example, if the OR voltage was less than 80 V, fragments derived from glycosidic bond cleavages were not significant. As the CID energy further increased to 120 V, the sodiated molecular ions fragmented to lower-mass ions and the fragments (also sodium adducts) increased up to 15% in relative abundance, **Figure 4.5**.

Glycosidic bond cleavages and cross-ring cleavages have been reported as the two dominant processes in the fragmentation of protonated oligosaccharide ions and alkali metal ion adducts, together with the loss of metal ions (e.g. Na^+) in the fragmentation of the metal ion adducts[13,20]. Dissociation from glycosidic bond cleavage and cross-ring cleavages are important for the determination of sequence and linkages of the oligosaccharides, respectively. In the present study, products from cross-ring cleavages were generally not observed with the investigated saccharides. It has been reported that complex glycan structures commonly suppress cross-ring cleavages in MS/MS experiments[19].

Figure 4.3. The μESI mass spectra of the TRSE-labeled sugars.

(A) Monosaccharide derivatized with TRSE (MR). (B) Disaccharide derivatized with TRSE (DR). (C) Trisaccharide derivatized with TRSE (TR). Samples were prepared in methanol at a concentration of 2 μM and infused at 200 nL/min for 1 min, i.e. 400 fmol was infused and 5 spectra were summed. Other conditions were as described in the experimental section.

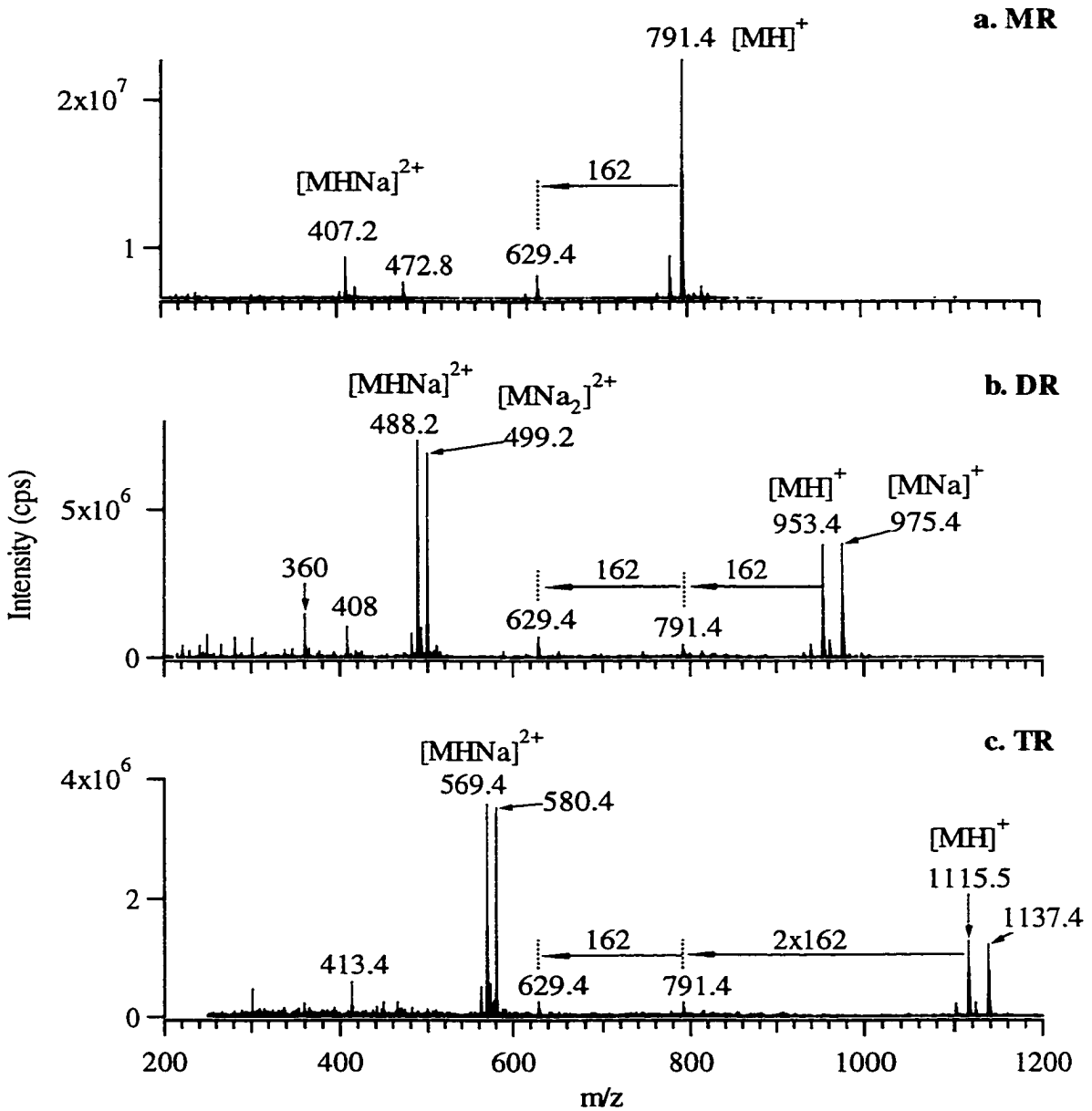

Figure 4.4. The μESI mass spectra of sugars without the TRSE label.

(A) Trisaccharide derivatized with a linker arm (Trig-L). (B) Lactose derivatized with a linker arm (Lac-L). (C) Lactose (Lac). Samples were prepared in methanol at a concentration of 2 μM and infused at 200 nL/min for 1 min, i.e. 400 fmol was infused and 5 spectrum was accumulated.

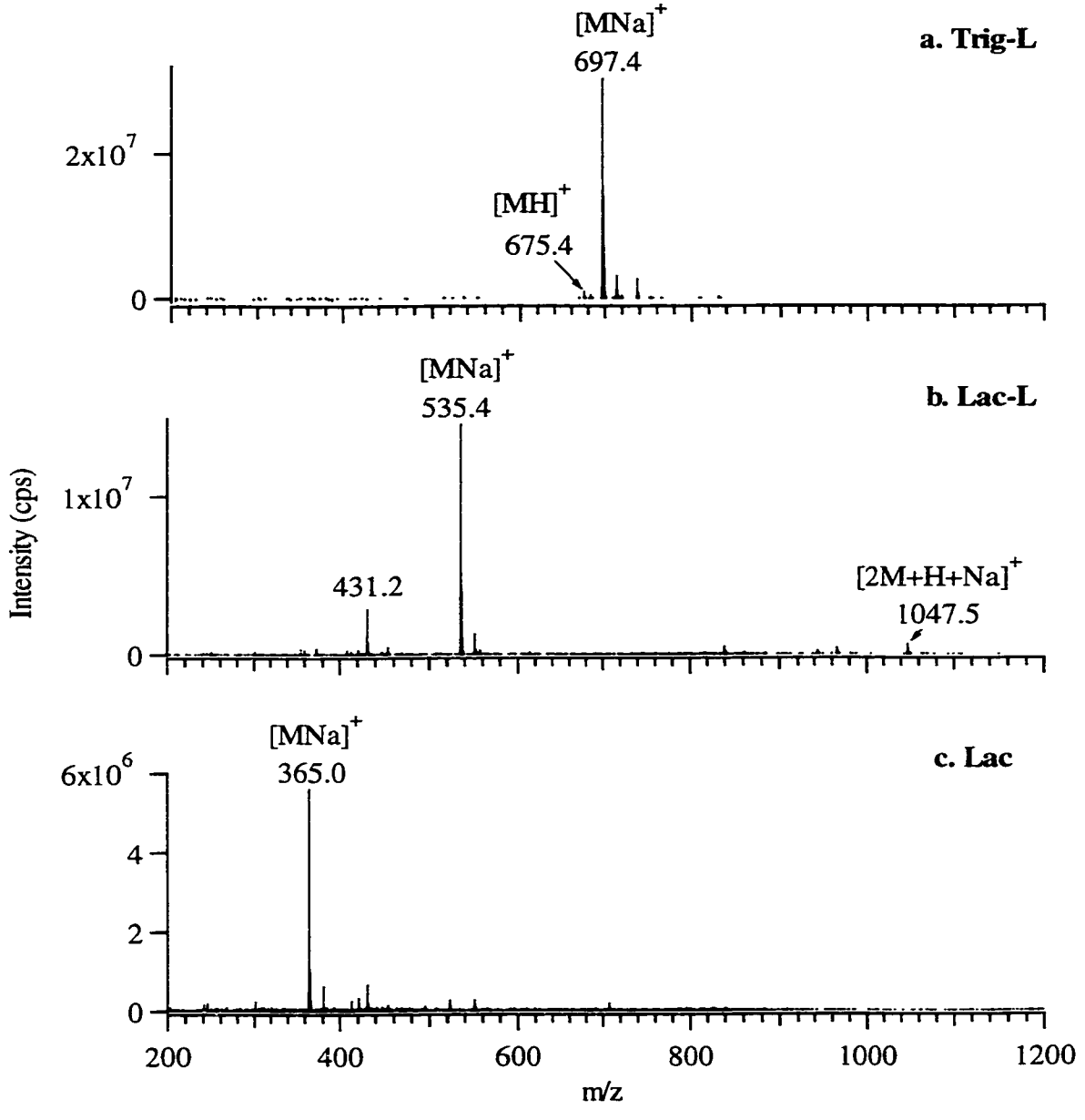

Figure 4.5. The μESI mass spectra of Trig-L at various orifice voltages.

The sample, 20 μM, was prepared in methanol and was infused at 200 nL/min for 1 min, i.e. 400 fmol was infused and 5 spectra were summed. (A) OR 60 V; (B) OR 80 V; (C) OR 120 V. Other conditions were as described in the experimental section.

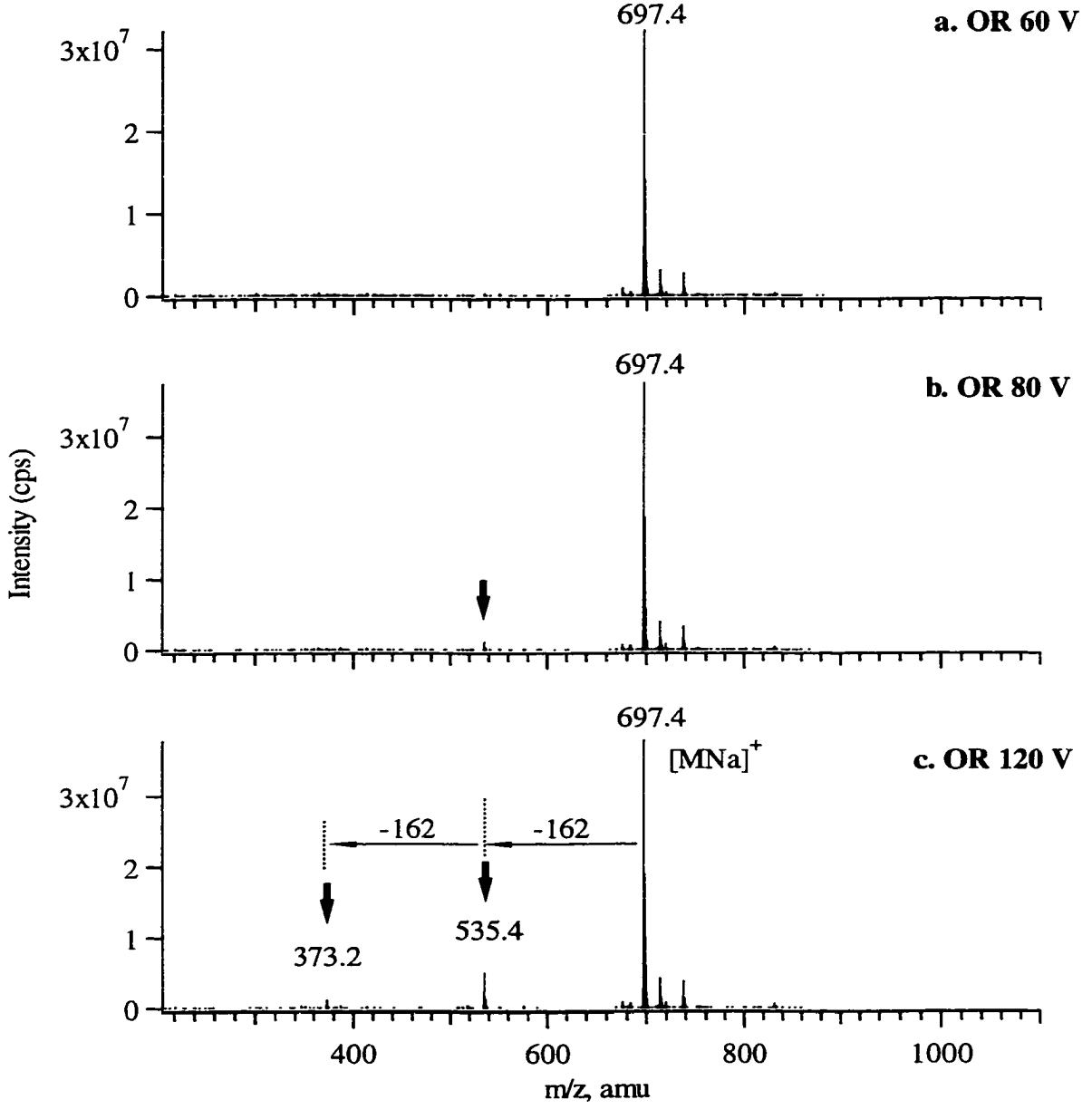

The calibration curves of the TRSE-labeled saccharides show that linearity is obtained in the range of 20-2000 fmol of analyte infused, **Figure 4.6**. The 3σ concentration detection limits of the μESI-MS for MR, DR, TR and Trig-L were 8, 8, 60, and 5 nM, respectively, calculated from their $[M+Na]^+$ signals and their surrounding noise signals. The infusion volume for obtaining 5 accumulated spectra was 200 nL in 1 min, therefore the mass detection limits for MR, DR, TR and Trig-L were 1.6, 1.6, 12, and 1.0 fmol, respectively.

The μESI mass spectra of TR prepared in a cell media[35] exhibited more complex patterns than did TR in a pure solvent such as water and methanol, **Figure 4.7**. Although the presence of the TR was still detectable at a 10 μM concentration, the sensitivity has been largely suppressed by the presence of media matrices. Without chromatographic separation it would be extremely difficult to discriminate the analyte of interest from other species. An approach that utilizes an electrophoretic separation and an on-line ESI-MS detection has been investigated.

4.4.2 Aqueous CE in an APS Silane-Coated Column

The TRSE labeled saccharides possess a convenient fluorophore with maximum excitation at 552 nm and maximum emission at 570 nm. CE was first developed using borate buffers[32] that facilitate the separation of closely related monosaccharides via the formation of anionic complexes. This separation scheme is not suited to ESI-MS operation in either positive or negative ion mode due to the high chemical background leading to suppression of the analyte signal. Electrophoretic separations using volatile buffers such as aqueous ammonium acetate or nonaqueous ammonium acetate have been developed with the operation of electrospray ionization. Examples of electropherograms obtained utilizing MS detection with positive ion mode are presented in **Figure 4.8** and

Figure 4.6. Calibration curves of the TRSE labeled sugars obtained by μESI-MS.

Samples were prepared in methanol and infused at 200 nL/min to the μESI-MS. Other conditions were as described in the experimental section.

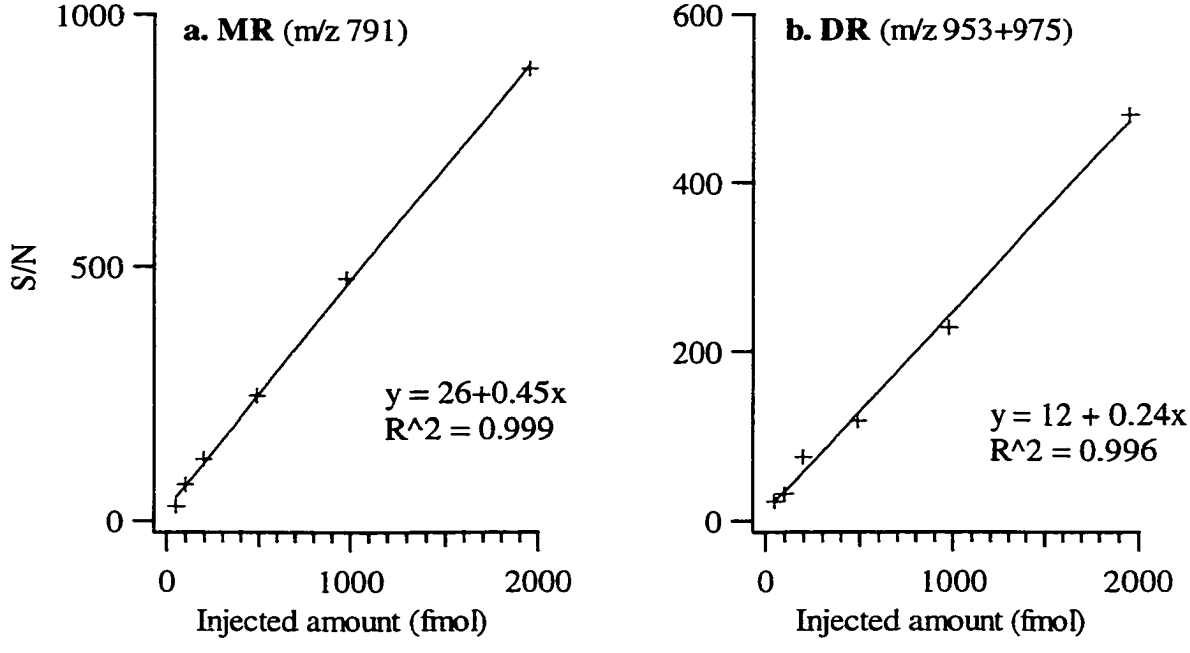

Figure 4.7. μESI mass spectra of 10 μM TR in a cell incubation media.

Sample was infused at 200 nL/min for 1 min. 5 spectra were summed. Other conditions were as described in the experimental section.

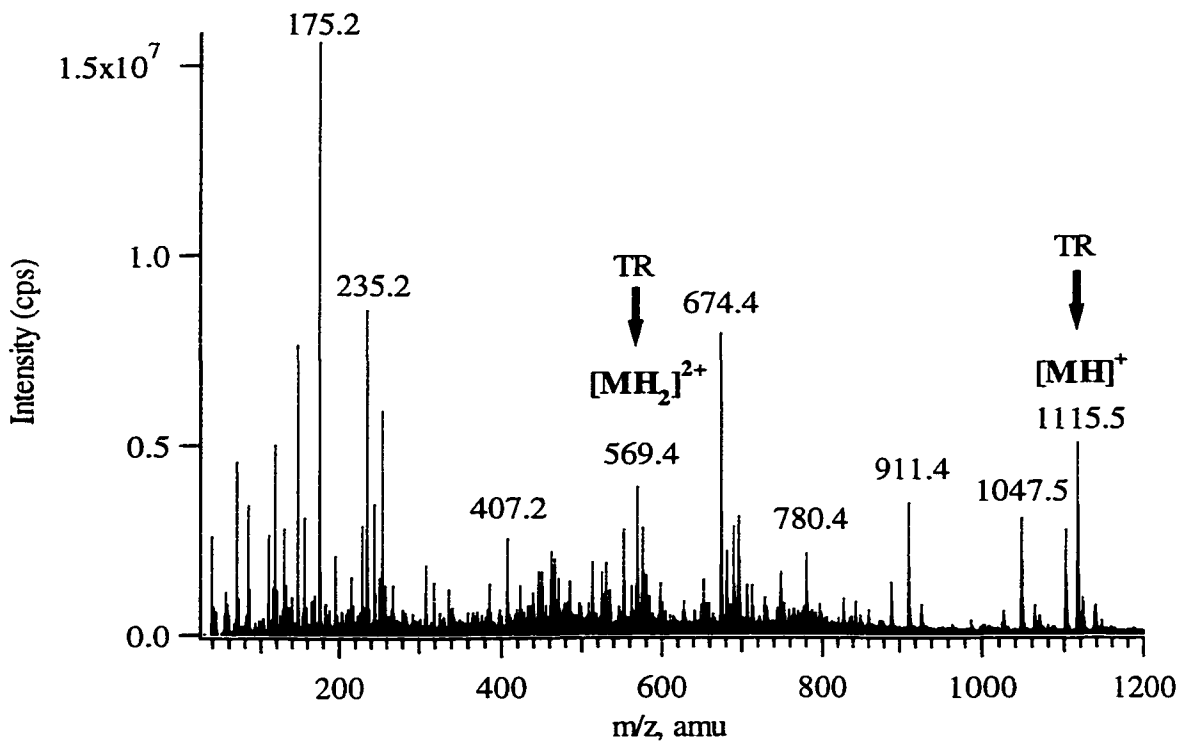

Figure 4.8. Total ion electropherogram showing the separation of the TRSE labeled and non-labeled sugars by CE-MS using an APS coated column and acidic separation buffer.

The sample was a 10 μM mixture prepared in 50% (v/v) BGE and injected at 18 cm for 30 s, i.e. a volume of 14 nL was injected. The separation column was APS coated with 50 μm ID x 150 μm OD x 60 cm. Separation was performed at -200 V/cm with a current of 3 μA. The BGE was 10 mM acetic acid. Other conditions were as described in the experimental section.

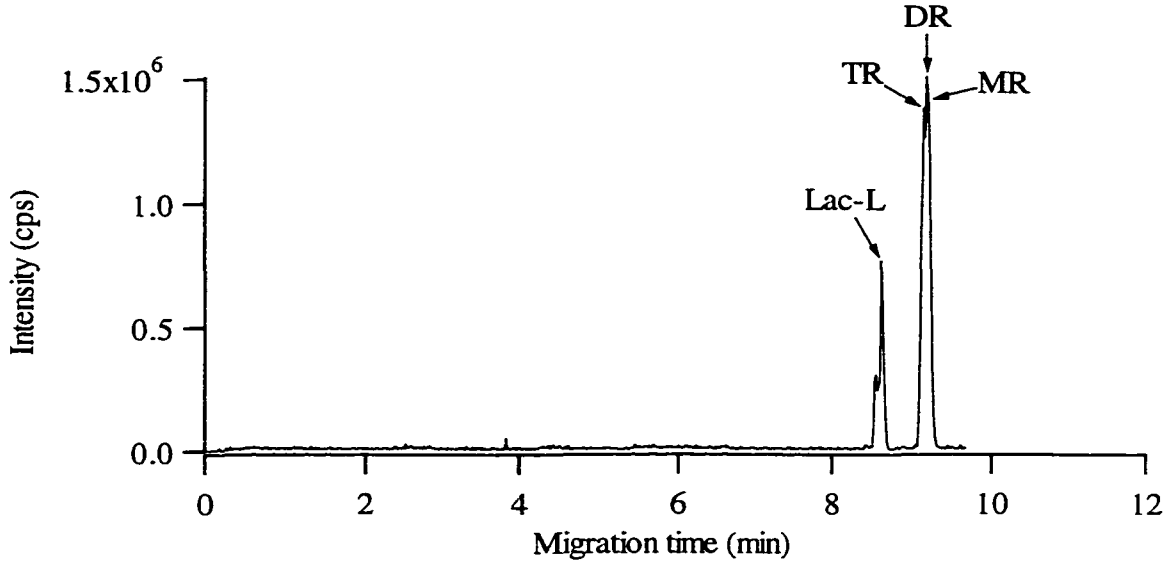

Figure 4.9. The separations were performed in an APS Silane coated capillary column using acidic separation buffer system and reversed electrical field. The TRSE-labeled disaccharide (DR) is well separated from the disaccharide with a linker arm as depicted in **Figure 4.8**. The three saccharides labeled with TRSE are slightly resolved from one another when the analysis was conducted using selected ion monitoring. For example, the three labeled sugars were observed at 9.23 (TR), 9.19 (DR), and 9.12 (MR) minutes in the reconstructed (extracted) ion electropherogram obtained from the same analysis as shown in **Figure 4.9**. The TRSE-labeling through a reductive amination produces relative neutral species under the solution pH of the separation background electrolyte, which explains why these analytes are not well separated by the free zone CE.

Extracted mass spectra taken at the crest of each peak are presented in **Figure 4.10**. In each case, the mass spectrum is dominated by ions corresponding to the protonated molecule $[MH]^+$ and protonated fragments arose from the cleavages of the glycosidic bonds and the side chain linkage; few sodium adducts were present. Note that the orifice voltage associated with the in-source collision induced dissociated was set to 80 V for more fragmentation information. Nevertheless, these spectra obtained after CE separations were slightly different from those appeared in the micro-electrospray experiments (**Figure 4.3**), where the sodium adducts were predominant. The information of molecular weight and bond cleavages shown in the mass spectra allows ambiguous assignment of sugar identity, though these sugars are not completely resolved by CE.

4.4.3 Nonaqueous CE in an Untreated Column

Separation of the TRSE-labeled sugars has also been developed using a nonaqueous buffering system in an untreated capillary column with positive ion ESI-MS detection. Nonaqueous CE-ESI-MS has been successfully employed for studies of structurally

Figure 4.9. Extracted ion electropherograms showing the separation of mono-, di-, and tri-saccharide labeled with TRSE.

Conditions was as in **Figure 4.8**.

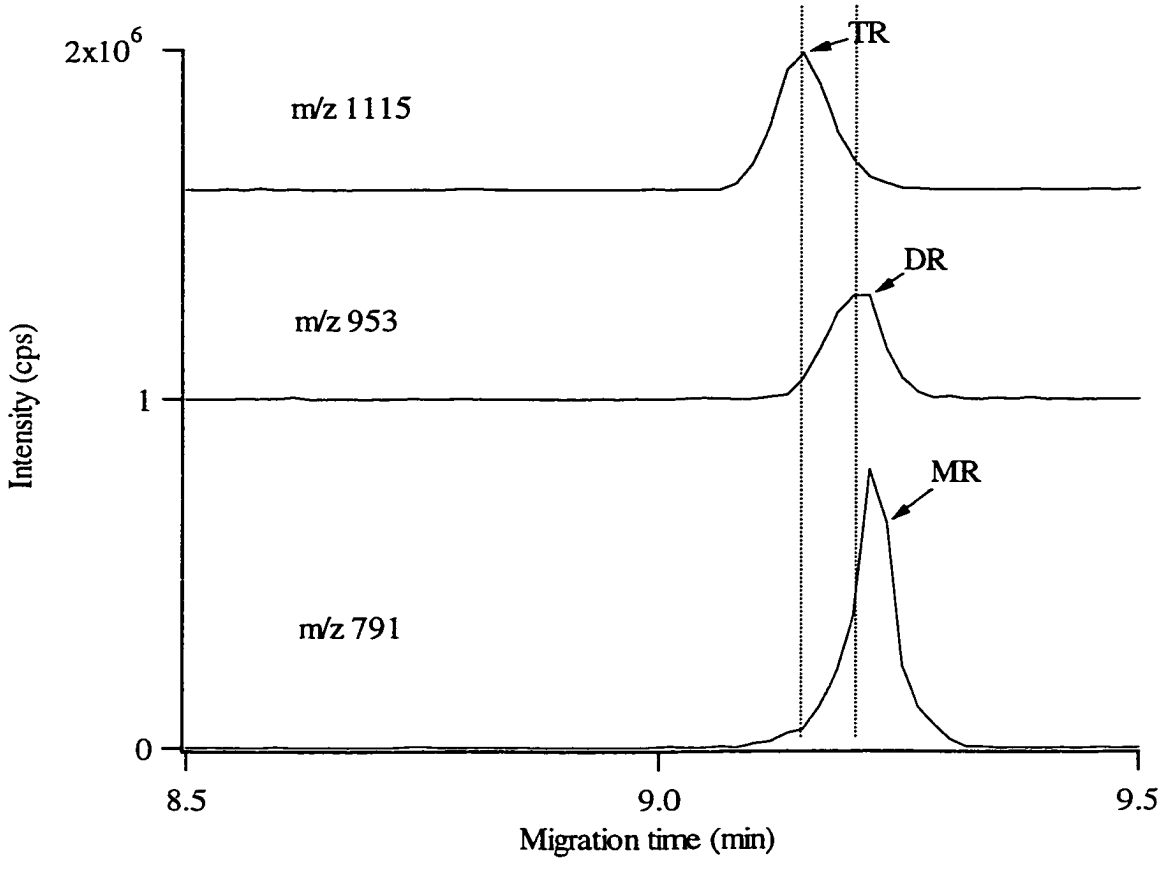

Figure 4.10. The ESI mass spectra of the TRSE-labeled sugars separated by CE-MS showing in **Figure 4.8**.

The potentials applied at the ion sprayer, the orifice, and the ring were 5.0 kV, 80 V, and 400 V, respectively.

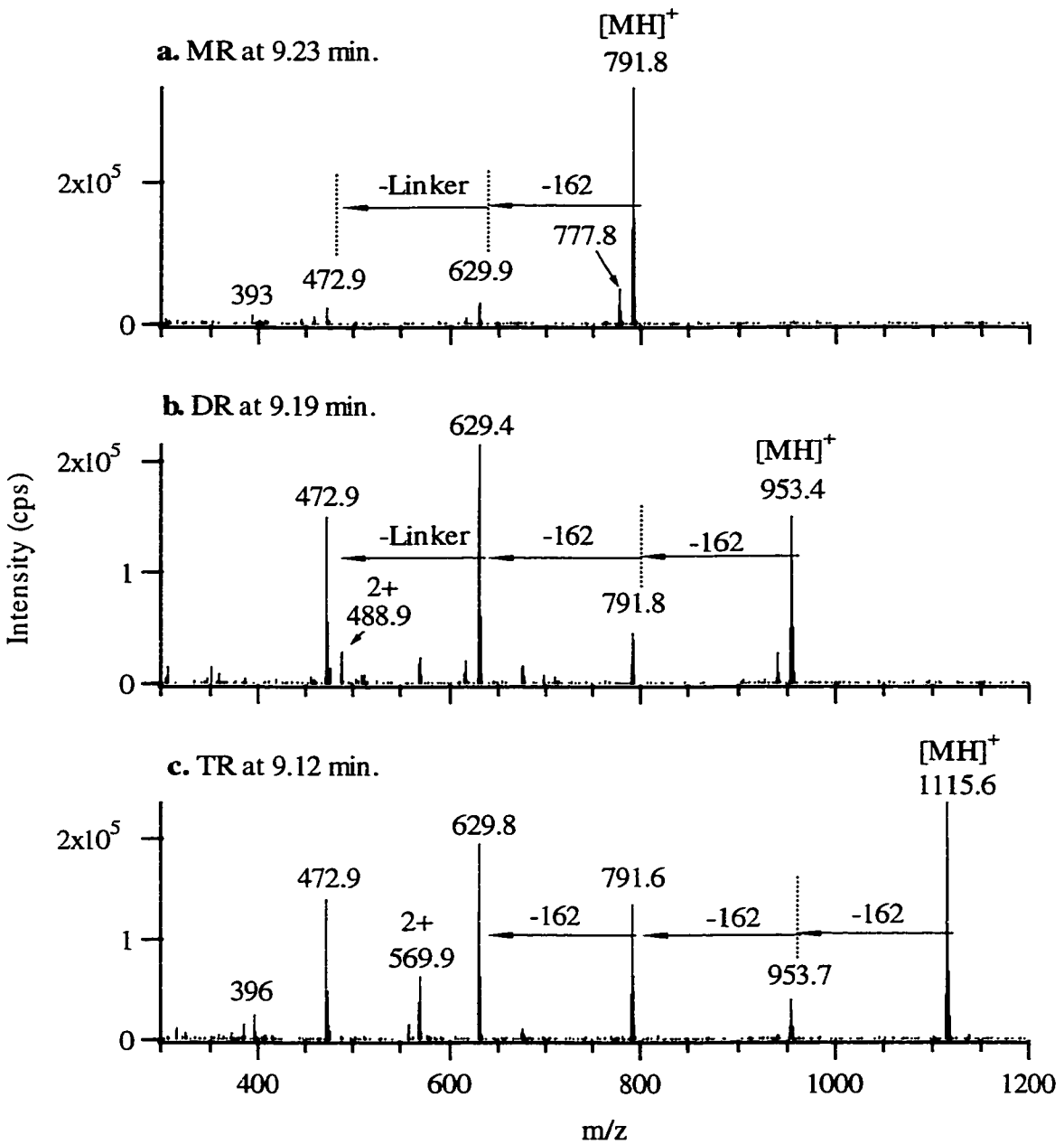

similar antidepressants and metabolites[54]. Similar to that in **Figure 4.8**, the TRSE-labeled sugars were partially resolved with one another in the nonaqueous CE-MS as demonstrated in **Figure 4.11**.

4.5 CONCLUSION

Microelectrospray MS provided sensitive detection of fluorophore-labeled and non-labeled oligosaccharide standards. Sub-femtomole detection limits were obtained. The CE separation systems were shown to be compatible with direct CE-ESI-MS coupling analysis. Structural information was obtained in the CE-MS profiles of standards. The present CE separation systems however, are not able to completely separate the three tetramethylrhodamine-labeled sugars. As such the structure elucidation of unknown co-migrating species will be complicated. Further development of a separation scheme based on capillary electrochromatography (CEC)[55] or CEC coupled to electrospray mass spectrometry (CEC-ESI-MS)[56] for analysis of these TRSE labeled sugars and related species should be investigated. Another possible solution is to employ an alternative labeling approach to generate negatively charged adducts that are separated in an untreated capillary column with a volatile buffer at neutral to basic pH solutions[44-47]. Future work is being directed to the application of these analytical approaches to model compounds and to complex mixtures of carbohydrates extracted from an HT29 cell incubation mixture with the trisaccharide.

Figure 4.11. Total ion electropherogram showing the separation of the TRSE labeled sugars by CE-MS using an untreated column and nonaqueous separation buffer.

The sample was a 10 μM mixture prepared in 50% (v/v) BGE and injected at 10 kV for 10 s. The separation column was an untreated capillary of 50 μm ID x 150 μm OD x 60 cm. Separation was performed at +260 V/cm. The BGE was 40 mM NH_4Ac in methanol-acetonitrile (70:30). Other conditions were as described in the experimental section. (*) unknown compound.

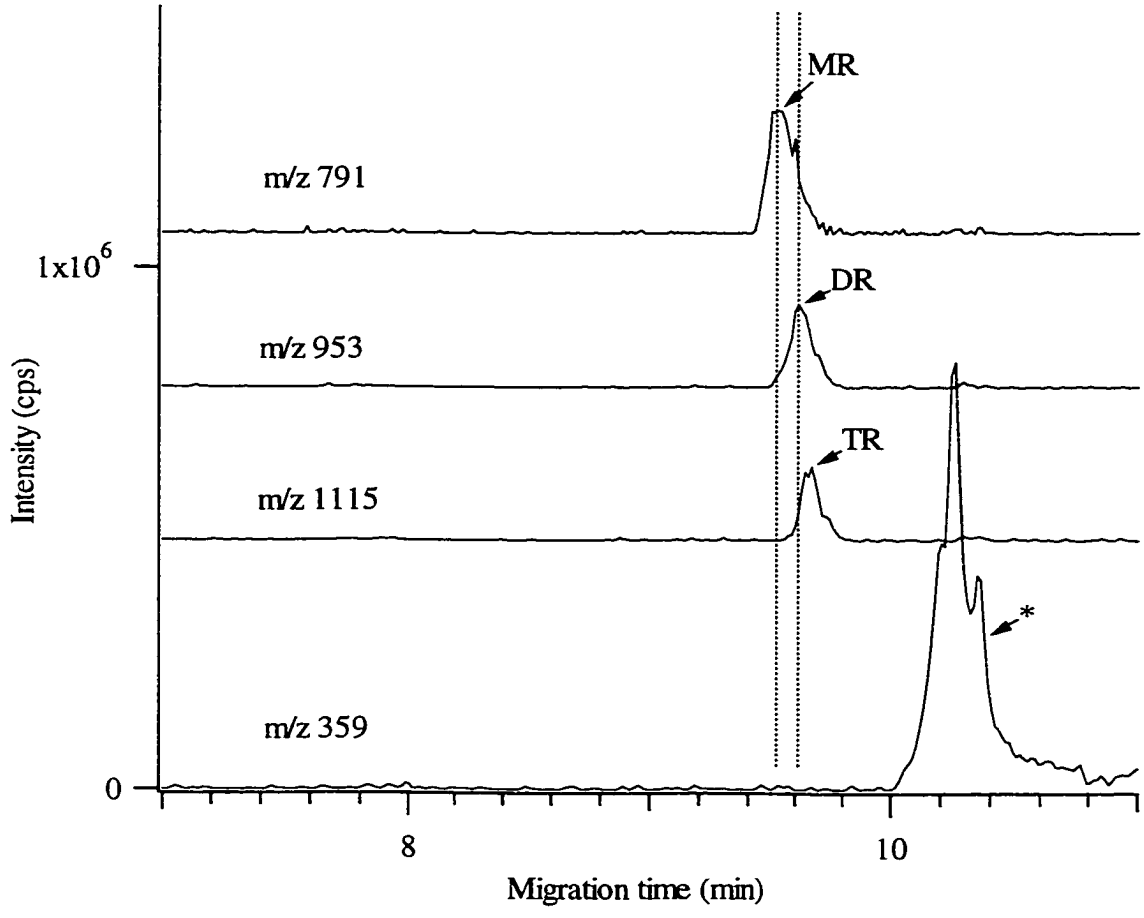

4.6 BIBLIOGRAPHY

(1) Elbein, A.D. *Trends Biotech.* **1991**, *9*, 346-52.

(2) Warren, C.E. *Curr. Opin. Biotech.* **1993**, *4*, 596-602.

(3) Yarema, K.J.; Bertozzi, C.R. *Curr. Opin. Chem. Biol.* **1998**, *2*, 49-61.

(4) Crowther, M.; Hirsh, J. *Seminars in Thrombosis & Homeostasis* **1997**, *23*, 77-81.

(5) Galustian, C.; Childs, R.A.; Yuen, C.T.; Hasegawa, A.; Kiso, M.; Lubineau, A.; Shaw, G.; Feizi, T. *Biochemistry* **1997**, *36*, 5260-6.

(6) Haurum, J.S.; Thiel, S.; Haagsman, H.P.; Laursen, S.B.; Larsen, B.; Jensenius, J.C. *Biochem. J.* **1993**, *293*, 873-8.

(7) Panchal, R.G. *Biochem. Pharmacol.* **1998**, *55*, 247-52.

(8) Lee, K.B.; Loganathan, D.; Merchant, Z.M.; Linardt, R.J. *Appl. Biochem. Biotech.* **1990**, *23*, 53-80.

(9) Yeung, B.; Porter, T.J.; Vath, J.E. *Anal. Chem.* **1997**, *69*, 2510-2516.

(10) Packer, N.H.; Harrison, M.J. *Electrophoresis* **1998**, *19*, 1872-1882.

(11) Krylov, S.N.; Zhang, Z.; Chan, N.W.C.; Arriaga, E.; Palcic, M.M.; Dovichi, N.J. *Cytometry* **1999**, *37*, 14-20.

(12) Turkova, J. *J. Chromatogr. B,* **1999**, *722*, 11-31.

(13) Olechno, J.D.; Ulfelder, K.J. in Landers, J.P. (Editor), *Handbook of Capillary Electrophoresis,* CRC Press, Boca Raton, London, **1994**, pp 255.

(14) Orlando, R.; Bush, C.A.; Fenselau, C. *Biomed. Environ. Mass Spectrom.* **1990**, *19*, 747-754.

(15) Stahl, B.; Steup, M.; Karas, M.; Hillenkamp, F. *Anal. Chem.* **1991**, *63*, 1463-1466.

(16) Duffin, K.L.; Welply, J.K.; Huang, E.; Henion, J.D. *Anal. Chem.* **1992**, *64*, 1440-1448.

(17) Reinhold, V.N.; Reinhold, B.B.; Costello, C.E. *Anal. Chem.* **1995**, *67*, 1772-1784.

(18) Bahr, U.; Pfenninger, A.; Karas, M.; Stahl, B. *Anal. Chem.* **1997**, *69*, 4530-4535.

(19) Welskopf, A.S.; Vouros, P.; Harvey, D.J. *Anal. Chem.* **1998**, *70*, 4441-4447.

(20) Cancilla, M.T.; Wong, A.W.; Voss, L.R.; Lebrilla, C.B. *Anal. Chem.* **1999**, *71*, 3206-3218.

(21) Chen, P.; Werner-Zwanziger, U.; Wiesler, D.; Pagel, M.; Novotny, M.V. *Anal. Chem.* **1999**, *71*, 4969-4973.

(22) Gu, J.; Hiraga, T.; Wada, Y. *Biol. Mass Spectrom.* **1994**, *23*, 212-217.

(23) Churms, S.C. *J. Chromatogr.* **1990**, *500*, 555-583

(24) Molle, D.; Leonil, J. *J. Chromatogr. A*, **1995**, *708*, 223-30.

(25) Kohler, M.; Leary, J.A. *Anal. Chem.* **1995**, *67*, 3501-3508.

(26) Rush R.S.; Derby, P.L.; Smith, D.M.; Merry, C.; Rogers, G.; Rohde, M.F.; Katta, V. *Anal. Chem.* **1995**, *67*, 1442-1452.

(27) Jorgenson, J.W.; Lukacs, K.D. *Science* **1983**, *222*, 266-272.

(28) Linhardt, R.J.; Pervin, A. *J. Chromatogr. A.* **1996**, *720*, 323-335.

(29) Ruiz-Calero, V.; Puignou, L.; Galceran, M.T. *J. Chromatogr. A,* **1998**, *828*, 497-508.

(30) Guttman, A.; Cooke, N.; Starr, C.M. *Electrophoresis* **1994**, *15*, 1518-1522.

(31) Stefansson, M.; Novotny, M. *Anal. Chem.* **1994**, *66*, 1134-1140.

(32) Zhao, J.Y.; Diedrich, P.; Zhang, Y.; Hindsgaul, O.; Dovichi, N.J. *J. Chromatogr. B,* **1994**, *657*, 307-313.

(33) Paulus, A.; Klockow, A. *J. Chromatogr. A*, **1996**, *720*, 353-376.

(34) Hoffstetter, S.; Paulus, A.; Gassmann, E.; Widmer, H.M. *Anal. Chem.* **1991**, *63*, 1541-1547.

(35) Zhang, Y.; Le, X, Dovichi, N.J.; Compston, C.A.; Palcic, M.M.; Diedrich, P.; Hindsgaul, O. *Anal. Biochem.* **1995,** *227*, 368-376.

(36) Honda, S.; Yamamoto, K.; Suzuki, S.; Ueda, M.; Kakehi, K. *J. Chromatogr.* **1991**, *588*, 327-333.

(37) Schwaiger, H.; Oefner, P.J.; Huber, C.; Grill, E.; Bonn, G.K. *Electrophoresis* **1994**, *15*, 941-952.

(38) Klockow, A.; Paulus, A.; Figueiredo, V.; Amado, R.; Widmer, H.M. *J. Chromatogr. A*, **1994**, *680*, 187-200.

(39) Honda, S.; Iwase, S.; Makino, A.; Fujiwara, S. *Anal. Biochem.* **1989**, *176*, 72-77.

(40) El Rassi, Z.; Postlewait, J.; Mechref, Y.; Ostrander, G.K. *Anal. Biochem.* **1997**, *244*, 283-290.

(41) Ma, S.; Nashabeh, W. *Anal. Chem.* **1999**, *71*, 5185-5192.

(42) Colon, L.A.; Dadoo, R.; Zare, R.N. *Anal. Chem.* **1993**, *65*, 476-481.

(43) Krattiger, B.; Bruno, A.E.; Widmer, H.M.; Dandliker, R. *Anal. Chem.* **1995**, *67*, 124-130.

(44) Monsarrat, B.; Brando, T.; Condouret, P.; Nigou, J.; Puzo, G. *Glycobiology.* **1999**, *9*, 335-342.

(45) Kelly, J.; Masoud, H.; Perry, M.B.; Richards, J.C.; Thibault, P. *Anal. Biochem.* **1996**, *233*, 15-30.

(46) Li, D.T.; Sheen, J.F.; Her, G.R. *J. Am. Soc. Mass Spectrom.* **2000**, *11*, 292-301.

(47) Duteil, S.; Gareil, P.; Girault, S.; Mallet, A.; Feve, C.; Siret, L. *Rapid Commun. Mass Spectrom.* **1999**, *13*, 1889-1898.

(48) Che, F.Y.; Song, J.F.; Zeng, R.; Wang, K.Y.; Xia, Q.C. *J. Chromatogr. A,* **1999**, *858*, 229-238.

(49) Auriola, S.; Thibault, P.; Sadovskaya, I.; Altman, E. *Electrophoresis* **1998,** *19*, 2665-2676.

(50) Kelly, F.F.; Locke, S.J.; Ramaley, L.; Thibault, P. *J. Chromatogr. A*, **1996**, *720*, 409-427.

(51) Zhao, J.Y.; Dovichi, N.J.; Hindsgaul, O.; Gosselin, S.; Palcic, M.M. *Glycobiology* **1994**, *4*, 239-242.

(52) Scaman, C.H.; Hindsgaul, O.; Palcic, M.M.; Srivastava, O.P. *Carbohydr. Res.* **1996**, *296*, 203-213.

(53) Weinmann, W.; Maier, C.; Baumeister, K.; Przybylski, M.; Parker, C.E.; Tomer, K.B. *J. Chromatogr. A*, **1994**, *664*, 271-275.

(54) Liu, C.S.; Li, X.F.; Pinto, D.; Hansen, E.B., Jr.; Cerniglia, C.E.; Dovichi, N.J. *Electrophoresis* **1998**, *19*, 3183-3189.

(55) Yang, C.; El Rassi, Z. *Electrophoresis* **1998**, *19*, 2061-2067.

(56) Hau, J.; Roberts, M. *Anal. Chem.* **1999**, *71*, 3977-3984.

CHAPTER 5 [1,2]

A Novel Electrospray Interface for Capillary Electrophoresis-Mass Spectrometry

[1] Part of this work has been presented at the 48th ASMS Conference on Mass Spectrometry and Allied Topics, Long Beach, CA, June 2000.

[2] A version of this chapter has been submitted for publication.
Liu, C.S.; Zhang, J.Z.; Dovichi, N.J. 2000. Analytical Chemistry.

5.1 ABSTRACT

This chapter presents a reliable sheath interface for low-flow electrospray ionization mass spectrometry (ESI-MS) and capillary electrophoresis-electrospray mass spectrometry (CE-ESI-MS). The interface emitter is made of a fused-silica capillary suitable for microliter and nanoliter flow-rate electrospray. A capillary for direct infusion or a detection end gold-coated capillary column for capillary electrophoresis (CE) is inserted into the emitter with a concentric configuration until a junction is formed at the tip of the emitter. A sheath liquid, usually methanol, is pumped through the void space between the column and the emitter and is used as the conducting media for ESI and the CE circuit.

This novel design has been evaluated by an infusion-ESI analysis of peptides and the most common antiretroviral dideoxynucleosides. The effects of the sheath and the sample flow rates on detection sensitivity and signal stability were investigated. For an emitter with an internal diameter of 30 μm, the optimum flow rates for the sheath and the sample are 200 nL/min and 300 nL/min, respectively. Enhanced sensitivity (3 times) for the detection of dideoxynucleosides was obtained by using this low-flow interface in comparison with a conventional electrospray interface.

This design has also been tested on a CE separation with on-line ESI-MS detection of five antidepressant drugs. A layer of gold film coated on the CE column detection end is crucial for durable and sensitive performance of the coupled CE-ESI-MS analysis. Utilizing this design, detection sensitivities 12 times higher than those of conventional CE-MS using an ion spray interface were obtained, and no apparent degradation of CE separation efficiency is observed. The interface is rugged and simple to fabricate.

5.2 INTRODUCTION

Since its introduction in 1985[1], ESI has revolutionized the MS technology in bioanalytical chemistry with its ability to transfer thermally labile and macromolecular species from the liquid phase to the gas-phase as intact molecular ions with multiple charges. In the past decade the electrospray interface has grown into a family with a variety of novel designs. In terms of the spray formation, pure electrospray [1-3] and pneumatically assisted electrospray (also called ion spray) [4-6] are two major operational modes along with others including the lately developed sonic spray[7-9]. A conventional ESI sprayer tip is around 100-200 μm in internal diameter, and the sample flow rates are typically in the range of 1-20 μL/min. Electrospray performed with smaller tips and at lower flow rates is known as microspray [10,11] or nanospray[12,13].

A requirement of ESI is that analytes must be in solution, which results in the natural compatibility of ESI with many types of separation techniques, such as liquid chromatography[1,14-19], CE[20-28], and capillary electrochromatography[29-31]. A number of research groups have developed methods for decreased sample consumption by utilizing much lower flow rates and a capillary separation method in a coupled technique[18,32-40]. CE-MS has shown unparalleled advantage over other coupled techniques for its small sample requirement and ease of operation.

In coupled CE-MS analysis, coaxial liquid sheath[20,25,41], liquid junction[23,42-47], microdialysis junction[48-50] and sheathless[37,51-55] interfaces have been widely employed. The coaxial liquid sheath interfaces utilize a coaxial make-up flow pumped through a stainless steel tube to provide stable electrospray and to complete the CE electrical circuit[20]. Although optimizations have improved performance[25], the sheath interface suffers from impaired sensitivity due to the dilution of the analyte by the sheath liquid.

However, the sheath interface design is the most useful one for stable and long-lasting performance of electrospray with total flow rates higher than a couple of microliters per minute. In the liquid junction designs, a liquid gap is introduced between the CE column and the sprayer[23]. The sensitivity is decreased as in the case of the sheath interface, and the separation efficiency can be compromised by the introduction of a gap in the system[57].

In a sheathless style interface design for CE-ESI-MS applications, the emitter is often a CE separation capillary coated with a conductive material such as silver[33], gold [58-60], chromium-gold[61], gold particles[55], conductive epoxy adhesives[62], carbon[63], or polyaniline[64]. Other possibilities tend to be more complicated and delicate, for example inserting a metal electrode inside the outlet of the CE capillary[51,65]. A conductively coated piece of fused-silica capillary butted to the CE separation capillary as a disposable emitter has also been used[66-68]. These interfaces are actually microspray or nanospray interfaces. In recent years, a sheathless interface has been favored for increasing the sensitivity of CE-MS analysis. The high sensitivity is believed to be due to the low flow rate and the high electrospray efficiency[10-13,69]. Compared to a sheath liquid assisted electrospray, the microspray and nanospray CE-MS do not dilute the analyte and thus a larger portion of the ions should be generated and sampled to the MS. The major reported drawback of these sheathless designs is the short lifetime mainly due to particle clogging and deterioration of the metal coating by electrical discharge. Although improved coating methods have been developed to increase metallized emitter lifetime[55,58,70,71], the methods are tedious and time-consuming. Another limitation of the sheathless interface for CE-MS analysis is that gas bubbles formed or transported to the tip can often terminate the electrospray and/or CE process. Further, the choice of CE buffers is also restricted to a very narrow range due to the lack of post-column solution chemistry. Last, in some

applications the electro-osmotic flow is not sufficient to cover the demand of the electrospray process, especially with the use of acidic buffers in, e.g., peptides analysis. Reproducibility of injections and migration times are poor, and the sensitivity gain is often compromised by poor signal stability[55].

To overcome limitations of the sheathless interface, a silica sheath interface for low flow rate electrospray CE-MS has been introduced[72,73]. The sprayer tip is made of a fused silica capillary or a borosilicate glass tube with a large internal diameter (ID) and outer diameter (OD) pulled and tapered to a small opening. A sampling capillary is inserted to the end of the sprayer, and the ESI high voltage is applied through the sheath fluid which is pumped concentrically to the sprayer. The use of this interface for CE-MS applications, although reported to be successful[72,73], does not always result in a stable spray in our experience; the baseline is unstable and noisy, and the signals of interest are insensitive and irreproducible. Thus, we have developed a modified version of the low-flow interface for CE-MS. In this case, the sampling capillary is a detection end gold-coated CE column. The sheath liquid and the gold layer both function to complete the ESI and the CE circuits. Application of this interface to on-line CE-MS analysis of several antidepressants is demonstrated, and the performance of this low flow electrospray interface is compared to that of a conventional ionspray interface.

5.3 EXPERIMENTAL

5.3.1 Reagents and Materials

Fused-silica capillaries were purchased from Polymicro Technologies (Phoenix, AZ). Dideoxycytidine (ddC), azodothymidine (AZT), dideoxythiacytidine (3TC), didanosine (ddI), stavudine (d4T), bradykinin, desipramine, nortriptyline, imipramine,

amitriptyline and clomipramine were from Sigma (St. Louis, MO). Rhodamine 6G was from Aldrich (Milwaukee, MI). AttoPhos substrate was obtained from JBL Scientific (San Luis Obispo, CA). HPLC-grade methanol and acetonitrile was purchased from BDH (Toronto, ON, Canada). Sodium borate was purchased from J.T. Baker (Phillipsburg, NJ). Ammonium acetate, acetic acid and formic acid were obtained from Anachemia (Montreal, PQ, Canada). Stock solutions of 10^{-2} M didexoynucleosides were prepared using water prepurified by a Nanopure II system (Barnstead, MA) and then diluted to 10^{-3} to 10^{-8} M with methanol-water (95:5). Preparation of stock and test solutions of antidepressant drugs was as described in another paper[74]. A 0.22 μm syringe filter (Waters, MA) was used to filter all solutions passing through the interface.

5.3.2 Sheath Low-Flow Interface for Infusion-ESI-MS

A fused-silica capillary of 204 μm ID and 360 μm OD was cut to 10 cm-long pieces and then heated by electric spark and pulled apart manually on a fiber optic splicer (Orionics, Bozeman, MT). Tips of the two tapered halves (each 5 cm in length) were then carefully inspected and cut to the desired dimensions with flat and round openings on the tip. The exact size of the opening was measured using an optical microscope (E. Leitz Wetzlar, Toronto, Canada) attached to a CCD camera (Sanyo, Japan) and a Macintosh computer. A series of tapered tips with internal diameters of 1 μm to 104 μm were constructed. A tip with a diameter of 30 μm ID was used for the present study. Tips were labeled and taped on a glass chip and stored in a plastic box. A sampling column with 50 μm ID and 150 μm OD and a length of 50 cm was inserted inside the tapered tip, **Figure 5.1**. This tip was then mounted in a stainless steel hold-down tee modified from a commercial tee (Valco Instruments, Houston, TX).

Figure 5.1. Schematic diagram of the sheath low-flow electrospray interface.

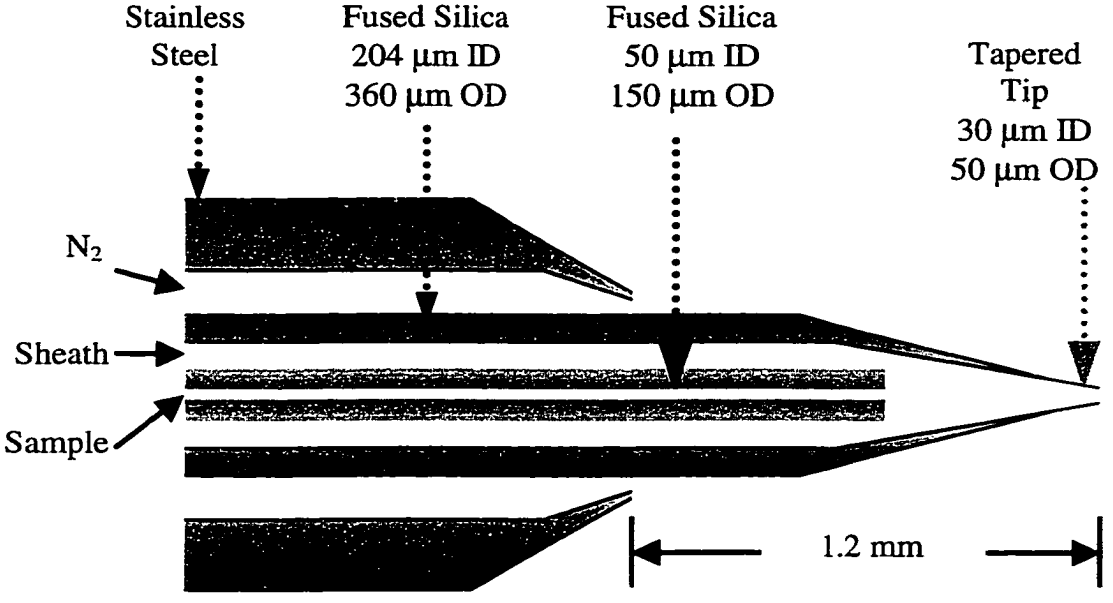

5.3.3 Sheath Low-Flow Interface for CE-ESI-MS

Based on the design of the sheath tip for infusion ESI-MS, a modified version of the interface was fabricated for on-line CE-MS analysis. Ten capillaries with 50 μm ID and 150 μm OD and a length of 62 cm, both end openings sealed on the fiber optic splicer, were grouped together and put in a plastic bag with a 6 cm length of capillaries left outside. The plastic bag was sealed by a transparent tape and put in a Lesker Sputter System II (Kurt J. Lesker Co., Clairton, PA). The exposed ends were sputter-coated with gold atoms under a vacuum of 10^{-7} torr. The end-coated capillaries were cut into 60 cm long pieces and used as CE columns. The 5-cm gold-coated end of the column was inserted in the tapered tip and mounted, **Figure 5.2.**

5.3.4 ESI-MS and CE-ESI-MS.

All experiments were performed using a PE/Sciex API 100 single quadrupole mass spectrometer from Sciex (Thornhill, ON, Canada). For comparison, a commercial ion spray interface (Sciex) and the in-house built low-flow interfaces were employed for separate studies. A sheath flow of methanol was delivered using a syringe pump (Harvard Apparatus, South Natick, MA). Samples or buffer solutions were infused through the sampling capillary using another syringe pump for direct infusion study and for tuning purposes. CE was performed using an in-house built injector and a high voltage supply (Spellman CZE 1000R, Plainview, NY). A fresh running buffer, 50 mM ammonium acetate in a mixed solvent of methanol-acetonitrile (70:30), was used to flush the capillaries before and between CE runs. CE separations were performed at 200 V/cm or more. Samples were electrokinetically injected at 10 kV for 10 s. Injection volume was around 11 nL, calculated using an equation of $V_{inj} = V_{cap}(t_{mig}/t_{inj})(E_{inj}/E_{CE})$. For negative detection of AttoPhos, potentials applied to the sprayer (IS), the orifice (OR), and the

Figure 5.2. A modified version of the sheath low-flow electrospray interface for CE-MS.

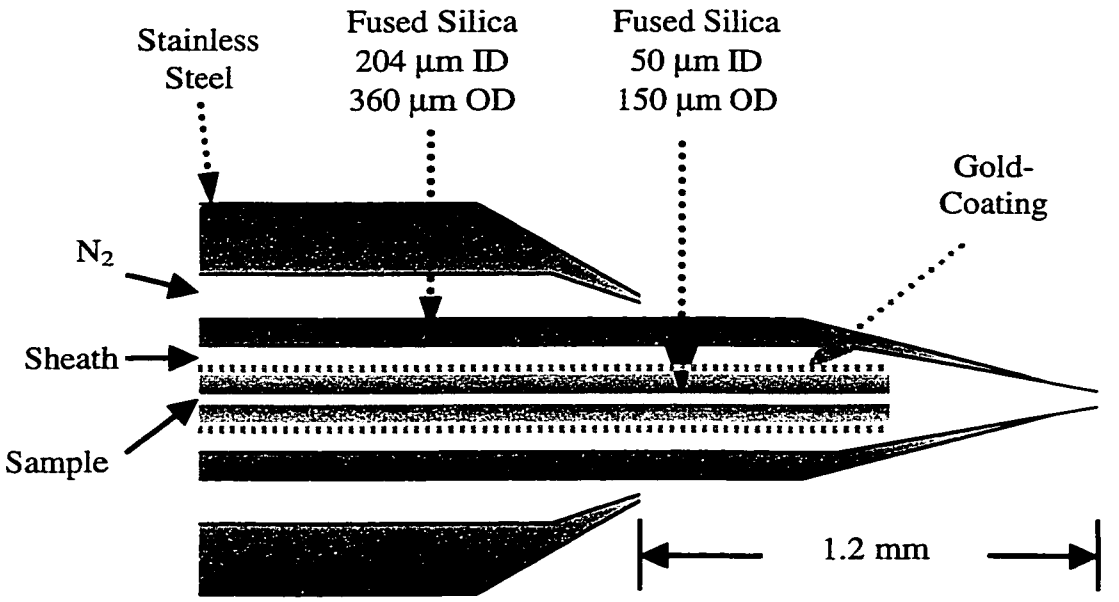

focusing ring (RNG) were optimized and set to -3.5 kV, -45 V and -320 V for low-flow interface, respectively. For positive ESI-MS, potentials applied to the IS, the OR, and the RNG were optimized and set to 4.6 kV, 30 V and 220V for ion spray interface and to 2.8 kV, 30 V and 170 V for low-flow interface, respectively, unless otherwise indicated. It should be noted that the curtain plate was always under a potential of 1 kV. Therefore the net electrospray voltage applied were 3.6 kV for the ion spray interface and 1.8 kV for the low flow interface, respectively. A mass range of m/z 30-1200 and a step size of 1.0 Da were scanned with a speed of 2.4 s/scan for infusion studies. A mass range of m/z 65-400 and a step size of 1 mass unit and a speed of 0.99 s/scan were used for CE-MS analysis. The curtain gas flow rate was 1.1 L/min (CUR 9). No nebulizing gas was applied in the present study; i.e. the instrument was operated as a pure electrospray instead of ion spray process. Raw data was acquired by LCTune software (Sciex) and processed by the MultiView software (Sciex).

5.4 RESULTS AND DISCUSSION

5.4.1 Sheath Liquid Low Flow Electrospray for CE-MS

The main goal of this study was to develop an electrospray interface that combines the high sensitivity feature of a microspray or a nanospray interface and the high stability feature of the sheath-flow configuration for CE-MS on-line coupled analysis. In a conventional sheath-flow interface design[25], a stainless steel (SS) electrode tube has been commonly employed with an internal diameter of over 200 μm which is large enough for a capillary column to insert inside and to protrude out. A similar design has also been employed in which the CE column is pulled back 1 mm with reference to the SS electrode outlet[74]. A terminal junction is, therefore, formed at the exit of the column and serves as the CE terminal reservoir. It is obvious that this interface can be adapted for

low-flow electrospray by reducing the terminal opening of the SS tube. However, it is difficult to manufacture a metal sprayer with an internal diameter of 200 μm and an end opening of 50 μm ID. A fused-silica capillary with a large ID pulled and tapered to a small opening suitable for micro- and nanospray should be a good alternative. In this case, the sheath liquid is the only means to apply the electrospray voltage at the silica sprayer tip and thus also close the electrical circuit required for CE operation. With this consideration in mind, we have manufactured a sheath flow fused-silica emitter (**Figure 5.1**). This emitter was initially tested by an infusion experiment prior to on-line CE-MS studies.

5.4.2 Sample Flow Effect on Sensitivity

Since this interface is operated at low-flow rates, it is important to test the influence of flow rates on sensitivity. **Figure 5.3** shows the effects of the sample flow on ion intensity for continuous infusion of a 50 μM ddC in 90% methanol. The sheath flow was fixed at 0.4 μL/min, and the signal of a base fragment of ddC, m/z 112, was extracted from a total ion chromatogram. At flow rates up to 0.15 μL/min, the mass spectrometric detection is sample-flow sensitive. The signal of m/z 112 then reaches a plateau in the range of 0.20-0.30 μL/min. **Figure 5.4** shows a similar flow-rate response relationship except that the sheath flow is much lower, i.e., 0.10 μL/min. The ion signal is nearly constant over a flow range of 0.10-0.40 μL/min although a slightly higher response was obtained at the flow rate of 0.10 μL/min. It should be noted that the ion signal becomes noisy as the sample flow rate decreases to less than 0.10 μL/min, i.e. a total flow rate (sample flow plus sheath flow) of at least 0.20 μL/min is required to maintain a stable electrospray process.

Figure 5.3. Effects of sample-flow rates on the selected ion signal of ddC.

The ddC was 50 μM in 90% MeOH. Sheath flow-rate was fixed at 0.40 μL/min. The emitter was 30 μm ID.

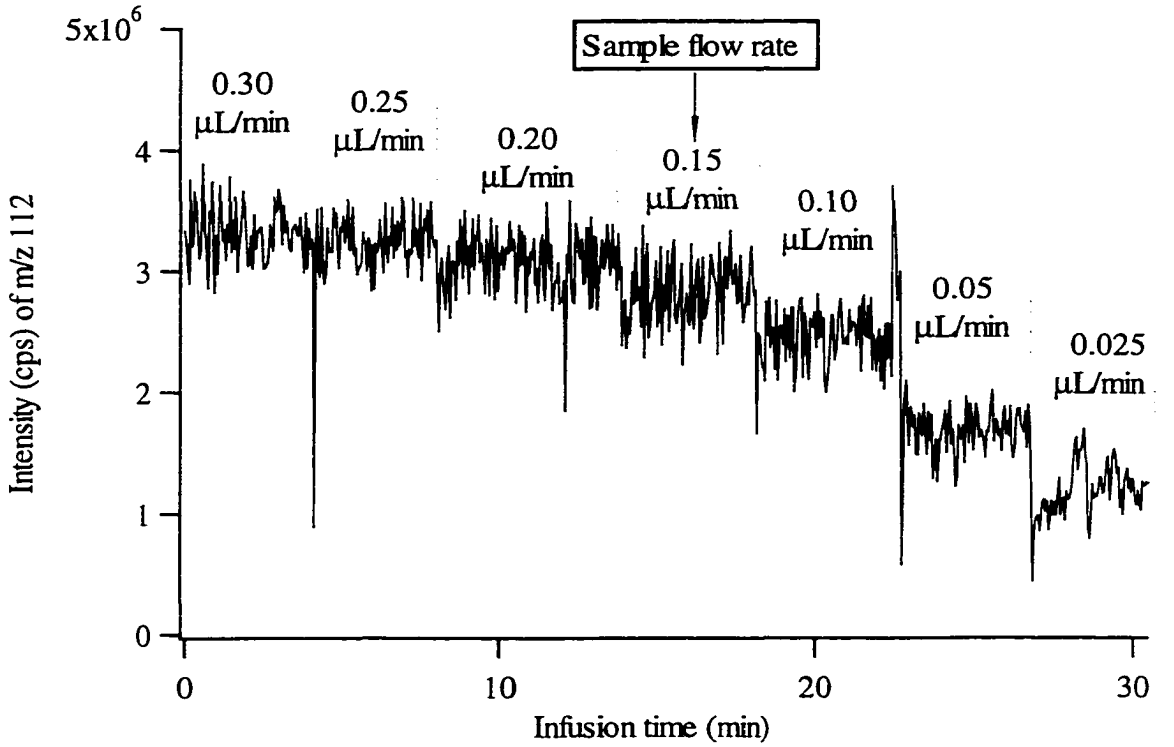

Figure 5.4. Effects of sample flow rates on the selected ion signal of ddC.

The ddC was 50 μM in 90% MeOH. Sheath flow-rate was fixed at 0.10 μL/min. The emitter was 30-μm ID.

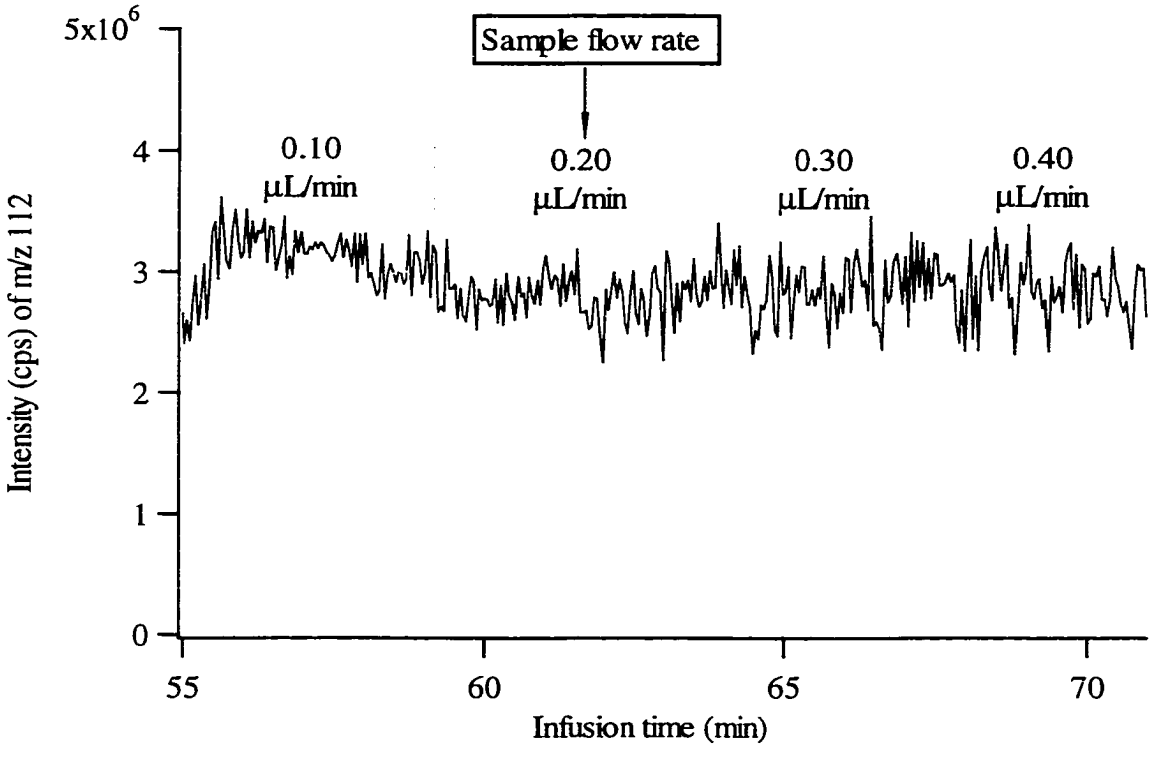

Figure 5.5 shows a typical relationship between a sample flow rate and total ion current of analyte. In order to maintain a minimum flow for stable electrospray over a broad range of sample flow rates, a sheath liquid of methanol at 0.20 μL/min was supplied. With the help of MultiView software functions, the TIC signal of an analyte was obtained by subtracting the signal of a blank solvent from that of a compound dissolved in the solvent in a total ion chromatogram traced with infusion time (refer to Figure 3). Pseudo-molecular ions, mainly H^+, Na^+ and K^+ adducts, and major fragments produced from glycosidic bond cleavage ($[B+2H]^+$, $[B+H+Na]^+$, $[B+H+K]^+$, and $[BH2-NH3]^+$), as well as clusters are typical ions in an ESI mass spectrum of a ddN. The observed signal intensities were the summation of total ion current in a cleaned spectrum calculated manually. At a low sample flow rate, the analyte concentration in the sprayer tip is low due to a dilution by the sheath fluid. Since the response of ESI-MS is concentration dependent,[75] at low sample flow rates (<0.20 μL/min) where the sheath liquid flow is dominating, the signal intensities are proportional to the sample rate; the electrospray interface behaves like a mass-flow sensitive detector. Whilst for higher flow rates (0.20-0.50 μL/min), where the dilution of analyte by the sheath liquid is not apparent, the interface changes to a concentration sensitive detector, and the signal reaches its maximum. As the sample flow further increases, the TIC of ddI decreases and gradually reaches a plateau. The drop in signal intensity at high flow rates may be due to an insufficient desolvation process. The optimum sample flow rates are in the range of 0.20-0.40 μL/min, and a sample flow rate of 0.30 μL/min was chosen for the rest of infusion experiments.

Figure 5.5. Total ion current (TIC) signal intensity of ddI vs. sample flow rate. The ddI was 50 μM in 95% MeOH. The sheath flow was fixed at 0.20 μL/min.

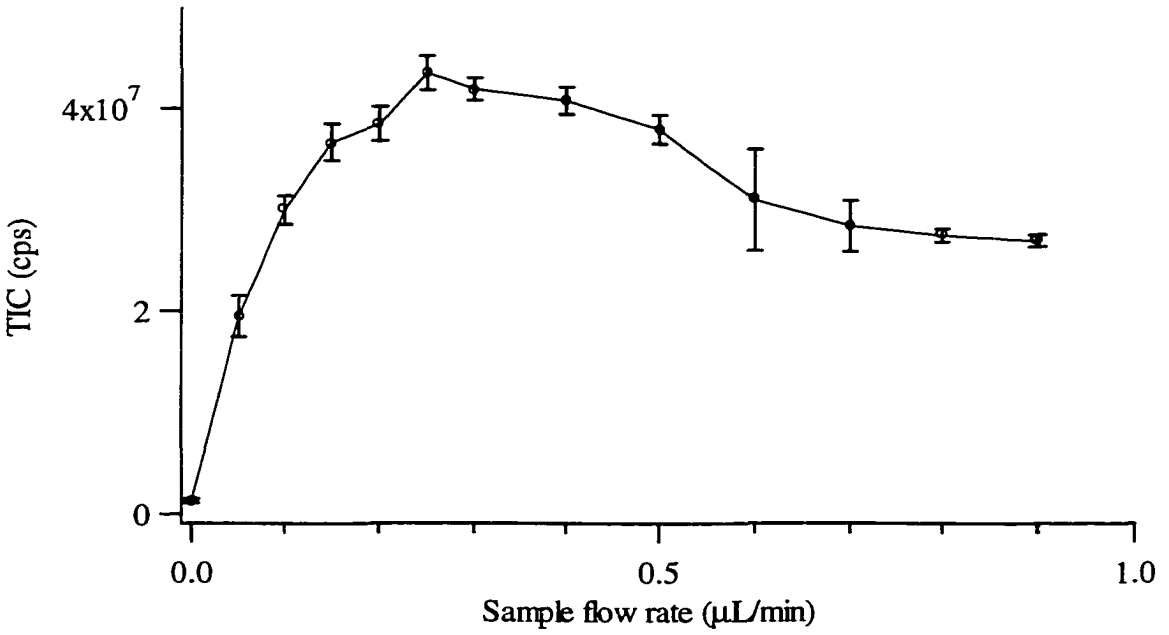

5.4.3 Sheath Flow Effects on Sensitivity

As shown in an infusion total ion chromatogram, **Figure 5.6**, the sheath flow rate also has a significant effect on signal intensity. As the sheath flow increases from 0.10 μL/min to 0.40 μL/min, the ion intensity decreases. When this rate is less than 0.10 μL/min, the signal is not stable. Here, a 50 μM ddC in 90% methanol was infused at a flow rate of 0.10 μL/min.

Figure 5.7 shows a typical plot of the sheath flow-rate response while maintaining a sample flow at 0.30 μL/min. As the sheath flow decreases to 0.050 μL/min, unstable signals are produced. The optimum rates are in the range of 0.10-0.30 μL/min. As the sheath exceeds 0.30 μL/min, the signal decreases. The drop of signal intensity may be again due to an incomplete desolvation process at high sheath flow rates. A 50 μM ddI solution prepared in 95% methanol was infused in this experiment. To obtain a stable signal with a small dilution factor, a sheath flow rate of 0.20 μL/min methanol was chosen for the rest of the experiments.

Although we have prepared a series of emitters with tip sizes from 1 to 104 μm ID, an emitter with an internal diameter of 30 μm was chosen for the present study to match a typical electro-osmotic flow in our CE-MS study. Generally, the dimensions of the tip determine the optimum total flow rate for stable and sensitive electrospray. For instance, we have found out that the optimum flow rates for a 200 μm ID tip and a 20 μm ID tip are 2.2 μL/min[74] and 0.20 μL/min, respectively. From the above results, a sample flow-rate of 0.20-0.50 μL/min and a sheath flow-rate of 0.10-0.30 μL/min are optimum choices for an emitter with a tip size of 30 μm ID. It is interesting to note that a typical range of electro-osmotic flow in CE and capillary electrochromatography (CEC) falls

Figure 5.6. Effects of sheath flow rates on the selected ion signal of ddC.

The sample was 50 μM in 90% MeOH. Sample flow-rate was fixed at 0.10 μL/min.

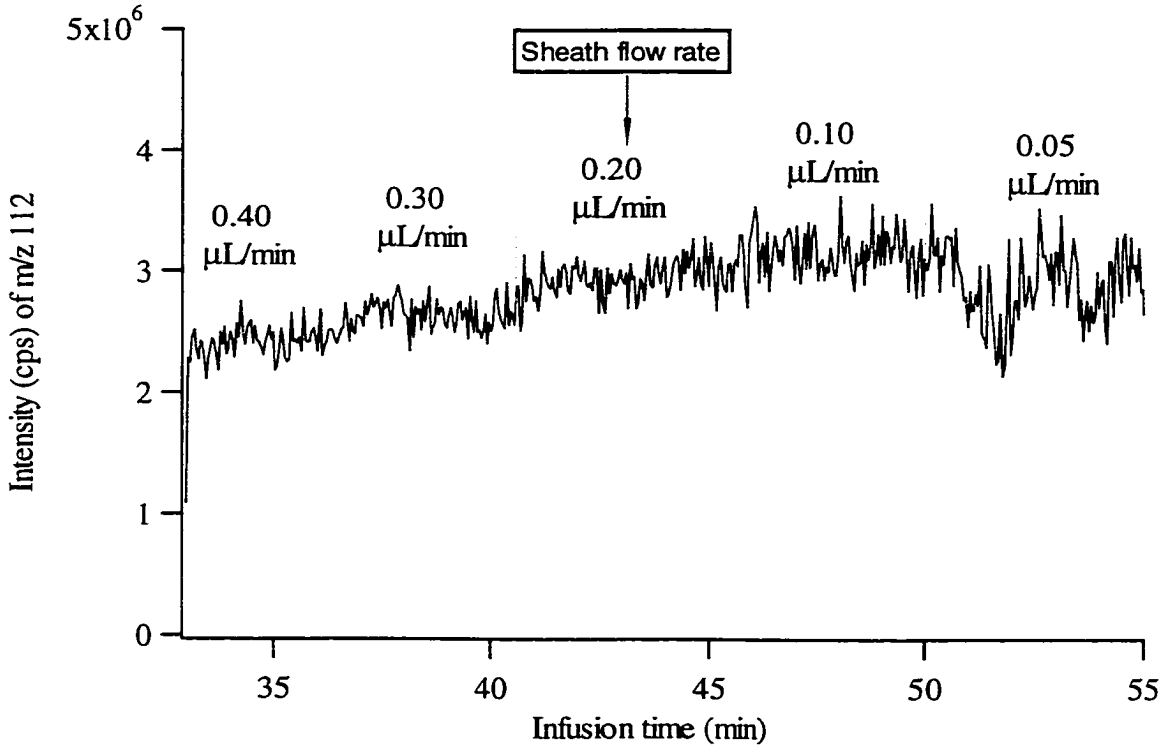

Figure 5.7. Effects of sheath-flow rates on observed signals (TIC) of ddI.

The ddI was 50 μM in 95% MeOH. Sampling rate was fixed at 0.3 μL/min. Only 4 groups of measurements were repeated.

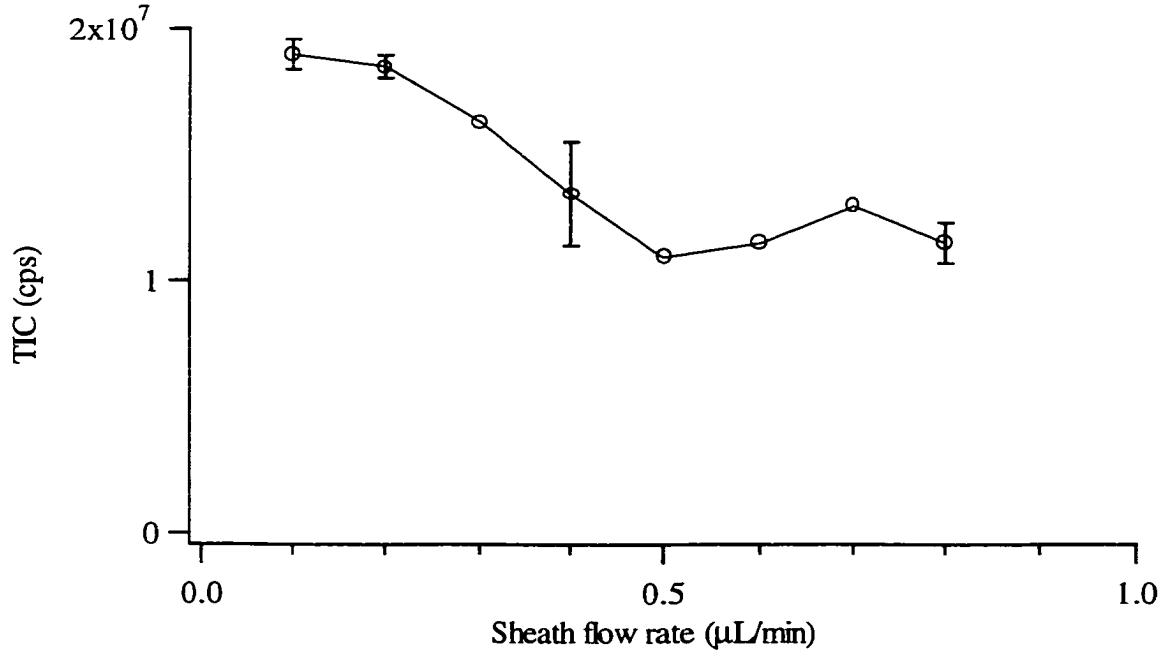

into this concentration-sensitive response region of the 30 μm ID electrospray emitter, making the low-flow interface well-suited for on-line CE-MS or CEC-MS analysis.

5.4.4 Calibration Curves

Calibration curves of ddNs were linear for three orders of magnitude across a concentration range of 10^{-7} to 10^{-4} M with R^2 of 0.99 in a log-log plot, **Figure 5.8,** obtained in a series of infusion full-scan experiments with a mass range of m/z 30-1200. Sensitivities are nearly the same for all compounds. Within a concentration range of 10^{-7} M to 5 x 10^{-4} M, these calibration curves can be described by the following equations:

ddI: $y = 0.927x + 11.2 \quad R^2 = 0.992$ (5.1)

ddC: $y = 1.18x + 12.5 \quad R^2 = 0.992$ (5.2)

d4T: $y = 0.925x + 11.3 \quad R^2 = 0.999$ (5.3)

3TC: $y = 0.796x + 10.6 \quad R^2 = 0.955$ (5.4)

AZT: $y = 0.894x + 10.8 \quad R^2 = 0.995$ (5.5).

The concentration limit of quantitation is 100 nM (S/N of 10) using a selected ion monitoring (SIM). The concentration limit of detection is 30 nM of ddNs determined in an infusion ESI-MS using SIM.

5.4.5 Infusion-ESI Mass Spectra

Use of the silica sheath flow emitter for infusion-ESI-MS of several kinds of compounds is shown in **Figures 5.9-5.12.** The positive ESI mass spectrum of bradykinin (10 μM in 90% methanol, 10% aqueous 10mM formic acid) is shown in **Figure 5.9a.** **Figure 5.9b** is an ESI mass spectrum of the same compound obtained from ionspray. No

Figure 5.8. Calibration curves for ddNs by infusion ESI-MS.

Sheath flow and sample flow rates were 0.20 and 0.30 μL/min, respectively.

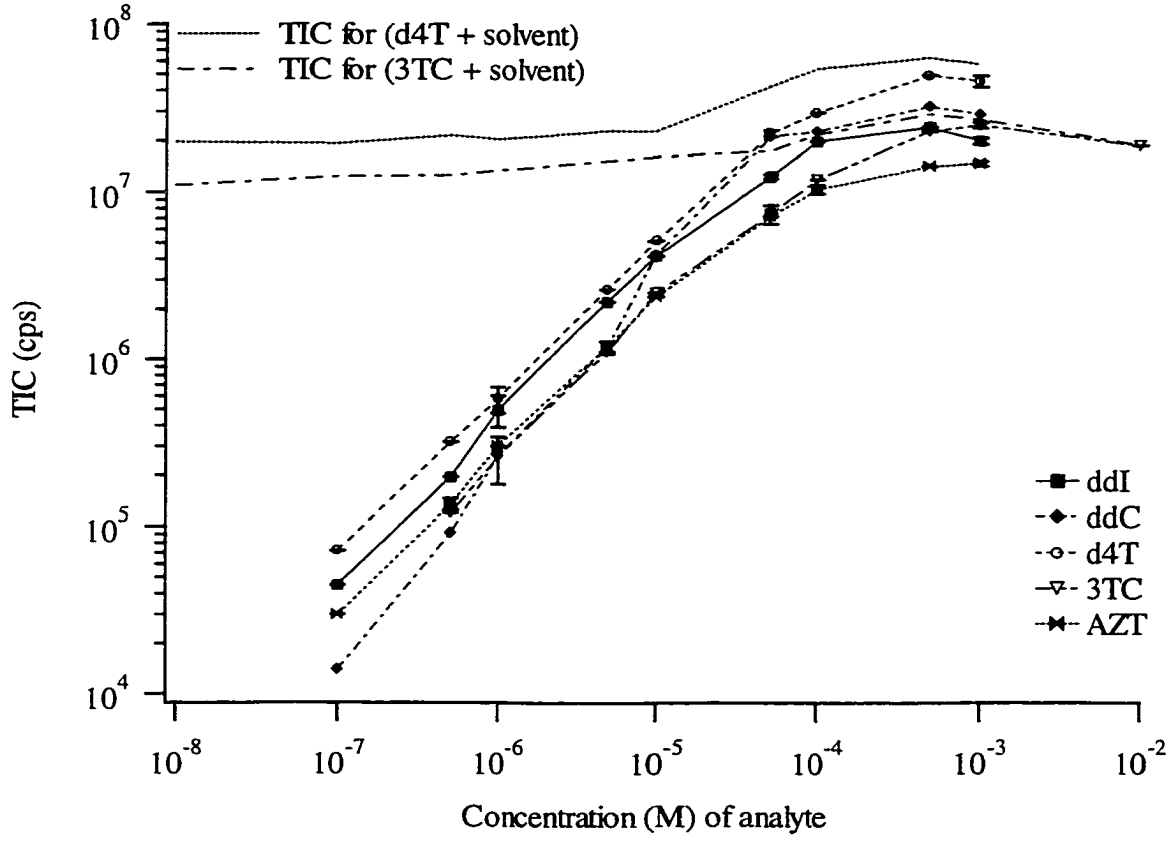

Figure 5.9. ESI mass spectra of bradykinin obtained from (a) ion spray and (b) low-flow interfaces.

The sample was 10 μM in 90% MeOH. It was infused to (a) low-flow interface at 0.30 μL/min and a sheath flow at 0.20 μL/min; (b) ion spray interface at 2.0 μL/min and the sheath flow rate was at 0.20 μL/min. OR voltages were (a) 20 V and (b) 50 V, respectively. Other conditions were as described in the experimental section.

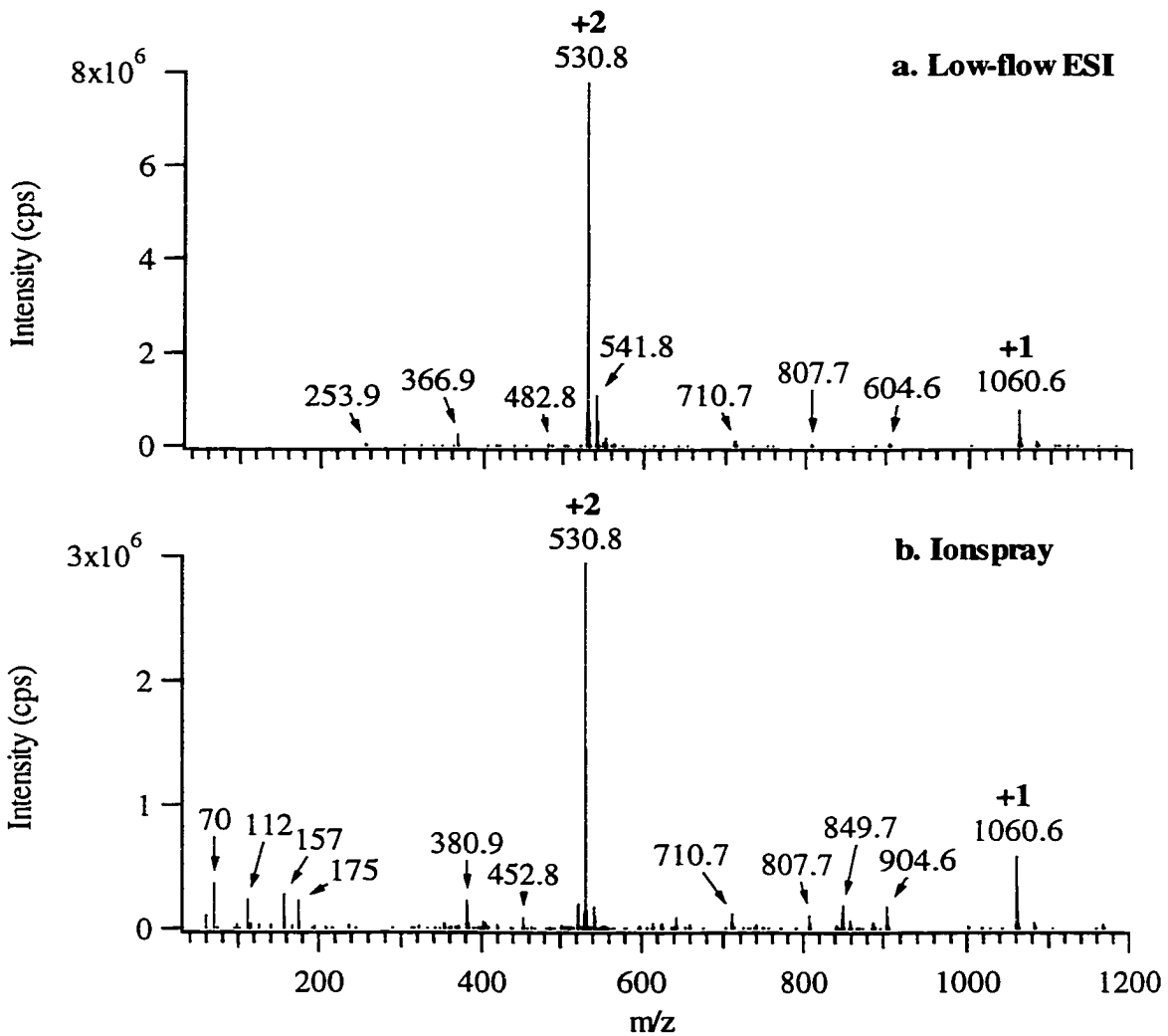

Figure 5.10. ESI mass spectra of rhodamine obtained from the sheath silica low-flow interface.

The sample was (a) 10 μM (b) 5 μM (c) 1 μM in 90% MeOH, 10% 10 mM formic acid and infused at 0.30 μL/min. The sheath flow was at 0.20 μL/min. Positive ESI-MS was performed. Other conditions were as described in the experimental section.

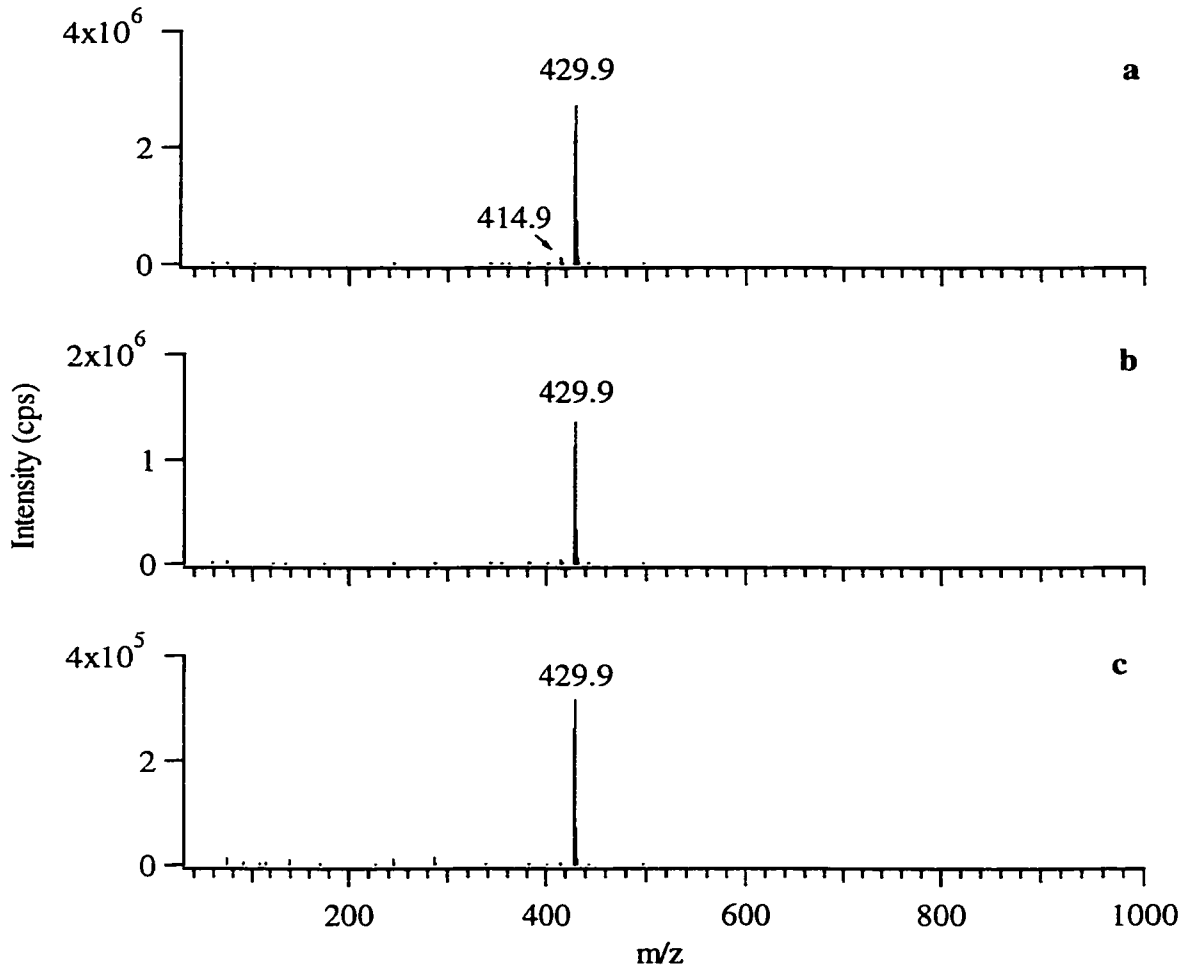

Figure 5.11. Negative and positive ESI mass spectra of AttoPhos obtained from the sheath silica low-flow interface.

The sample was 1 mM in acetonitrile-water (50:50) (a, b) or in 45 mM borate at pH 9.5 (c). Samples were infused at 0.30 µL/min. The sheath flow was at 0.20 µL/min. Other conditions were as described in the experimental section.

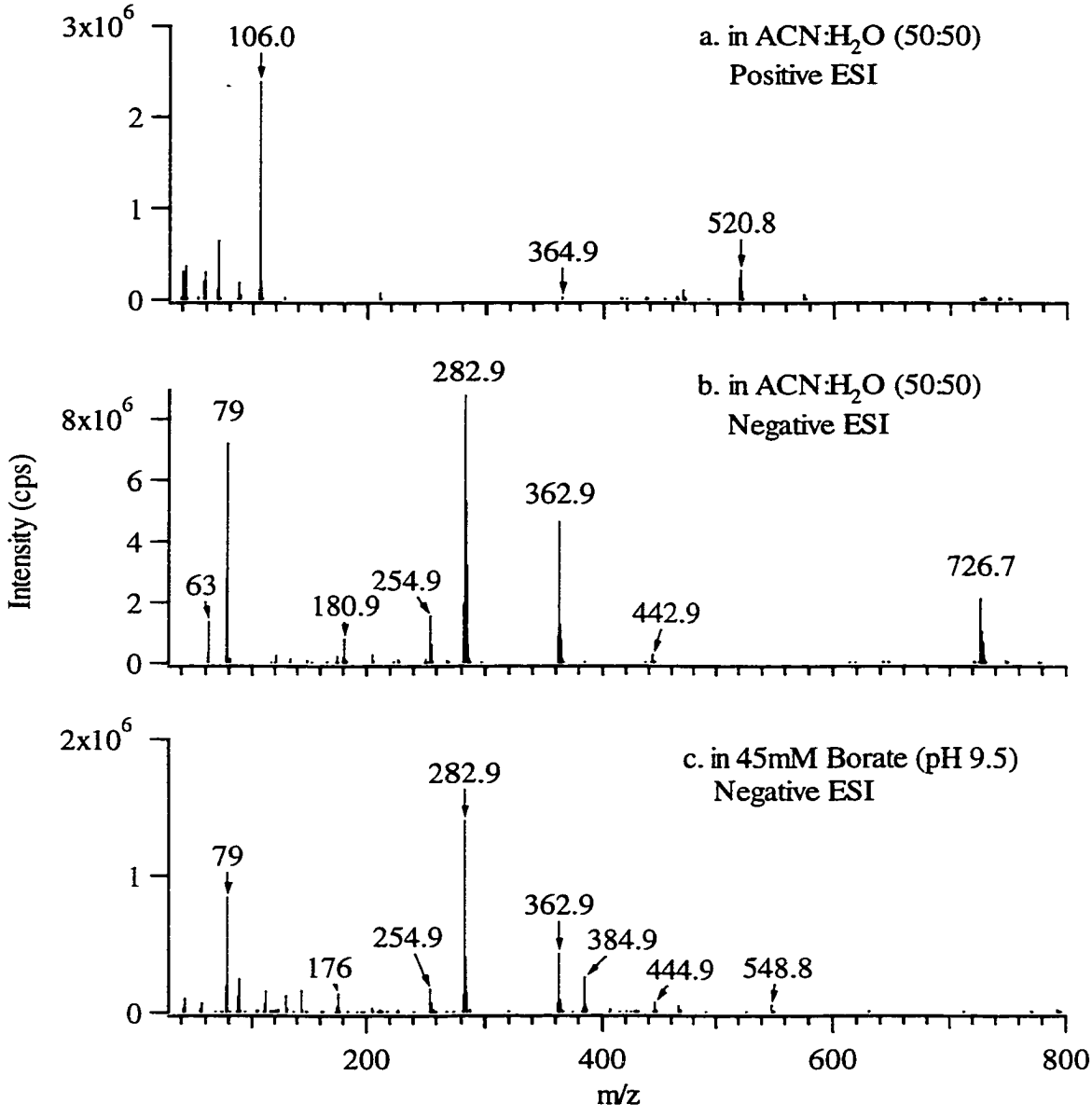

Figure 5.12. ESI mass spectra of ddI showing the sensitivity comparison of ion spray and low-flow interfaces.

Samples were 50 μM ddI dissolved in 90% MeOH and infused to (a) ion spray interface at 2.0 μL/min and the sheath flow rate was at 0.20 μL/min; (b) low-flow interface at 0.30 μL/min and a sheath flow at 0.20 μL/min. Other operational conditions were nearly the same for both interfaces.

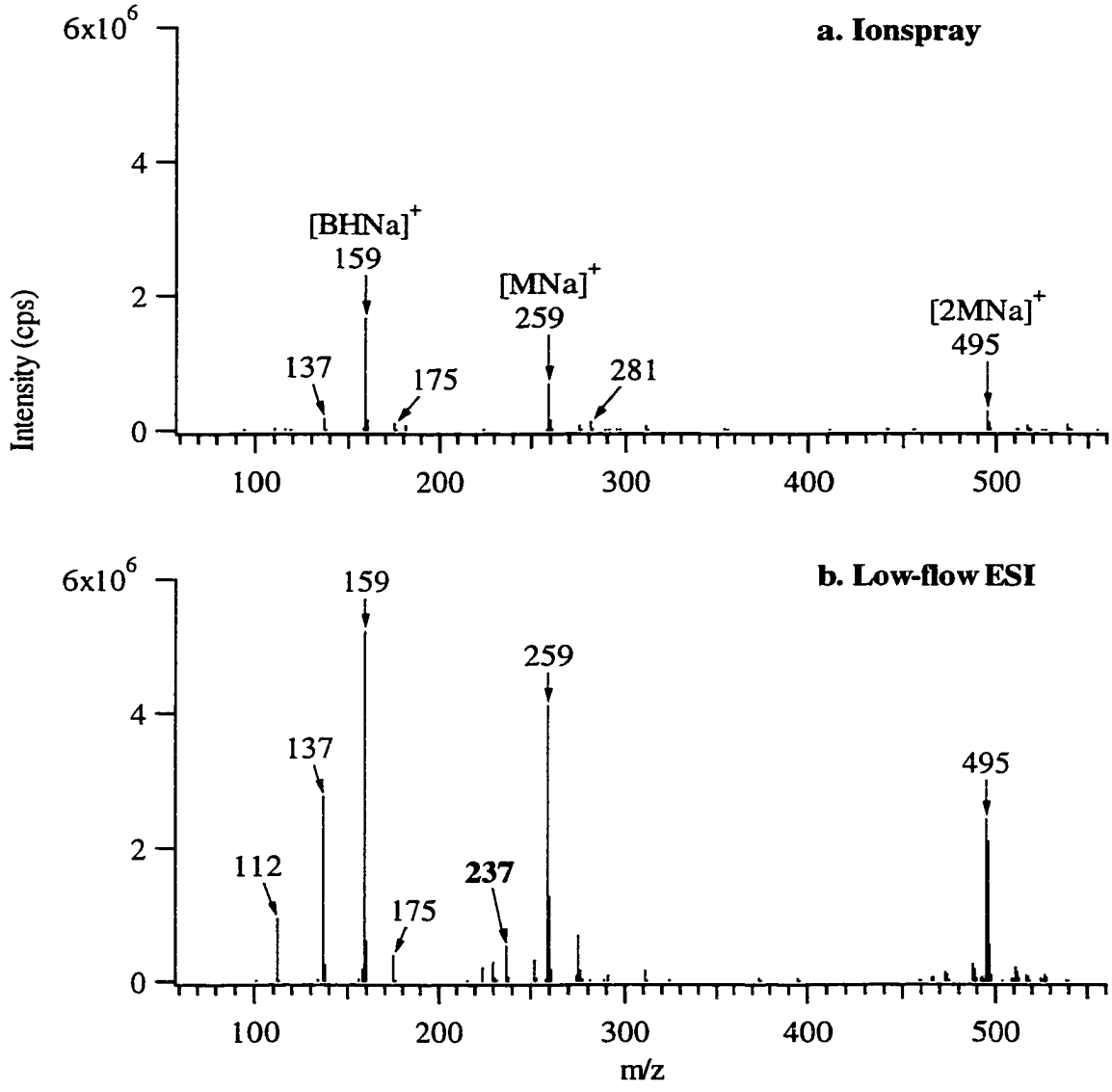

obvious discrepancy between charge state distribution for bradykinin using ionspray and the low flow electrospray is observed, though the low flow ESI spectrum reveals more intensive doubly-charged ions and an enhanced total ion intensity of nearly 3 times. Other ions in the spectra are from the cleavage of peptide bonds. Both spectra were obtained under optimal ESI conditions that were nearly identical for both the low flow electrospray and the ionspray interfaces. The in-source CID voltages (OR) were 50 V and 20 V for ionspray and the low flow ESI, respectively.

Figure 5.10 shows a clean and sensitive mass spectrum of rhodamine obtained from the low flow interface in a positive ESI detection mode.

Figure 5.11 shows negative and positive ESI mass spectra of AttoPhos, a highly fluorogenic substrate for Alkaline Phosphotase used in single enzyme molecule assays in this lab[76]. An interpretable spectrum was obtained of the analyte in even a 45 mM borate solution at pH 9.5, though the detection sensitivity was lower compared to that obtained for the analyte dissolved in a volatile solvent, acetonitrile-water (50:50). Borate is a well-known CE separation buffer that is not appropriate for on-line applications of CE-MS due to a severe ion suppression by borate.

One of the key attributes of low flow ESI that has been noted is its high sensitivity[10-13,36,66,71]. We compared the sensitivity of the low-flow interface with a conventional ion spray interface, **Figure 5.12**. Both the low-flow electrospray and ion spray interfaces were located 10 mm away from the sampling orifice, and nearly identical operating conditions were used for the two interfaces. Low-flow electrospray gave an enhanced signal (3 times) for the base peak in the spectra, the sodiated base fragment of ddI. The spectrum from low-flow interface also showed the molecular ion (m/z = 237), which was not observed in the ion spray spectrum. Instead, the ion spray spectrum was

dominated by sodium adducts (m/z 259 and 281). The high flow rate ionspray produces large initial charged droplets, which experience prolonged desolvation process in the gas-phase until droplets are sufficiently small for ions to be released. The concentration of impurities and analyte in such a droplet after extensive evaporation is increased and thus a suppression (competition) of gas-phase ion production and an increased amount of metal ion adducts occur. In contrast, in the low flow electrospray, the initial droplets are much smaller; ion ejection may occur in the first or early droplet fissions. The offspring droplet at this stage should contain a relatively low concentration of salt residue; thus a higher response of analyte from the low flow electrospray should be obtained and the protonated ions, in addition to the metal ion adducts, should be observed. The higher tolerance towards salt contamination in samples has been reported by other groups[13,77].

5.4.6 CE-MS Performance

Figure 5.13 shows an electropherogram of five antidepressants with similar masses and structures obtained utilizing CE-MS with the interface depicted in **Figure 5.1**. Although peaks of interest are seen, the sensitivity is not better than results obtained using an ionspray interface (**Figure 5.14a**). A noisy background signal in the electropherogram pose additional difficulties in assigning peaks of interest. The unstable electrospray process is probably caused by an insufficient charge separation of buffer counterions at the time of the charged-droplet formation. However, it is not immediately clear why the charge separation should be any different in an SS tube of ionspray as oppose to a silica emitter of the low flow interface. A modified low-flow interface was then fabricated in which the detection end of the CE column was sputter-coated with gold. The coated layer of gold, in addition to the charged sheath liquid, may be crucial for the charge separation. **Figure 5.14** shows total ion electropherograms of a 10 μM mixture

Figure 5.13. Total ion electropherogram of antidepressants by CE-MS using a low flow rate ESI interface shown in **Figure 5.1**.

The sample was a 20 μM mixture of 5 antidepressants in 10% BGE. CE was performed at 267 V/cm. Injection was made electrokinetically at 10 kV for 10 s. Sheath flow rate was at 0.40 μL/min methanol. Other conditions were as described in the experimental section.

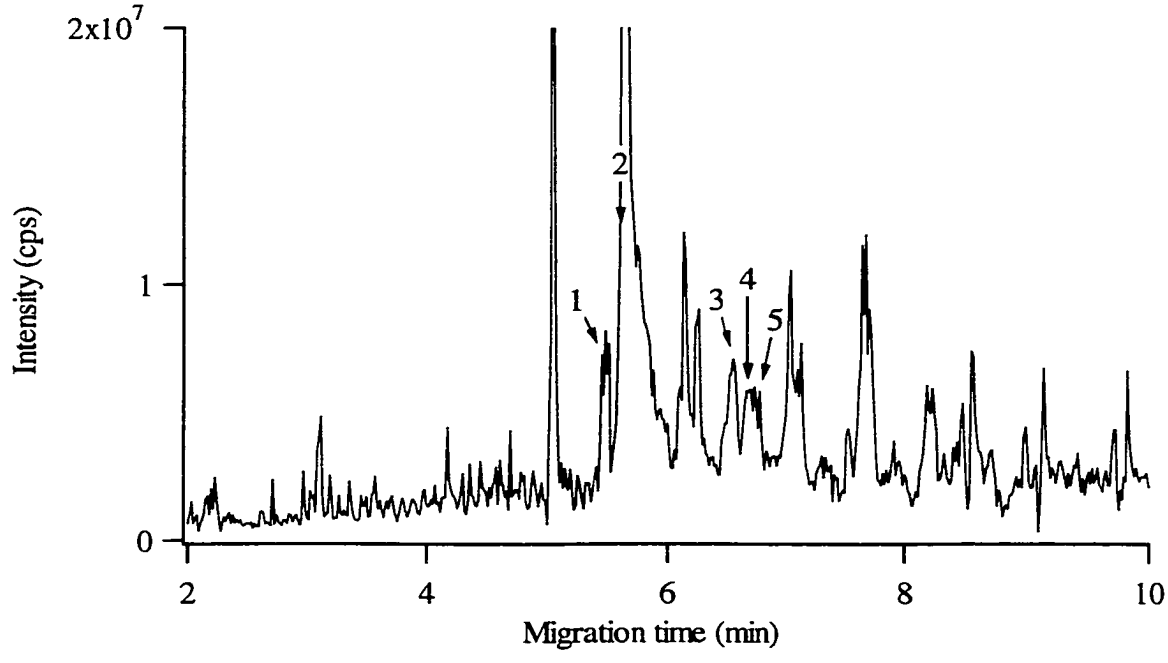

Figure 5.14. Total ion electropherograms of tricyclic antidepressants by CE-MS.

Separations were performed at (a) 200 V/cm (b) 207 V/cm in a 50 μm x 150 μm x 59 cm long capillary using a buffer of 50 mM ammonium acetate in 70:30 methanol-acetonitrile. A 10-μM mixture of 6 compounds was injected at 10 kV for 10 s. All electropherograms were baseline subtracted. Positive ionization ESI was operated with a mass scan speed of 1 s/scan over a range of m/z 65-400. (a) Ion spray interface, (b) low-flow interface with CE column gold-coated at the detection end. Peak orders: (1) desipramine, (2) nortriptyline, (3) imipramine, (4) amitriptyline, (5) clomipramine, (6) tamoxifen, (*) decomposed products.

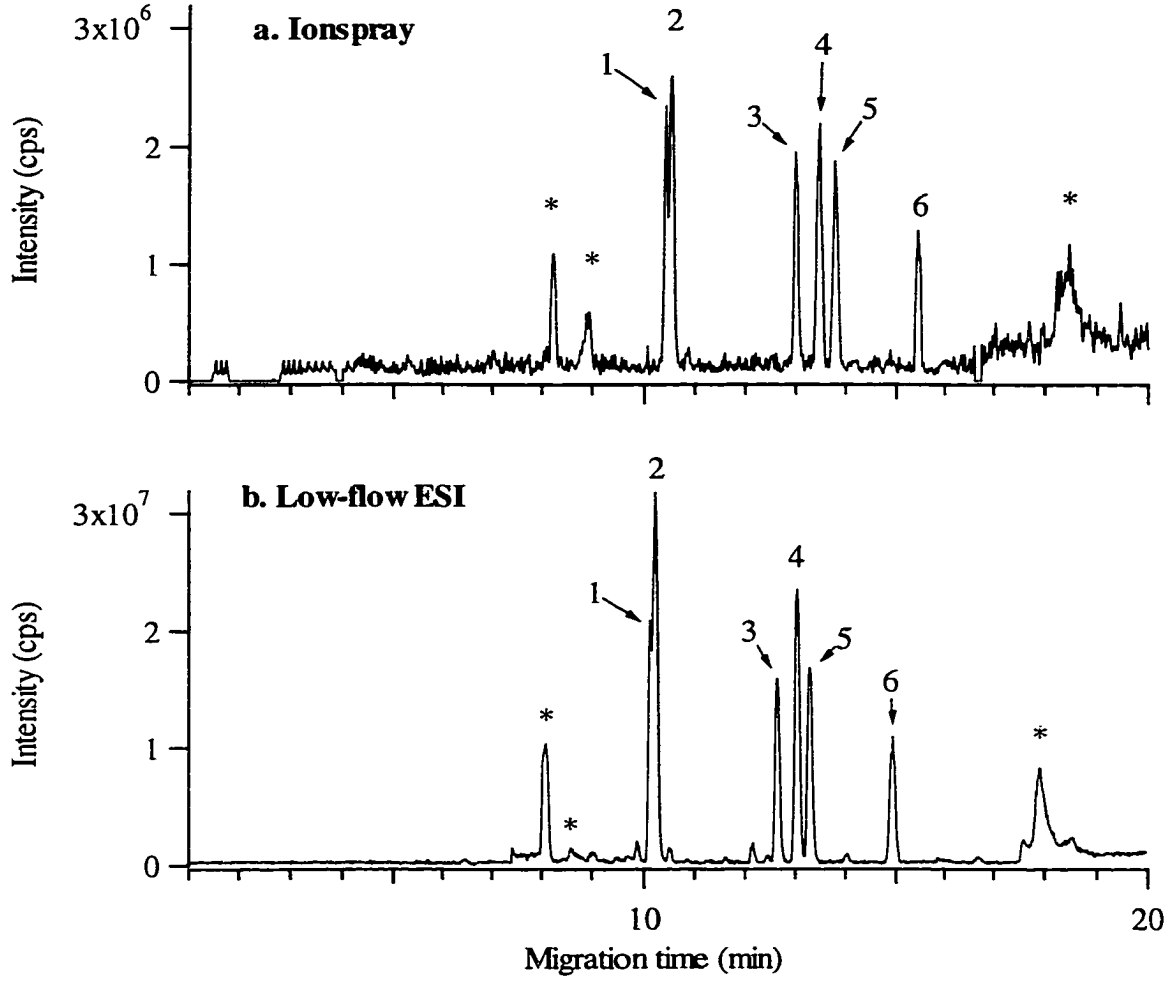

of antidepressant drugs prepared in 5 mM ammonium acetate and 70:30 methanol-acetonitrile, obtained from a conventional ion spray interface (**Figure 5.14a**) and the low-flow interface (**Figure 5.14b**). For comparison, both interfaces were optimized to their best conditions, and nearly identical parameters were used in the two experiments. The sample was electrokinetically injected, and the injection volume was estimated as 11 nL. Since the sample was dissolved in 10% of the running buffer, some stacking effects were present.[74] The tips in both interfaces were 10 mm apart from the curtain plate. In general, the sensitivity of the low-flow electrospray is 12+/-3 (n=3) times higher than ion spray. For instance, the S/N of peak 4 in ion spray is 60, while in low-flow electrospray 710. Some decomposed products can be observed in both experiments. The responses of these decomposed products also demonstrate the performance differences of the two interfaces.

The inherent advantage of the low-flow ESI interface is the spraying of droplets with diameters in the low nanometer range[12], while in ionspray they are believed to be about one order of magnitude larger, in the micrometer range[75,78]. The diameter of the initial droplets influences the evaporation efficiency of the droplets and, therefore, affects the number of ion entering the mass spectrometer. In the context of the widely accepted uneven-fission model,[78] the low-flow electrospray would experience at least one less fission generation before the size of the offspring droplets is small enough for ions to release, or in other words, in the low-flow electrospray, efficient ions are generated in early fissions without extensive evaporation, and the sensitivity is high.

Due to the presence of the liquid-junction inside the emitter tip, a loss of separation efficiency in CE is expected compared to that using an on-column UV detection method. We have reported a theoretical plate number of 240,000 for peak 4 in an identical CE separation of these antidepressants with on-column thermo-optical absorbance

detection,[79] and 200,000 in a CE-MS study using a conventional ion spray interface with a sheath flow of 2.0 μL/min.[74] The average separation efficiency in this study for peak 4 is 199,000, which is nearly the same as that in ion spray.

The lifetime of the sheath interface was tested. The only factor that effects the performance of the interface is the clogging of the tip by the dried buffer salt. To avoid this, water was used to flush the CE column and the emitter after use. The use of a syringe filter to filter all solutions passing through the interface is necessary. One sheath tip has been used for 3 weeks without degradation in performance.

5.5 CONCLUSION

The sheath flow silica emitter for low flow ESI and CE-ESI-MS has been demonstrated. The gold coating on the CE separation column is necessary for sensitive and stable performance of an on-line coupled CE-MS operation. There is a sensitivity enhancement of the low flow ESI when compared to conventional ionspray. Sensitivities 3 times and 12 times higher have been obtained for infusion ESI-MS and CE-MS analyses, respectively. These improvements are similar to that of sheathless gold-coated emitter versus normal ESI. Yet with the sheath-flow feature, the low flow ESI interface we have developed overcomes the most problematic limitations of metalized sheathless emitters; it provides long-term durability yet is simple to fabricate. The gold coating is only applied to the CE column. Future work will be centered on examination of the emitter tip size and how it effects the sensitivity improvements in various CE applications having different electro-osmotic flows, and on studies of the applicability of the interface in peptide and protein analysis by CE-MS.

5.6 BIBLIOGRAPHY

(1) Whitehouse, C.M.; Dreyer, R.N.; Yamashita, M.; Fenn, J.B. *Anal. Chem.* **1985**, *57*, 675-679.

(2) Fenn, J.B.; Mann, M.; Meng, C.K.; Whitehouse, C.M. *Science* **1989**, *246*, 64-71.

(3) Fenn, J.B. *J. Am. Soc. Mass Spectrom.* **1993**, *4*, 524.

(4) Bruins, A. P.; Covey, T. R.; Henion, J. D. *Anal. Chem.* **1987**, *59*, 2642-2646.

(5) Covey, T.T.; Bruins, A.P.; Henion, J.D. *Org. Mass Spectrom.* **1988**, *23*, 178-186.

(6) Covey, T.R.; Huang, E.C.; Henion, J.D. *Anal. Chem.* **1991**, *63*, 1193-1200.

(7) Banks, J.F. Jr.; Shen, S.; Whitehouse, C.M.; Fenn, J.B. *Anal. Chem.* **1994**, *66*, 406-414.

(8) Hirabayashi, A.; Sakairi, M.; Koizumi, H. *Anal. Chem.* **1994**, *66*, 4557-4559.

(9) Straub, R.; Linder, M.; Voyksner, R.D. *Anal. Chem.* **1994**, *66*, 3651-3658.

(10) Emmett, M.R.; Caprioli, R.M. *J. Am. Soc. Mass Spectrom.* **1994**, *5*, 605-613.

(11) Andren, P.E.; Emmett, M.R.; Caprioli, R.M. *J. Am. Soc. Mass Spectrom.* **1994**, *5*, 867-869.

(12) Wilm, M.S.; Mann, S. *Int. J. Mass Spectrom. Ion Processes* **1994**, *136*, 167-180.

(13) Wilm, M.; Mann, M. *Anal. Chem.* **1996**, *68*, 1-8.

(14) Lee, E.D.; Muck, W.; Henion, J.D.; Covey, T.R. *J. Chromatogr.* **1988**, *458*, 313-21.

(15) Shumate, C.B.; Hill, H.H., Jr. *Anal. Chem.* **1989**, *61*, 601-606.

(16) Huang, E.; Henion, J.; Covey, T.R. *J. Chromatogr.* **1990**, *511*, 257-270.

(17) Ikonomon, M.G.; Blades, A.T.; Kebarle, P. *Anal. Chem.* **1990**, *62*, 957-967.

(18) Griffin, P.R.; Coffman, J.A.; Hood, L.E.; Yates, J.R., III. *Int. J. Mass Spectrom. Ion Precesses* **1991**, *111*, 131-149.

(19) Deterding, L.J.; Parker, C.E.; Perkins, J.R.; Moseley, M.A.; Jorgenson, J.W.; Tomer, K.B. *J. Chromatogr.* **1991**, *554*, 329-338.

(20) Olivares, J.A.; Nguyen, N.T.; Yonker, C.R.; Smith, R.D. *Anal. Chem.* **1987**, *59*, 1230-1232.

(21) Smith, R.D.; Barinaga, C.J.; Udseth, H.R. *Anal. Chem.* **1988**, *60*, 1948-1952.

(22) Udseth, H.R.; Loo, J.A.; Smith, R.D. *Anal. Chem.* **1989**, *61*, 228-232.

(23) Lee, E.D.; Mueck, W.; Henion, J.D.; Covey, T.R. *Biomed. Environ. Mass Spectrom.* **1989**, *18*, 844-850.

(24) Smith, R.D.; Udseth, H.R.; Barinaga, C.J.; Edmonds, C.G. *J. Chromatogr.* **1991**, *559*, 197-208.

(25) Moseley, M.A.; Jorgenson, J.W.; Shabanowitz, J.; Hunt, D.F.; Tomer, K.B. *J. Am. Soc. Mass. Spec.* **1992**, *3*, 289-300.

(26) Garcia, F.; Henion, J.D. *Anal. Chem.* **1992**, *64*, 958-990.

(27) Yang, L.; Harrata, A.K.; Lee, C.S. *Anal. Chem.* **1997**, *69*, 1820-1826.

(28) Jensen, P.K.; Harrata, A.K.; Lee, C.S. *Anal. Chem.* **1998**, *70*, 2044-2049.

(29) Lane, S.J.; Boughtflower, R.; Paterson, C.; Underwood, T. *Rapid Commun. Mass Spectrom.* **1995**, *9*, 1283-1287.

(30) Schmeer, K.; Behnke, B.; Bayer, E. *Anal. Chem.* **1995**, *67*, 3656-3658.

(31) Wu, J.T.; Huang, P.; Li, M.X.; Qian, M.G.; Lubman, D.M. *Anal. Chem.* **1997**, *69*, 320-326.

(32) Perkins, J.R.; Parker, C.E.; Tomer, K.B. *J. Am. Soc. Mass Spectrom.* **1992**, *3*, 139-149.

(33) Wahl, J.H.; Gale, D.C.; Smith, R.D. *J. Chromatogr. A,* **1994**, *659*, 217-222.

(34) Davis, M.T.; Stahl, D.C.; Hefta, S.A.; Lee, T.D. *Anal. Chem.* **1995**, *67*, 4549-4556.

(35) Link, A.J.; Eng, J.; Yates, J.R., III. *Am. Lab.* **1996**, *28*, 27-30.

(36) Valaskovic, G.A.; Kelleher, N.L.; McLafferty, F.W. *Science* **1996**, *273*, 1199-202.

(37) Vanhoutte, K.; Van Dongen, W.; Hoes, I.; Lemiere, F.; Esmans, E.L.; Van Onckelen, H.; Van den Eeckhout, E.; van Soest, R.E.; Hudson, A.J. *Anal. Chem.* **1997**, *69*, 3161-3168.

(38) Moore, R.E.; Licklider, L.; Schumann, D.; Lee, T.D. *Anal. Chem.* **1998**, *70*, 4879-4884.

(39) Hulthe, G.; Petersson, M.A.; Fogelqvist, E. *Anal. Chem.* **1999**, *71*, 2915-2921.

(40) Zhang, C.X.; Xiang, F.; Pasa-Tolic, L.; Anderson, G.A.; Veenstra, T.D.; Smith, R.D. *Anal. Chem.* **2000**, *72*, 1462-1468.

(41) Wahl, J.H.; Goodlett, R.R.; Udseth, H.R.; Smith, R.D. *Electrophoresis* **1993**, *14*, 448-457.

(42) Johansson, I.M.; Huang, E.C.; Henion, J.D.; Zweigenbaum, J. *J. Chromatogr.* **1991**, *554*, 311-327.

(43) Wachs, T.; Sheppard, R.L.; Henion, J. *J. Chromatogr. B,* **1996**, *685*, 335-342.

(44) Gatlin, C.L.; Kleemann, G.R.; Hays, L.G.; Link, A.J.; Yates, J.R., 3rd. *Anal. Biochem.* **1998**, *263*, 93-101.

(45) Settlage, R.E.; Russo, P.S.; Shabanowitz, J.; Hunt, D.F. *J. Microcolumn Separations* **1998**, *10*, 281-285.

(46) Li, J.; Thibault, P.; Bings, N.H.; Skinner, C.D.; Wang, C.; Colyer, C.; Harrison, J. *Anal. Chem.* **1999**, *71*, 3036-3045.

(47) Zhang, B.; Foret, F.; Karger, B.L. *Anal. Chem.* **2000**, *72*, 1015-1022.

(48) Lamoree, M.H.; Tjaden, U.R.; van der Greef, J. *J. Chromatogr. A,* **1997**, *777*, 31-9.

(49) Liu, C.; Hofstadler, S.A.; Bresson, J.A.; Udseth, H.R.; Tsukuda, T.; Smith, R.D. *Anal. Chem.* **1998**, *70*, 1797-1801.

(50) Yang, L.; Lee, C.S.; Hofstadler, S.A.; Smith, R.D. *Anal. Chem.* **1998**, *70*, 4945-50.

(51) Fang, L.; Zhang, R.; Williams, E.R.; Zare, R.N. *Anal. Chem.* **1994**, *66*, 3696-3701.

(52) Mazereeuw, M.; Hofte, A.J.P.; Tjaden, U.R.; van der Greef, J. *Rapid Commun. Mass Spectrom.* **1997**, *11*, 981-986.

(53) Guo, X.; Chan, H.M.; Guevremont, R.; Siu, K.W.M. *Rapid Commun. Mass Spectrom.* **1999**, *13*, 500-507.

(54) Petersson, M.A.; Hulthe, G.; Fogelqvist, E. *J. Chromatogr. A.* **1999**, *854*, 141-154.

(55) Barnidge, D.R.; Nilsson, S.; Markides, K.E. *Anal. Chem.* **1999**, *71*, 4115-4118.

(56) Alexander, J.N. IV; Schultz, G.A.; Poli, J.B. *Rapid Commun. Mass Spectrom.* **1998**, *12*, 1187-1191.

(57) Pleasance, P.; Thibault, P.; Kelly, J. *J. Chromatogr.* **1992**, *591*, 325-329.

(58) Kriger, M.S.; Cook, K.D.; Ramsey, R.S. *Anal. Chem.* **1995**, *67*, 385-389.

(59) Hofstadler, S.A.; Severs, J.C.; Smith, R.D.; Swanek, F.D.; Ewing, A.G. *Rapid Commun. Mass Spectrom.* **1996**, *10*, 919-921.

(60) McComb, M.E.; Krutchinsky, A.N.; Ens, W.; Standing, K.G.; Perreault, H. *J. Chromatogr. A,* **1998**, *800*, 1-11.

(61) Barnidge, D.R.; Nilsson, S.; Markides, K.E., Rapp, H.; Hjort, K. *Rapid Commun. Mass Spectrom.* **1999**, *13*, 994-1002.

(62) Wahl, J.H.; Smith, R.D. *J. Cap. Electrophor.* **1994**, *136*, 167-171.

(63) Chang, Y.Z.; Her, G.R. *Anal. Chem.* **2000**, *72*, 626-630.

(64) Maziarz, E.P., III; Lorenz, S.A.; White, T.P.; Wood, T.D. *J. Am. Soc. Mass Spectrom.* **2000**, *11*, 659-663.

(65) Cao, P.; Moini, M. *J. Am. Soc. Mass Spectrom.* **1997**, *8*, 561-564.

(66) Valaskovic, G.A.; Kelleher, N.L.; Little, D.P.; Aaserud, D.J.; McLafferty, F.W. *Anal. Chem.* **1995**, *67*, 3802-3805.

(67) Bateman, K.P.; White, R.L.; Thibault, P. *Rapid Commun. Mass Spectrom.* **1997**, *11*, 307-312.

(68) Gucek, M.; Vreeken, R.J.; Verheij, E.R. *Rapid Commun. Mass Spectrom.* **1999**, *13*, 612-619.

(69) Jurashek, R.; Dulcks, T.; Karas, M. *J. Am. Soc. Mass Spectrom.* **1999**, *10*, 300-308.

(70) Valaskovic, G.A.; McLafferty, F.W. *J. Am. Soc. Mass Spectrom.* **1996**, *7*, 1270-2.

(71) Kelly, J.F.; Ramaley, L.; Thibault, P.; *Anal. Chem.* **1997**, *69*, 51-60.

(72) Lewis, K.C.; Opiteck, G.J.; Jorgenson, J.W.; Sheeleg, D.M. *J. Am. Soc. Mass Spectrom.* **1997**, *8*, 495-500.

(73) Hsieh, F.; Baronas, E.; Muir, C.; Martin, S. *Rapid Commun. Mass Spectrom.* **1999**, *13*, 67-72.

(74) Liu, C.S.; Li, X.; Pinto, D.; Hansen, E.B., Jr.; Cerniglia, C.E.; Dovichi, N.J. *Electrophoresis*, **1998**, *19*, 3183-3189.

(75) Tang, L.; Kebarle, P. *Anal. Chem.* **1993**, *65*, 3654-3668.

(76) Polakowski, R.; Craig, D.B.; Skelley, A.; Dovichi, N.J. *J. Am. Chem. Soc.* **2000**, *122*, 4853-4855.

(77) Juraschek, R.; Dulcks, T.; Karas, M. *J. Am. Mass Spectrom.* **1998**, *10*, 300-308.

(78) Kebarle, P.; Tang, L. *Anal. Chem.* **1993**, *65*, 972A-986A.

(79) Li, X.; Liu, C.S.; Roos, P.; Hansen, E.B. Jr.; Cerniglia, C.E.; Dovichi, N.J. *Electrophoresis* **1998**, *19*, 3178-3182.

CHAPTER 6

Electrospray Artifacts of Peptides: A Unique Behavior of Doubly Charged Ions

6.1 ABSTRACT

We report a distinctive ion appearance of small peptides in electrospray ionization mass spectrometry. By infusing a standard peptide solution into the spectrometer, we observed that ion signals of doubly-charged species predominate at low analyte concentrations, whereas at high concentrations singly-charged species are more abundant. This unique phenomenon was verified by capillary electrophoresis coupled with electrospray mass spectrometric detection. An electrophoretic peak, obtained by CE-MS analysis in either acidic or basic buffer systems, shows dynamically the effects of solute concentration on relative intensities of doubly- and singly-charged ions. In addition, the amount of doubly charged ions decreases substantially at elevated voltages applied at the orifice and the focusing ring.

6.2 INTRODUCTION

Capillary electrophoresis-mass spectrometry (CE-MS) has become an attractive coupling technique in solving complex analytical and biological problems since its first demonstrated success for separation and characterization of labile, polar or ionic constituents in biological mixtures in 1987[1]. A variety of MS techniques have been used for coupling to either capillary zone electrophoresis[1-10], capillary gel electrophoresis[11], capillary isoelectric focusing[12, 13], capillary isotachophoresis[4, 15], micellar electrokinetic capillary chromatography[16, 17], or capillary electrochromatography[18, 19]. A key point in these combinations is the electrospray interface by which the analyte of interest is ionized, desolvated, and transferred into the vacuum region of the mass spectrometer[20-23]. Electrospray ionization is a highly effective means for producing gas-phase peptide and protein ions with multiple charges from solution[24, 25]. The charge distribution of peptides and proteins in the gas phase has been reported to be a function of temperature[26], pH[27], solvent[22], anions[28], ionic strength[29], protein conformation[30, 31], nebulizing gas[25], and the number of basic or acidic sites in proteins or peptides[24]. Fenn *et al.*[24] reported that the relative intensities of singly- and doubly-charged parent peaks of a cyclic decapeptide, gramicidin S, are strongly dependent on solution composition as well as analyte concentration. The doubly-charged ions are predominant while the singly-charged ions almost vanishes at very low concentration. A subsequent explanation was proposed based on an ion evaporation theory[32, 33] or a total free energy study[34]. It is estimated that the total free energy of a doubly-charged ion is lower than that of a singly-charged ion[34].

We monitored the relative amounts of doubly-charged ions over singly-charged ions for two peptides, bradykinin and angiotensin II, over wide ranges of concentrations.

At low concentrations, doubly-charged species predominate, while at high concentrations, singly-charged ions are more abundant. The total free energy explanation does not satisfy the latter case. The effects of solute concentration on the distribution of doubly-and singly-charged ions are dynamically demonstrated in a CE-MS analysis. The relative intensities of the two kinds of ions are also investigated during their transit. Effects of solvent composition on charge state distribution were also investigated.

6.3 EXPERIMENTAL

6.3.1 Materials and Chemicals

Angiotensin II and bradykinin were purchased from Sigma (St. Louis, MO). Spectrophotometric grade methanol was purchased from BDH (Toronto, ON, Canada). Acetic acid (HAc) and ammonium acetate (NH_4Ac) were obtained from Anachemia (Montreal, PQ, Canada). Triethylamine was from Sigma. Peptide solutions of 2×10^{-3} M were prepared using water prepurified by a Nanopure II system (Barnstead, MA) and diluted to 10^{-4} - 10^{-8} M with methanol-water (95:5) or other solvent mixtures as indicated.

Untreated fused-silica capillaries (Polymicro Technologies, Phoenix, AZ) with 50 μm ID x 142 μm OD with a length of 60 cm were used for all experiments. Freshly prepared buffers were used for CE-MS experiments. A CZE 1000R high-voltage (HV) power supply (Spellman High-Voltage Electronics, Plainview, NY) was used to apply the HV for CE injections and separations.

6.3.2 CE-ESI-MS

An in-house built CE injector was used for all coupling analysis. ESI-MS studies were conducted on a PE/Sciex API 100 (Thornhill, Canada) single quadrupole mass

spectrometer equipped with an ion spray source. An in-house built stainless steel electrode with a tip internal diameter of around 50 μm was used to replace the commercial electrode. The interface set up was shown in **Figure 6.1**. Briefly, a 2 cm long piece of stainless steel (SS) tube with 50 μm ID and 200 μm OD was soldered to another 13 cm long SS tube with a 250 μm ID and 400 μm OD. Most of the small ID SS tube was then cut off leaving about 2 mm protruding with reference to the large ID SS tube. The CE column was inserted into the electrode, which was inside the SS nebulizing tube. The CE column exit end was withdrawn 1 mm once it reached the electrode tip, and the tip protruded 1 mm with reference to the nebulizing tube outlet. The electrode tip was 14 mm from the sampling cone (X-axis). The Y- and Z-axes of the tip were optimized for maximum sensitivity by a continuous injection method. Potentials applied at the ion sprayer (IS), the orifice (OR) and the focusing ring (RNG) were chosen for highest peptide signals, and were 4 kV, 50 V, and 240 V, respectively. The MS scan speed was 2.4 s/scan. When a continuous injection mode was performed, the standard solutions at various concentrations were infused at 2.0 μL/min; no sheath liquid was applied. When CE injection was performed, the ion spray voltage was set to 0. The sheath liquid, methanol, was pumped through the coaxial space between the silica column and the electrode inner wall at 2.0 μL/min by a syringe pump (Harvard Apparatus, South Natick, MA). No nebulizing gas was applied for this study; i.e. a pure electrospray (instead of ion spray) process was used. CE separations were performed at 300 V/cm in acidic (2 mM NH_4Ac in 1% HAc) or basic (0.4% triethylamine) buffer systems. Electrokinetic injections were made at 10 kV for 10 s. The sheath flow rate was 0.6 μL/min.

Figure 6.1. A schematic diagram of the interface set-up for electrospray and CE-MS.

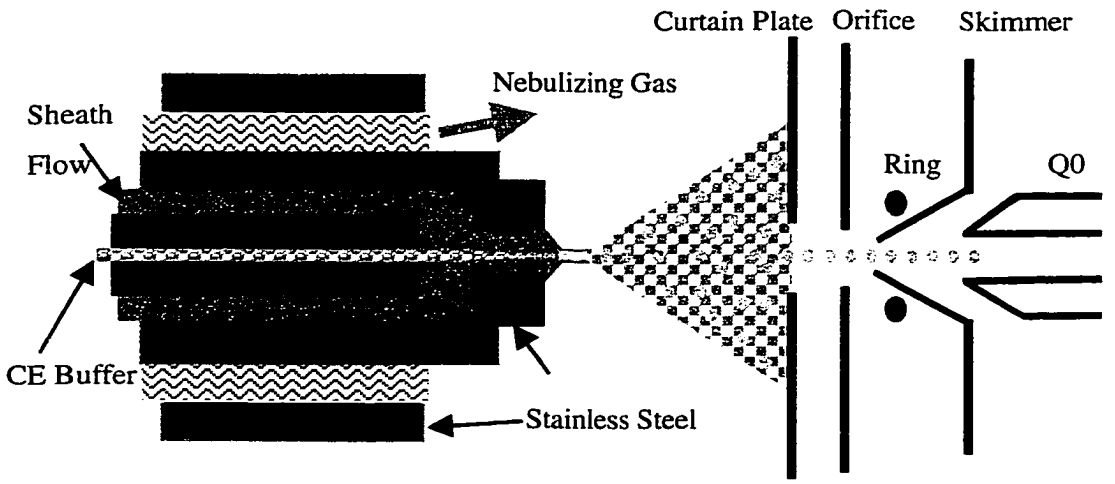

6.4 RESULTS AND DISCUSSION

In a series of infusion studies, standard solutions with concentrations varying from 10^{-8} to 10^{-4} M were infused to the ESI-MS via the CE separation capillary column. **Figure 6.2a** shows a typical ESI mass spectrum of bradykinin in which the singly-charged ions, the doubly-charged ions and the fragments, e.g. y" ions and b ions arising from the peptide bond cleavage, are clearly seen. There is a linear dependence of total ion current (TIC) on analyte concentrations at low range ($<10^{-5}$ M); above this range, signals level off as the concentration increases as described by Tang and Kebarle's theory[35, 36]. Surprisingly, when the sample concentration decreases, the relative ion intensities of the singly-charged ion decrease as illustrated in **Figure 6.2b**. Further, if the calibration curves for singly- and doubly-charged pseudo molecular ions were plotted separately, different behaviors were observed. The typical calibration curves are demonstrated in **Figure 6.3** and **Figure 6.4**. The plots in the figures show that doubly-charged ions predominate at low concentrations, while that at high concentrations the singly-charged ions are more abundant.

These phenomena were confirmed by on-line CE-ESI-MS analysis. Because of the presence of a concentration gradient in an electrophoretic peak (i.e., the analyte concentration is high at the center of the peak and is low on the sides) the extracted ion electropherogram (XIE) shows dynamically the effect of analyte concentration on charge distribution. The XIE was obtained from a total ion electropherogram (TIE) by extracting only signals of interested ions. The XIE for singly-charged ions gives a higher and narrower peak than that for doubly-charged ions which gives a lower and broader peak, **Figure 6.5**.

Figure 6.2. ESI mass spectra of bradykinin showing the influence of analyte concentration on relative intensities of doubly charged ions over singly charged ions.

The sample was prepared in 95% methanol and infused via the CE capillary column at a flow rate of 2 μL/min. Other conditions were as described in the experimental section.

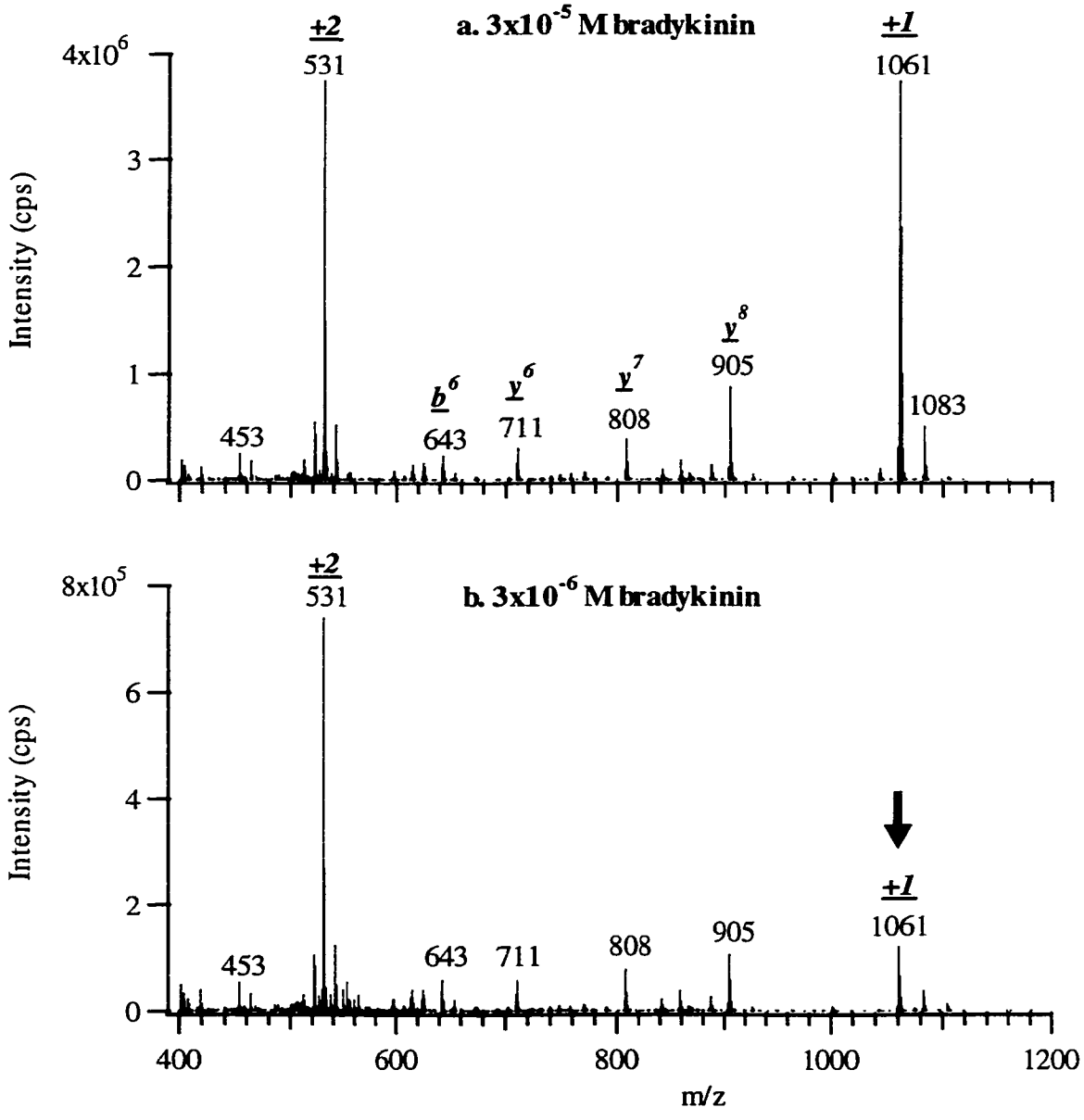

Figure 6.3. Calibration curves of bradykinin by infusion ESI-MS.

Samples in 95% methanol were continuously infused at 2 μL/min. The potentials applied at the ion sprayer, the orifice and the focusing ring were 4.0 kV, 50 V, and 240 V, respectively. The nebulizing gas was set to 0. Other conditions were as described in the experimental section

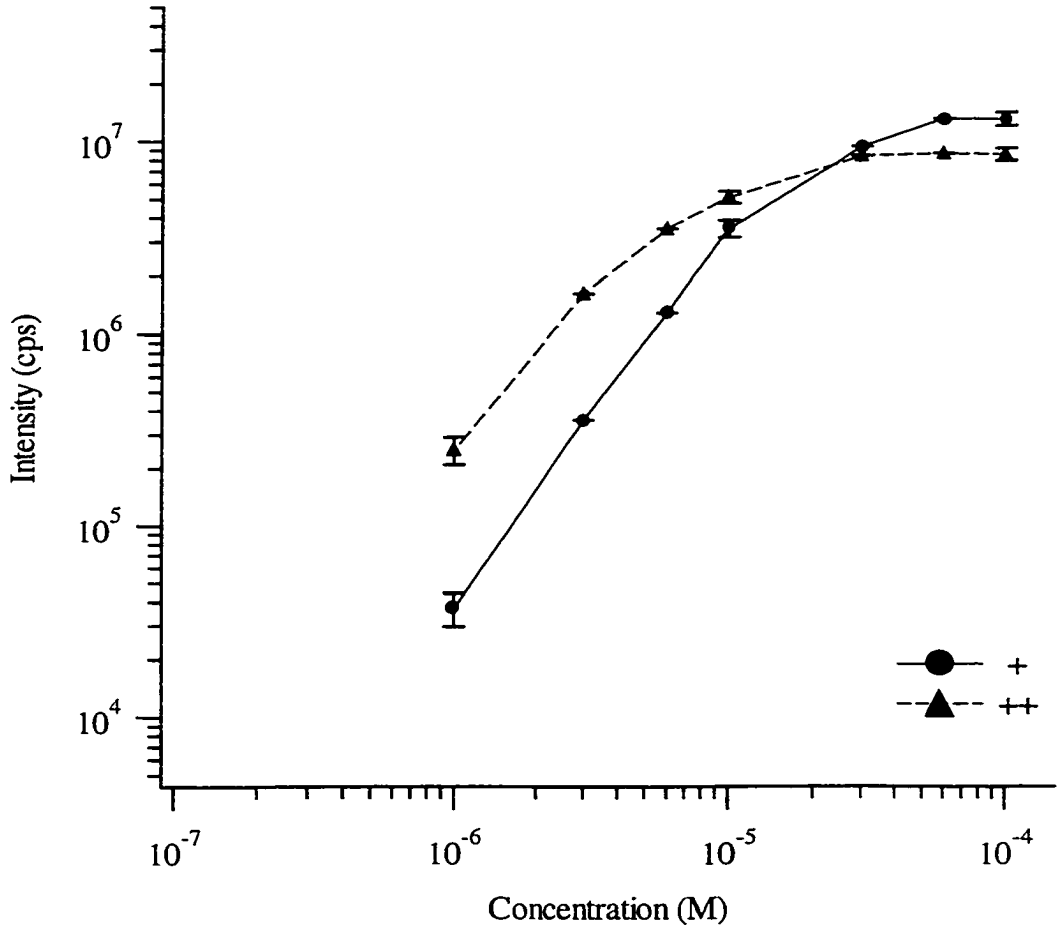

Figure 6.4. Calibration curves of angiotensin II by infusion ESI-MS.

Conditions were the same as in **Figure 6.3**.

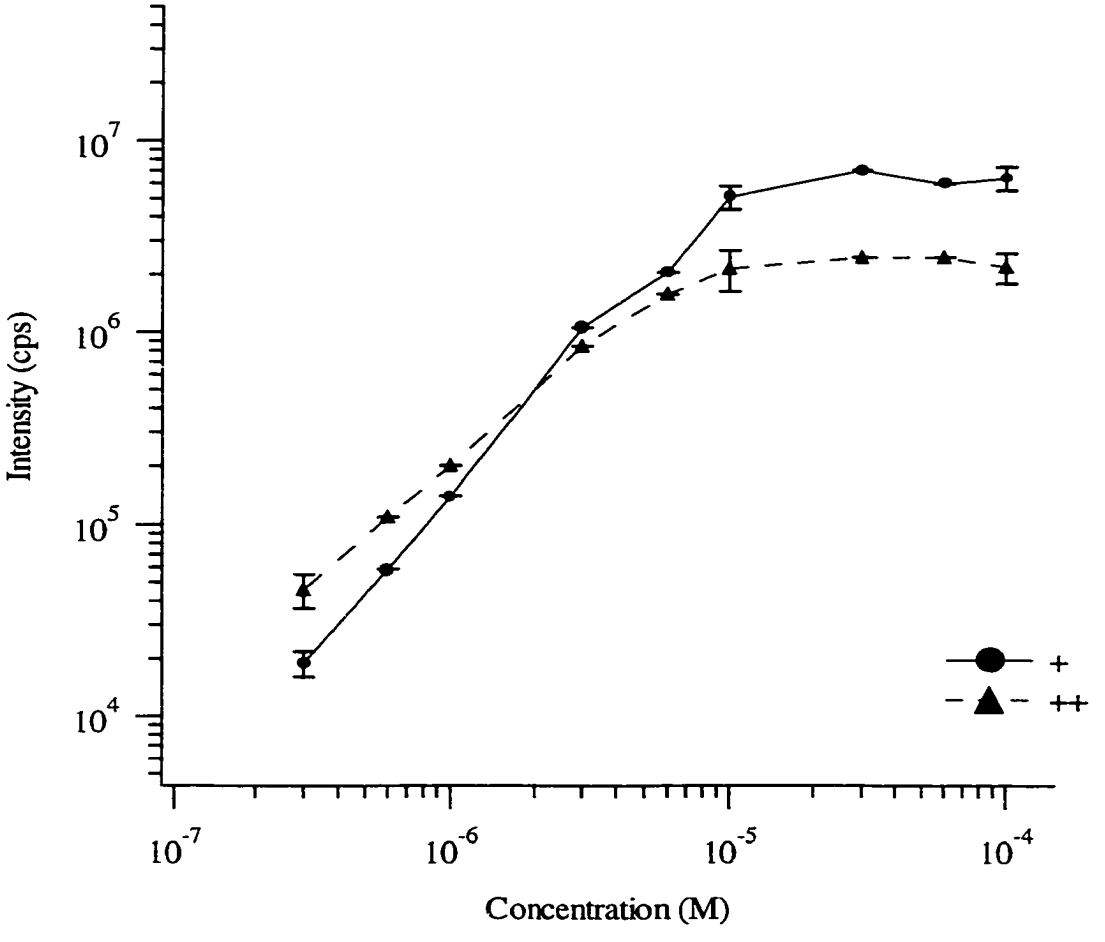

Figure 6.5. Extracted ion electropherogram (XIE) for singly charged ions (m/z 1040-1140) and doubly charged ions (m/z 520-570) obtained from a total ion electropherogram (TIE) of bradykinin.

The sample was 10^{-5} M bradykinin prepared in 95% methanol and was injected at 10 kV for 10 s. CE was performed at 250 V/cm in 2 mM ammonium acetate in 1% acetic acid (pH 2.9). Other conditions were as described in the experimental section. The trace for ++ was moved left for about 1.2 s to compensate the slow scanning speed (2.41 s/scan) of the quadrupole mass analyzer which scanned high mass first.

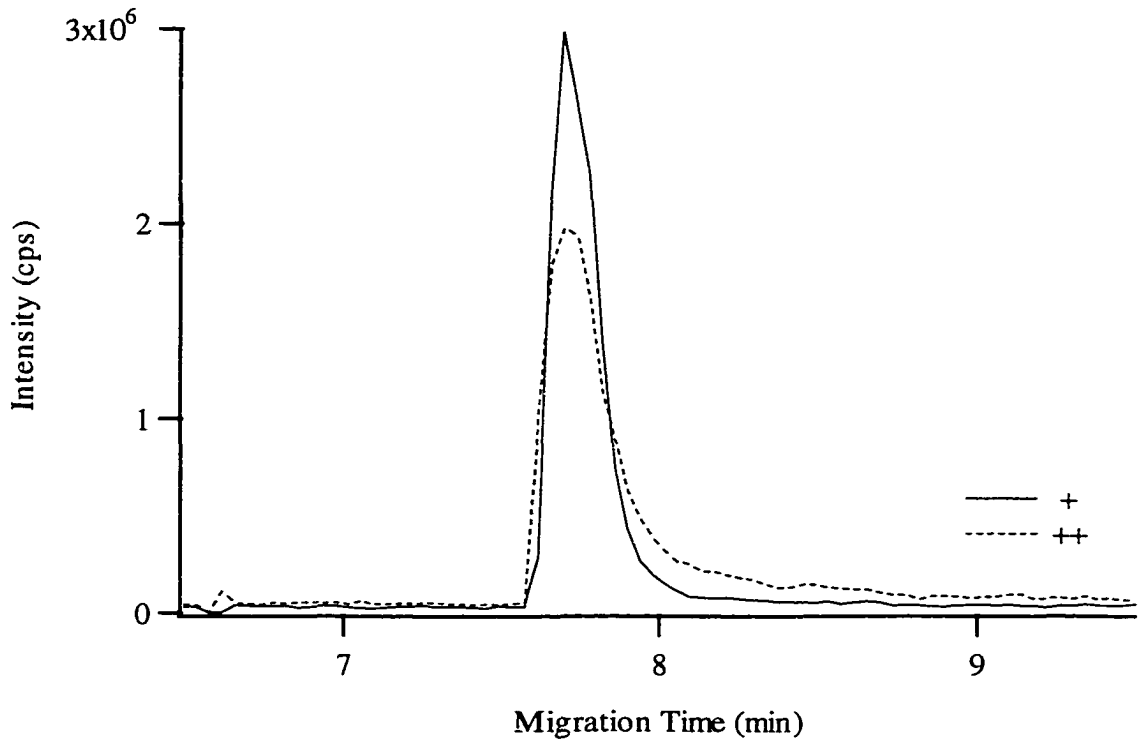

To explain these results, one could simply reason that there is a competition between analyte molecules in the charged droplets in gaining protons to become protonated molecular ions. If the analyte concentration is high, a limited number of protons on the charged surface are shared by many analyte molecules, so mostly singly-charged ions are observed. If the concentration is low, the same numbers of protons on the droplet surface are available for fewer analyte molecules in the droplet; therefore more doubly-charged ions are formed.

This simple argument is at least limited. It can not explain the experimental observations shown in **Figures 6.6 and 6.7**. In this case, 10^{-5} M angiotensin II was prepared in a series of mixed methanol-water solvents with different water content and infused into the ESI-MS. The noteworthy feature of **Figure 6.6** and **Figure 6.7** is the remarkable decrease in ion abundance of doubly-charged species as the water content of the solution rises, while the intensity of singly-charged species is nearly constant when the water content increases from 5% to 50%.

The Ion Desorption Model (IDM) proposed by Iribarne and Thomson[32] and further studies derived from the IDM[33, 36] offers a possible explanation. According to the IDM, the only charges available to produce free gas-phase ions from a droplet are the excess charges the droplet carries when it is formed from the jet of liquid emerging from the Taylor cone at the exit of the sprayer needle. Those excess charges are all at the droplet surface and have no accompanying counterions, as do all the solute ions in the sub-surface bulk solution which is therefore neutral. For most situations the total charge on the droplet when ion desorption begins is essentially independent of analyte type and concentration[36]. The charges are distributed over the droplet surface in an equidistant array to achieve the minimum electrostatic repulsive energy[33].

Figure 6.6. Intensity of singly-charged and doubly-charged ions versus water content in a sample solution prepared in methanol-water.

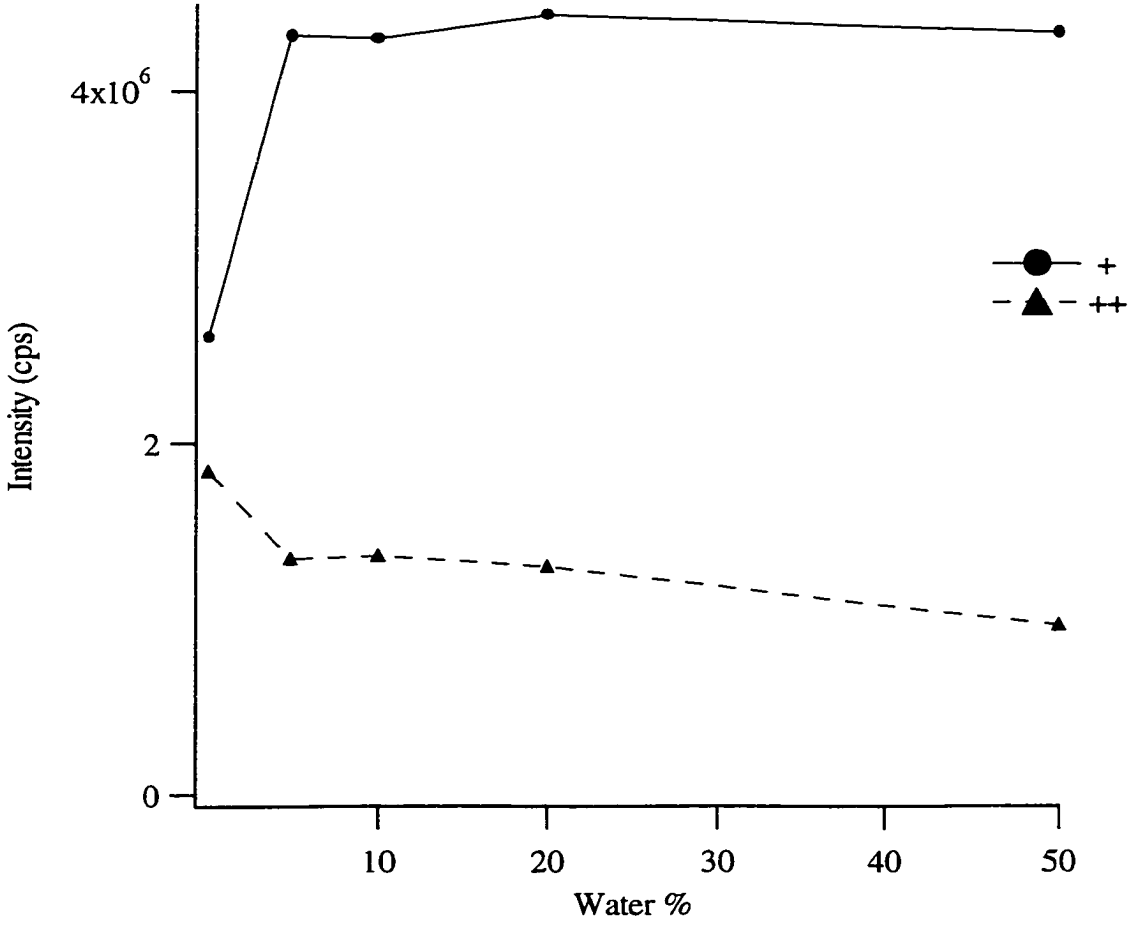

Figure 6.7. Intensity ratio of doubly-charged ions to singly-charged ions (++/+) *versus* water content in a sample solution prepared in methanol-water.

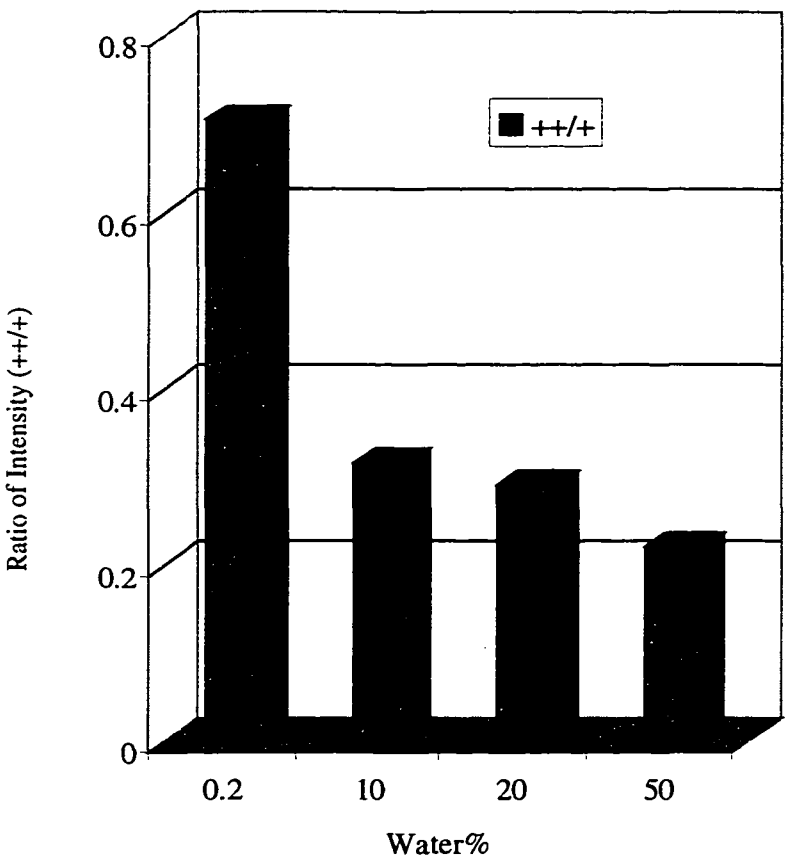

For high concentrations, as the droplet shrinks by solvent evaporation, the distance between the charges decreases. When a basic group on a peptide molecule approaches a surface charge, the group attaches to that charge and becomes pinned to its location. Once droplets of Iribarne ion desorption sizes are formed, the ion will be desorbed to a gas-phase, another analyte molecule will fill its location, and the subsequent shrinkage-fission process will occur. If the original analyte concentration is very low, few peptide molecules are present in the droplet. Once the charged peptide molecule is desorbed, few other molecules are available in the droplet to replace the peptide, and only when enough shrinkage-fission cycles have occurred, in the late droplet evaporation process (when the analyte is highly concentrated), will most of the analyte molecule approach the surface charges. At this stage, the droplet is so small and the surface charges are so close that a peptide molecule can span the distance between two of the charges and thus become doubly-charged.

This assumption that doubly-charged ions desorb in a late evaporation process is supported by the experimental results shown in **Figure 6.6**. Because the solvent evaporation rate of a charged droplet is proportional to the vapor pressure of the solvent, electrospray with less volatile solvents such as the higher water content solution may lead to lower ion intensities. This result suggests that doubly-charged ions are desorbed from the last offspring droplets, while the singly-charged ions are from the early droplet shrinkage process. High water content leads to a slower evaporation process, and therefore few later desorbed doubly-charged ions are produced.

A recent publication provided another explanation: the singly charged peptide ions might be actually aggregates of two singly-charged units[37]. This assumption can not be justified by the present experiment owing to limited resolution of our mass spectrometer.

The pH of spray solution has a larger effect on charge distribution, **Figure 6.8**. At higher pH, fewer-doubly charged ions occur. Because of neutralization in a basic buffer system there are fewer doubly-charged species than in acidic solutions. In acidic pH condition, more doubly-charged ions occur in the gas phase than singly-charged ions.

Effects from the spatial positioning effects of the ESI tip on signal ratios of singly-charged ions to doubly charged ions were studied. The sprayer was pointed off-axis to the sampling cone. When the other two dimensions were fixed at optimized positions and the Y-axis was moved from -3 to 0 mm, the TIC was nearly constant. The TIC decreased when the Y-axis was further moved from 0 to 1.5 mm, **Figure 6.9**. Although the ratio of $[M+H]^+$ / $[M+2H]^{2+}$ decreased along with the Y-axis, the change was insignificant, **Figure 6.10**. As the Y-axis reached 2 mm away from the center, the signal went to zero.

The influence of the infusion flow rate of sample solution on the ion distribution has also been investigated. **Figure 6.11** shows the extracted ion current traces of singly- and doubly-charged bradykinin obtained from a total ion current trace of infusion-ESI-MS. The infusion flow rate has no apparent influence on relative ion intensities of the singly-charged ions over doubly-charged ions, though the sensitivity and signal stability is affected by the flow rate as depicted in the figure.

It is interesting to note that the doubly-charged ion intensities change with voltages applied at the orifice and the focusing ring in a very different pattern than that of singly-charged ions. Although the maximum TIC occurs at an orifice potential of 50 V, the peak +1 ion signal occurs at OR 55 V, and that of +2 ions occurs at 35 V, **Figure 6.12**. $[M+2H]^{2+}$ substantially decreases at elevated potential of the orifice. The focusing ring potential has similar effects on the +2 ions, i.e., singly-charged species are more abundant

Figure 6.8. Effects of solution pH on ESI mass spectra of bradykinin.

The sample was 2 x 10^{-4} M in 90% methanol and electrokinetically injected onto the CE column. CE separation was performed at 300 V/cm. The CE separation buffers were (A) 2 mM ammonium acetate in 1% acetic acid at pH 3.0, and (B) 0.4 % triethylamine at pH 11.0. Other conditions were as described in the experimental section.

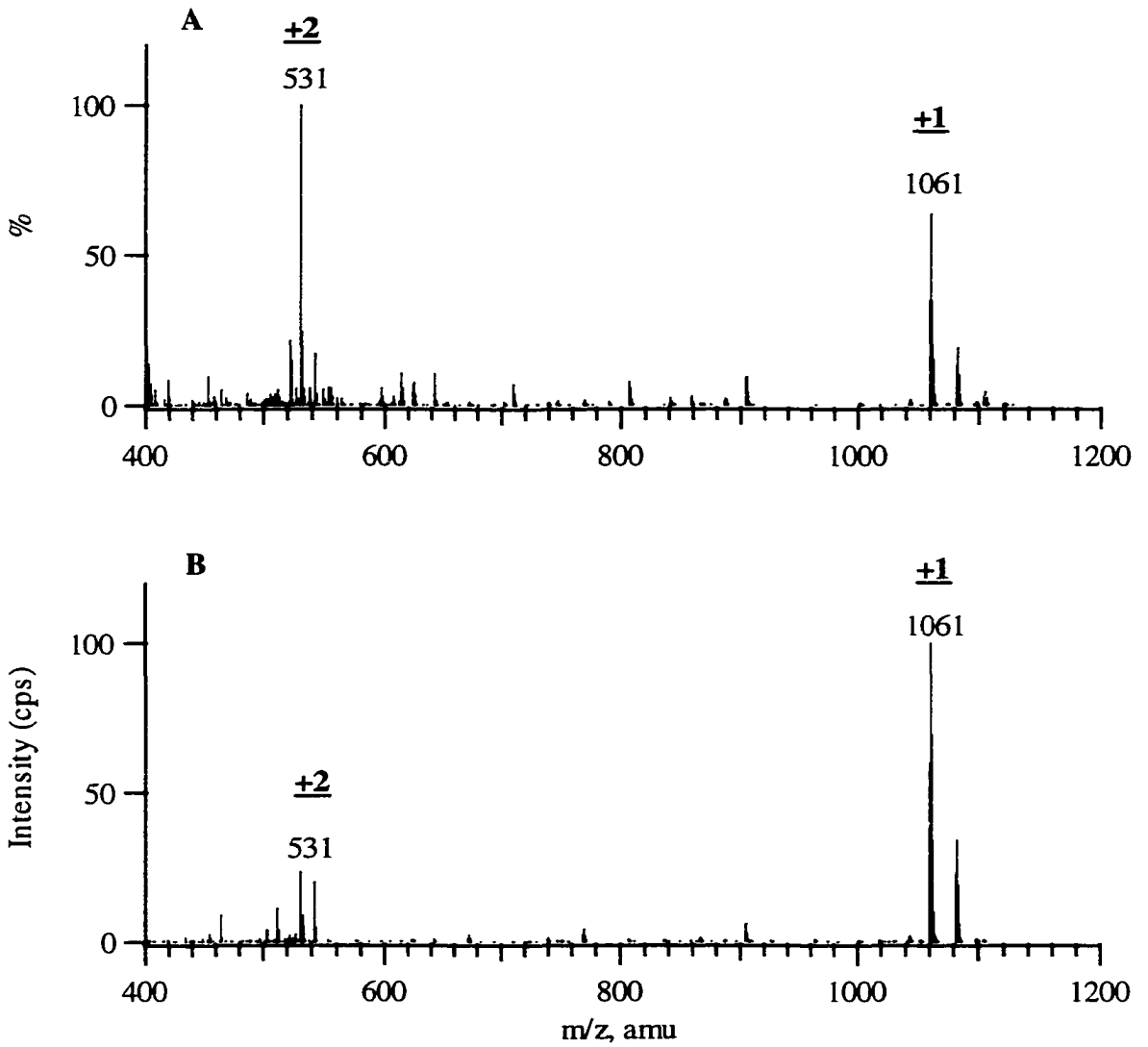

Figure 6.9. Spatial effects of Y-axis on charge distribution of bradykinin in the gas phase.

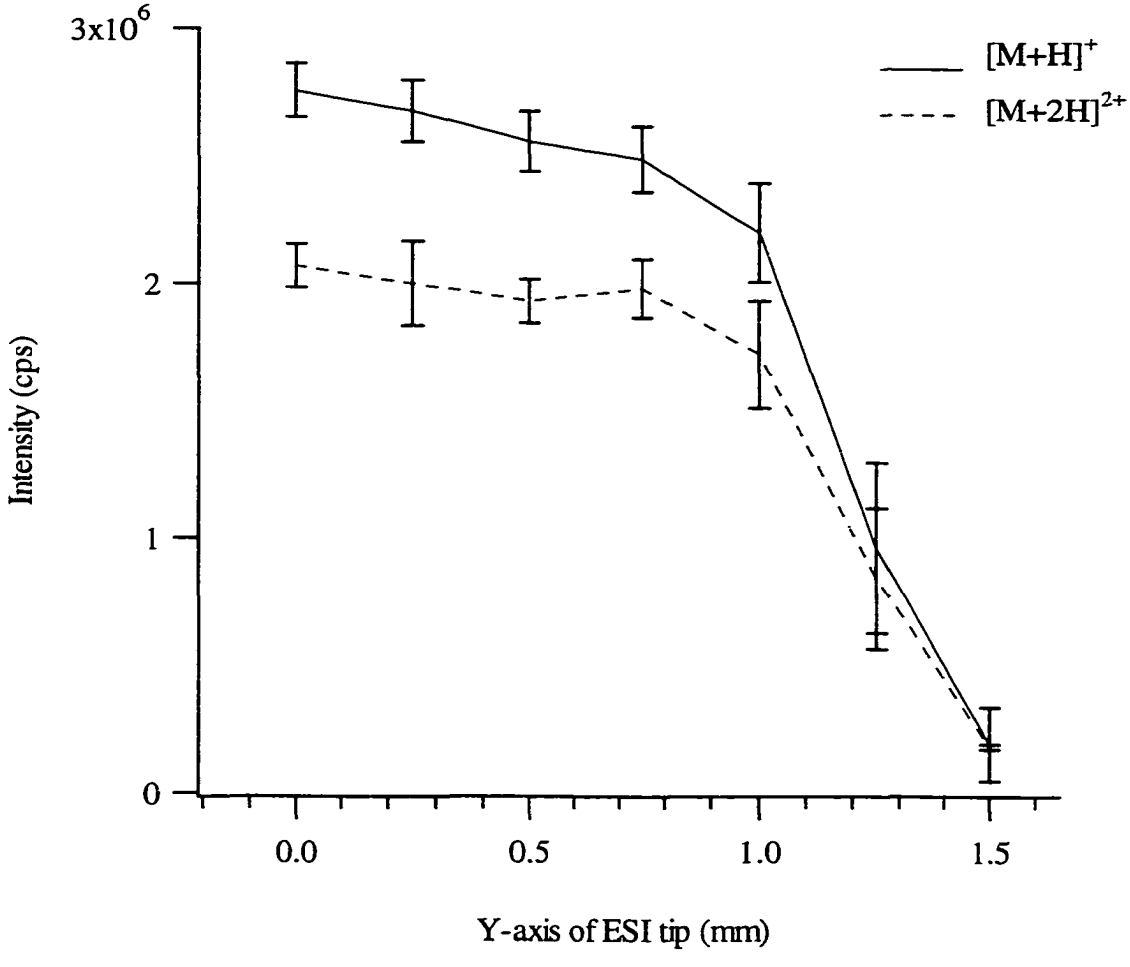

Figure 6.10. Spatial effects of Y-axis on charge formation as plotted with a ratio of ++/+ versus the Y-axis.

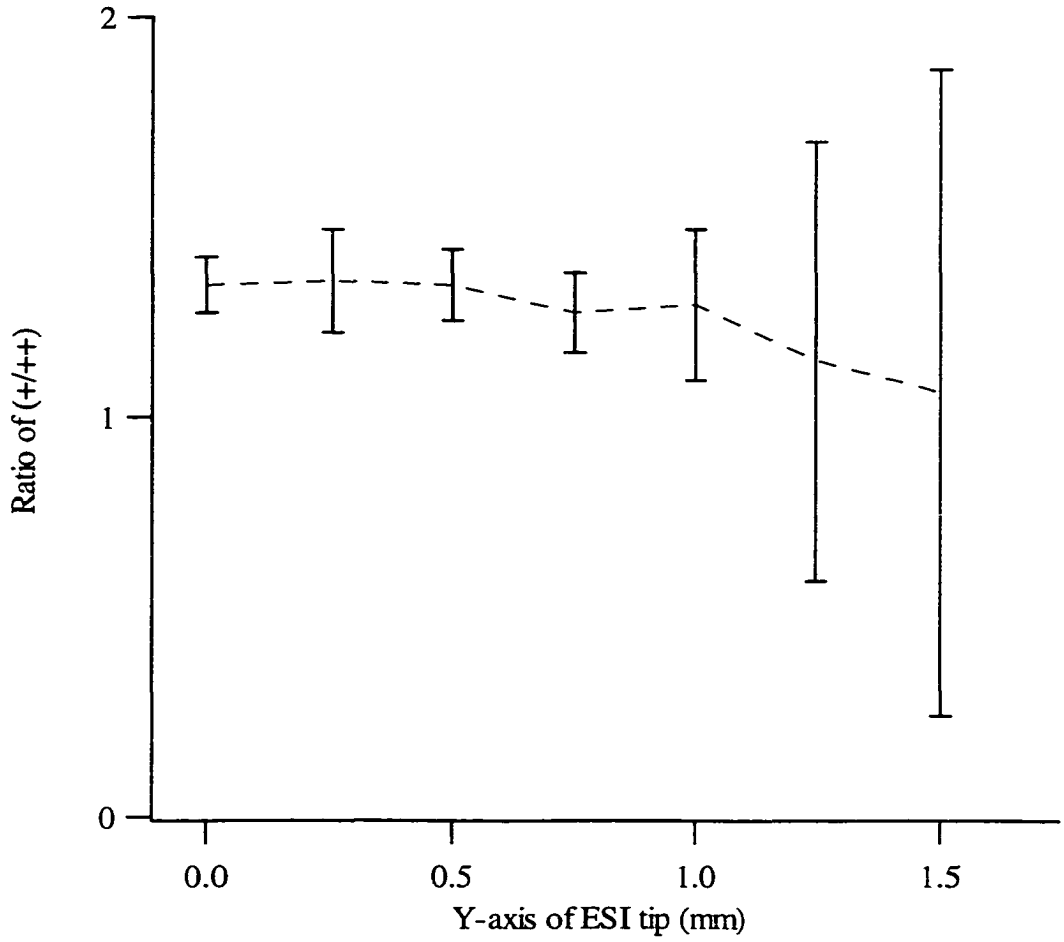

Figure 6.11. Effects of infusion flow rates of the sample solution on charge distribution of bradykinin in the gas phase.

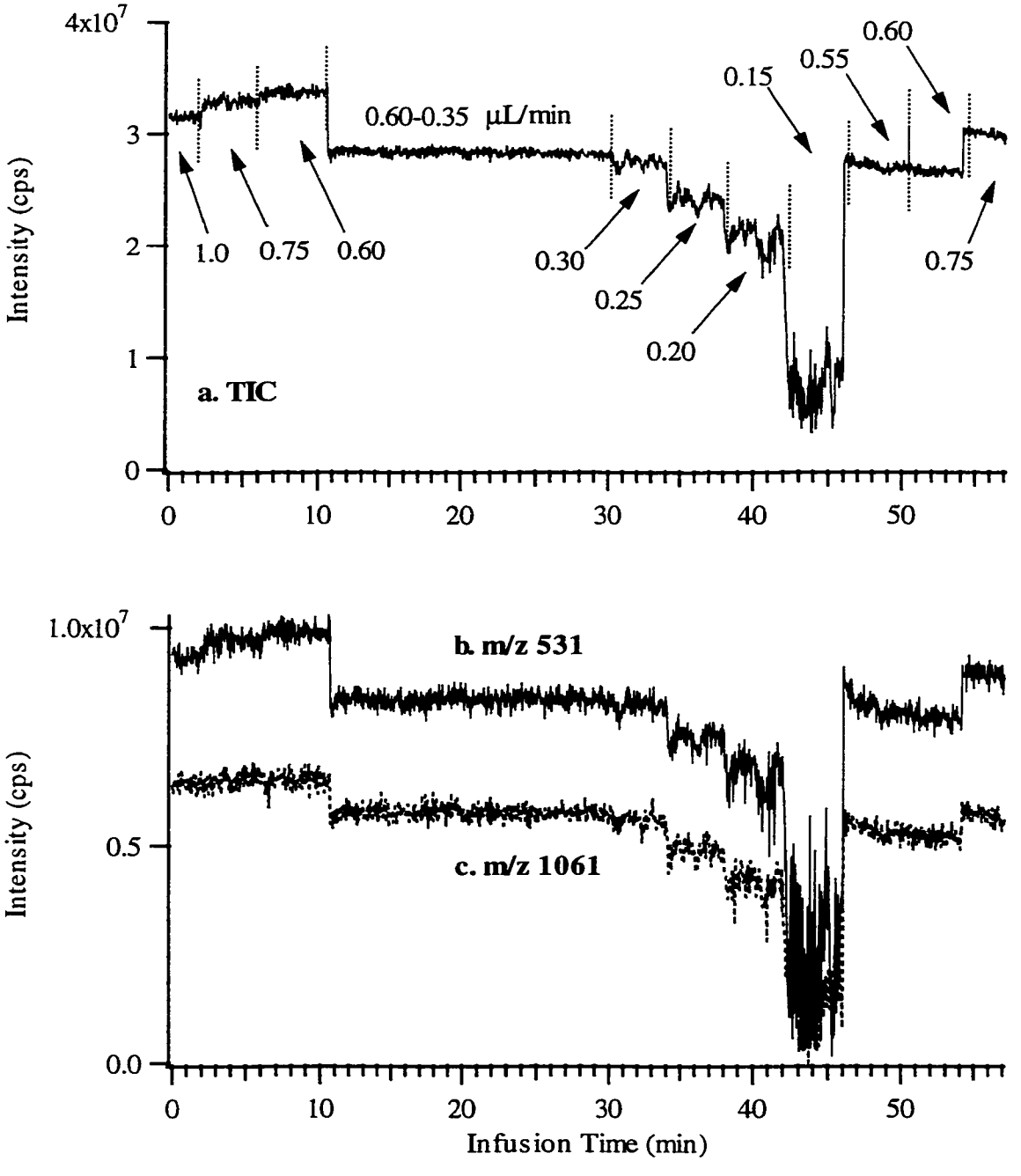

Figure 6.12. Effects of orifice potential on charge formation.

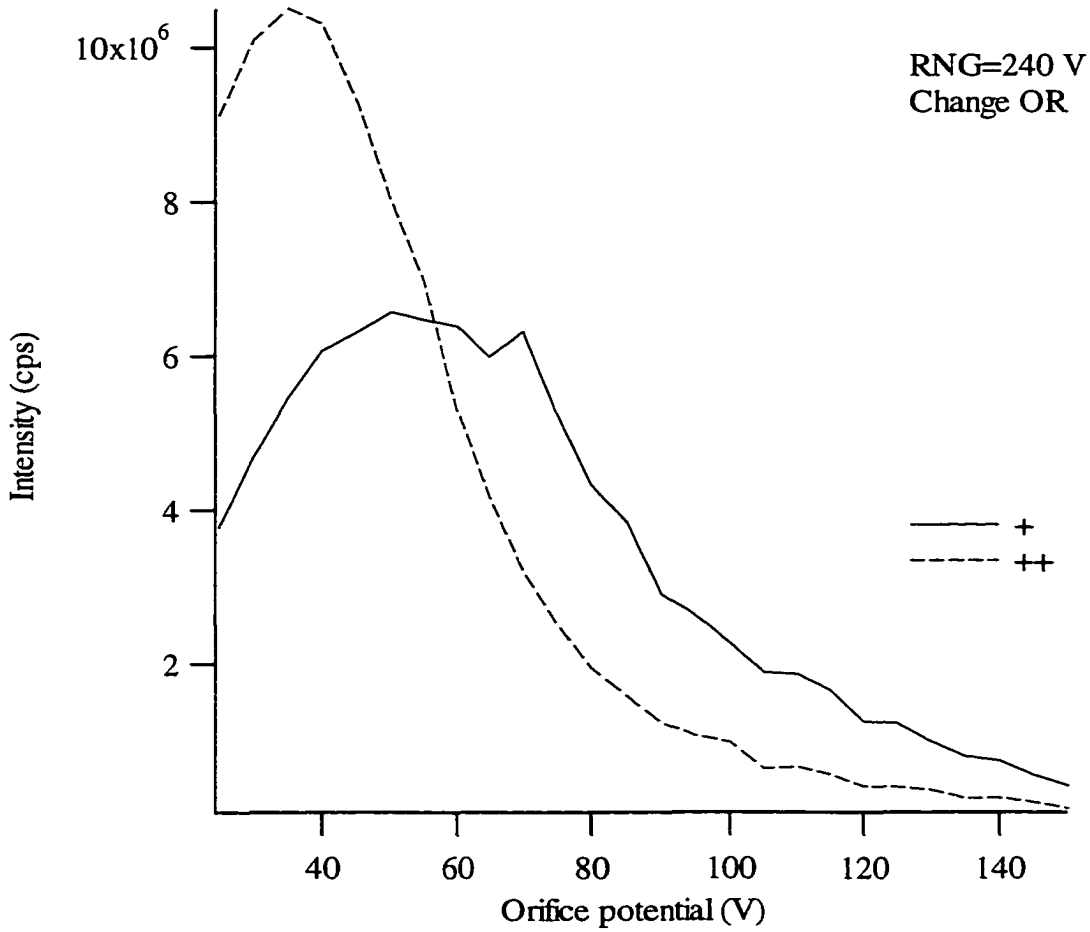

at around 240 V, while the doubly-charged ones are more prevalent at 200 V, **Figure 6.13**. The free-jet region between the orifice cone and the skimmer cone causes in-source collisional induced dissociation (CID) of ions.

The aforementioned results have been used to optimize the operating parameters of ESI-MS in a peptide analysis by CE-MS. The potentials applied at the interface region should be adjusted accordingly for maximum sensitivity of these ions. **Figure 6.14** shows a typical separation of the structurally similar peptides, bradykinin and tyr-bradykinin in an acidic separation buffer. Due to the mass range limit of our quadrupole analyzer, the molecular ions of tyr-bradykinin was not observed.

6.5 CONCLUSION

The separate behaviors of doubly-and singly-charged ions of small peptides in electrospray were studied by infusion ESI-MS and CE-ESI-MS analysis. The charge distribution of peptides in electrospray mass spectrometry is affected by the solute concentration, the solution pH, the solvent content, and the energy applied during ion transit. An attempt to explain the data based on ion evaporation theory is made. A more complete physical model should be employed for a more in-depth explanation. Nevertheless, the experimental results obtained have significance for the optimization of operational ESI parameters in peptide mapping by mass spectrometry.

Figure 6.13. Effects of ring potential on charge formation.

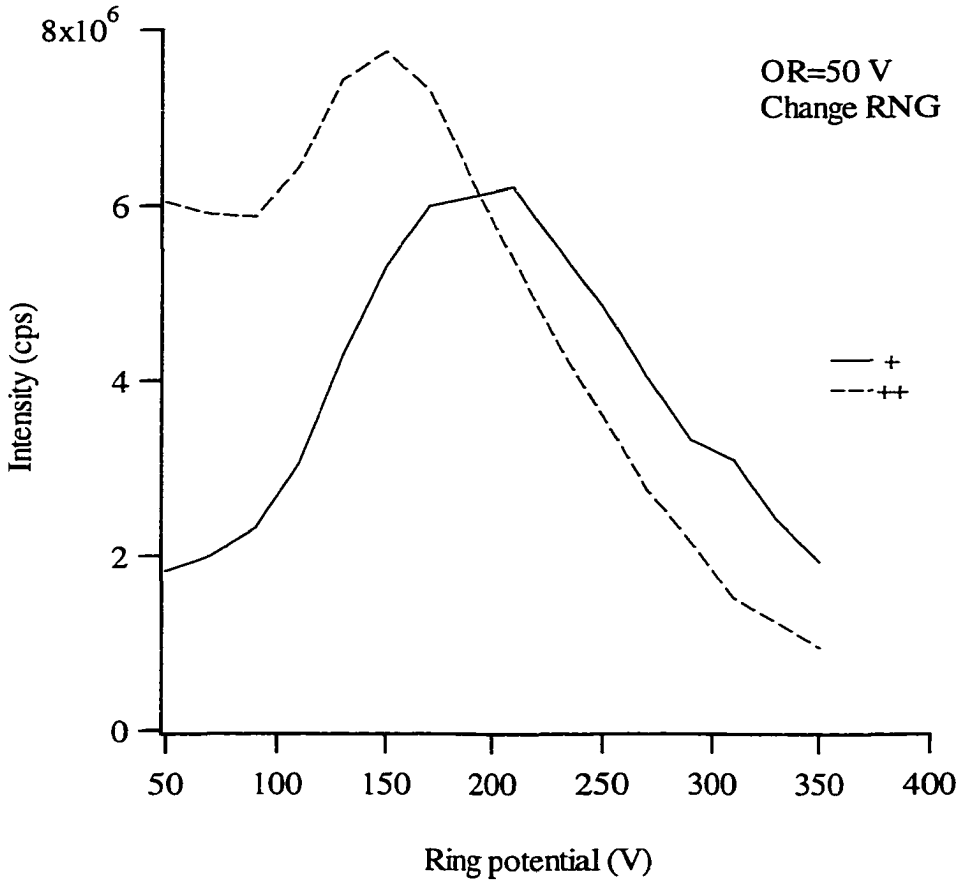

Figure 6.14. Total ion electropherogram showing the separation of bradykinin and tyr-bradykinin.

The sample was a 10^{-5} M mixture in 95% methanol and injected at 10 kV for 10s. CE was performed at 300 V/cm in a 2 mM ammonium acetate with 1% acetic acid. The column was an untreated fused silica capillary. Other conditions were as described in the experimental section.

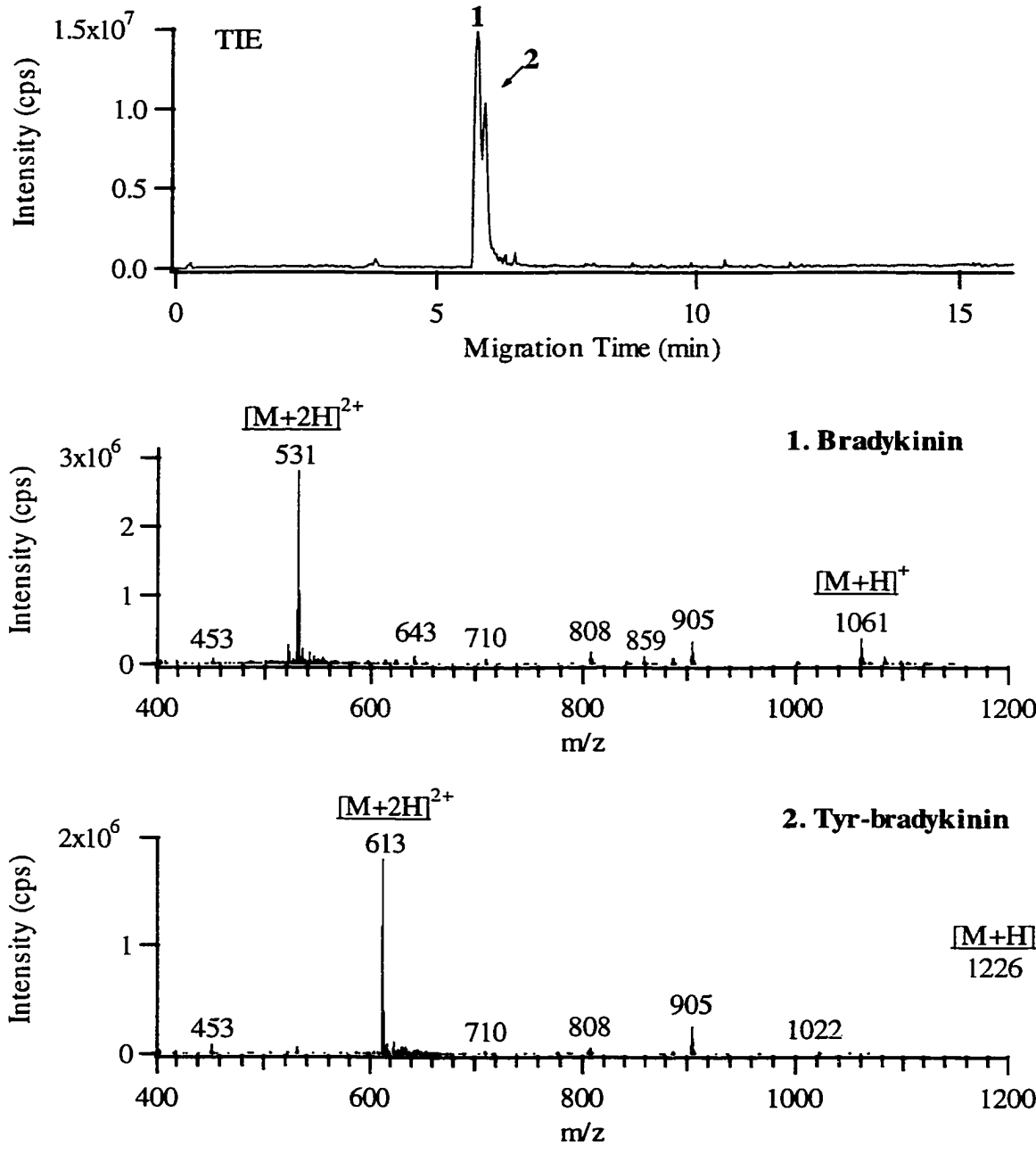

6.6 BIBLIOGRAPHY

(1) Olivares, J.A.; Nguyen, N.T.; Yonker, C.R.; Smith, R.D. *Anal. Chem.* **1987**, *59*, 1230-1232.

(2) Lee, E.D.; Muck, W.; Henion, J.D.; Covey, T.R. *J. Chromatogr.* **1988**, *458*, 313-321.

(3) Thibault, P.; Pleasance, S.; Laycock, M.V. *J. Chromatogr.* **1991**, *542*, 483-501.

(4) Lee, E.D.; Muck, W.; Henion, J.D.; Covey, T.R. *Biomed. Environ. Mass Spectrom.* **1989**, *18*, 253-257.

(5) Harsch, A. and Vouros, P. *Anal. Chem.* **1998**, *70*, 3021-3027.

(6) Figeys, D. and Aebersold, R. *Electrophoresis* **1997**, *18*, 360-368.

(7) Perkins, J.R. and Tomer, K.B. *Anal. Chem.* **1994**, *66*, 2835-2840.

(8) Henry, K.D.; Quinn, J.P.; McLafferty, F.W. *J. Am. Chem. Soc.* **1991**, *113*, 5447-5449.

(9) Hofstadler, S.A.; Swanek, F.D.; Gale, D.C.; Ewing, A.G.; Smith, R. *Anal. Chem.* **1995**, *67*, 1477-1480.

(10) Fang, L.; Zhang, R.; William, E.R.; Zare, R.N. *Anal. Chem.* **1994**, *66*, 3696-3701.

(11) Garcia, F. and Henion, J.D. *Anal. Chem.* **1992**, *64*, 985-992.

(12) Tang, Q.; Harrata, A.K.; Lee, C.S. *Anal. Chem.* **1995**, *67*, 3515-3519.

(13) Yang, L.Y., Lee, C.S.; Hofstadler, S.A.; Pasa-Tolic, L.; Smith, R.D. *Anal. Chem.* **1998**, *70*, 3235-3241.

(14) Smith, R.D.; Loo, J.A.; Barinaga, C.J.; Edmonds, C.G.; Udseth, H.R. *J. Chromatogr.* **1989**, *480*, 211-232.

(15) Zhao, Z.; Wahl, J.H.; Udseth, H.R.; Hofstadler, S.A.; Fuciarelli, A.F.; Smith, R.D. *Electrophoresis*, **1995**, *16*, 389-395.

(16) Yang, L.Y.; Harrata, A.K.; Lee, C.S. *Anal. Chem.* **1997**, *69*, 1820-1826.

(17) Lamoree, M.H.; Tjaden, U.R.; van der Greef, J. *J. Chromatogr. A.* **1995**, *712*, 219-225.

(18) Ding, J. and Vouros, P. *Anal. Chem.* **1997**, *69*, 379-384.

(19) Lord, G.A.; Gordon, D.B.; Myers, P.; King, B.W. *J. Chromatogr. A.* **1997**, *768*, 9-16.

(20) Whitehouse, C.M.; Dreyer, R.N.; Yamashita, M.; Fenn, J.B. *Anal. Chem.* **1985**, *57*, 675-682.

(21) Yamashita, M; Fenn, J.B. *J. Phys. Chem.* **1984**, *88*, 4451-4459.

(22) Edmonds, C.G.; Loo, J.A.; Barinaga, C.J.; Udseth, H.R.; Smith, R.D. *J. Chromatogr.* **1989**, *474*, 21-37.

(23) Smith, R.D.; Udseth, H.R.; Barinaga, C.J.; Edmonds, C.G. *J. Chromatogr.* **1991**, *559*, 197-208.

(24) Fenn, J.B.; Mann, M.; Meng, C.K.; Whitehouse, C.M. *Science* **1989**, *246*, 64-71.

(25) Fenn, J.B. *J. Am. Soc. Mass Spectrom.* **1993**, *4*, 524-535.

(26) Mirza, U.A.; Cohen, S.L.; Chait, B.T. *Anal. Chem.* **1993**, *65*, 1-6.

(27) Chowdhury, S.K.; Katta, V.; Chait, B.T. *J. Am. Chem. Soc.* **1990**, *112*, 9012-9013.

(28) Mirza, U.A. and Chait, B.T. *Anal. Chem.* **1994**, *66*, 2898-2904.

(29) Wang, G. and Cole, R.B. *Anal. Chem.* **1994**, *66*, 3702-3708.

(30) Katta, V.; Chait, B.T. *Rapid Communications in Mass Spectrometry* **1991**, *5*, 214-217.

(31) Loo, J.A.; Ogorzalek, RR.; Udseth, H.R.; Edmonds, C.G.; Smith, R.D. *Rapid Commun. Mass Spectrom.* **1991**, *5*, 101-105.

(32) Iribarne, J.V.; Thomson, B.A. *J. Chem. Phys.* **1976**, *64*, 2287.

(33) Fenn, J.B.; Rossel, J.; Nohmi, T.; Shen, S.; Banks, Jr., F.J., Editor: Snyder, A.P. *Biochemical and Biotechnological Applications of Electrospray Ionization Mass Spectrometry* **1995,** ACS, Washington, DC, 61-80.

(34) Sakairi, M.; Yergey, A.L. *Rapid Commun. Mass Spectrom.* **1991**, *5*, 349-353.

(35) Tang, L. and Kebarle, P. *Anal. Chem.* **1991**, *63*, 2709-2715.

(36) Tang, L. and Kebarle, P. *Anal. Chem.* **1993**, *65*, 3654-3668.

(37) Counterman, A.E.; Valentine, S.J.; Srebalus, C.A.; Henderson, S.C.; Hoaglund, C.S.; Clemmer, D.E. *J. Am. Soc. Mass Spectrom.* **1998**, *9*, 743-759.

CHAPTER 7 [1]

An Observation of Clusters in Electrospray Mass Spectra of Dideoxynucleosides

[1] Part of this work has been presented at the 47th ASMS Conference on Mass Spectrometry and Allied Topics, Dallas, TX, June 1999.

7.1 ABSTRACT

This chapter presents the occurrence and behavior of cluster ions of nucleosides in the gas phase. In electrospray ionization (ESI) mass spectra of nucleosides, the most intense signals were protonated and sodiated molecular ions, and base fragments originating from glycosidic bond cleavages, as well as cluster ions such as dimers, trimers, tetramers, and pentamers. The cluster signals increased as the solute concentration increased. Base ions, molecular ions and cluster ions showed distinctive characteristics under variable conditions in the in-source collisional induced dissociation (CID) region. Specifically, at elevated potentials applied to the orifice, the base fragments increased, while the dimers and oligomers decreased. Interestingly, proton and sodium ion adducts were two major dimeric species of nucleosides, while oligomers are composed of only sodiated adducts. The binding energy in the protonated dimer is weaker than in the sodiated dimer as revealed in the experimental results.

7.2 INTRODUCTION

Gas-phase studies have offered appreciable insight into the mysterious electrospray process. The gas-phase ion current that observed by a mass spectrometer provides one of the best tools in elucidating the intrinsic mechanism of electrospray ionization. For example, mass-spectrometric determinations of gas-phase ions have been employed to distinguish between the predictions of the Iribarne-Thomsom ion evaporation theory and the Dole charged-residue theory[1] of electrospray ionization. Also as an example, the observation of the suppressed ion intensity of a given analyte in the presence of other analytes has been investigated and explained based on a competition mechanism in the ion desorption process[2-4]. The observation and investigation of the charge state distribution of proteins have promoted a better understanding of the complex process of the electrospray ionization of macromolecules[5] and the functions of proton transfer reactions in the gas-phase ion production[1]. This chapter presents a compilation of results observed in electrospray mass spectrometric analyses of dideoxynucleosides regarding formation of cluster ions of nucleosides in the gas phase. The occurrence of clusters of nucleosides has been noted previously[6, 7]. However, the mechanism governing the formation of aggregated species in the gas phase has not been reported. It is hoped that the results presented in this chapter will help to add new evidence in drawing a clear picture of the electrospray mechanism relevant to the cluster ion production of nucleosides in the gas phase.

7.3 EXPERIMENTAL

7.3.1 Chemicals and Materials

Dideoxycytidine (ddC), azodothymidine (AZT), didanosine (ddI), stavudine (d4T), dideoxythiacytidine (3TC) and triethylamine were all purchased from Sigma (St. Louis, MO). HPLC-grade methanol was purchased from BDH (Toronto, ON, Canada). Acetic acid was obtained from Anachemia (Montreal, PQ, Canada). Syringe filters (0.45 μm) from Fisher Scientific (Eden Prairie, MN) were used to filter the solvents used. Stock solutions of 10^{-2} M ddNs were prepared using water and then diluted to 10^{-3} to 10^{-8} M with methanol-water (95:5) or 10 mM HAc or 0.4% triethylamine as indicated in the text. Fused silica capillaries were from Polymicro Technologies (Phoenix, AZ).

7.3.2 Procedures

The PE/Sciex API 100 single quadrupole mass spectrometer (Thornhill, ON, Canada) equipped with an in-house built low-flow electrospray interface was used in this study. The fabrication of the low-flow electrospray interface has been described in **Chapter 5, Figure 5.1**. Standards were diluted in 95% MeOH and infused at 0.3 μL/min with a syringe infusion pump from Harvard Apparatus (Southnatick, MA). The sheath liquid was methanol at 0.2 μL/min. Positive detection mode was conducted with potentials applied at the ion sprayer, the orifice and the focusing ring of 4.6 kV, 30 V and 170 V, respectively, unless otherwise stated. Typically, a mass range of 30-1200 Da was scanned at a speed of 2.4 s/scan with a mass step size of 1.0 Da and a dwell time of 2 ms. Spectra were acquired using LCTune software from Sciex and processed using MultiView software from Sciex and IgorPro software from WaveMetrics (Lake Oswego, OR).

7.4 RESULTS AND DISCUSSION

7.4.1 ESI Mass Spectra of Dideoxynucleosides

Figure 7.1A shows the ESI mass spectra of the commonly used antiretroviral dideoxynucleoside ddI obtained from an infusion experiment. The analyte was dissolved in a solution of methanol-water (95:5) and the spectrum was the average from 10 scans. The protonated molecular ion appears at m/z 237, also present are Na^+ and K^+ adducts of molecular ions, $[M+Na]^+$ and $[M+K]^+$. Major fragments are protonated and sodiated adducts of base fragments, $[BH_2]^+$, $[BHNa]^+$ and $[BHK]^+$, arose from the cleavage of a glycosidic bond (base-sugar linkage). The so-called in-source collision induced dissociation (CID) occurs in the free-jet region between the orifice cone and the skimmer cone, and results in the fragmentation of molecular ions to the low-mass species. Also ddI gives rise to protonated and sodiated adducts of dimers (e.g. $[2M+H]^+$, $[2M+Na]^+$ and $[2M+K]^+$), trimers ($[3M+Na]^+$), and tetramers ($[4M+Na]^+$). The ESI mass spectra of other dideoxynucleosides exhibit similar occurrence of ions i.e. protonated and/or alkali ion adducts of molecular ions, base fragments and clusters, **Figure 7.1B-7.1E**.

7.4.2 Pseudo-Molecular Ions and Base Fragments

A subtle, interesting difference should be noted in comparing the mass spectra of these different compounds. The mass spectra of ddI and d4T show that the sodiated adducts of the base fragments and the sodiated molecular ions are predominant. For example, the intensity ratio of $[M+Na]^+/[M+H]^+$ in the spectrum of ddI is 4.6, and that of d4T is 14. The mass spectra of ddC and 3TC, however, appear to have more protonated ions species. For example, the pseudo-molecular ion $[M+H]^+$ of 3TC at m/z 230 is about three times more intense than the sodiated adduct ion $[M+Na]^+$ at m/z 252; no significant

Figure 7.1. Average of 10 spectra of (A) ddI, (B) d4T, (C) ddC, (D) AZT, and (E) 3TC.

Samples were at 50 μM in 95% methanol and infused at 0.3 μL/min with a sheath of 0.2 μL/min methanol.

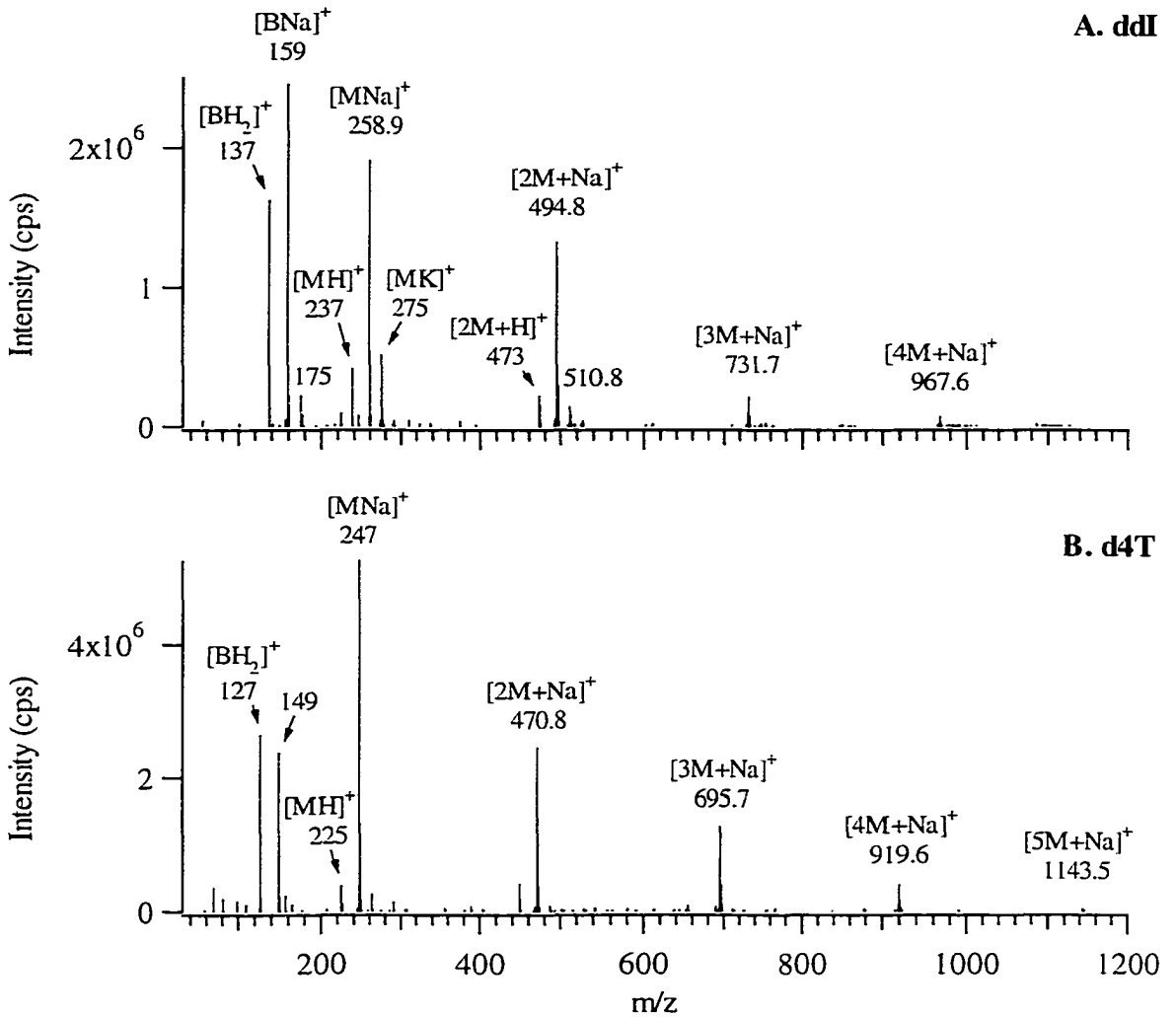

Figure 7.1. (cont'd).

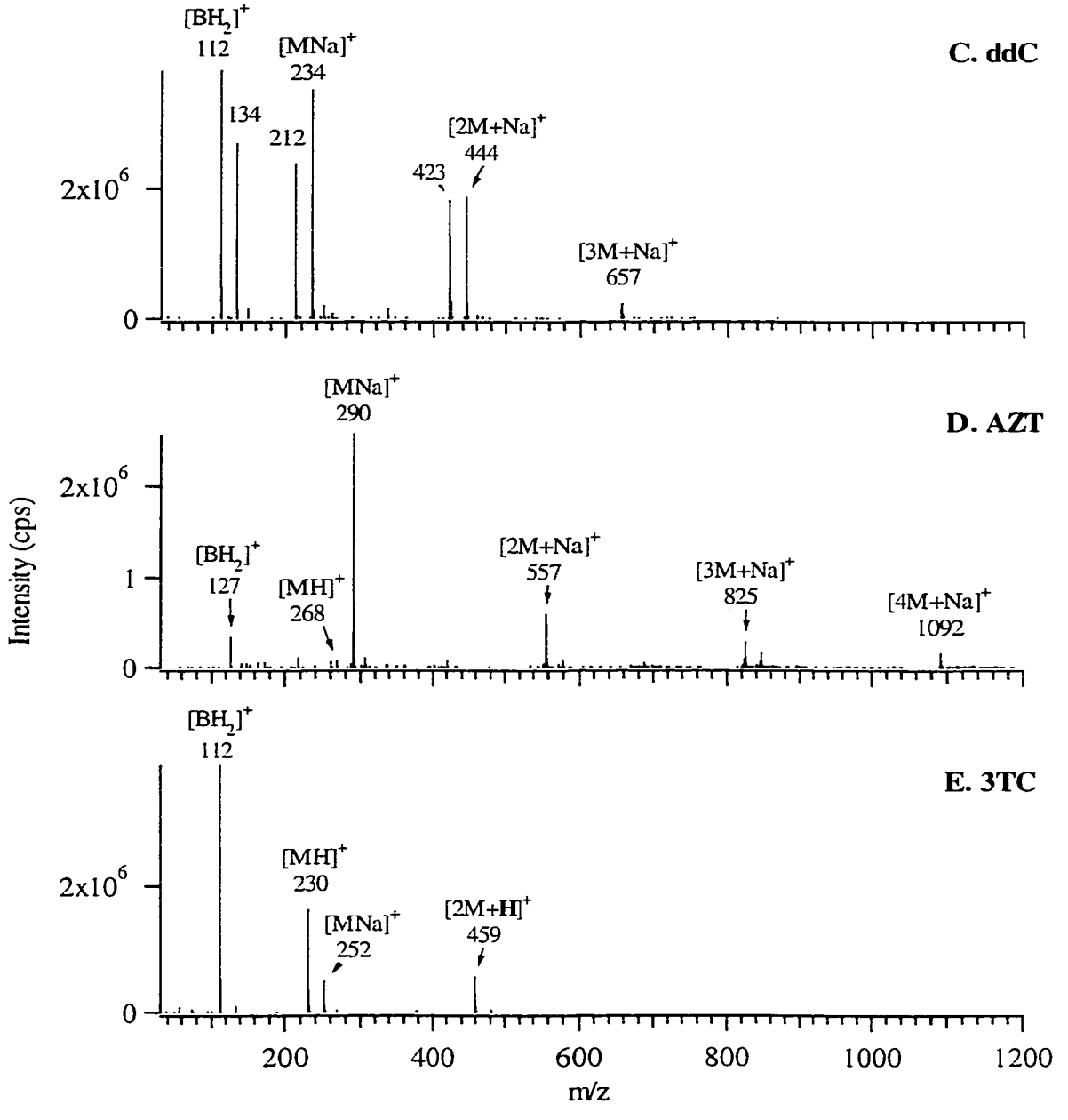

sodiated adducts of the base fragments are observed. It has been reported[8,9] that the proton affinity (PA) of the ring nitrogen is increased by the $-NH_2$ substitution, and that the PA of deoxynucleosides yield an order of dG>dA~=dC>>dT. Although there are no reports on the PA values of dideoxynucleosides, based on the above results showing the relative abundance of protonated molecular species, a similar order of the PA of dideoxynucleosides can be rationalized as 3TC>ddC>>ddI~=d4T.

The metal adduct species are frequently observed in the electrospray mass spectra of organic compounds. A mass spectrometric study of structural analysis on metal ion-nucleoside interactions has suggested that the metal cation is linked to purine's N7 site[10].

7.4.3 Dimers and Oligomers of Dideoxynucleosides in the Gas-Phase

It is interesting to note that, except for 3TC, the studied dideoxynucleosides demonstrate, in going from base fragments to cluster ions, an increased relative abundance of the sodiated adducts to the protonated species. For example, in the spectrum of ddI, the intensity ratios of $[BH+Na]^+/[BH+H]^+$, $[M+Na]^+/[M+H]^+$, and $[2M+Na]^+/[2M+H]^+$ are 1.5, 4.6, and 6.0, respectively, in cases of trimers and tetramers, no appreciable amounts of protonated ions appear. Similarly, in the spectrum of d4T, the ratios of $[BH+Na]^+/[BH+H]^+$, $[M+Na]^+/[M+H]^+$, and $[2M+Na]^+/[2M+H]^+$ are 0.9, 14, and 6.0, respectively, no significant protonated trimers and tetramers are present. Also, the aggregated species increase as the analyte concentrations increase as depicted in **Figure 7.2.**

As exhibited in **Figure 7.1**, the dimeric ions observed in the spectra of dideoxynucleosides mainly appeared as both the protonated ions $[2M+H]^+$ and the sodiated ions $[2M+Na]^+$. The formation of the protonated dimers has been observed and

Figure 7.2. Cluster intensities (total ion current) versus. concentration of d4T.

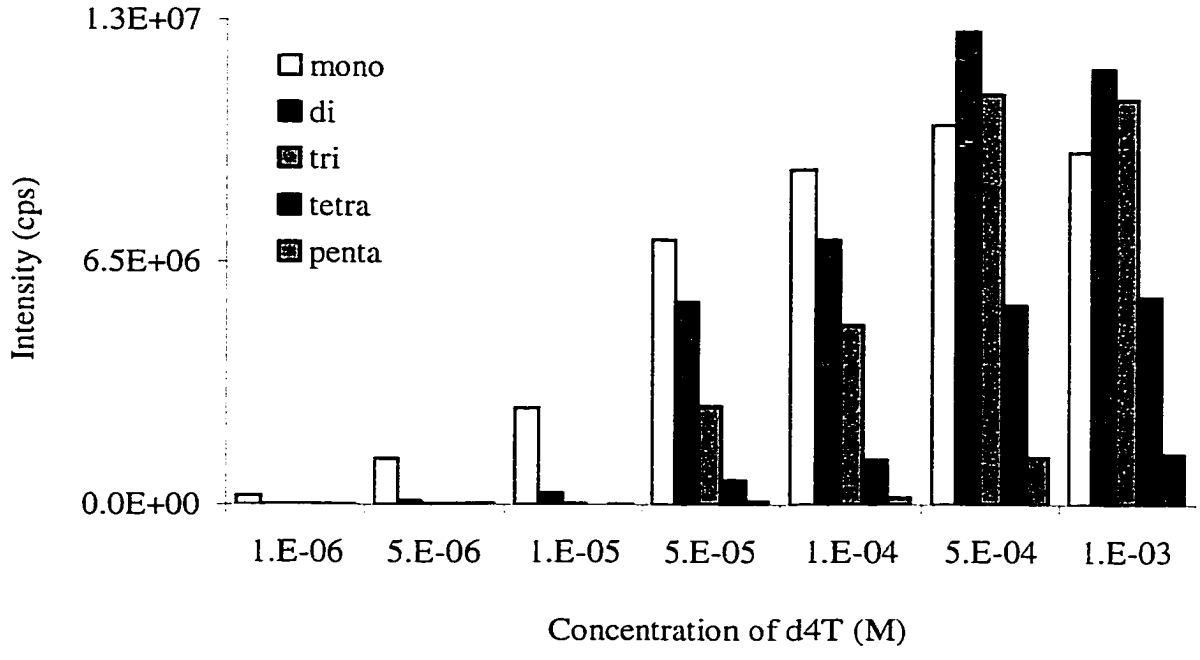

investigated by Meot-Ner[11], Dey and co-workers[12], and hydrogen bonds between nucleobases have been claimed as the driving force for base-pairing in the gas phase[11,12]. It has also been noted that the degree of hydrogen bonding in the gas-phase dimeric ions, as suggested by the thermodynamic data, is interestingly parallel to the degree of hydrogen bonding in DNA[11]. The formation of the complimentary nucleobase pairs in the gas phase, as that in DNA (i.e. A-T and C-G), is found to be in preference to noncomplimentary base pairs[12].

However, the origin and the structural aspects of sodiated dimer ions in the gas phase have not been revealed. Studies have demonstrated that the presence of a metal ion promotes self-stacking of nucleosides[13], and the stacked configuration is preferred in aqueous solution phase[14]. It is therefore suggested that the formation of the sodiated dimer follows a different route from that of the protonated dimers. The protonated dimers are formed by hydrogen bonds, while the sodiated dimers are formed by agglomeration of two molecules. At low concentrations, the protonated dimeric products (via hydrogen bonding) dominate; as the concentration increases, the sodiated dimers increase while the protonated dimers decrease, **Figure 7.3**. Based on this result, one can rationalize that protonated dimers form early in the fission process of charged droplets where the solute concentration is low, and the sodiated dimers occur at late fission generations where the solute concentration is high due to solvent evaporation. The presence of the sodiated (instead of protonated) oligomers, especially at high concentrations of analyte, further indicates that agglomeration occurs prior to desorption of the ions from the surface of the charged droplets. As shown in **Figure 7.2**, although the absolute signal stabilizes (and then decreases) at sample concentrations of 10^{-4} M and above, the relative amount of clusters compared to monomers continues to increase. It is then reasonable to assume that, at very high concentration levels, the solute precipitates as the droplet evaporates to

Figure 7.3. Effects of analyte concentration on dimer formation for ddC.

Samples were ddC in 95% methanol and infused at 0.3 μL/min with a sheath of 0.2 μL/min methanol.

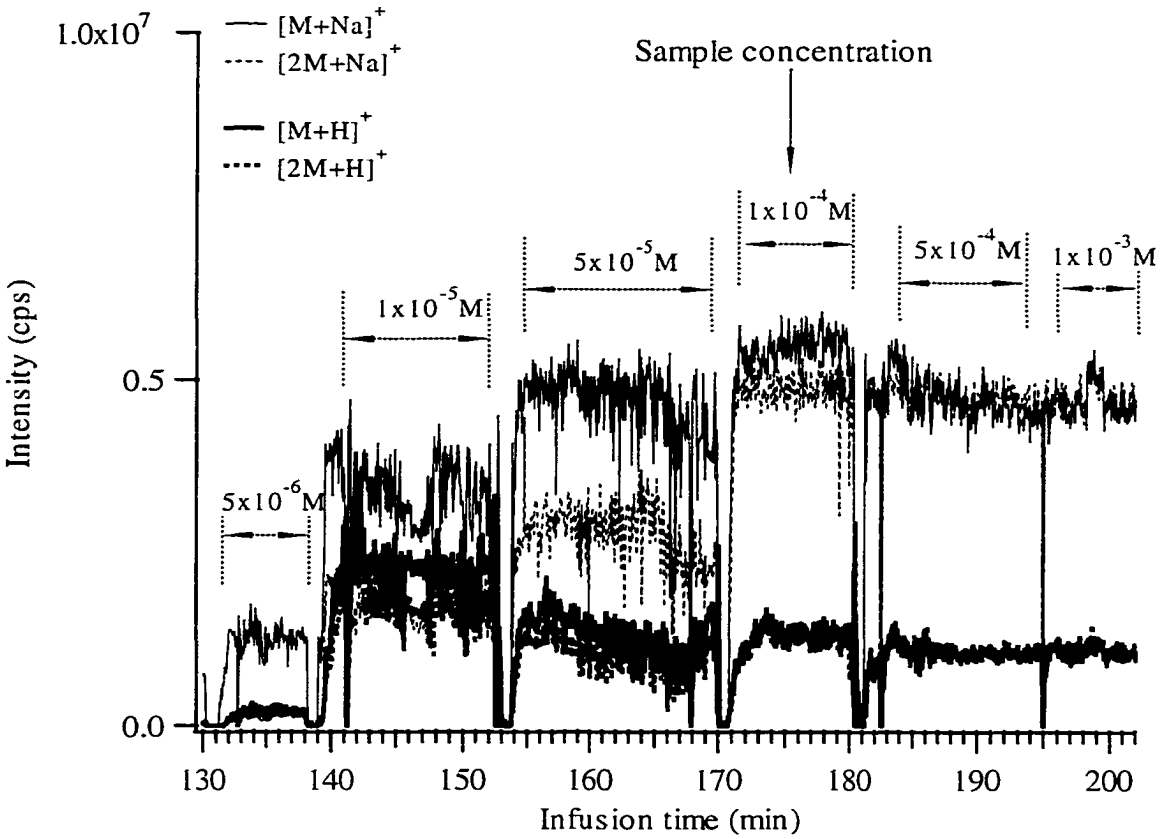

smaller size, and the analyte ionization through electrospray no longer exists, resulting in an observed decrease of absolute signals and an increase of oligomers.

The in-source CID voltage applied at the orifice has substantial effects on ion intensities of base, monomer, and oligomers as depicted in **Figure 7.4**. At higher orifice voltages (OR), more fragments are observed due to an elevated CID process. And the cluster signals decrease as the voltage increase. For instance, the greatest amount of pseudo-molecular ions occur at an orifice potential of 25 V, while the greatest amount of base fragments appear at a higher potential, 40 V, and the most dimers appear at 20 V.

Further investigations of the dimeric ions reveal another interesting phenomenon: the most protonated ion $[2M+H]^+$ appears at a lower CID voltage, 10 V for the orifice potential, whereas the most sodiated ion $[2M+Na]^+$ at 25 V, **Figure 7.5**. These results suggest that the protonated and the sodiated dimers are two different noncovalently bonded complexes with different dissociation constants.

In contrast, protonated and sodiated molecular ions do not show much difference. The highest $[M+H]^+$ and $[M+Na]^+$ both occur at 25 V. Similarly, both $[BH_2]^+$ and $[BH+Na]^+$ are intense at 40 V. The right-shift of the crest in **Figure 7.5C** is mainly due to the elevated CID process of molecular ions. It is believed that if a pure nucleobase and a pure nucleoside are infused into the ESI-MS separately, the crests of Intensity-OR plots for the nucleobase and the nucleoside should be both at 25 V of OR. Last, a re-arrangement of **Figure 7.5** for sodiated monomer and oligomer traces reveals that the stability of sodiated clusters is nearly the same, **Figure 7.6**.

Figure 7.4. Orifice voltage versus total ion intensities of base, molecular, and dimer ions of ddC.

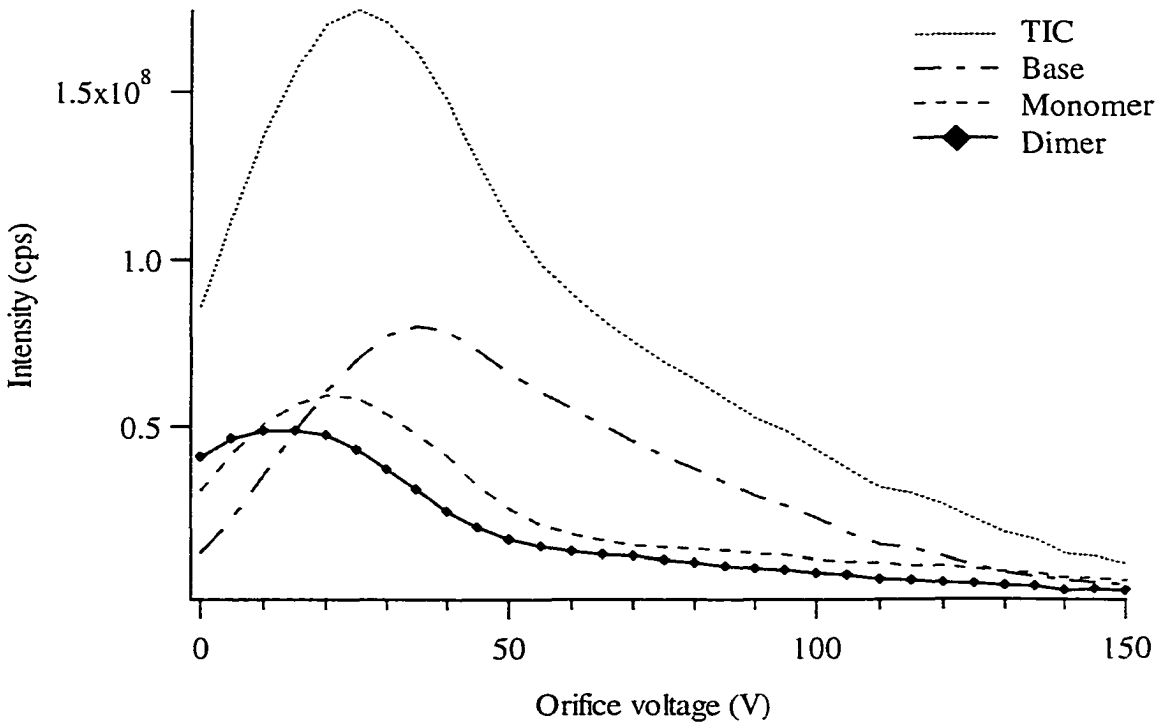

Figure 7.5. Orifice voltage vs. signal intensities of protonated and sodiated ions of ddC. (A) dimers, (B) monomers, (C) base fragments.

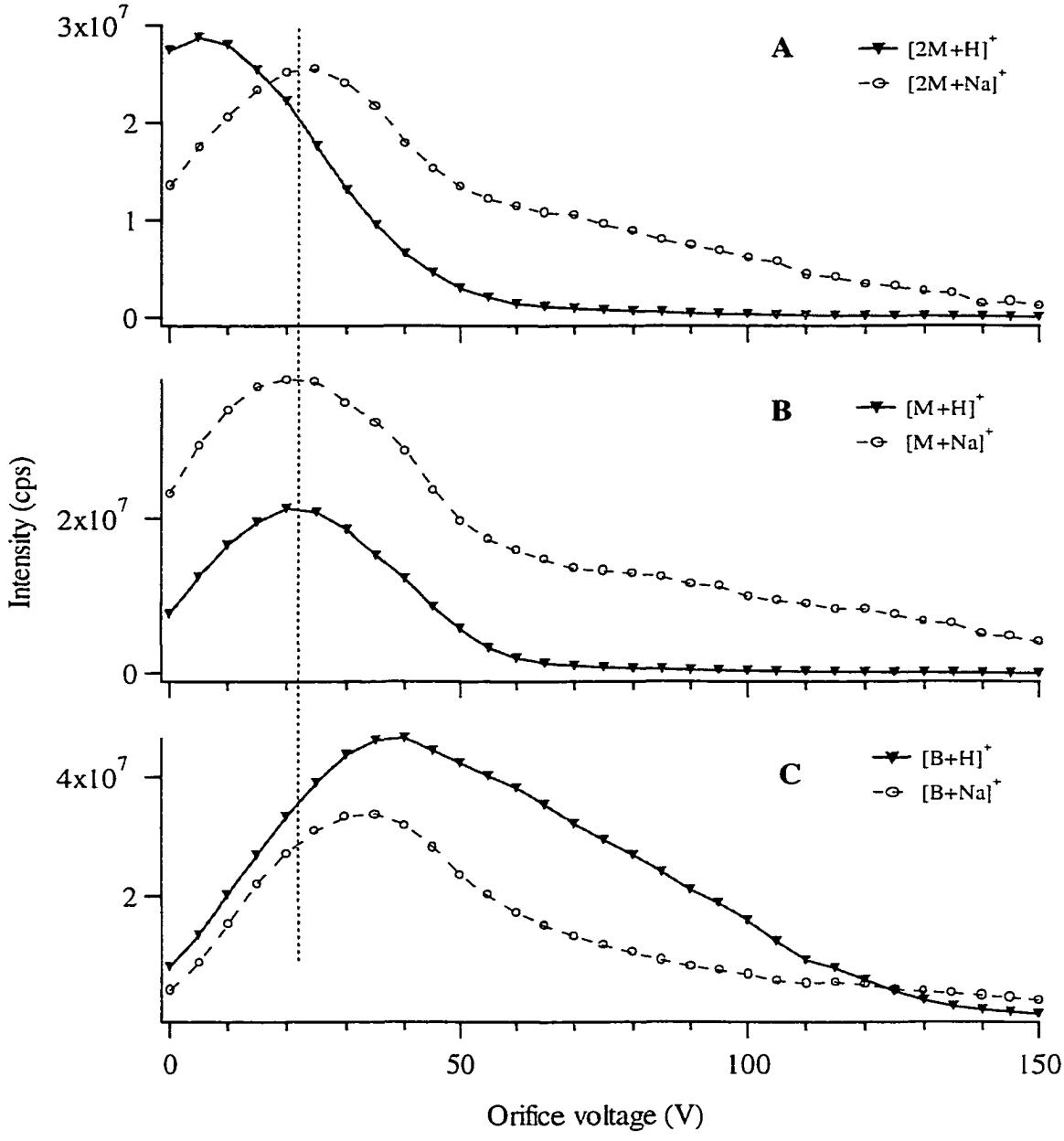

Figure 7.6. Orifice voltage vs. ion intensities of sodiated monomer and ologomers of ddC (a re-plot of **Figure 7.5**).

Traces for dimer and monomer were moved left for 1.67 and 3.34 V, respectively in relative to the trace for trimer to compensate the slow scanning speed of qualdrupole analyzer that scans high masses first for 1.14 s or 1.67 V per 211 Da.

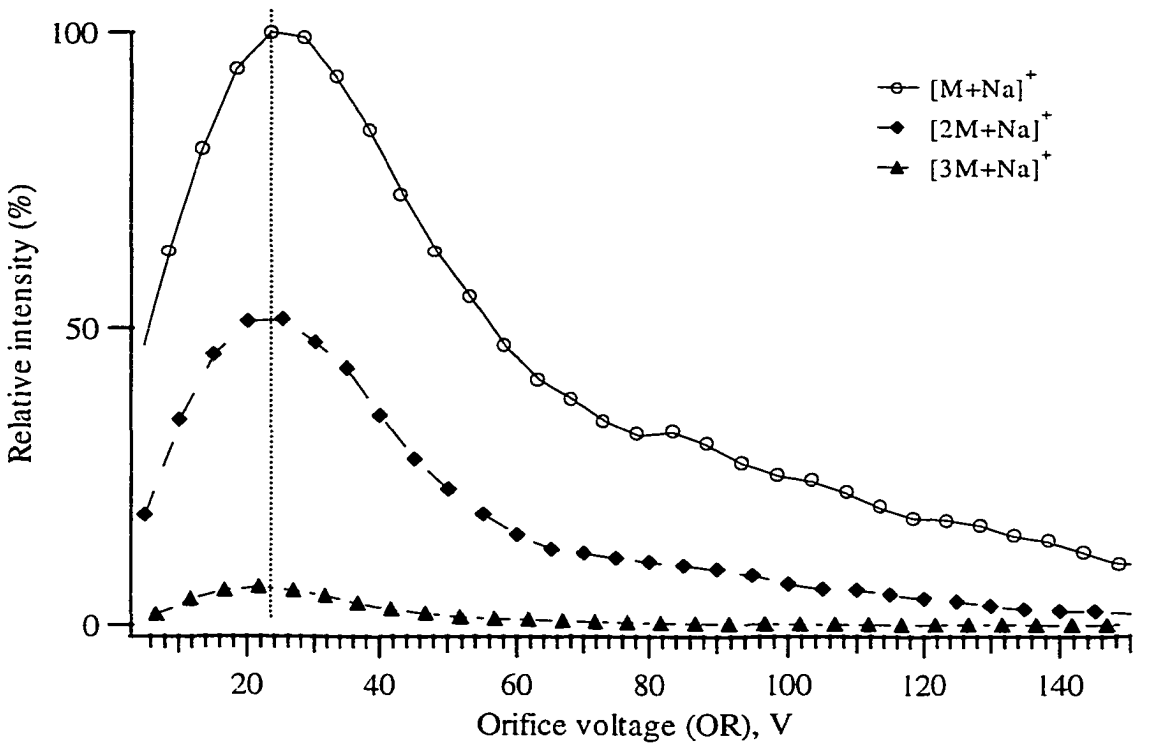

7.5 CONCLUSION

The mass spectra of dideoxynucleosides generated in the electrospray ionization exhibit interesting similarities and differences. Generally, in a spectrum of a dideoxynucleoside dissolved in a solution of methanol-water, the protonated molecular ion and base fragments and their metal ion adducts appear with high intensity, also present are protonated and sodiated dimers, as well as sodiated oligomers. Cluster signals increase as the sample concentration increases. Some spectral differences among five dideoxynucleosides have also been observed. Analytes with high proton affinity show more intense protonated species. More interestingly, two kinds of dimeric species show distinctive stability in the gas phase. Compared to the sodiated dimers, the protonated dimers are readily dissociated upon elevated energies applied in the in-source CID region, which indicates the (hydrogen) bonding force between two nucleoside molecules with a proton adducted is relative weak compared to the (static) bonding force in sodiated dimers. A detailed study of the structural aspects of dimers is beyond the scope of this thesis. Nevertheless, observations of clusters of dideoxynucleosides in the gas-phase should have provided new evidence in depicting the mechanism of cluster ion occurrence in the electrospray process.

7.6 BIBLIOGRAPHY

(1) Kebarle, P.; Yeunghaw, H. *Electrospray Ioniz. Mass Spectrom.* **1997**, Cole, R.B., Ed. Wiley: New York, NY. pp 3-63.

(2) Tang, L.; Kebarle, P. *Anal. Chem.* **1991**, *63*, 2709-2715.

(3) Tang, L.; Kebarle, P. *Anal. Chem.* **1993**, *65*, 3654-3668.

(4) Kebarle, P.; Tang, L. *Anal. Chem.* **1993**, *65*, 972A-986A.

(5) Wang, G.; Cole, R.B. *Electrospray Ioniz. Mass Spectrom.* **1997**, Edited by Cole, R.B., Wiley: New York, NY. pp 137-174.

(6) Banks, J.F., Jr.; Shen, S.; Whitehouse, C.M.; Fenn, J.B. *Anal. Chem.* **1994**, *66*, 406-414.

(7) Kamel, A.M.; Brown, P.R.; Munson, B. *Anal. Chem.* **1999**, *71*, 5481-5492.

(8) Greco, F.; Liguor, A.; Sindona, G.; Uccella, N. *J. Am. Chem. Soc.* **1990**, *112*, 9092-9096.

(9) Liguori, A.; Napoli, A.; Sindona, G. *Rapid Commun. Mass Spectrom.* **1994**, *8*, 89-93.

(10) Theophanides, T.; Bariyanga, J. *J. Mol. Struct.* **1989**, *214*, 177-184.

(11) Meot-Ner, M. *J. Am. Chem. Soc.* **1979**, *101*, 2396-2403.

(12) Dey, M.; Moritz, F.; Grotemeyer, J.; Schlag, E.W. *J. Am. Chem. Soc.* **1994**, *116*, 9211-9215.

(13) Scheller, K.H.; Sigel, H. *J. Am. Chem. Soc.* **1983**, *105*, 5891-5900.

(14) Imoto, T. *Biochem. Biophys. Acta* **1977**, *475*, 409-416.

CONCLUSION

The joy of establishing a new achievement in developing and applying a novel technology after hard work of learning and studying is indeed enormous. Several years of experimentation have passed since I started the projects on capillary electrophoresis-electrospray mass spectrometry in early 1997. This coupling technology has truly evolved over that time into a readily applicable, high-performance analytical tool for solving the real problems deeply related to human diseases, drug discovery, and bioanalytical chemistry. The marriage of electrospray mass spectrometry to capillary electrophoresis with a thorough optimization of separation and detection conditions has made the coupling technology routine. The analyst can now readily employ an assortment of methodologies described in this thesis for real-time detailed structural and quantitative analysis.

However, the commercialization of the coupled CE-ESI-MS system for widespread applications on a routine basis, as in the case of liquid chromatography-mass spectrometry, has not yet occurred. This is mainly due to the lack of robustness of the CE methodology and the coupling interface. The dependence of the CE separation on use of highly conductive buffer salts further limits the performance of the coupled technique because of the competitive ionization feature in electrospray ionization process. However, improvement in CE method development for the on-line CE-MS analysis has proven the robustness of this technique in a research lab. With the employment of a nonaqueous buffering system as presented in **Chapter 2**, the on-line coupled analysis can be very sensitive and reproducible in analyte migration (RSD < 1%) and peak area (RSD < 8%) detected by ESI-MS in a full scan mode. Detection limits are in the sub-femtomole or 10^{-7} M range of analytes dissolved in 10% buffer; these limits can be even lower for samples prepared in pure solvent for an increased stacking effect as discussed in the chapter. The established method has been successfully employed in metabolism studies of

amitriptyline by *C. elegans*. Sixteen metabolites were detected and their structures were elucidated, most of them have been reported previously in publications utilizing other methods such as nuclear magnetic resonance (NMR) analysis after high performance liquid chromatographic fractionation. More interestingly, this nonaqueous CE system coupled with ESI-MS has been tested in a summer workshop held in 1999 in this department. All participants with various backgrounds achieved nearly equal separation efficiency and signal sensitivity for test compounds studied in Chapter 2. Thereafter, a few students have successfully adopted this analytical protocol with minor modification for studies of various organic compounds.

Aqueous CE separations coupled with ESI-MS detection have also been developed for analyses of nucleosides, nucleotides, carbohydrates, and peptides. With the use of volatile separation background electrolytes such as ammonium acetate, ammonium carbonate, and acetic acid, sufficient sensitive ESI-MS detection and adequate CE separation efficiency have been achieved. As presented in **Chapter 3**, an exemplary separation of 14 nucleosides and nucleotides has been optimized in ammonium acetate buffer at pH 10. Optimization of component separations was accomplished based on studies on their solution chemistry-specifically their pKa. Electrospray ionization of both nucleosides and nucleotides in negative ion mode provides sensitive ion signals with high stability. Similar sensitivities are obtained for nucleosides in positive ion detection mode. Surprisingly, nucleotides can also be detected in positive ion mode although sensitivities are one third of that observed for nucleosides. It is concluded that proton transfer must have occurred in the gas phase between nucleotide molecules and cations, such as ammonium, present in the ESI process. The influence of operational parameters of quadrupole mass analyzers, for instance the scan speed and the mass step size, on ion intensity and sensitivity has been studied. The total ion electropherogram (TIE) shows

higher signals when the quadrupole analyzer scans at a fixed speed, but at a smaller mass interval and a smaller dwell time. However, the sensitivity remains the same (determined by the signal to noise ratio in the TIE). To increase the scan speed, one must either increase the step size or decrease the dwell time; either will decrease the ion intensity and sensitivity as well. It is clear that in order to gain sufficient data points to describe an electrophoretic peak and for high sensitivity, a non-scanning mass analyzer such as time of flight must be employed. The present method has been used for detection and recognition of nucleotides in a cell extract. Applications of this methodology to intracellular characterization of 3TC, a popular anti-HIV agent, have also been demonstrated. Detection limits in the low femtomole or sub-micromolar range with an injection volume of tens of nanoliters have been obtained.

Microspray MS and CE-ESI-MS have been explored as structural analysis techniques for carbohydrates in **Chapter 4**. While an impressive and useful accomplishment, the methods are presently not competitive with other chromatographic methods mainly because the separation of neutral carbohydrates is not successful without employing complexing agents in the separation buffer. These complexation agents are believed to suppress the ionization of analytes in electrospray. Alternative methods employing either derivatization of carbohydrates with a charged tag for improved separation in free zone CE or the employment of capillary electrochromatographic separation should be explored. Nevertheless, the demonstrated CE-MS methodology for carbohydrate analysis can be very useful for desalting a sample and providing rough separation for improved electrospray ionization efficiency, for which traditional methods such as infusion-ESI-MS are more difficult to implement.

Since our quadrupole mass analyzer has limited mass range up to 1200 Da, my research has been emphasized on investigations associated with small molecules such as organic compounds, carbohydrates, small peptides, and nucleotides.

Micro- and nano- electrospray sheathless interfaces operated at low sample flow rates provide superior sensitivity for analytes in minimal amounts. Problems associated with bubble formation and tip deterioration often terminate the CE and ESI process in direct coupling of CE with MS via this sheathless configuration. To take advantage of an increased ESI efficiency of a microspray interface and the long-term stability of a conventional stainless-steel sheath flow interface, **Chapter 5** presents a silica sheath liquid interface that has been constructed and operated at a flow rate in the mid- to high-nanoliter per minute range. The liquid sheath and the gold layer deposited on the outer surface of the CE column at the detection end make the electrical contact for CE and ESI. Overall, the interface showed a gain in sensitivity of at least one order of magnitude over the conventional interface. This low flow interface also shows promise in terms of its endurance and ability in producing highly stable ion signals.

Understanding of the intrinsic mechanism governing the ion desorption from the charged droplets in the electrospray process and the modifications of gas phase ions produced thereafter in the sub-atmospheric pressure sampling regions of the mass spectrometer should aid in elucidation of the mass spectrometric data. **Chapter 5** presents observations of distinctive behavior of doubly-charged and singly-charged ions as revealed in the ESI mass spectra and on-line CE-MS analysis of small peptides. At high analyte concentrations singly-charged species predominate; at low concentrations doubly-charged ions increase. Multiple-charged ions of protein and peptides formed in ESI have long been topics of interest for mass spectrometrists since the invention of ESI-MS. Two

theoretical models and subsequent implementations have been employed extensively in accounting for experimentally observed results, although these theories have not been accepted unanimously. In this chapter, the unique appearance of the doubly-charged peptide ions is implemented employing a prediction of the well-known ion evaporation model (IEM). The rationale that the singly-charged ions are produced early in the fission process of the charged droplets while the doubly-charged ions occur in a later process has been deduced.

Furthermore, an observation of cluster ions of nucleosides in the electrospray mass spectra is presented in **Chapter 7**. These clusters increase at elevated analyte concentrations. Dimers are composed of proton and sodium ion adducts while other oligomers such as trimers and higher are mainly sodiated species. Protonated dimeric ions dissociate readily upon collisional dissociation in the sub-atmospheric pressure region, while sodiated dimeric and other oligomeric ions show similar stability in the gas phase. It is clear that bonding forces and types are different in protonated and sodiated cluster ions. While protonated dimers are formed via hydrogen bonding, sodiated clusters may be aggregated together through electrostatic forces. The origin and implementation of these clusters are still areas of research and are not well elucidated. Nevertheless results shown in this chapter and chapter 6 are important references in interpreting the electrospray mass spectrometric data and in optimization of the instrumental parameters for desired sensitivity and structural information.

Finally, this thesis provides clear evidence of the extraordinary performance of CE-ESI-MS that can be achieved in terms of resolution, efficiency, sensitivity, and specificity of compound information. Preliminary data also demonstrate that CE-ESI-MS and ESI-MS can become extremely useful in studies of electrosprayed ion-molecule and ion-ion

reactions. With new capabilities in the hands of many more scientists, the area of study will undoubtedly see future growth and lead to commercialization and application of the CE-MS coupling technology and thus enlightening biochemical discoveries.